LAKE SEDIMENT RECORDS OF LATE QUATERNARY PALEOCLIMATE CHANGE FROM ALASKA AND NEWFOUNDLAND DEVELOPED USING SEDIMENTOLOGY AND GEOCHEMICAL PROXIES

by

Matthew Scott Finkenbinder

B.S. Shippensburg University, 2005

M.S. West Virginia University, 2008

Submitted to the Graduate Faculty of the

Kenneth P. Dietrich School of Arts and Sciences in partial fulfillment

of the requirements for the degree of

Doctor of Philosophy

University of Pittsburgh

2015

UNIVERSITY OF PITTSBURGH

DIETRICH SCHOOL OF ARTS AND SCIENCES

This dissertation was presented

by

Matthew S. Finkenbinder

It was defended on

April 16, 2015

and approved by

Byron Steinman, Assistant Professor, Large Lakes Observatory, University of Minnesota Duluth

Joseph Ortiz, Professor, Geology, Kent State University

Charles Jones, Lecturer, Geology and Planetary Science

William Harbert, Professor, Geology and Planetary Science

Daniel Bain, Assistant Professor, Geology and Planetary Science

Dissertation Advisor: Mark Abbott, Professor, Geology and Planetary Science

LAKE SEDIMENT RECORDS OF LATE QUATERNARY PALEOCLIMATE CHANGE FROM ALASKA AND NEWFOUNDLAND DEVELOPED USING SEDIMENTOLOGY AND GEOCHEMICAL PROXIES

Matthew S. Finkenbinder, Ph.D.

University of Pittsburgh, 2015

High-latitude regions are particularly sensitive to climate change through positive feedbacks linked with cryospheric processes and further exert a significant influence on the global climate system. Long term records of natural climate variability are essential to give context to potential future climatic scenarios and to put them into perspective. Sediments from Harding Lake in the interior and Burial Lake in northwest Alaska were used to reconstruct lake-levels and paleoenvironmental conditions spanning the Last Glacial Maximum using a detailed analysis of core sedimentology and a multiproxy geochemical approach. Relatively high lake-levels during late Marine Isotope Stage 3 are followed by extremely arid and windy conditions evinced from very low lake-levels during the Last Glacial Maximum (LGM). Ameliorating climate conditions and rising

lake-levels commence by 19,600 cal yr BP at Burial Lake and by 15,700 cal yr BP at Harding Lake. Holocene hydroclimate conditions are broadly characterized by high and stable lake-levels along with variable levels of terrestrial and aquatic productivity. Major climatic transitions in Alaska coincide with changes in summer insolation, Laurentide Ice Sheet extent, eustatic sea level, and related changes in paleogeography. Millennial variations in aquatic productivity at Burial Lake occur over the last 10,000 cal yr BP, which are related to changes in the duration of the ice-free season and the availability of limiting nutrients. Productivity variations coincide with changes in the mean-state Arctic Oscillation on millennial time scales, suggesting the millennial variations are driven by an internal forcing mechanism related to an ocean-atmosphere interaction. Sediments from Cheeseman Lake in Newfoundland were used to reconstruct hydroclimate variability using the oxygen isotopic composition of authigenic carbonates ($\delta^{18}O$). Increasing $\delta^{18}O$ values from 10,200 to 7,950 cal yr BP reflect warming temperatures that are superimposed by abrupt negative $\delta^{18}O$ shifts at 9,700 and 8,500 cal yr BP from short lived cooling events. Decreasing $\delta^{18}O$ values after 7,950 to 1,200 cal yr BP indicate a cooling trend consistent with declining insolation, cooling surface temperatures, and a cooling trend inferred from Greenland ice cores. The results highlight the sensitivity of Newfoundland climate to ocean-atmosphere interactions on century to orbital time scales.

TABLE OF CONTENTS

LIST OF TABLES

LIST OF FIGURES

LIST OF EQUATIONS

PREFACE

I would foremost like to express gratitude to my doctoral advisor Dr. Mark Abbott for his guidance and encouragement throughout the duration of my graduate studies. I am incredibly grateful for all the research opportunities and intellectual freedom you provided me to complete this dissertation. I would also like to thank my committee members; Dr. Byron Steinman, Dr. Daniel Bain, Dr. William Harbert, Dr. Charles Jones, and Dr. Joseph Ortiz for the helpful discussions and input. To Byron, for being a great mentor in the field, the lab, and in reviewing rough drafts of manuscripts that were initially quite rough. To Bill, for your enthusiasm and assistance with quantitative analysis. To Dan, for the critical discussions on sedimentary trace metals and nutrients. To Charlie, for the opportunity to teach Sedimentology and Stratigraphy lab and the fun weekend fieldtrips. To Joe, for the discussions and perspective linking marine and terrestrial climate conditions in the Arctic.

I also want to thank the many collaborators that assisted in my Alaska and Newfoundland research. Thank you to Dr. Joe Stoner and Jason Dorfman at Oregon State University, for all the great discussions and critical input on the Burial Lake sediment record. It has been a great pleasure working with you both over the last several years. Thank you to Dr. Bruce Finney at Idaho State University, Dr. Mary Edwards at Southampton University, and Dr. Nancy Bigelow at University of Alaska

Fairbanks, for use of coring equipment during the July 2012 field season, the helpful discussions related to Alaskan paleoclimatology, insights with proxy interpretation, and patience during the review process of manuscripts. Thank you to Dr. John Southon and Dr. Guaciarra dos Santos at the University of California Irvine, for allowing me to visit the Accelerator Mass Spectrometry lab to prepare and measure radiocarbon samples. Thank you to Chanda Bertrand at the University of California Irvine radiocarbon prep lab, for all your help in converting very tiny pieces of charcoal to carbon dioxide to filamentous graphite for measurement. Thank you to Dr. Emily Elliot for use of your spectrophotometer to measure sedimentary biogenic silica, which proved to be crucial for unravelling the paleoenvironmental history of Alaska. Thank you to Dr. Nathan Stansell, for your help with field work at Burial Lake, processing radiocarbon samples, and for always being responsive with an endless stream of proxy questions. Thank you to Dr. Broxton Bird, for analyzing water isotope samples from Alaska and Newfoundland. Thank you to Dr. Tom Edwards for providing precipitation isotope data from the Bay d'Espoir station in Newfoundland. Thank you to Katie Redling for the measurement of carbonate stable isotopes. This research was supported by funding from the National Science Foundation, the Geological Society of America, the University of Pittsburgh Leighton Memorial Scholarship, and the University of Pittsburgh Andrew Mellon Predoctoral Fellowship.

I am very grateful for the support and discussions with my office mates and fellow lab members, in particular a special thank you to Aubrey Hillman and David Pompeani. At many times through this adventure, I felt lost and completely overwhelmed, yet you always made the time to discuss the interpretation of a 'wiggle' or some facet of

paleolimnology. Thank you to Dr. Darren Larsen for the motivation to write a separate Burial Lake paper describing the opal variations and reviews of early drafts of my dissertation chapters. I would also like to thank my other friends and colleagues in the Department of Geology and Planetary Science, past and present, including Chris Purcell, Alan Mur, Kaitlin Clarke, and Molly O'Beirne. You have all made my time in Pittsburgh a great pleasure. Thank you to the army of undergraduate lab assistants who assisted in preparing sediment samples for geochemical analysis, especially Rob McDermott, Adam Ofstun, and Justin Coughlin.

I would also like to thank the College of Arts and Sciences Machine Shop, which provided invaluable support for my research. To Tom Gasmire, thank you for your willingness to create and fabricate coring equipment with nothing less than a poor sketch and a few crude ideas about raw materials. To Jeff Sicher, thank you for all the help keeping our vacuum pumps running and for your assistance in building a frame for our glass vacuum line. To Shawn Artman and Josh Byler, thank you for your assistance with all the projects over the years in machining and drafting. You all made it possible to collect sediment cores from lakes with a range of water depths from a variety of coring frames.

Finally, I want to thank my family for their continuous love and support. Thank you to my parents, Dewaine and Theresa, for instilling in me their work ethic. Thank you to my brother David, for his friendship and encouragement. Most importantly, thank you to my best friend and wife Crissy for your unending support, encouragement, and love. And to my little girl, Evelyn Fjord who is 1 year and 2 months old as I write this, for providing me a greater perspective and for reprioritizing my life. And to Olivia Grace, it

was the greatest pleasure to have met you - you forever changed my life. This dissertation is dedicated in your memory.

1.0 INTRODUCTION

Global temperatures have risen by 0.6° C over the last century (IPCC, 2007) and Arctic temperatures have increased by double that over the last several decades (ACIA, 2005). Physical observations and climate model simulations demonstrate that higher temperatures are directly related to rising greenhouse gas (CO_2 and methane) concentrations primarily from fossil fuel combustion and global deforestation. Arctic and sub-arctic regions are particularly sensitive to climatic change primarily through positive feedbacks linked with cryospheric processes (snow and ice losses or gains) and associated changes in surface albedo (ACIA, 2005). Arctic warming and associated consequences further exert a significant influence on global climate via positive feedbacks that include: (1) increased absorbance of solar energy through melting of sea ice and snow, (2) rising sea levels and alterations in ocean circulation through melting ice sheets, and (3) enhanced greenhouse gas emissions from the breakdown of permafrost (ACIA, 2005). Accelerated warming in the Arctic has resulted in adverse impacts to the hydrologic cycle, with increasing evaporation since the late 20th century and permafrost degradation resulting in a reduction in lake surface areas and the drying out and disappearance of thaw lakes in Alaska (Jepsen et al., 2013). Alarmingly, average annual temperatures in the Arctic are projected to increase from 3° to 5° C by 2100 (IPCC, 2007), with winter temperatures projected to rise even more (4° to 7° C).

In light of the these changes and the importance of high-latitude regions to global climate change, long term records of natural climate variability are essential to give context to potential future climatic scenarios and to put them into perspective.

Lakes and their sediments provide an excellent means to reconstruct long-term terrestrial climatic and paleoenvironmental change because lakes are ubiquitous features across Arctic and subarctic regions. Lakes integrate changes in the surrounding watershed and atmosphere (Carpenter et al., 2007), and further respond rapidly and are sensitive to climatic change (Adrian et al., 2009). In addition, lake sediments can provide continuous archives, are easily constrained with radiometric dating techniques, and can be analyzed for multiple indicators or proxies of environmental change. This dissertation utilizes the sedimentary record from small lakes in Alaska and Newfoundland, combined with detailed analyses of core sedimentology and geochemical proxy analysis, to investigate the timing, magnitude, and underlying causes of natural climate variability spanning the late-Quaternary period.

1.1 OBJECTIVE

The main objective of my dissertation is to produce continuous, well-dated lake records of paleoenvironmental change using sedimentology and multiple geochemical proxies at high temporal resolution (decadal to centennial scale) from 1) Arctic and subarctic Alaska spanning the Last Glacial Maximum through to the present and from 2) subarctic Newfoundland, Canada since deglaciation in the Holocene. The Alaskan research seeks to reconstruct hydroclimate variability, aquatic and terrestrial

productivity, and paleoenvironmental changes within the study lakes and surrounding watersheds. The Newfoundland research seeks to investigate changes in hydroclimate and the isotopic composition of paleo-precipitation since regional deglaciation over the Holocene. The motivation for these studies relates to the general lack of well-dated, high-resolution, and quantitative paleo records from these regions. The subsequent sections in this dissertation are organized by the corresponding lake sites from Alaska and Newfoundland, with a brief overview of the late-Quaternary climatic history for each region and a short literature review showing important data gaps.

1.2 ALASKA

Paleoclimate variability during the Late-Quaternary was influenced by large changes in Earth's orbital parameters and surface boundary conditions. Specifically, Bartlein et al. (1991) indicate that Late-Quaternary paleoclimate variations in Alaska were controlled by (1) the size of the Laurentide Ice Sheet and the associated influences on atmospheric circulation and temperature, (2) insolation and its associated influences on temperature and seasonality, (3) temperature variability associated with atmospheric [CO_2], and (4) additional feedbacks associated with cryospheric conditions (sea ice and snow cover) and sea surface temperatures. The gradual and substantial changes in incoming solar radiation (insolation) are attributed to the combined effects of eccentricity, obliquity, and axial precession (Berger and Loutre, 1991). Specifically, the large changes in high-latitude, northern hemisphere (65° N) summer insolation directly control the size of northern hemisphere ice sheets through control of ice ablation during

warm summers (Hays et al., 1976). The global buildup of continental ice sheets and extensive alpine glaciers during the Last Glacial Maximum (LGM; 19,000 – 26,500 cal yr BP) (Clark et al., 2009) resulted in eustatic sea level lowering (-120 m compared to modern) and exposure of the shallow Bering and Chukchi continental shelves (Hopkins, 1982). The formation of the Bering Land Bridge enhanced the continentality of interior and lowland regions of Alaska by increasing the transport distance from marine moisture sources in the North Pacific Ocean. As a consequence, interior and lowland regions of Alaska remained ice-free during the LGM with glaciers restricted to high-elevation mountainous areas (Coulter et al., 1965; Kaufman et al., 2011).

The broad unglaciated lowland regions in Alaska, collectively known as Eastern Beringia, contains numerous lakes and therefore represent one of the few regions in the Arctic where continuous geologic archives dating back to the LGM may be found. To date, however, only a handful of lacustrine records from western Alaska that continuously cover the transition into the LGM through to the present have been reported (Ager, 2003; Kaufman et al., 2003). In contrast, the vast majority of small, shallow (< 15 m deep) lakes in the interior of Alaska were dry prior to 15,000 cal yr (Abbott et al., 2000) and indicate substantial aridity during the LGM. Collectively, these lake records provide important archives to reconstruct glacial age environments and the transition from glacial to interglacial conditions. However, the use of bulk sediment radiocarbon dating and questionable chronological control, comparatively low-resolution (multi-century to millennial scale) proxy sampling, historical emphasis on pollen analysis to reconstruct vegetation, and general lack of detailed sedimentological analysis to

verify continuous deposition of sediment (eg. lack of unconformities) limits these paleoenvironmental interpretations.

Numerous questions regarding the late Pleistocene paleoenvironmental history of Alaska remain unanswered. For example, at what time and how did lake levels and environmental conditions respond to the gradual changes in insolation forcing and eustatic sea level lowering during the LGM onset and subsequent sea level rise during the Lateglacial transition? Although evidence for millennial scale climate variability has been reported over the Holocene in Alaska (Hu et al., 2003), to date no evidence has been found of the rapid glacial age Dansgaard-Oeschger cycles found in Greenland ice cores (Dansgaard et al., 1993). Were lacustrine sedimentation rates to slow to resolve these abrupt climate change events or alternatively has low-resolution sampling of proxies resulted in aliasing of paleoclimate records and hindered their discovery? And lastly, several recently published marine sediment records from the North Pacific Ocean (Davies et al., 2011) and Bering, Chukchi, and Beaufort seas (Caissie et al., 2010; Darby et al., 2012; Katsuki et al., 2009; Max et al., 2012) permit critical analysis of land-ocean feedbacks and interactions. Were dramatic changes in arctic sea ice extent and sea surface temperature synchronous with changes in terrestrial climate variability? To investigate these specific questions and to refine our understanding of the timing and magnitude of paleoenvironmental conditions preceding and during the LGM and subsequently during the late-glacial transition and Holocene, this dissertation uses sediment core analysis from Harding Lake in the interior of Alaska and Burial Lake in northwest Alaska.

1.3 NEWFOUNDLAND

The island of Newfoundland in eastern Canada was completely covered by the Laurentide Ice Sheet during the LGM (Dyke and Prest, 1987). The Newfoundland ice cap retreated to the interior of the island by 12,000 ^{14}C yr BP (~14,000 cal yr) and resulted in topographic control of residual ice, with melting of the last remnants by 10,000 ^{14}C yr BP (~11,500 cal yr) (Shaw et al., 2006). After deglaciation, the early Holocene climate of Newfoundland and eastern Canada was largely influenced by the residual Laurentide Ice Sheet, which cooled the adjacent region through its impact on surface energy balance and ocean circulation (Kaufman et al., 2004). In addition, paleoclimate variability since deglaciation was influenced by the monotonic decline in summer insolation since peak early Holocene values (Laskar et al., 2004) and abrupt climate events attributed to glacial lake outburst floods and corresponding changes in North Atlantic Ocean overturning circulation (Alley et al., 1997; Yu et al., 2010).

Lakes that precipitate carbonate minerals within their water column provide an important archive to quantitatively investigate hydroclimate variability. Specifically, the oxygen isotope composition of authigenic carbonate minerals ($\delta^{18}O_{cal}$) that form in small, through flow lakes with short water residence times generally reflects variations in temperature or the isotopic composition of paleo-precipitation (Leng and Marshall, 2004). Terrestrial stable isotope records of paleo-precipitation spanning the Holocene from sub-Arctic eastern Canada are quite rare. For example, Daley et al. (2009) measured the oxygen isotope ($\delta^{18}O$) composition of bog cellulose at Norden's Bog Pond in eastern Newfoundland and interpret their isotope data to represent the isotopic composition of precipitation over the last 8,500 cal yr. However, $\delta^{18}O$ variations on the

order of 6.0 ‰ and stable isotope analysis of bog surface waters that indicate evaporation is a substantial source of water loss during summer months are inconsistent with these interpretations. Additional stable isotope records of precipitation from Newfoundland are therefore necessary to improve our understanding of the spatial and temporal variability in terrestrial hydroclimate over the Holocene and to test specific paleoclimate-related hypothesis. For example, how did the isotopic composition of paleo-precipitation over Newfoundland respond to the abrupt cooling event at 8,200 cal yr (Alley et al., 1997) centered in the North Atlantic region? Given the sensitivity of climate conditions in Newfoundland to North Atlantic ocean-atmospheric conditions (Banfield and Jacobs, 1998; Hurrell, 1995), did the $\delta^{18}O$ of precipitation in Newfoundland vary synchronously with the inferred temperatures from Greenland (Vinther et al., 2009)? Finally, climate model simulations are increasingly using precipitation stable isotope data because water isotopes are useful tracers of the global hydrologic system (LeGrande and Schmidt, 2009). As such, a dense network of paleoclimate observations are necessary to improve the predictive ability of climate models to simulate changes in hydroclimate conditions under future climate scenarios. To investigate these specific questions, this dissertation uses stable isotope analysis of authigenic carbonate minerals from Cheeseman Lake in west-central Newfoundland.

1.4 THESIS FORMAT

This doctoral thesis comprises a collection of five chapters, the first four of which represent individual papers to submit for publication in peer reviewed journals. One

chapter has already been published (chapter 2) and another (chapter 3) is currently in review for publication in a peer-reviewed scientific journal. The final chapter summarizes the major results and conclusions of each chapter.

2.0 A 31,000 YEAR RECORD OF PALEOENVIRONMENTAL AND LAKE-LEVEL CHANGE FROM HARDING LAKE, INTERIOR ALASKA

Physical and geochemical proxy analyses of sediment cores from Harding Lake in central Alaska are used to reconstruct paleoenvironmental change and millennial scale fluctuations in lake level for the last ~ 31,000 years. We analyzed a composite 422 cm core from the lake depocenter (42.1 m water depth) and identified 4 distinct lithologic units based on variability in dry bulk density, organic matter, biogenic silica, carbon to nitrogen (C/N) atomic ratios, organic matter carbon ($\delta^{13}C$) isotopes, pollen, and elemental abundances via scanning X-ray fluorescence, with age control provided by 16 Accelerator Mass Spectrometry radiocarbon dates and ^{210}Pb dating. In addition, we analyzed a transect of cores from 7.1m, 10.75m, 15.91m, and 38.05m water depths to identify lake level fluctuations and to characterize sediment compositional changes as a function of water depth. Organic matter content and magnetic susceptibility values in surface sediments from all transect cores show a strong correlation with water depth. Interpretation of four lithologic units with well-dated contacts produced a record of water-depth variations that is consistent with independent climate records from eastern Beringia. Basal coarse-grained sediments (quartz pebble diamicton) were deposited prior to 30,700 calendar years before present (yr BP), possibly from fluvial reworking or deflation during a period of severe aridity. Unit 1 sediments were deposited between

30,700 and 15,700 cal yr BP and are characterized by a low organic matter content, a high magnetic susceptibility, and low biogenic silica concentrations resulting from very low lake levels, low terrestrial and in-lake productivity and a high flux of clastic sediment. An abrupt increase in organic matter and biogenic silica concentration marks the transition into Unit 2 sediments, which were deposited between 15,700 and 9,400 cal yr BP when lake levels were higher and variable (relative to Unit 1). The transition to full interglacial conditions at 9,400 cal yr BP marks the beginning of Unit 3. Here an abrupt increase in the sedimentation rate, organic matter and biogenic silica concentration occurs (along with a corresponding decrease to low magnetic susceptibility). These high values persist until 8,700 cal yr BP, signifying a rapid rise to higher lake levels (in comparison to Units 1 and 2). Unit 4 sediments were deposited between 8,700 cal yr BP to 2010 AD and generally contain high concentrations of organic matter and biogenic silica with low magnetic susceptibility, suggesting that lake levels were relatively high and stable during the middle to late Holocene.

2.1 INTRODUCTION

The Tanana valley in the interior of Alaska, encompassing the broad unglaciated lowland of eastern Beringia (Péwé, 1975) remained ice-free during the Last Glacial Maximum (LGM; 26,500 to 19,000 years before present [cal yr BP]). Regionally, glaciers were restricted to the Alaska Range to the south and the Yukon-Tanana Uplands to the north (Coulter et al., 1965). Evidence suggests much colder, drier, and windier conditions than at present occurred during the LGM (Hopkins, 1982). However,

these observations from interior Alaska, based on investigation of loess (Muhs et al., 2003), frozen silt and permafrost (Hamilton et al., 1988), lake sediments (Nakao and Ager, 1985), and an alluvial basin (Matthews, 1974) are poorly resolved, discontinuous, and beset by chronological problems. For example, pollen analysis of drilled cores from Harding Lake (analyzed at sub-millennial scale resolution and radiocarbon dated using bulk sediments) reveal an age reversal at the core bottom but suggest lacustrine sediments span the last 26,500 ± 400 ^{14}C years (Nakao and Ager, 1985). Several lake records with basal ages of ~ 15,000 yr BP from this region (Abbott et al., 2000; Ager, 1975, 1983; Bigelow and Edwards, 2001; Carlson and Finney, 2004) indicate substantial climatic change during the late glacial period with increases in temperature and effective moisture (precipitation minus evaporation). Cosmogenic exposure (CE) dating of moraines has yielded several late Pleistocene glacial records indicating the LGM glacial maxima occurred between 16,000 to 17,000 yr BP on the north slope of the Alaska Range (Matmon et al., 2010; Young et al., 2009) and between 21,000 to 23,000 yr BP in the Yukon-Tanana Uplands (Briner et al., 2005). While helpful, these records of moraine stabilization offer only 'snap-shot' views of paleoclimate and are of limited utility in documenting paleoclimatic conditions between dated glacier advances. Given the lack of continuous, well-dated paleoclimate records spanning the LGM in interior Alaska and the need for records against which to compare paleoclimate model simulations (Otto-Bliesner et al., 2006), additional work is necessary to investigate the timing and magnitude of late Quaternary climatic change and the resulting paleoenvironmental effects in central Alaska.

In this study, we present a ~ 31,000 year record of paleoenvironmental change inferred from analyses of overlapping sediment cores from Harding Lake. We analyzed multiple physical and geochemical proxies (including dry bulk density, organic matter, biogenic silica, carbon to nitrogen (C/N) atomic ratios, bulk sediment organic matter carbon isotopes ($\delta^{13}C$), pollen, and elemental abundances via scanning X-ray fluorescence), using Accelerator Mass Spectrometry (AMS) radiocarbon and a surface ^{210}Pb profile to establish age control. The Harding Lake sedimentary record continuously spans the period prior to the LGM through to the present. In addition, we analyzed a depth transect of cores from 7.1 m, 10.75 m, 15.91 m, and 38.05 m water depths to track lake-level fluctuations and to characterize shallow water sediments. We compare the Harding Lake record to other regional glacial and lacustrine records to examine the timing of paleoenvironmental responses to insolation forcing and the climatic effects of the exposure and later submergence of the Bering and Chukchi continental shelves during the late Pleistocene and earliest Holocene.

2.2 STUDY SITE AND REGIONAL SETTING

Harding Lake (64.42° N, 146.85° W; 217 m ASL) is located in the interior of central Alaska in the Tanana valley, approximately 60 km southeast of Fairbanks (Figure 2-1). The maximum and mean water depths are 43 meters and 16 meters, respectively. The lake has a surface area of 9.88 km^2 and a watershed area of roughly 20 km^2 (LaPerriere, 2003). Harding Lake is oligotrophic and usually dimictic, with overturning and mixing occurring in the spring and fall (LaPerriere, 2003). Infrequently

spring overturn events do not occur, leading to meromixis during these years. Water quality data collected in March 2010 from core site D-10 (Figure 2-1) reveal thermal and chemical stratification of the water column (Figure 2-2). Surface lake water had a temperature of 0.5° Celsius, a specific conductivity of 0.102 µS/cm, a pH of 7.13, and dissolved oxygen of 12.95 mg/L. The oxygen ($\delta^{18}O$) and hydrogen (δD) isotopic values of lake water collected in July, 1996 were -12.59 ‰ and -116.91 ‰ (VSMOW), respectively. Water isotope data from several lakes and rivers in the Tanana Valley (Wooller et al., 2012) show that Harding Lake water isotopic values plot along the regional evaporation line, indicating that water loss via evaporation is a considerable flux in the lake hydrologic budget.

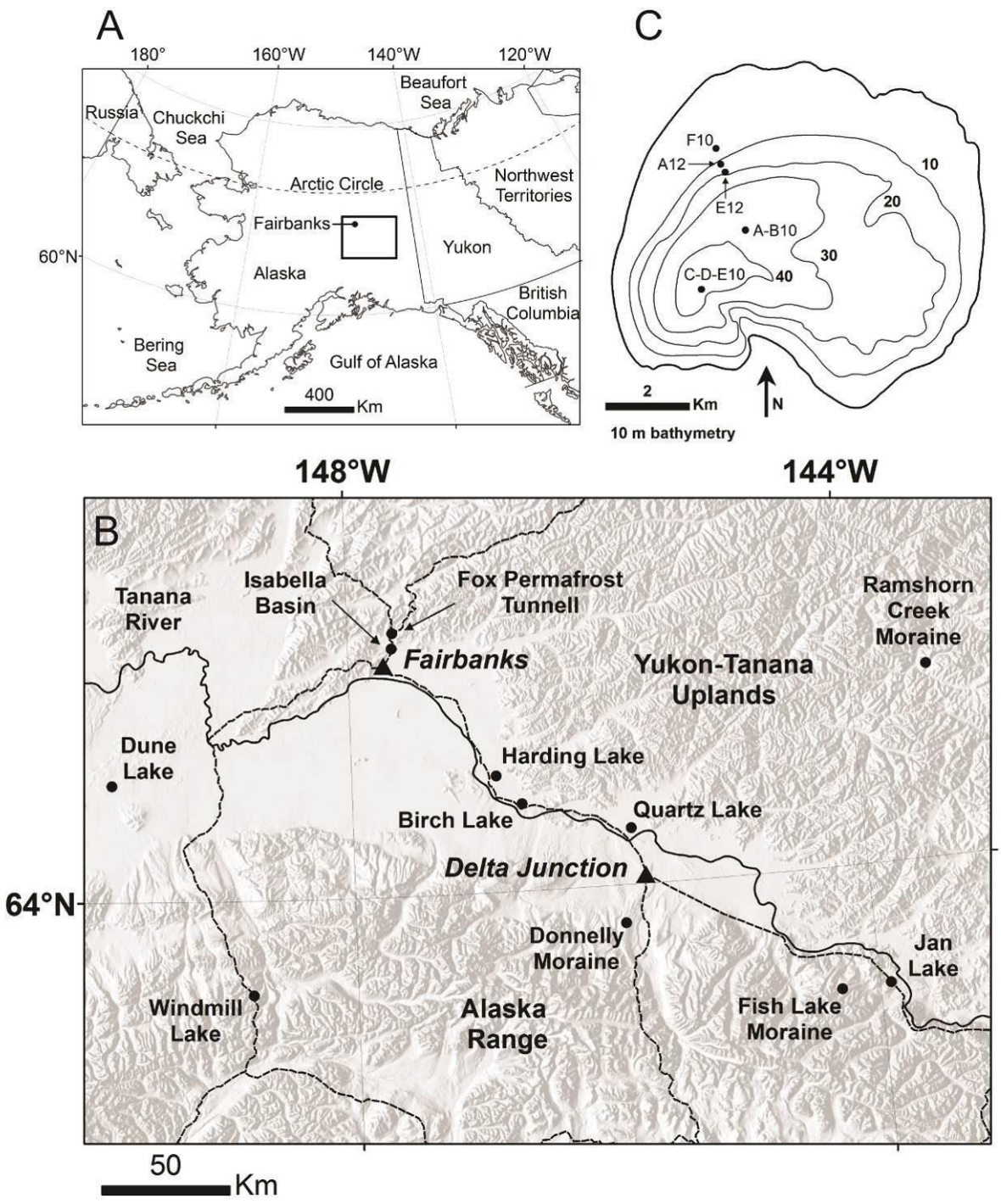

Figure 2-1. A) Location map of Alaska and the surrounding area. B) Shaded relief map of the Harding Lake area with sites mentioned in the text. Dashed lines are major roads and solid lines are major rivers. C) Bathymetric map of Harding Lake showing 10 m depth contours and core sites.

Surface inflow to the lake periodically occurs from the outflow of Little Harding Lake (0.18 km^2 lake surface area, 2.88 km^2 watershed area) to the southwest and a small stream on the northeastern shore. Harding is a topographically closed-basin lake with respect to surface outflow. Lake levels are primarily controlled by variations in the balance between evaporation and precipitation falling directly on the lake surface, because of the small watershed size (relative to the lake surface area) and the lack of a surface outflow. Variability in lake levels have been noted in the recent past; for example, low lake levels in the 1930's and early 1970's were followed by higher lake levels in late 1970's and early 1980's (LaPerriere, 2003). During times of low lake level, the shallow shelf at the northern edge of Harding Lake is exposed. Review of historical aerial photos shows a relatively higher lake level in 1978 and relatively lower lake levels in 1996 and 2003. Quantitative assessments of historical lake level changes are not available; however, frequent exposure and submergence of the shelf along the northern shore suggests fluctuations on the scale of a few meters.

Harding Lake is located at the southern edge of the Yukon-Tanana Uplands Physiographic Province, which is characterized by rounded, gentle relief ridges and broad interfluves (Wahrhaftig, 1965). Tributary streams in the southern portion flow south into the Tanana River, including the Salcha River located north of Harding Lake. Bedrock geology in the watershed consists of medium to high grade pelitic schist (Wilson et al., 1998) with few exposures. The majority of the landscape and low-relief hills to the south and east of Harding Lake are mantled with loess (Blackwell, 1965). Extensive sand dune and loess deposits exist throughout the Tanana River Valley in the Fairbanks area (Péwé, 1975) along with discontinuous permafrost (Jorgenson et al.,

2008). Blackwell (1965) attributed the origin of Harding Lake to aggradation of Tanana River during the Delta Glaciation (penultimate) and damming of a tributary flowing south from the Yukon-Tanana Uplands. The formation of several other lakes abutting the Yukon-Tanana Uplands, including Birch Lake, Quartz Lake, and Chisholm Lake, are hypothesized to result from the same process. Nakao et al. (1981) conducted a gravimetric survey from the surface of Harding and Little Harding Lake and suggested that a fault valley and trough exists underneath the area. They concluded the lake formed as a result of tectonic activity and faulting, and the subsequent damming of a small tributary resulting from aggradation of the Tanana River (Nakao and Ager, 1985).

The regional climate is classified as Interior (Sub-Arctic), with maximum summer temperatures above 30° C and minimum winter temperatures below -40° C (Stafford et al., 2000). Climate data from Fairbanks International Airport (Figure 2-2; 64.818° N, 146.863° W; 135 m ASL; 1948-2010 AD) reveal average winter (January-February-March) and summer (June-July-August) temperatures of -18° C and 15.2° C, respectively. The Interior is bounded by the Brooks Range to the north and Alaska Range to the south, which produce significant orographic barriers to moisture transport leading to annual precipitation values ranging from 200 to 400 mm (Stafford et al., 2000). Numerous studies suggest the location and strength of the Aleutian Low and Siberian/Beaufort High pressure cells have a strong influence on atmospheric circulation and temperature and precipitation patterns in interior Alaska (Cassano et al., 2011; Mock et al., 1998). Specifically, warmer temperatures occur when the Aleutian Low is strong and located over the Aleutian Islands, a scenario that produces a southerly air mass trajectory (Cassano et al., 2011). Colder temperatures result when

low pressure systems are positioned to the southwest of the Aleutian Islands and over the Canadian Archipelago, along with an area of high pressure centered over eastern Siberia (Siberian High). Positive precipitation anomalies (wet conditions) are associated with a weakened Aleutian Low positioned to the west over the Aleutian Islands. In contrast, negative precipitation anomalies (dry conditions) typically occur when the Aleutian Low is in a more easterly position in the Gulf of Alaska, a configuration that produces more southerly winds and less moisture delivery across the Alaska Range into the interior (Streten, 1974). The above synoptic climate controls are more important for winter conditions due to their association with the Aleutian Low pressure system, which is stronger in winter months. In contrast, summer climate is more influenced by mid-tropospheric variations of ridges and troughs (Streten, 1974) that control atmospheric circulation and the resultant trajectory of air masses travelling to the interior. Instrumental weather data from Fairbanks (Figure 2-2) and across interior Alaska indicate the majority of annual precipitation occurs during summer months, with peak values typically occurring in July and August.

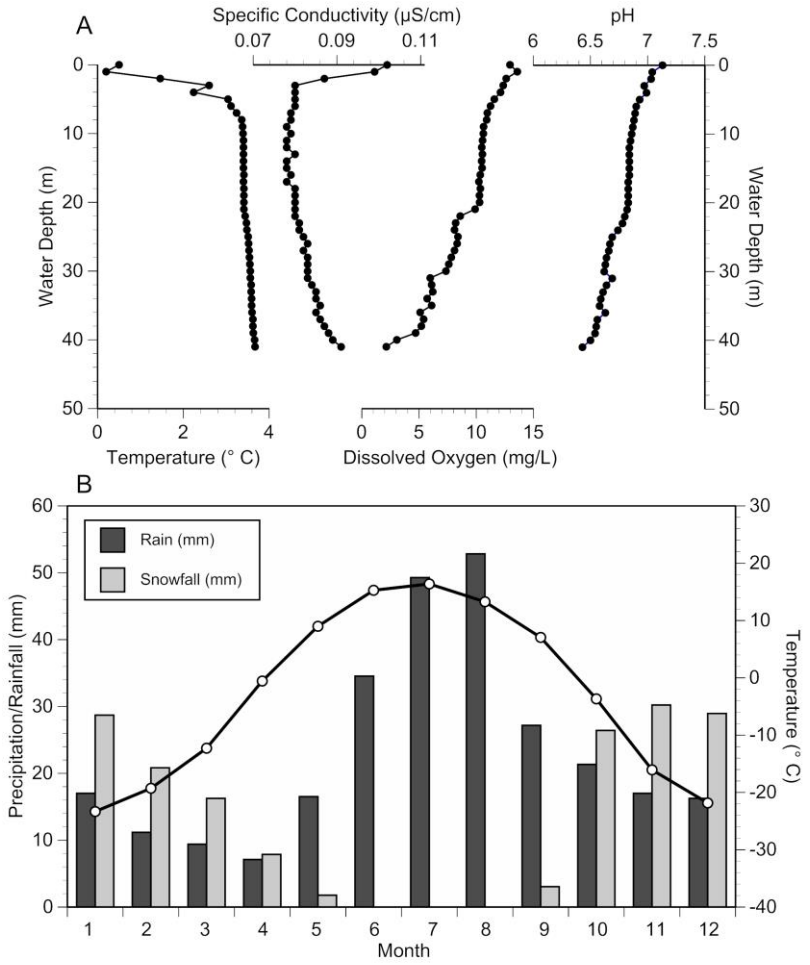

Figure 2-2. Harding Lake water column physical water quality data and Fairbanks International Airport mean annual climate data for the period 1948 to 2010 AD.

2.3 METHODS

2.3.1 Sediment Coring

Sediment cores were collected through the ice from multiple locations on Harding Lake in March, 2010 (Figure 2-1). A surface core (D-10) with intact sediment-water

interface was recovered from 42.1 m water depth using a UWITEC surface corer. Upon recovery, the flocculate upper portion of the sediment was extruded in the field at 0.5 cm intervals to a depth of 34 cm. Multiple overlapping long cores were recovered from core sites A-10 and B-10 in 38.05 m water (64.422° N, 146.854° W) , and C-10, D-10, and E-10 in 42.1 m water (64.419° N, 146.858° W) using a 9 cm diameter UWITEC percussion coring system. Core F-10 (64.425° N, 146.857° W) was recovered from 7.1 m water depth using a square rod Livingston corer. To better characterize shallow and intermediate water depth sediments and to track lake-level fluctuations, two additional cores were recovered from an inflatable raft in July, 2012 (Figure 2-1). Core A-12 (64.425° N, 146.856° W) was recovered from 10.75 m water depth and core E-12 (64.424° N, 146.856° W) from 15.91 m water depth using a square rod Livingston corer. After recovery, all long cores were sealed in plastic, capped, wrapped with duct tape, and transported to the Department of Geology and Planetary Science at the University of Pittsburgh.

2.3.2 Geochronology

The composite core age model was developed from ^{210}Pb dating of surface sediments and AMS radiocarbon analyses of 16 terrestrial macrofossils (Table 2.1). Freeze dried and homogenized aliquots of the top 15 cm of surface core D-10 were analyzed for radioisotope (^{210}Pb, ^{214}Pb, ^{137}Cs and ^{226}Ra) activities by direct gamma counting using a high purity germanium detector (Canberra model BE-3825) with a closed-end coaxial well located in the Department of Geology and Planetary Science at the University of Pittsburgh. Detector efficiency was determined by counting a

Canberra MGS-1 multi-gamma standard for which peak efficiencies have been established using a National Institute of Standards traceable standard. Excess ^{210}Pb activities were calculated by subtracting the background ^{214}Pb activity, sourced from in-situ decay of ^{226}Ra within the sediment matrix, from the ^{210}Pb activity sourced from direct atmospheric deposition. Sediment ages were calculated using the Constant Rate of Supply (CRS) method, which accounts for variability in both the sedimentation rate and dry bulk density, according to the methodology of Binford (1990). Bulk sediment samples were disaggregated and wet-sieved to separate terrestrial macrofossils for AMS radiocarbon measurement. Organic samples were pre-treated using standard acid-base-acid wash techniques (Abbott and Stafford, 1996) and were combusted, graphitized, and measured at the W.M. Keck Carbon Cycle AMS Laboratory, University of California, Irvine. Radiocarbon ages were calibrated to calendar years BP (cal yr BP; 1950 AD) using CALIB 6.0 and the INTCAL09 calibration curve (Reimer et al., 2009). Radiocarbon samples from charcoal, wood, plant material, and seeds (Table 2.1) were analyzed from the composite core. An age-depth model was created using point to point, linear interpolation with the classical age modeling (CLAM) code v2.1 for the statistical software R (Blaauw, 2010). In addition, one radiocarbon sample from core A-12 and three samples from core E-12 (Table 2.1) were analyzed to constrain the timing of sediment deposition and subsequent lake-level fluctuations at each core site.

Table 2.1. Harding Lake AMS radiocarbon dates with calibrated 2s error ranges. Samples highlighted with an asterisk are rejected from the age model.

Sample ID (UCIAMS #)	Core-Drive	Total Depth (cm)	Material	Raw Age (^{14}C yr BP)	Error (yr)	Calib Age (2σ) (yr BP)
Core C-10/E-10 Composite						
89203	C10-D1	22.5	Charcoal	380	30	319-505
109356	C10-D1	36.5	Charcoal	1,245	25	1,082-1,267
89204	C10-D1	46.5	Wood	1,570	40	1,375-1,541
89205	C10-D1	65.0	Seeds	2,700	15	2,761-2,844
89206	C10-D1	101.0	Wood	4,160	45	4,538-4,834
89207	C10-D1	165.0	Charcoal	6,960	70	7,673-7,935
89208	C10-D2	195.5	Charcoal	8,000	100	8,585-9,134
89209	C10-D2	200.5	Charcoal	8,130	60	8,795-9,285
89210	E10-D2	277.5	Charcoal	8,450	80	9,272-9,550
89211	E10-D2	281.0	Charcoal	8,820	160	9,537-10,233
109357	E10-D2	302.5	Charcoal	10,310	160	11,407-12,577
109358	E10-D2	320.5	Plant material	10,690	190	12,059-13,068
* 109359	E10-D2	351.5	Seeds	8,770	370	8,787-11,065
89212	E10-D2	362.5	Wood	13,560	100	16,359-16,967
* 109360	E10-D2	383.5	Plant material	10,740	310	11,643-13,285
89213	E10-D2	412.5	Charcoal	25,900	320	29,848-31,193
Core A-12						
131490	A12-D1	73.5	Seed	12,670	380	13,854-16,526
Core E-12						
131489	E12-D1	93.5	Wood	8,650	100	9,468-10,119
131489	E12-D2	118.5	Wood	11,820	300	13,093-14,841
116879	E12-D2	120.5	Wood	12,175	35	13,872-14,174

2.3.3 Lithostratigraphy

Sediment cores were split, described, and photographed at the Department of Geology and Planetary Science at the University of Pittsburgh. Notable sedimentary structures, grain-size, and Munsell color were characterized for each core. A composite depth scale of 422 cm was created with surface core D-10, and long cores C-10 Drive

1, D-10 Drive 1, C-10 Drive 2, and E-10 Drive 2 based on anomaly matching proxy data (Figure 2-3) and visible stratigraphic markers. Thirty, 1 cm samples (spanning the entirety of the composite record) were analyzed via smear-slide mineralogy and described according to the lacustrine sediment classification scheme of Schnurrenberger et al. (2003). Dry bulk density and weight percent organic matter values were measured on all cores at continuous 1 cm intervals via loss-on-ignition (LOI) at 550° C for 4 hours (Heiri et al., 2001). Magnetic susceptibility was measured on all split cores at 2 mm intervals using a Bartington MS2 Magnetic Susceptibility Meter.

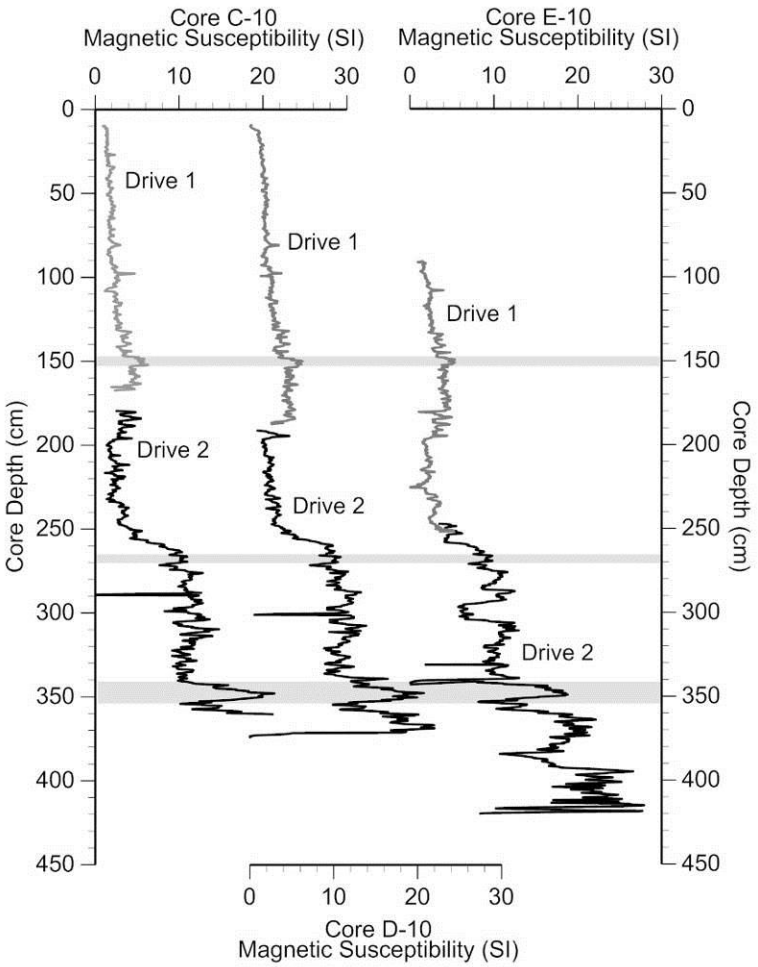

Figure 2-3. Magnetic susceptibility for Harding Lake cores C-10, D-10, and E-10 showing the anomaly match used to construct the 422 cm composite depth scale.

Weight percent Biogenic Silica (BSi) was measured at 2 cm intervals on 209 samples (including 20 replicates) from the composite core using a wet-chemistry, alkaline extraction adapted from Mortlock and Froelich (1989). Prior to analysis wet samples were freeze-dried, homogenized to a fine powder, and treated with 30% H_2O_2 and 1M HCl to remove organic matter and carbonate minerals, respectively. BSi was extracted with a 10% Na_2CO_3 solution and determined by molybdate blue spectrophotometry at 812 nm (Mortlock and Froelich, 1989) using a Thermo Scientific Evolution 60s UV-Visible Spectrophotometer. Replicate measurements of internal

sediment standards from Laguna de Los Anteojos (Stansell et al., 2010) run during sample analysis produced an average error of 3.1 %.

Carbon to nitrogen mass ratios (C/N) and bulk sediment organic matter stable isotopes of carbon ($\delta^{13}C$) were measured at 1 cm intervals from 0-25 cm and at 2 cm intervals over the remainder of the composite core at the Stable Isotope Laboratory at Idaho State University. Total organic carbon (TOC), total nitrogen (TN), and organic matter $\delta^{13}C$ measurements were obtained using an Elemental Combustion System 4010 interfaced to a Delta V Advantage mass spectrometer through the ConFlo IV system. Samples were treated with 1M HCl to remove carbonate minerals and subsequently freeze-dried and homogenized prior to analysis. The mass ratio of TOC to TN (C/N) was calculated to assess organic matter sources. Values of $\delta^{13}C$ are reported as ‰ values relative to the VPDB scale. Replicate measurements of internal standards yielded coefficients of variation of 1.4 % and 1.5 % for total organic carbon and total nitrogen, and precision better than 0.15 ‰ for the stable isotope measurements.

Bulk sediment geochemistry was measured continuously at 1 cm intervals with 60 second count times on the split composite cores using the ITRAX X-ray fluorescence (XRF) core scanner at the Large Lakes Observatory, University of Minnesota Duluth. The D-10 D1 core was not scanned because an earlier composite depth scale based on field measurements did not include this drive. As a result, an 11 cm gap in XRF data exists in the composite depth scale (168 – 179 cm) where core D-10 D1 spans the overlap between core C-10 D1 and C-10 D2. The ITRAX XRF provides a non-destructive, high resolution and semi-quantitative record of elemental abundances

(Croudace et al., 2006). Values are reported as counts per second. We focus our paleoenvironmental interpretation on titanium concentrations, which are typically used as proxy for detrital clastic flux (Balascio and Bradley, 2012).

Pollen analysis was carried out at approximately 20 cm intervals through the upper 350 cm and approximately 10 cm intervals through the basal 80 cm of the composite core. We used conventional methodologies for preparation, identification, and counting (Faegri et al., 1989), plus heavy-liquid separation (sodium polytungstate) (Elias et al., 1999) and extra sieving for silt- and sand-rich samples. The pollen sum was typically ≥300 terrestrial pollen grains, excluding spores and aquatic taxa, but lower in the inorganic basal 80 cm. Pollen reference material held at the University Southampton was consulted when necessary. The pollen diagram was plotted using TILIA software (Grimm, 1990).

2.4 RESULTS AND INTERPRETATIONS

2.4.1 Sediment Core Geochronology

The composite core sedimentology and depth to age model, based on 16 AMS radiocarbon dates and the ^{210}Pb profile (as well as linear sedimentation rates (cm/yr)) are presented in Figure 2-4. Two samples (UCIAMS # 109359 and # 109360) produced stratigraphic age reversals and were excluded prior to generating the age model. The first sample (UCIAMS # 109359, at 351.5 cm) was a seed that yielded an extremely small carbon yield (10 µg) and very large analytical uncertainty (Table 2.1). The second

sample (UCIAMS # 109360, at 383.5 cm) was plant material that also yielded a small carbon yield (17 µg) and large analytical uncertainty (Table 2.1). Inclusion of either of these dates would necessitate rejecting other radiocarbon measurements from much larger samples with smaller analytical uncertainty. The exact cause of these age discrepancies is unknown, however we hypothesize the very small Carbon yields, which are near the threshold limit for AMS radiocarbon analysis at UCI KCCAMS, are the most likely source of error. For example, the influence of modern carbon contamination through sample processing (e.g. pretreatment, combustion, and graphitization) increases with decreasing sample size for radiocarbon analysis (Santos et al., 2010). In an investigation of the effects of sample mass on radiocarbon dates from Arctic lake sediments, Oswald et al. (2005) found that ages for samples of > 50 µg carbon from the same macrofossil produced statistically indistinguishable ages. However, ages for samples of < 50 µg carbon were substantially younger and had greater uncertainty, which they attributed to the combined effects of incomplete graphitization and a larger influence from background contamination. As a result, we consider the reported ages of the samples at 351.5 cm and 383.5 cm (UCIAMS # 109359 and # 109360) to be too young given more robust, adjacent dates and therefore reject both from the age model.

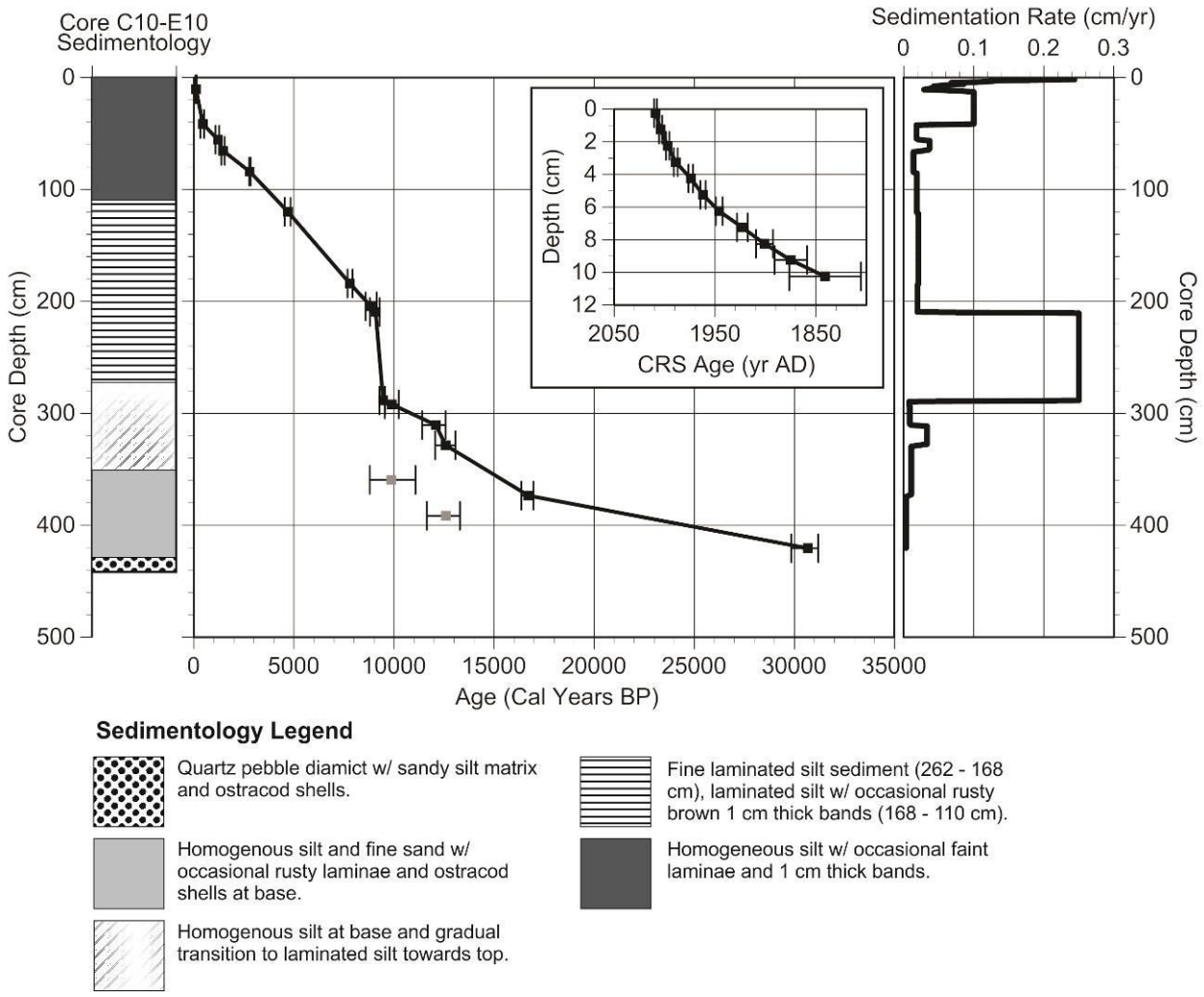

Figure 2-4. Harding Lake composite core sedimentology, age model, and linear sedimentation rates. Gray squares indicate dates that were rejected from the age model.

Sedimentation rates, calculated as sediment accumulation per unit time (cm/year), reveal considerable temporal variability in sediment deposition (Figure 2-4). Sedimentation rates were extremely low (0.004 cm/yr) from 30,700 to 16,800 cal yr BP, assuming the reliability of our basal AMS radiocarbon age on charcoal (UCIAMS # 89213). However, our proxy data from Unit 1 sediments (see discussion) suggest the possibility that old organic material was reworked into presumably younger sediments, and thus age constraints and calculated sedimentation rates prior to 16,800 cal yr BP

may be erroneous. Subsequently, sedimentation rates increased to 0.010 cm/yr from 16,800 yr BP to 12,700 cal yr BP. At 12,700 yr BP, the sedimentation rate again increased to 0.031 cm/yr until 12,000 cal yr BP. Thereafter (between 12,000 and 9,400 cal yr BP) sedimentation rates were lower, ~ 0.01 cm/yr. At 9,400 cal yr BP, the sedimentation rate greatly increased to 0.225 cm/yr, a rate that was maintained until 9,100 cal yr BP. During this interval sediment accumulated more rapidly at Harding Lake than any other time during the late Quaternary (see results and discussion for Lithologic Unit 3). Subsequently, sedimentation rates were lower from 9,100 to 109 cal yr BP, with values between ~ 0.015 to ~ 0.040 cm/yr. Sedimentation rates for the upper 10 cm were calculated from ^{210}Pb ages and increase from 0.03 cm/yr to 0.2 cm/yr from 109 to -60 cal yr BP (2010 AD), respectively.

2.4.2 Composite Core Lithologic Units

Paleoenvironmental interpretation of the Harding Lake record is based on lithologic units defined using the sediment physical and geochemical data. We identified 4 lithologic units based primarily on variations in organic matter (wt %), biogenic silica (wt %), and magnetic susceptibility (Table 2.2; Figure 2-5; Figure 2-6) as well as 4 pollen zones (Table 2.3; Figure 2-7). The lithologic unit boundaries do not correspond to the changes in sedimentation rate (Figure 2-4); however, this is not expected given these calculations are based on a linear interpolation between the radiocarbon and ^{210}Pb ages. In addition, the lithologic and pollen boundaries are broadly similar, but do not correspond exactly.

Table 2.2. Harding Lake lithologic units.

Lithologic unit	Core Depth (cm)	Age Range (cal yr BP)
4	193-0	8,700-2010 AD
3	262-193	9,400-8,700
2	352-262	15,700-9,400
1	422-352	30,700-15,700

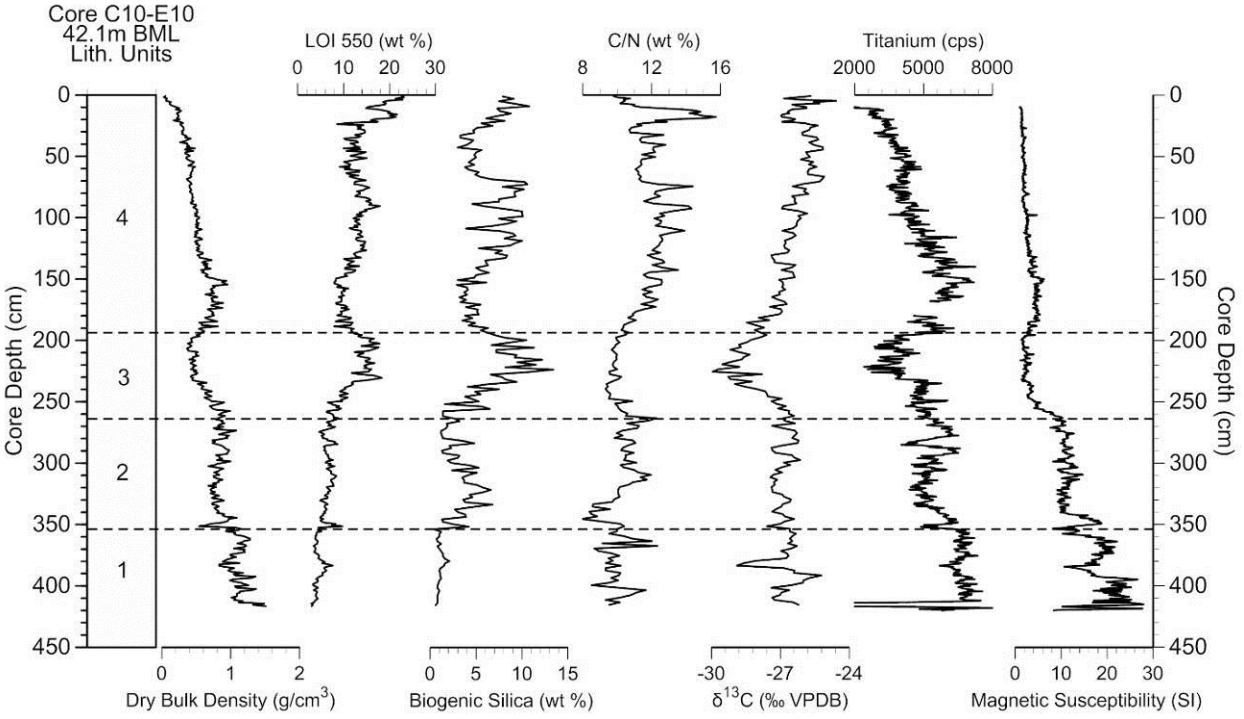

Figure 2-5. Harding Lake composite core proxy data plotted against core depth (cm).

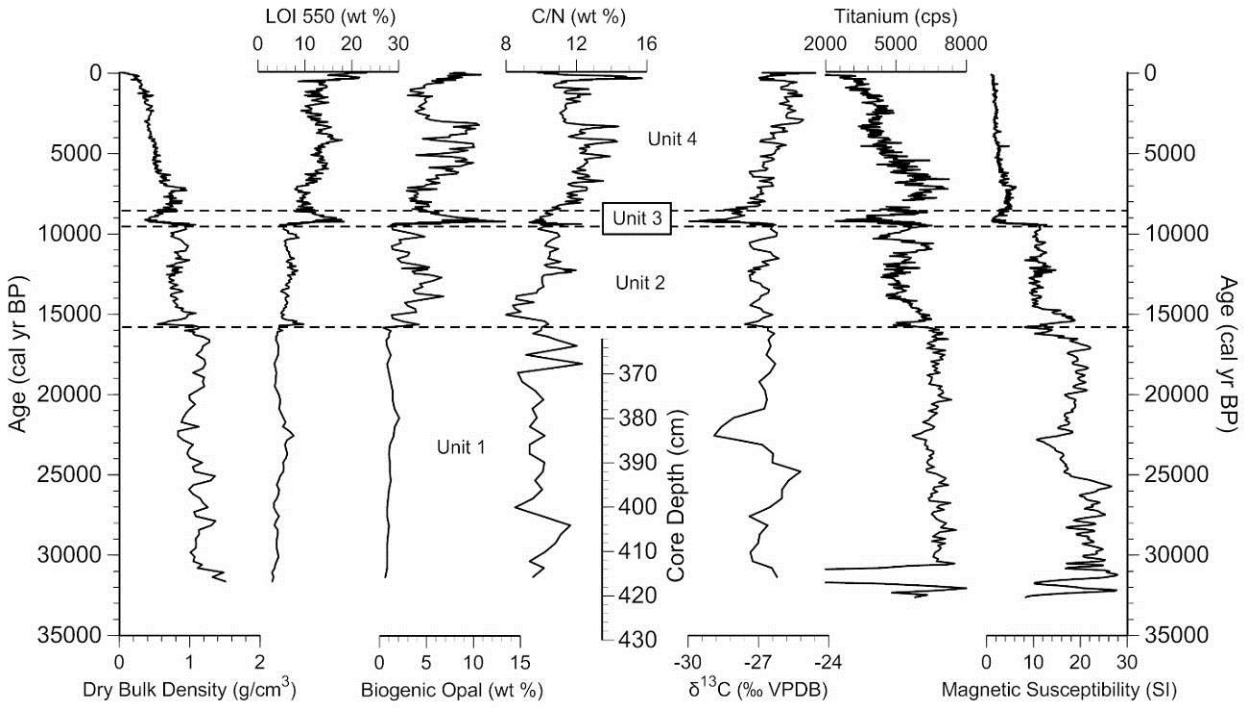

Figure 2-6. Harding Lake composite core proxy data plotted against age in cal yr BP.

Table 2.3. Harding Lake pollen zones.

Pollen zone	Core Depth (cm)	Age Range (cal yr BP)	Dominant taxa
3	200-0	9,100-present	Betula, Alnus, and Picea
2	341-200	14,600-9,100	Betula
1	422-341	30,700-14,600	Herb

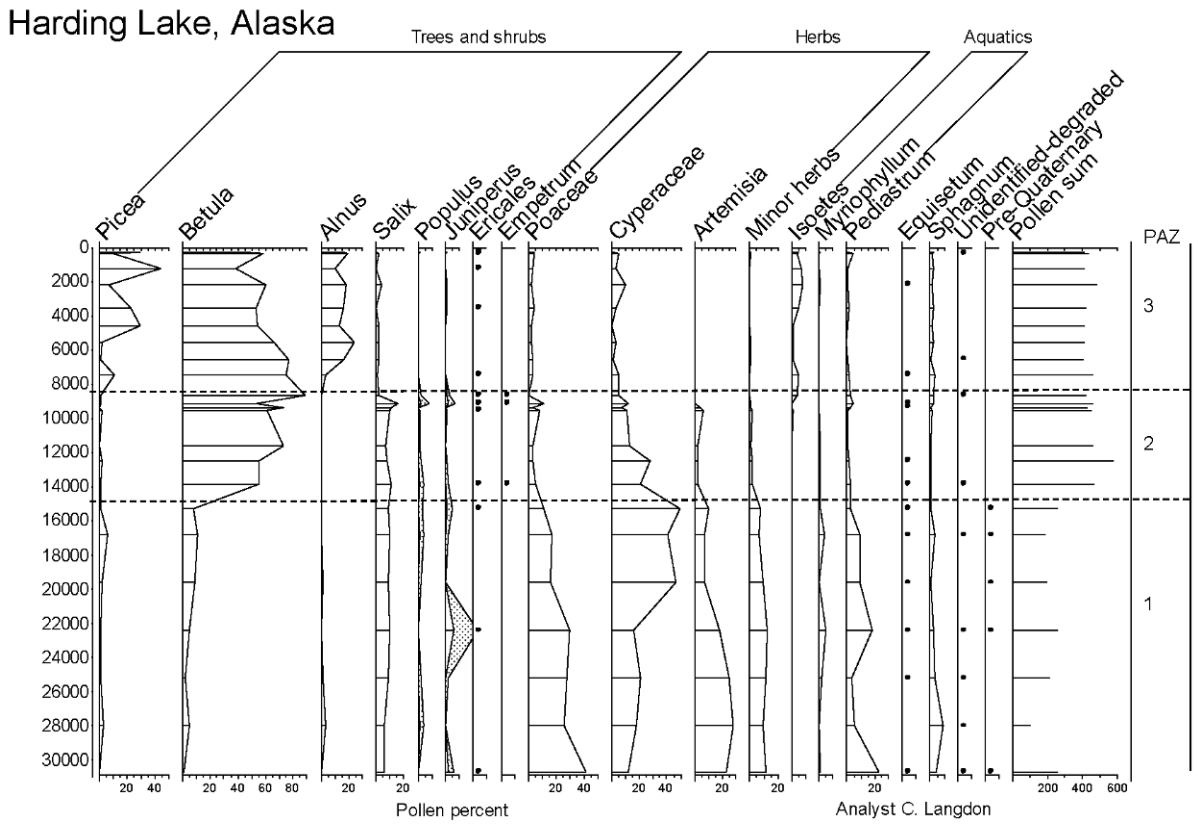

Figure 2-7. Harding Lake percentages of major pollen and spore taxa plotted against age in cal yr BP.

Unit 1 extends from the base of the composite core (422 cm) to 352 cm depth and spans the period 30,700 to 15,700 yr BP. The basal 7 cm (422 to 416 cm) consist of a dusky brown (5YR 2/2), quartz pebble diamicton with abundant ostracod shells and a sandy silt matrix. The upper portion (416 to 352 cm) gradually transitions to pale brown (5YR 5/2) to pale yellowish brown (10YR 6/2), homogenous silt and fine sand with occasional rusty laminae and ostracod shells at the base. Smear-slide analysis of several samples shows very few diatom frustules or sponge spicules and a large proportion of mineral matter. Diatoms in this unit are often fragmented and appear to have been partially dissolved. Unit 1 sediments are characterized by relatively coarse grain size (silt to fine sand), along with high and variable magnetic susceptibility (19 ± 4

SI) and dry bulk density values (1.1 ± 0.1 g/cm^3) (Figure 2-6). Organic matter (4 ± 1 %) and biogenic silica (1 ± 0.3 %) contents are very low while titanium (6300 ± 1300 cps) concentrations are relatively high (Figure 2-6). The organic matter and biogenic silica content in Unit 1 gradually increases and peaks at 383 cm and 380 cm, respectively, and subsequently decreases gradually until the Unit 2 boundary (Figure 2-6). Organic matter $\delta^{13}C$ (-27 ± 0.7 ‰) values are high and exhibit considerable variability. C/N ratios are on average low (10 ± 0.9) during this interval (Figure 2-6). Pollen zone 1 spans the entirety of lithologic Unit 1 and is predominated by herb taxa including *Cyperaceae*, *Poaceae*, and *Artemisia* (Figure 2-7). *Salix* and *Betula* are a minor component of the pollen assemblage. Pre-Quaternary pollen and spores are present in low amounts, indicating possible reworking of older sediments into the lake basin. The aquatic taxa *Myriophyllum* and *Pediastrum* (Figure 2-7) are also consistently present.

Unit 2 extends from 352 cm to 262 cm depth and spans the period 15,700 to 9,400 yr BP. The contact with Unit 1 sediments is gradual, and the lower portion (352 to 272 cm) consists of dusky brown (5YR 2/2) to pale brown (5YR 5/2) silt, homogenous at the base and increasingly laminated towards 261 cm. The upper portion (272 to 262 cm) consists of dark yellowish brown (10YR 4/2), dusky yellowish brown (10YR 2/2), and dusky brown (5YR 2/2) laminated silt. Smear slide analysis shows a higher proportion and increased diversity in diatom frustules and sponge spicules compared to Unit 1. Unit 2 sediments are characterized by decreasing grain size (silt), along with intermediate magnetic susceptibility (10 ± 3 SI) and titanium (5400 ± 500 cps) values compared to Units 1 and 3-4 (Figure 2-6). Dry bulk density (0.9 ± 0.9 g/cm^3) abruptly decreases then increases at the base of Unit 2, and subsequently decreases again up

core (Figure 2-6). Organic matter (7 ± 1 %) values are higher compared to Unit 1 and increase at the base of Unit 2 then rapidly decrease (Figure 2-6). The organic matter content gradually increases up core with minor variability to 12,300 cal yr BP then steadily decreases to 9,400 cal yr BP, with minor variability at the top of Unit 2 (Figure 2-6). Biogenic silica (3 ± 1 %) values are also higher than Unit 1, and gradually increase and peak between 13,900 and 12,700 cal yr BP then gradually decrease to 9,400 cal yr BP, with some variability during this interval (Figure 2-6). Organic matter $\delta^{13}C$ (-27 ± 0.4 ‰) values are similar to Unit 1 and fluctuate substantially. C/N ratios (10 ± 1) initially decline and gradually increase up section through Unit 2 (Figure 2-6). Pollen zone 1 persists until 341 cm (14,600 cal yr BP) (Figure 2-7), and thereafter pollen zone 2 begins and is marked by a fourfold increase in pollen concentration (not shown). It is characterized by the *Betula* rise, a regional feature, and subsequent high *Betula* values (> 50 %). *Salix* is a minor component (< 10 %) of the pollen assemblage during this interval. There is a corresponding decline in herb taxa (Figure 2-7), but *Cyperaceae* values remain moderately high, possibly reflecting local vegetation associated with the lake basin.

Unit 3 extends from 262 cm to 193 cm and spans the period 9,400 to 8,700 yr BP. Sediments consist of dark yellowish brown (10YR 4/2), dusky yellowish brown (10YR 2/2), and dusky brown (5YR 2/2) laminated silt. The contact between Unit 2 sediments is gradational. Smear slide analysis shows the highest proportion and diversity in diatom frustules and sponge spicules for the entire record. Unit 3 sediments are characterized by silty sediments with an abrupt and sustained increased in organic matter (13 ± 3 %) and biogenic silica (7 ± 3 %) concentration, and a corresponding

decrease in dry bulk density (0.6 ± 0.1 g/cm^3) (Figure 2-6). Biogenic silica content peaks and attains the highest value (13 %) for the entire Holocene at 9,200 cal yr BP. In addition, the organic matter content peaks (18 %) at 9,200 cal yr BP (Figure 2-6), reaching a level that matches late Holocene values. Magnetic susceptibility (3 ± 2 SI), titanium (4300 ± 800 cps), and dry bulk density (0.6 ± 0.1 g/cm^3) are much lower in comparison to Units 1 and 2 (Figure 2-6). Organic matter $\delta^{13}C$ (-28 ± 0.2 ‰) values abruptly decrease and are the most negative for the entire record. C/N ratios (10 ± 0.4) are generally low, stable, and comparable to Unit 1 and 2 sediments, although with much less variability (Figure 2-6). We suggest the abrupt and sustained decrease in $\delta^{13}C$ and low C/N values is a result of increased aquatic productivity and loading of dissolved relatively depleted $\delta^{13}C$ carbon to the lake from the watershed. This interval overlaps with the time of highest sedimentation (0.225 cm/yr) throughout the entire record (Figure 2-4) and indicates a major change within the lake and the surrounding landscape. Given that sedimentation rates increase through this interval and titanium values decrease, likely caused by dilution from organic matter, we interpret the increase in organic matter and biogenic silica content as a result of increased in-lake productivity. The main components of the pollen spectra retain the features of pollen zone 2 (Figure 2-7).

Unit 4 extends from 193 cm to the top of the composite core (0 cm) and spans the period 8,700 cal yr BP to 2010 AD. The contact between Unit 3 sediments is gradational. The lower portion (193 to 168 cm) consists of consists of dark yellowish brown (10YR 4/2), dusky yellowish brown (10YR 2/2), and dusky brown (5YR 2/2) laminated silt. The middle portion (168 to 110 cm) consists of dark yellowish brown

(10YR 4/2) laminated silt with occasional dusky brown (5YR 2/2) 1 cm thick bands. The upper portion consists of dark yellowish brown (10YR 4/2) to brownish black (5YR 2/1) homogeneous silt with occasional faint laminae and banding. Smear slide analysis shows a high proportion and diversity in diatom frustules and sponge spicules throughout this interval. Unit 4 sediments are characterized by fine-grained sediments (silt), along with moderately high and variable organic matter (13 ± 3 %) and biogenic silica (6 ± 2 %) concentrations with slightly different trends (Figure 2-6). Biogenic silica gradually increases up section and peaks at values > 10 % between 120 to 70 cm (5,500 and 3,100 cal yr BP) with substantial variability (Figure 2-6). Generally low values of biogenic silica are found between 70 to ~ 26 cm (3,100 to 600 cal yr BP) with a generally rising trend up core to ~ 10 % near the core top (Figure 2-6). In contrast, organic matter steadily increases and peaks at 18 % at a depth of 91 cm (4,100 cal yr BP), exhibiting minimal variability. Above this, organic matter decreases up core with values generally < 15 % until 23 cm (450 cal yr BP) (Figure 2-6). Organic matter values increase to the highest levels of the entire record (23 %) near the core top (over last 450 yr) with substantial variability. Organic matter $\delta^{13}C$ (-26 ± 0.7 ‰) gradually increases up core from -28 ‰ and approach values of -25 ‰ between 70 to ~ 25 cm (3,100 to 600 cal yr BP) and near the core top at 5 cm (Figure 2-6). C/N ratios (12 ± 1) gradually increase up section from the base of Unit 4 to high values (~ 14) with substantial variability (~ 2) from 110 to 74 cm (5,100 to 3,300 cal yr BP) (Figure 2-6). The highest C/N ratios are found near the core top between 19 to 13 cm and peak at values > 15. Magnetic susceptibility (3 ± 1 SI), titanium (4800 ± 1000 cps), and dry bulk density (0.5 ± 0.1 g/cm^3) values steadily increase and peak by 7,100 cal yr BP and gradually

decrease up section to the core top (Figure 2-6). Sedimentation rates (~ 0.015 to ~ 0.04 cm/yr) were generally stable and low throughout Unit 4 until ~ 109 yr BP and thereafter gradually increase towards the core top to 0.2 cm/yr, indicating stability in landscape and climatic conditions. Pollen zone 3 begins about 9,100 cal yr BP (Figure 2-7) and covers the uppermost part of the record. High *Betula* (> 75 %) pollen predominates, and values of *Picea* and *Alnus* increase between 8,600 to 7,500 cal yr BP. *Isoetes* predominates the aquatic taxa and *Myriophyllum* is absent.

2.4.3 Core F-10 Sediments

Core F-10 was recovered in 7.1 m water depth, is 32.5 cm in length, and spans the sediment-water interface (Figure 2-8). The upper 8 cm consist of dark yellowish brown (10YR 4/2) to pale yellowish brown (10YR 6/2) homogenous silt to fine sand. The remainder of the sediment between 8 and 32.5 cm consists of grayish brown (5YR 3/2) homogenous silt to fine sand interrupted by grayish brown sand layers. The medium to coarse grained sand layers are from 13 to 15.5 cm and 20 to 20.5 cm, with erosive contacts and load structures immediately below the sand. Smear slide analysis of select samples shows diatom frustules in the upper portion (0 to 13 cm) while the basal sediments consist entirely of mineral sediment with no diatoms. Dry bulk density (1 ± 0.3 g/cm^3) is generally high throughout and gradually decreases up core. Organic matter (7 ± 3 %) is low at the core bottom and generally increases towards the core top. Magnetic susceptibility (49 ± 82 SI) is very high at the core bottom and gradually decreases towards the top. No terrestrial macrofossils were found for radiocarbon dating of core F-10.

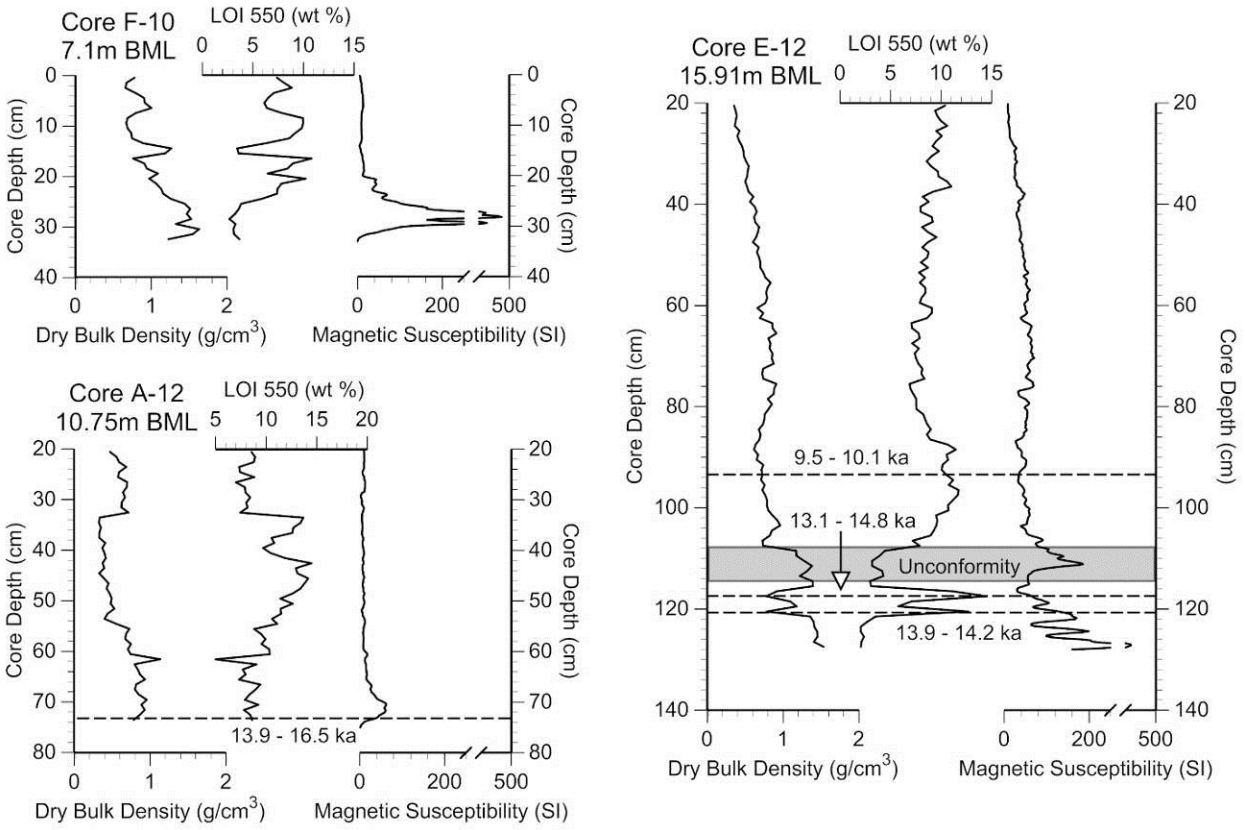

Figure 2-8. Harding Lake cores F-10, A-12, and E-12 proxy data plotted against depth. Dashed lines indicate radiocarbon samples, reported as the calibrated 2s error range in thousands of years (ka) cal before present.

2.4.4 Core A-12 Sediments

Core A-12 was recovered in 10.75 m water depth, is 55 cm in length, and starts 20 cm below the sediment-water interface (Figure 2-8). The upper portion (20 to 74 cm) consists of dark yellowish brown (10YR 4/2) homogeneous to faintly banded silt to find sand and the basal 1 cm (74 to 75 cm) consists of medium sand. Smear slide analysis of select samples shows diatom frustules in the upper portion (20 to 74 cm) of the sediments. Dry bulk density (0.6 ± 0.2 g/cm^3) values gradually decrease up core while

organic matter (10 ± 2 %) values generally increase towards the core top. Magnetic susceptibility (14 ± 13 SI) is very high at the core bottom and gradually decreases towards the top. Radiocarbon analysis of a seed at 73 to 74 cm constrains the onset of lacustrine sedimentation at the core site (11.48 m below modern level; BML) to 15,050 cal yr BP (Table 2.1; 13,910 to 16,520 cal yr BP error range). No other terrestrial macrofossils were found for radiocarbon dating of core A-12.

2.4.5 Core E-12 Sediments

Core E-12 was recovered in 15.91 m water depth, is 108 cm in length, and starts 20 cm below the sediment-water interface (Figure 2-8). The upper portion (20 to 110 cm) consists of moderate yellowish brown (10YR 5/4) to dark yellowish brown (10YR 4/2) homogenous to faintly banded silt. The middle portion (110 to 118 cm) consists of disturbed, moderate yellowish brown (10YR 5/4) to dark yellowish brown (10YR 4/2) silt to fine sand sediment with a clear erosional unconformity. The basal sediments (118 to 128 cm) consist of dark yellowish brown (10YR 4/2) silt and fine to medium sand with organic rich layers from 118 to 123 cm. Smear slide analysis of select samples shows diatom frustules in the upper 90 cm (20 to 110 cm) while the basal sediments largely consist of mineral matter. Dry bulk density (0.8 ± 0.3 g/cm^3) values generally decrease up core, aside from the unconformity interval resulting from erosion and re-working (Figure 2-8). Organic matter (8 ± 2 %) values generally increase and magnetic susceptibility (57 ± 40 SI) values generally decrease towards the core top, again aside from the unconformity interval (Figure 2-8). Radiocarbon analysis was conducted on three samples from core E-12 (Table 2.1). A sample of wood from 120 to 121 cm

constrains the onset of lacustrine sedimentation at the core site (17.11 m BML) to 14,020 cal yr BP (13,870 to 14,170 cal yr BP error range). An additional sample of wood from 118 to 119 cm has a median age of 13,720 yr BP (13,110 to 14,830 yr BP error range) and provides further evidence of the initial major rise in lake level. The median ages of these samples are in stratigraphic order; however the calibrated error ranges overlap. A sample of wood from 93 to 94 cm, located stratigraphically above the erosional unconformity in the E-12 core, constrains the subsequent rise in lake level (16.84 m BML) to before 9,660 yr BP (9,470 to 10,120 cal yr BP error range). No other terrestrial macrofossils were available for radiocarbon dating of core E-12.

2.5 DISCUSSION

The specific climatic controls on lake level at multi-centennial to millennial timescales at Harding Lake are poorly understood, though must be related to changes in regional effective moisture (precipitation minus evaporation). Analysis of sediment proxies from Harding Lake shows variability in organic matter content and magnetic susceptibility are coeval with many regional hydroclimate transitions evidenced from other paleoproxy datasets. Scatterplot analysis of organic matter content and magnetic susceptibility (Figure 2-9) demonstrates clustering of the lithologic units into distinct groups. Unit 1 (30,700 to 15,700 cal yr BP) sediments, characterized by the lowest organic matter content and highest magnetic susceptibility during the entire record, correspond to the interval when most small, shallow lakes in central Alaska were dry (Abbott et al., 2000; Ager, 1983; Bigelow and Edwards, 2001; Carlson and Finney,

2004; Wooller et al., 2012). Unit 2 (15,700 to 9,400 cal yr BP) sediments, characterized by intermediate organic matter content and magnetic susceptibility, parallel the initial formation of lacustrine sediment in many lakes in central Alaska, indicating rising and fluctuating water levels (Abbott et al., 2000). In contrast, Unit 3 to 4 (9,400 cal yr BP to present) sediments, characterized by high organic matter content and low magnetic susceptibility, were deposited during the Holocene when regional lake levels were rising and near overflow levels (Abbott et al., 2000; Ager, 1983; Bigelow and Edwards, 2001; Carlson and Finney, 2004; Finney et al., 2012; Wooller et al., 2012). However, variability in organic matter content and magnetic susceptibility may also in part reflect changes in soil stabilization within Harding Lake's watershed associated with major vegetation shifts. For example, Hu et al. (1993) suggested that shrub tundra conditions between 12,000 – 10,500 ^{14}C yr BP (~13,900 to ~12,500 cal yr BP) at Wien Lake (central Alaska) were accompanied by intensive soil erosion, inferred from high allogenic metal and low sediment organic content. The relatively sparse vegetative cover during this time likely promoted weathering and erosion of bare mineral soils in the surrounding watershed. The subsequent transition to shrub and boreal forest beginning at 10,500 ^{14}C yr BP (~12,500 cal yr BP) was marked by lower allogenic metal and higher sediment organic content, which Hu et al. (1993) attributed to the buildup of humic compounds and stabilization of watershed soils. Additional lake studies from northwestern (Hu et al., 1996) and southwestern (Hu et al., 2001) Alaska revealed similar vegetation-landscape development associated with the tundra to boreal forest transition during the late Pleistocene and early Holocene.

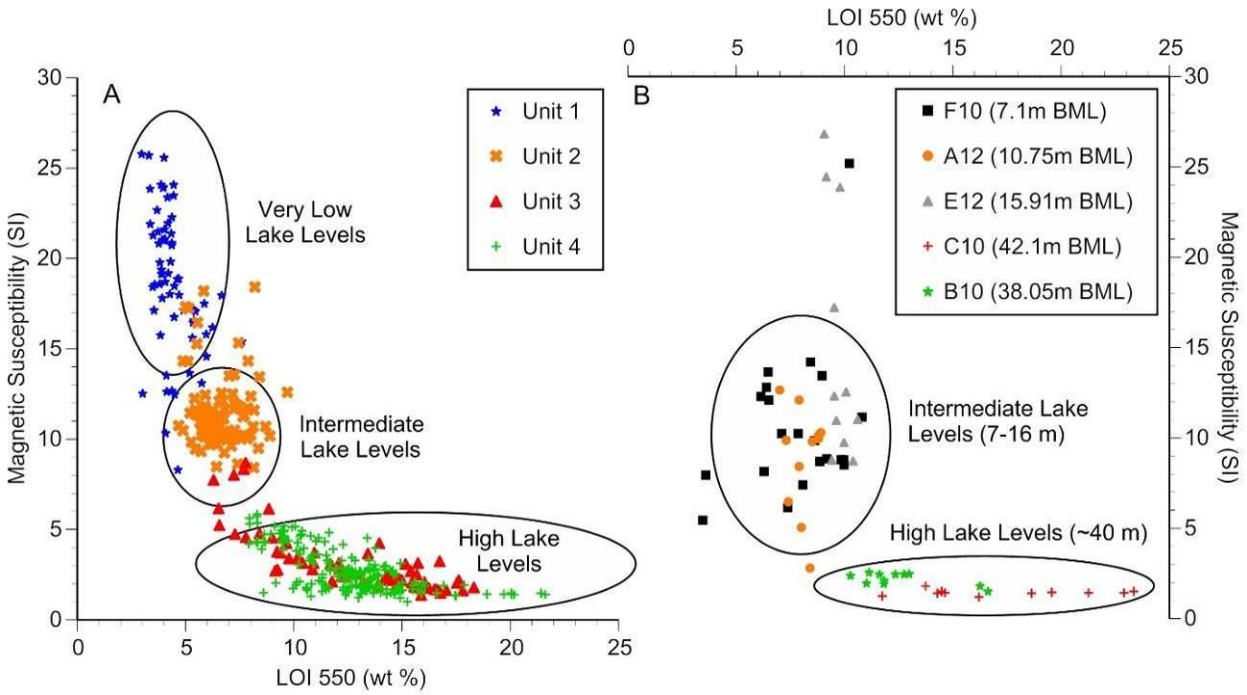

Figure 2-9. Scatterplot of organic matter content versus magnetic susceptibility for A) the Harding Lake composite core plotted by lithologic unit and B) surface sediments from core F-10, A-12, E-12, B-10, and C-10.

Scatterplot analysis of organic matter content and magnetic susceptibility from the upper portion (10 to 20 cm) of cores collected along a depth transect (Figure 2-9) confirms the aforementioned relationship and provides semi-quantitative constraints on lake-levels. For example, core top sediments from deep water cores B-10 and C-10 recovered from 38.05 and 42.1 m BML, and characterized by high organic matter content and low magnetic susceptibility (Figure 2-9), indicate that modern deep water sediments are most similar to middle to late-Holocene sediments from the composite core. In addition, surface sediments from shallow water cores F-10, A-12, and E-12 recovered from 7.1, 10.75, and 15.91 m BML and characterized by intermediate organic matter content and magnetic susceptibility (Figure 2-9), indicate that modern shallow to

intermediate water sediments are most similar to late-glacial sediments. Although a minor component of the down-core variability in organic matter content and magnetic susceptibility may be related to vegetation-landscape development (described above), the substantial variation in sediment properties along a water depth transect in the modern system suggests that vegetation-landscape changes were likely a small influence. We therefore assert that water depth is the dominant control at multi-centennial to millennial timescales on organic matter content and magnetic susceptibility. The lack of fine sediment deposition in water levels shallower than 7 m indicates that wave base erosion occurs to this depth in the modern lake.

Pompeani et al. (2012) used scatterplot analysis for Rantin Lake sediments in the Yukon (Canada) to distinguish deep versus shallow water sediment properties. In addition, Edwards et al. (2000) used a similar model in their investigation of Birch Lake using surface sediments along a water depth transect, where trends in sediment properties (aquatic pollen along with organic matter and magnetic susceptibility) reflected similar lake-level changes as determined from transect based lake-level reconstructions (Abbott et al., 2000). Edwards et al. (2000) also collected surface sediment samples from modern lakes in interior Alaska and used pollen analysis to investigate the relationship between aquatic taxa and water depth. Notably, a higher diversity of aquatic taxa was found at shallower (< 5 m) water depths, with little to no aquatic taxa found at depths > 20 m. Core transect data also demonstrate a substantial lake-level rise and fluctuating water levels occurred during the late-glacial period. The basal radiocarbon age from core A-12 suggests the initial rise in lake level to < 11.5 m BML occurred ~ 13,900 – 16,500 cal yr BP. This sample (UCIAMS # 131490) has large

analytical uncertainty, and the basal radiocarbon ages from core E-12 better constrain the lake level rise (to < 17.1 m BML) at ~ 14,000 cal yr BP. The erosional unconformity in core E-12 above the basal sediments (Figure 2-8) represents a period of non-deposition at this core site or erosion of previously deposited sediments during a time of lower or fluctuating lake levels after ~ 14,000 cal yr BP. The subsequent rise in lake-level to < 16.8 m BML is constrained by the uppermost radiocarbon age of 9,660 cal yr BP from core E-12 in fine-grained lacustrine sediment located above the erosional unconformity. There is no evidence that lake level dropped below the E-12 core site after this time. Accordingly, we combine the organic matter to magnetic susceptibility conceptual model with core-transect data to infer semi-quantitative changes in lake-level at Harding Lake (Figure 2-10) and compare these results with paleoclimate datasets from eastern Beringia. We do not account for the depth of wave base erosion in our lake level curve (Figure 2-10) and therefore our lake level constraints are semi-quantitative. However, we surmise the wave base erosion depth was of a lower magnitude during the period of rapid lake level change (during the late glacial) when the lake surface area was presumably smaller.

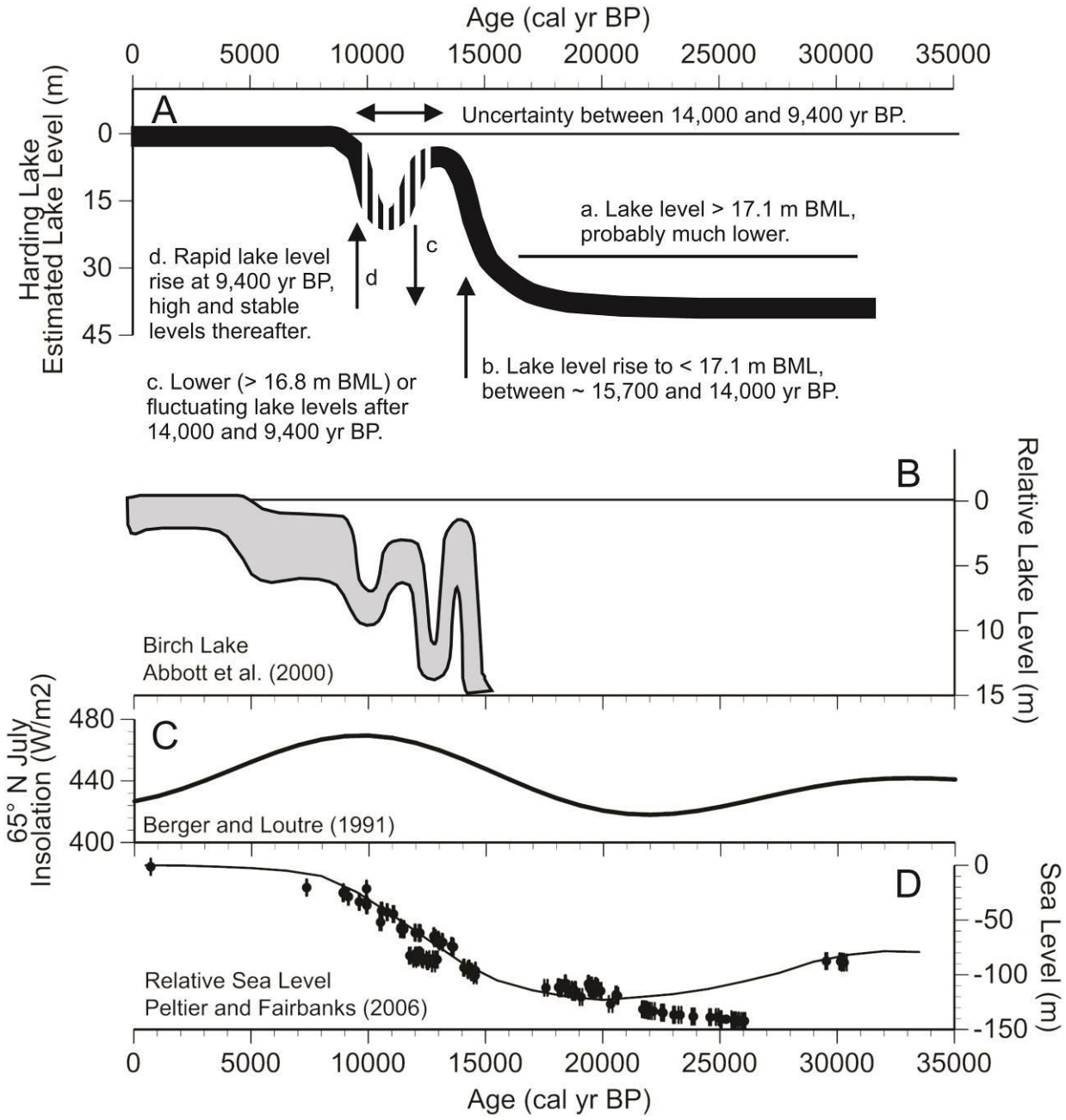

Figure 2-10. A) Harding Lake relative lake-level curve compared with regional climate records including B) a lake-level reconstruction for Birch Lake, Alaska (Abbott et al., 2000), C) July insolation for 65° North (Berger and Loutre, 1991), and D) Relative sea level data (Peltier and Fairbanks, 2006) and the ice-equivalent eustatic sea level history (smooth black line) (Waelbroeck et al., 2002).

2.5.1 Pre-Last Glacial Maximum (> 30,700 cal yr BP)

The presence of coarse sediments (pebble diamicton), low concentrations of organic matter and biogenic silica, and high and variable magnetic susceptibility, titanium, and dry bulk density indicate the basal 7 cm of Unit 1 are the lake bottom substrate (Figure 2-6). The lack of finer grained lacustrine sediments further indicates that prior to 30,700 cal yr BP the lake was either seasonally desiccated or dry for a long period of time, with any previously deposited sediment removed by deflation or fluvial reworking. The occurrence of these coarse sediments is consistent with the conclusions of Blackwell (1965) that Harding Lake was formed by aggradation of Tanana River through deposition of braided stream sediments and subsequent damming of the proto Salcha River draining from the north. Blackwell (1965) suggested the lake basin formed during the Delta Glaciation (penultimate), which has recently been dated by cosmogenic exposure ages to late Marine Isotope Stage (MIS) 4 or early MIS3, approximately 60,000 to 50,000 cal yr BP (Kaufman et al., 2011). If this age assignment is correct, the absence of lacustrine sediments dating to this time indicates generally unstable and variable climatic conditions with significant aridity during MIS3 in central Alaska, which may have caused multiple transgression/regression events that eroded sediment from the basin. Alternatively, previously deposited sediments may have been subsequently removed via fluvial erosion or deflation when lake levels were lower.

The existence of loess deposits stratigraphically above palaeosols dating to 32,000 to 30,000 ^{14}C yr BP (36,500 to 34,700 cal yr BP) at Halfway House, Gold Hill, and Birch Hill near Fairbanks (Muhs et al., 2003) indicates this was a time of extremely

arid and windy conditions. Pollen data from Isabella Basin demonstrate high percentages of Cyperaceae and Artemisia and low percentages of Alnus and Picea after ~ 32,000 ^{14}C yr BP until the Holocene (Matthews, 1974). Matthews (1974) interpreted these data to represent arctic climatic conditions in central Alaska, similar to that of the present day tundra in northern Alaska. Pollen and grain size data are available from a previous investigation of Harding Lake sediments (Nakao and Ager, 1985). While relatively coarse sediments (sand to granule) are recorded prior to 26,500 ± 460 ^{14}C yr BP (31,000 cal yr BP), pollen data are interpreted to show a vegetational mosaic characterized by Picea, Betula, Ericales, Cyperaceae and Sphagnum. Nakao and Ager (1985) suggest these proxies represent middle Wisconsian Interstadial conditions and a cool, wet climate; however, the use of bulk sediment radiocarbon dating, the presence of an age reversal in this interval, and the use of conventional drilling techniques to recover sediments may compromise their interpretation.

2.5.2 The Global Last Glacial Maximum (30,700 to 15,700 cal yr BP)

The portion of Unit 1 stratigraphically above the coarse basal sediment is characterized by decreasing grain size (silt to fine sand) with high and variable dry bulk density and generally constant titanium content (Figure 2-6), and an extremely low sedimentation rate (Figure 2-4), assuming reliability of our basal radiocarbon age on fine (< 250 μm) charcoal. Sediments are homogenous with occasional rusty banding, and there is no evidence of unconformities (eg. mud cracks, erosional surfaces, etc.) that would indicate discontinuous sedimentation. We suggest these sediments were deposited in a nearly perennially frozen, shallow lake with a very short ice free summer

season. Low organic matter and biogenic silica concentration imply that terrestrial vegetation was scarce in the vicinity and that in-lake productivity levels were low, due to cold and potentially turbid waters. High magnetic susceptibility and low organic matter content, combined with the absence of glacial age sediments in cores from shallower water depths, suggest very shallow lake levels (Figure 2-10). The general absence of terrestrial macrofossils in Unit 1 sediments further indicate the surrounding landscape had sparse vegetation. The predominance of herb taxa (*Cyperaceae*, *Poaceae*, and *Artemisia*) during the LGM (Figure 2-7) suggests a tundra environment with cold and dry conditions relative to today. The aquatic taxa *Myriophyllum* and *Pediastrum* (Figure 2-7) are consistently present and together indicate shallow water conditions (Edwards et al., 2000), which is coherent with low organic matter content and high magnetic susceptibility values in Unit 1 and the absence of LGM age sediments in shallow water cores. The high magnetic susceptibility and titanium values resulted from a high concentration of fine-grained clastic-rich sediments, which likely originated from wind-blown loess or intensive erosion of watershed soils. Age control during this interval rests on the basal charcoal sample at 412.5 cm (UCIAMS # 89213) and a linear interpolation to the next age at 362.5 cm. While the analytical uncertainty of the basal sample is generally low considering its age (Table 2.1), the question remains whether the organic material formed and subsequently deposited contemporaneously with the enclosing sediments. We believe the charcoal sample was formed and deposited simultaneously with the surrounding sediments because charcoal is extremely friable and easily disintegrates with minimal physical erosion. Given that Unit 1 sediments above the coarse basal gravel lack any convincing evidence of unconformities

(explained above), we infer these sediments represent temporally continuous sedimentation from ~ 30,700 to 15,700 cal yr BP. Alternatively, it is possible that the basal charcoal material could be reworked from older sediments, and therefore the timing of initiation of lacustrine sedimentation may be younger than its reported radiocarbon age. This scenario is consistent with the presence of only tundra type vegetation in Unit 1 sediments, which typify LGM conditions in interior Alaska, but continuous records dating the onset of tundra vegetation are lacking.

The proxy data from Harding Lake are consistent with evidence from central Alaska showing extremely arid conditions during the LGM. A revised model for loess deposition indicates that loess production and windiness increased during the LGM in central Alaska while accumulation decreased because of a lack of vegetative cover (Muhs et al., 2003). AMS radiocarbon and ^{10}Be dates from loess deposits near Fairbanks (Halfway House, Gold Hill, and Birch Hills) (Muhs et al., 2003) also suggest minimal loess deposition occurred during the global LGM because of the presence of sparse herb-tundra vegetation and minimal ground surface roughness. Nakao and Ager (1985) report the predominance of herb taxa from Harding Lake and suggest that climate was extremely cold and dry between 26,500 ± 460 and 13,690 ± 500 ^{14}C yr BP (31,000 to 16,500 cal yr BP). An unconformity in the sedimentary record from Burial Lake in northwest Alaska indicates a significant drop in lake level and a hiatus in deposition between 34,800 and 23,200 cal yr BP (Abbott et al., 2010). Core transect data from Birch Lake in the Tanana Valley indicate lake levels were 18 m lower prior to 15,000 cal yr BP (Figure 2-10) (Abbott et al., 2000). Evidence from elsewhere in the unglaciated interior of Alaska show that most small lakes were dry prior to the late-

glacial (15,000 cal yr BP) (Abbott et al., 2000; Ager, 1983; Bigelow and Edwards, 2001; Carlson and Finney, 2004; Wooller et al., 2012).

Collectively, these proxy records demonstrate an extremely dry climate in central Alaska during the global LGM that is, in part, attributed to changes in atmospheric circulation and exposure of the Bering Land Bridge. In climate model simulations for the LGM (18,000 cal yr BP), the winter jet-stream is split into a northern and southern component by the high-altitude dome of the Laurentide Ice Sheet (COHMAP, 1988). Simultaneously, an anti-cyclonic circulation ('glacial anti-cyclone') developed at the surface with enhanced easterly winds at the southern margin and southerly winds at the western margin of the ice sheet (Bartlein et al., 1991). The climatic effects of changing circulation were spatially variable and complicated, but likely produced windy and dry conditions downwind of the Laurentide Ice Sheet. Eustatic sea level lowering of -120 m (Figure 2-10) (Peltier and Fairbanks, 2006) resulted in exposure of the Bering and Chukchi continental shelves (Hopkins, 1982), forming the land bridge and increasing the transport distance of moisture from the North Pacific Ocean and Bering Sea to interior Alaska. The substantial increase in distance from oceanic moisture sources caused the climate of interior regions to become even more continental and dry.

Several recently published glacial records using cosmogenic exposure dates from moraines further document climatic conditions during the LGM. Evidence from Ramshorn Creek valley in the Yukon-Tanana Uplands shows the LGM maxima (Salcha moraine) occurred between 23,000 to 21,000 cal yr BP during the northern hemisphere summer insolation minima (Figure 2-10), while a recessional moraine located ~ 3.5 km up-valley (Ramshorn moraine) dates to between 19,000 to 18,000 cal yr BP (Briner et

al., 2005). A cosmogenic exposure chronology from Fish Lake valley in the northeast Alaska Range shows the LGM maxima may have occurred by 22,400 ± 600 cal yr BP (Young et al., 2009); however this age is based on only one date. Young et al. (2009) report a clustering of younger ages that suggest the Fish Lake glacier remained near the LGM maxima until ~ 16,500 cal yr BP. Evidence from the Delta River valley, the type section for late Pleistocene (Wisconsinan) glaciation in the northeast Alaska Range, dates the Donnelly moraine to 17,300 ± 600 cal yr BP (Matmon et al., 2010). These cosmogenic exposure chronologies suggest that regional glaciers persisted at or near their LGM maxima until near the late-glacial transition, implying that climatic conditions remained favorable (likely colder) for positive glacier mass balance until 17,000 to 16,000 cal yr BP. Glacier mass balance is controlled by both temperature and precipitation conditions, and while the LGM climate of interior Alaska is considered extremely dry (Hopkins, 1982), glacial maxima during the LGM likely resulted from colder temperatures. Therefore, the timing of alpine glacier retreat during the late-glacial (beginning around ~ 16,000 to 17,000 cal yr BP) likely indicates the initiation of warmer conditions.

Although our age control is limited during the LGM, proxy data from Harding Lake permit critical testing of an LGM (21,000 cal yr BP) climate model simulation that indicate annual temperatures up to 4° C warmer than present in central Alaska (Otto-Bliesner et al., 2006). Likewise, these conclusions are broadly supported by a pollen based LGM climate reconstruction (Bartlein et al., 2011) that relies on several pollen records constrained with bulk sediment radiocarbon dates. The anomalously warmer temperatures are hypothetically explained by the aforementioned changes in

atmospheric circulation associated with the increasing size and altitude of the Laurentide Ice Sheet (COHMAP, 1988). Otto-Bliesner et al. (2006) suggest the strong pressure gradient between the high pressure cell over the Laurentide Ice Sheet centered near Hudson Bay and a low pressure region in the North Pacific (Aleutian low) resulted in stronger southerly surface winds on the western margin of the ice sheet. Model simulations indicate the enhanced winds produced poleward advection of warmer air into Alaska, especially during winter (COHMAP, 1988). Although our age control is limited, evidence of very low aquatic (biogenic silica) and terrestrial (organic matter, absence of macrofossils) productivity throughout LGM age sediments at Harding Lake indicate generally dry and cold conditions with a short ice free (growing) season. Accordingly, proxy evidence from Harding Lake contradict the climate model simulation conclusions of Otto-Bliesner et al. (2006) and pollen based climate reconstructions of Bartlein et al. (2011). This apparent discrepancy may result from contrasting seasonal influences, whereby lacustrine proxies are responding to summer, growing season conditions. Mean annual temperatures in interior Alaska during the LGM, on the other hand, may be more influenced by winter season temperature variability.

2.5.3 The late-Glacial and early Holocene (15,700 to 9,400 cal yr BP)

The abrupt increase in organic matter and biogenic silica concentration at 15,700 cal yr BP marks the transition into the late-glacial and indicates wetter conditions at Harding Lake. A corresponding decrease in dry bulk density, magnetic susceptibility, and titanium values further suggests a decrease in windiness and ameliorating climatic conditions (Figure 2-6). The intermediate organic matter and biogenic silica content of

Unit 2 sediments suggests that although aquatic and terrestrial productivity levels were higher than before, they were still lower than modern levels. These results combined with a subtle increase in the sedimentation rate as well as lower magnetic susceptibility and titanium values imply that lake levels were higher relative to Unit 1. Rising and high Betula (> 50 %) pollen and a corresponding decline in herb taxa beginning shortly before 14,600 cal yr BP (Figure 2-7) further suggests that climatic conditions were warmer and wetter compared to the LGM. Comparison with other AMS dated lake records from interior Alaska show the Betula rise occurred between 13,500 to 14,000 cal yr BP at Jan Lake (Carlson and Finney, 2004) and Birch Lake (Bigelow, 1997), and thus suggest the Betula rise occurred contemporaneously or slightly earlier at Harding Lake. Collectively, proxy and core-transect evidence indicates a rapid lake level rise beginning at 15,700 cal yr BP reaching above 17 m BML by ~ 14,000 cal yr BP (Figure 2-10). The presence of an erosional unconformity in core E-12 demonstrates that lake level fluctuated or dropped after the initial rise. Regardless, the preservation of lacustrine sediment above this interval provides evidence that lake-levels did not drop below 17 m BML again for any sustained time.

The proxy data from Harding Lake support existing evidence for significant climatic change during the late-glacial in Alaska. For example, a pollen based reconstruction for eastern Beringia (Viau et al., 2008) indicates rising mean annual temperatures beginning around 16,000 yr BP and peak late-glacial mean annual temperatures by 12,000 cal yr BP. The onset of inferred warming at Harding Lake occurred during a time of increasing summer insolation (Figure 2-10) and rapid deglaciation in the Alaska Range (Young et al., 2009). Notably, the late-glacial

transition at Harding Lake also corresponds to a rapid 18 m lake level rise at Birch Lake at ~ 15,000 cal yr BP (Figure 2-10) (Abbott et al., 2000), suggesting that climate was substantially wetter than before. This assertion is supported by evidence that numerous small lakes began accumulating lacustrine sediment between 15,000 and 13,000 cal yr BP in lowland central Alaska (Ager, 1983; Bigelow and Edwards, 2001; Carlson and Finney, 2004) as well as evidence for deglaciation and warmer temperatures in the lower Fish Lake valley (located in the northeastern Alaska Range) by 15,000 to 14,000 cal yr BP (Young et al., 2009).

Marine sediments from the southeastern Bering Sea (HLY0502-51JPC) do not contain detectable amounts of C_{37} alkenones prior to ~ 16,700 cal yr BP (Caissie et al., 2010), implying perennial sea ice cover during the LGM. Alkenone derived sea surface temperature estimates and diatom assemblage data indicate warming sea surface temperatures and a transition from sea-ice to open water species during the late-glacial period (Caissie et al., 2010). In general, the available evidence from Harding Lake and comparison with other paleoproxy records shows the late-glacial was a time of wetter and warmer conditions, compared to the LGM, in central Alaska.

2.5.4 The early to mid-Holocene (9,400 to 8,700 cal yr BP)

The abrupt increase in organic matter and biogenic silica content (Figure 2-6) along with the highest sedimentation rates (0.225 cm/yr) of the entire record (Figure 2-4), and the simultaneous decline in magnetic susceptibility and titanium content indicate that considerable climatic and environmental changes occurred at Harding Lake at 9,400 cal yr BP. We suggest the abrupt change in the sediment physical and

geochemical data signifies rapidly rising and much higher lake levels between 9,400 to 8,700 cal yr BP. This interpretation is consistent with the accumulation of lacustrine sediment above the erosional unconformity in core E-12 by 9,660 cal yr BP. The marked increase in organic matter and biogenic silica can be attributed to a further increase in precipitation and rising lake levels, along with an increase in the length of the summer ice-free season from warmer temperatures associated with the summer insolation maxima (Berger and Loutre, 1991). The increase in biogenic silica is likely also caused, in part, by increased availability of nutrients and autochthonous organic sediment flux. Continued predominance of *Betula* (> 50 %) pollen, along with a concomitant decline in herb taxa and subtle increase in Sphagnum and *Isoetes* at 9,100 cal yr BP (Figure 2-7), further demonstrate increasingly wet conditions and higher lake levels. The corresponding decrease in titanium and magnetic susceptibility represents the final transition to interglacial climatic conditions, wherein a generally stable climate characteristic of the Holocene prevailed.

The Harding Lake sediment signal at 9,400 cal yr BP is explainable in the context of numerous other terrestrial records from central Alaska that demonstrate an increase in precipitation and potentially warmer conditions. Sedimentary evidence from Birch Lake shows rising lake levels to near the overflow level between 10,000 and 9,000 cal yr BP (Figure 2-10) (Abbott et al., 2000). Rising lake-levels also occurred at this time at Marcella Lake in the southwest Yukon (Anderson et al., 2005) and after 9,500 cal yr BP at Dune Lake (Finney et al., 2012). In addition, this period broadly corresponds with the early Holocene peak in summer insolation (Figure 2-10) as well as rising sea levels (Figure 2-10) and the final submergence of the Bering land bridge (Elias et al., 1996),

which would have reduced the transport distance of warm, moist North Pacific air masses traveling towards interior Alaska. Nevertheless, the gradual change in insolation forcing and eustatic sea level rise during this interval precludes a direct linkage between these forcings and the sediment anomaly. We therefore suggest the rapid changes in sedimentation at Harding Lake likely reflect an abrupt (and probably temporary) change in atmospheric circulation, possibly associated with further retreat of the Laurentide Ice Sheet.

2.5.5 The middle to late-Holocene (8,700 cal yr BP to 2010 AD)

Proxy evidence from Harding Lake suggests that water levels were generally high (Figure 2-10) for the remainder of the Holocene. The decline in sedimentation rates to lower and stable Holocene levels (0.015 to 0.04 cm/yr), along with the subtle increase and peak in magnetic susceptibility and titanium by 7,100 cal yr BP implies that lake levels were higher and that shoreline reworking provided a source of minerogenic sediments to the lake depocenter. The remainder of Holocene sediment is characterized by low and declining magnetic susceptibility and titanium values. The appearance of *Alnus* and *Picea* between 8,600 to 7,500 cal yr BP (Figure 2-7), and later increases in *Alnus* by 7,000 cal yr BP and *Picea* by 5,600 cal yr BP, respectively, indicate development of coniferous forest quite similar to present and further imply warm and wet conditions. *Isoetes* predominates the aquatic taxa and *Myriophyllum* is absent, consistent with deeper water at the depocenter (Edwards et al., 2000). The higher organic matter content and generally low and declining magnetic susceptibility (Figure 2-6) values suggest relatively high lake levels through the middle to late

Holocene. Substantially lower magnetic susceptibility values suggest that sediment composition in this interval is relatively insensitive to further low magnitude lake-level changes (Figure 2-9). A gradual trend toward higher C/N values indicates organic matter increasingly originated from terrestrial sources during the middle to late Holocene (Figure 2-6). In addition, organic matter $\delta^{13}C$ values gradually increase (Figure 2-6) becoming more enriched, and combined with higher organic matter content, suggest increasing levels of aquatic productivity within Harding Lake. Notably, biogenic silica concentrations peak during the mid-Holocene between 5,500 and 3,100 cal yr BP and fluctuate at millennial time scales (Figure 2-6). Given that magnetic susceptibility and titanium values are generally stable and decreasing throughout the Holocene (with minimal evidence of diatom dissolution), we attribute the variability in biogenic silica content to fluctuations in aquatic productivity.

Unchanging to overflowing lake levels persisted from ~ 6,000 cal yr BP to the present at Birch Lake (Figure 2-10) (Abbott et al., 2000), suggesting the middle to late Holocene climate of central Alaska was generally moist and stable. Core transect data from Jan Lake in the middle Tanana Valley suggest rising lake levels from 9,000 cal yr BP to the present, indicating a trend towards wetter conditions through the Holocene (Barber and Finney, 2000). Historical observations from Harding Lake demonstrate lake level fluctuations on the order of several meters since the 1930's (LaPerriere, 2003), with periodic exposure of the shallow shelf along the northern shore. Given the substantial water depth of the depocenter at Harding Lake (> 42 m), this deep core site appears relatively insensitive to recent low-magnitude lake level fluctuations.

2.6 CONCLUSIONS

A multi-proxy geochemical investigation of sediments from Harding Lake in interior Alaska reveal millennial scale changes in lake level, vegetation patterns, and paleoclimate over the last 31,000 cal yr BP. Detailed analysis of core sedimentology along with AMS radiocarbon dates on terrestrial macrofossils from a depocenter core (42 m water depth) collectively indicate Harding Lake persisted as a shallow, low productivity lake during the LGM, a known period of extreme aridity. The general absence of terrestrial macrofossils for radiocarbon dating and low organic matter and biogenic silica content suggest sparse terrestrial vegetation in the vicinity and low in-lake productivity. Pollen data show a predominance of herb taxa during this time that is likely indicative of tundra conditions. An increase in organic matter and biogenic silica content at 15,700 cal yr BP marks the transition into the late-glacial and indicates rising lake levels at Harding Lake and variable hydroclimatic conditions thereafter until 9,400 cal yr BP. Core transect data confirm a substantial lake-level rise with the onset of lacustrine sedimentation at 17.1 m BML by ~ 14,000 cal yr BP and lower or fluctuating lake-levels thereafter until 9,400 cal yr BP. Combined with evidence for a decrease in windiness (lower magnetic susceptibility and titanium) and expansion of *Betula* forest at 14,600 cal yr BP, the proxy data indicate wetter and potentially warmer conditions. A rapid increase in sedimentation rate and rising organic matter and biogenic silica content with a simultaneous decline in magnetic susceptibility and titanium values indicate that considerable environmental changes occurred at Harding Lake between 9,400 and 8,700 cal yr BP. Core transect data and composite core proxy evidence suggests rapidly rising and much higher lake levels than at any previous time during the

record. The increase in organic matter and biogenic silica is attributed to a further increase in the length of the summer ice-free season and high nutrient loads, while declining titanium and magnetic susceptibility resulted from the final transition to interglacial climatic conditions. High *Betula* pollen and a minor component of Sphagnum and *Isoetes* indicate wetter conditions and higher lake-levels. This period of rapid environmental change broadly corresponds to the submergence of the Bering land bridge and early Holocene maxima in summer insolation; however the abruptness of this transition precludes a direct linkage from insolation forcing and sea level rise. We alternatively suggest the rapid changes in sedimentation at Harding Lake beginning at 9,400 cal yr BP likely reflect an abrupt change in atmospheric circulation, possibly associated with further retreat of the Laurentide Ice Sheet and wetter conditions in interior Alaska. A return to stable and lower sedimentation rates by 8,700 cal yr BP, along with higher organic matter and low magnetic susceptibility, suggest generally high and stable lake levels over the middle to late-Holocene with conditions similar to the modern lake. Increases in *Alnus* by 7,000 cal yr BP and *Picea* by 5,600 cal yr BP, combined with continued predominance of *Betula* through the Holocene, indicate substantial expansion of forest around Harding Lake.

The use of AMS radiocarbon dating of terrestrial macrofossils and higher resolution proxy analysis relative to a previous study of Harding Lake sediments provide a better understanding of both the timing and magnitude of late-Quaternary climate variability in interior Alaska. Analysis of both a depocenter core and transect of cores from varying depths demonstrate that lake level reconstructions using a combination of methods are more robust than a single core approach, and provide quantitative

information regarding past hydroclimate variability. Further, deep lake basins in the unglaciated interior of Alaska preserve older sedimentary records than small, shallow lakes and therefore provide an important terrestrial archive to investigate paleoenvironmental change across the LGM to Holocene transition.

3.0 A MULTI-DECADAL TO CENTENNIAL SCALE MULTI-PROXY RECONSTRUCTION OF ENVIRONMENTAL CHANGE FROM BURIAL LAKE, ARCTIC ALASKA

Sediment cores from Burial Lake located in the western Brooks Range in Arctic Alaska record paleoenvironmental changes that span the last ~ 37,000 calendar years before present (cal yr BP). To our knowledge, the sediment sequence represents the oldest continuous lacustrine record from eastern Beringia to date. We identified four distinct lithologic subunits based on an analysis of physical properties (dry bulk density, magnetic susceptibility), sediment composition, and geochemical proxies (organic matter, biogenic silica, C/N, organic matter $\delta^{13}C$ and $\delta^{15}N$, and elemental data from scanning X-ray Fluorescence). The multi-proxy approach and relatively high temporal resolution (at multi-decadal to centennial time scales,) of our proxy analysis, compared with previous studies of intermediate water depth cores from Burial Lake, provides new insights into the paleoenvironmental history of the region spanning the period prior to the Last Glacial Maximum. Relatively high lake-levels and gradually decreasing in-lake and terrestrial productivity occur during the mid-Wisconsinan interstadial between 37,200 to ~ 29,600 cal yr BP. The subsequent period is defined by falling and lower lake-levels with decreasing effective-moisture, windier conditions, and sustained and low levels of aquatic productivity throughout the LGM between ~ 29,600 to ~19,600 cal

yr BP. The last deglaciation that commenced by ~19,600 cal yr BP is characterized by gradual changes in several sediment physical and geochemical proxies, including increasing C/N ratios and terrestrial productivity, decreasing magnetic susceptibility and clastic sediment flux, along with rising and relatively higher lake-levels. A decrease in aeolian activity after 16,500 cal yr BP is inferred from the appearance of fine (very fine sandy silt) sediment, compared to coarse sediments through the LGM and last deglaciation. The highest levels of terrestrial productivity along with increasing and variable aquatic productivity occurs during the Lateglacial to early Holocene interval between 16,500 to 8,800 cal yr BP. The absence of multi-proxy evidence for a climatic reversal during the Younger Dryas from Burial Lake sediments contrasts with other paleorecords showing cooler temperatures and/or dry conditions in northern Alaska at this time. Peak levels of sediment organic content and terrestrial productivity at Burial Lake between ~ 10,500 to 9,900 cal yr BP coincide with the early Holocene summer insolation maxima and Holocene Thermal Maximum in the western Arctic, which likely represents summertime warming and an enhanced flux of watershed derived organic matter from permafrost degradation. The remainder of the Holocene (since 8,800 cal yr BP) at Burial Lake is characterized by relatively high and stable lake levels, landscape stabilization, and relatively high and variable levels of aquatic productivity.

3.1 INTRODUCTION

Recent climate change in the Alaskan Arctic is a having a profound effect on aquatic and terrestrial ecosystems, the surface hydrology of lakes and ponds, and the

stability of permafrost landscapes. For example, warming temperatures from 1990 to 2009 coincide with an increase in the abundance of shrubs and terrestrial productivity in tundra landscapes across Arctic Alaska (Swanson, 2010). Accelerated permafrost degradation and thaw slumping observed in the Noatak Basin have been attributed to general climate warming and shifting trends in the seasonality of weather (Balser et al., 2014). Further, an ~ 30% decrease in pond and thaw lake surface area on the Alaskan north slope from 1948 to 2013 corresponded with increases in air temperature and permafrost active layer thickness (Andresen and Lougheed, 2015). The drying and disappearance of these tundra ponds near Barrow, Alaska has been linked with increased evaporation from warming, permafrost degradation, and increased emergent vegetation. Additional changes include a decrease in lake ice cover duration by 24 days from 1950 to 2011 on the Alaskan North Slope (Surdu et al., 2014) and shrinking sea-ice cover in the adjacent Chukchi Sea (Wendler et al., 2014). Understanding the significance of these terrestrial ecosystem changes and of natural climate variability in the Alaskan Arctic requires a longer-term perspective than is provided by instrumental weather records and satellite observations, so that they might be placed in an appropriate context.

The late-Quaternary climatic and environmental history of the Arctic Noatak Basin in the western Brooks Range in Alaska, confined by the Delong Mountains to the north and Baird Mountains to the south, is primarily based on extensive surficial mapping and analysis of alluvial, lacustrine, and glacial deposits (Hamilton, 2001, 2010; Hamilton et al., 1987; Hamilton and Van Etten, 1984). Alluvial deposits along Noatak River and tributaries show extensive aggradation during stadial periods and channel

incision, floodplain construction, and soil formation during interstadial periods (Hamilton, 2001). Glaciolacustrine and ice-contact glacial deposits are scattered throughout the basin and provide evidence for large proglacial lakes and periods of moraine construction spanning the middle Pleistocene to the Last Glacial Maximum (LGM) or late Wisconsinan (Hamilton et al., 1987; Hamilton and Van Etten, 1984). For instance, bracketing radiocarbon ages constrain the LGM to between 35 to 13.6 ka ^{14}C years in the western Noatak Basin (Hamilton, 2001). Floodplain aggradation on Noatak River ended by or shortly after 13.6 ka ^{14}C years and was followed by Holocene channel incision and down-cutting (Hamilton, 2001). Further evidence for climatic and environmental changes in the Noatak Basin are inferred from palynological analysis of lake sediment cores (Anderson, 1985, 1988; Eisner and Colinvaux, 1992) and analysis of fossil beetle assemblages to interpret temperatures (Elias, 2000; Elias et al., 1999). More recently, core-transect and multi-proxy analysis (pollen, organic geochemical proxies, and chironomids) of intermediate water depth (7.9 m) cores from Burial Lake reconstructed changes in relative lake-levels, vegetational patterns, and summer temperatures across the last 40,000 years (Abbott et al., 2010; Kurek et al., 2009), however an unconformity and missing sediments spanning the LGM limited the scope of these studies. Collectively, the previous studies and environmental interpretations are limited by the complex and discontinuous nature of surficial stratigraphic deposits (Elias, 2000; Hamilton, 2001), bulk sediment radiocarbon dating and emphasis on pollen analysis to assess vegetational changes (Anderson, 1985, 1988; Eisner and Colinvaux, 1992), and the coarse resolution of proxy analysis and missing sediments that did not permit continuous analysis of LGM to preceding interstadial conditions (Abbott et al.,

2010; Kurek et al., 2009). Further, these previous studies did not assess temporal trends in aquatic and terrestrial ecosystem productivity directly, through analysis of sedimentary biogenic silica along with Carbon and Nitrogen stable isotopes of organic matter.

The primary objective of this study was to investigate climatic and environmental changes extending back through the LGM to the present from multi-proxy analysis of newly recovered Burial Lake depocenter cores (21.5 m water depth). In this study, we analyze multiple physical and geochemical proxies (including dry bulk density, organic matter, biogenic silica, carbon to nitrogen mass ratios (C/N), stable carbon and nitrogen isotopes ($\delta^{13}C$ and $\delta^{15}N$) of organic matter, and elemental abundances via scanning X-ray fluorescence) along with sediment description and use Accelerator Mass Spectrometry (AMS) radiocarbon dating of discrete terrestrial macrofossils to establish age control. Proxies in this study were analyzed at much higher temporal resolution than previous works at Burial Lake to investigate multi-decadal to century scale variations in environmental conditions extending through the LGM. Comparison with a newly developed environmental magnetic record from the same sediment cores (Dorfman, 2013), other regional glacial and lacustrine records from northwest Alaska, along with nearby marine records provides an assessment and new synthesis of regional climatic change in the western Brooks Range during the late Quaternary.

3.2 SITE LOCATION AND REGIONAL SETTING

Burial Lake (68.43°N, 159.17°W; 460 m ASL) is located in the upper Anisak River drainage within the Noatak Basin in the northwestern Brooks Range, Alaska (Figure 3-1). The lake surface is approximately circular (0.8 km^2) and has a maximum water depth of 21.5 meters. The lake is situated on a subtle topographic high between Setting Sun Creek to the west and a small tributary to the east (Figure 3-1) that drains to Anisak River and eventually Noatak River. The surrounding catchment is small (3.3 km^2) with steep (3-5 m high) slopes along much of the lake's shoreline that transition to a low-relief plateau. The lake receives inflow from several ephemeral gullies along the northern shoreline and contains a small outlet stream at the southwest shoreline. Burial Lake is oligotrophic (Abbott et al., 2010) and a hydrologically open system. Lake surface water stable isotopes of $\delta^{18}O$ (-17.58 ‰ VSMOW) and δD (-138.58 ‰ VSMOW) collected in July, 2010 are similar to the isotopic composition of Anisak River waters ($\delta^{18}O$ = -16.83 ‰ VSMOW; δD = -136.47 ‰ VSMOW). Both Burial Lake and Anisak River water isotope values plot on the Global Meteoric Water Line, demonstrating water loss is primarily controlled by non-fractionating pathways (surficial outflow and/or groundwater outseepage) with minimal evaporative effects. Vegetation is low-arctic tundra, dominated by sedges, *Salix*, shrub-*Betula*, and *Alnus crispa*, with sparse stands of *Populus balsamifera* found in river valleys and along creek beds (Abbott et al., 2010). Tree-line for the nearest *Picea glauca* (Spruce) forest lies ~100 km to the west, and also encroaches on the Basin from the south.

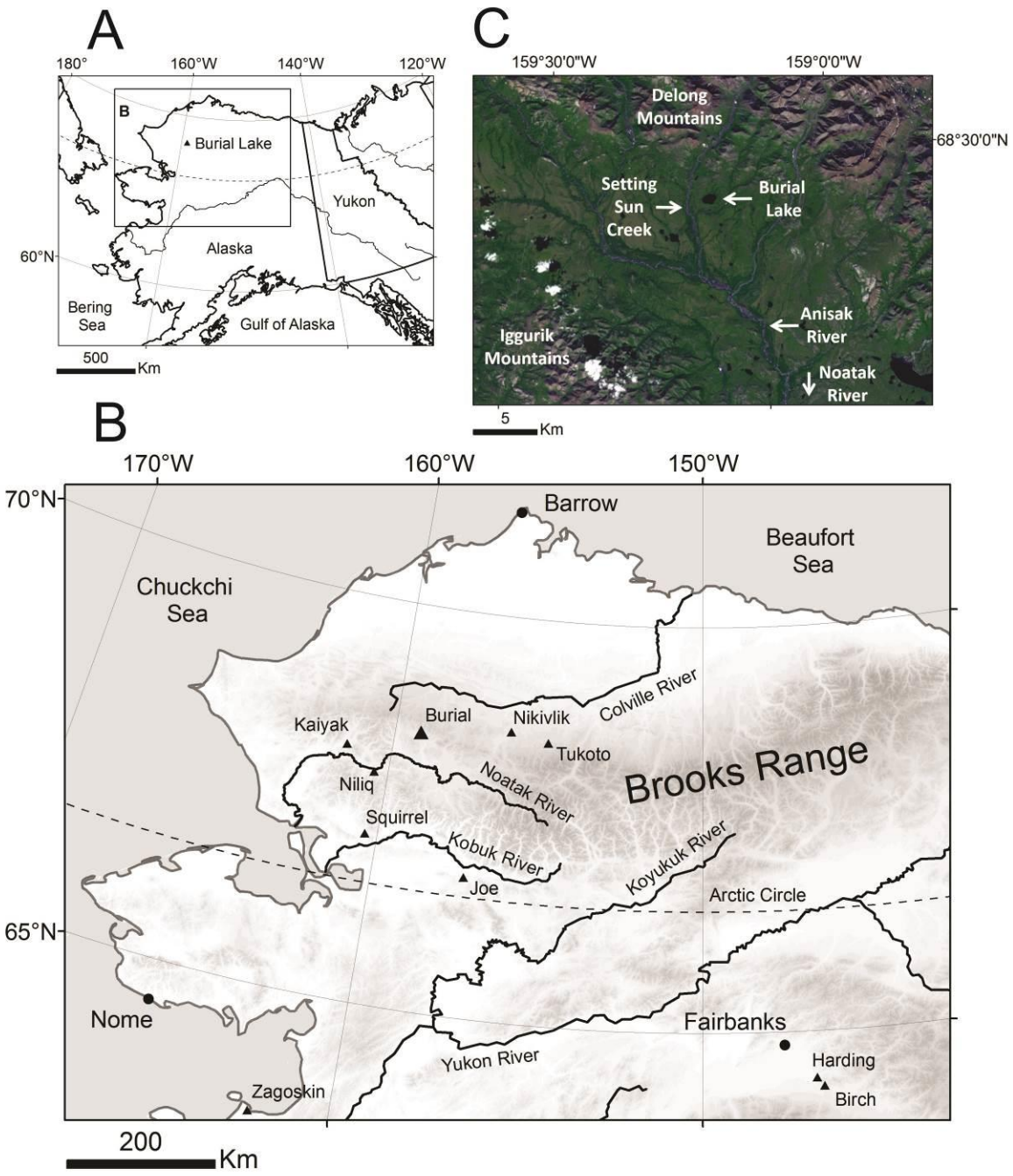

Figure 3-1. A) Map of Alaska showing the location of Burial Lake. B) Shaded relief map of the western Brooks Range in Alaska with sites mentioned in the text. Solid lines are major rivers. C) Aerial photograph of the Upper Anisak River drainage showing Burial Lake and the surrounding area.

The lake is located in the Aniuk Lowland sub-province within the Noatak Lowland physiographic province, an irregular rolling plain that slopes gradually to the south (Wahrhaftig, 1965). The Delong Mountains flank the lake and catchment to the north and consist of a series of rugged glaciated ridges with altitudes > 1250 m (Wahrhaftig, 1965), while the lower altitude (> 900 m) Iggiruk Mountains are located to the south. Bedrock geology in the catchment consists of Mississippian age carbonate and clastic sedimentary rocks, consisting of limestone and subordinate shale, chert, and dolomite (Grybeck et al., 1977). Surficial geology in the catchment is mapped as Itkillik I age (early Wisconsinan) lake deposits, Holocene to late Pleistocene age solifluction deposits, and silt-covered bedrock (Hamilton, 2010). The catchment and surrounding region is underlain by continuous permafrost and ground ice is mapped as low or < 10% volume (Jorgenson et al., 2008). During the Sagavanirktok River glaciation (middle Pleistocene age), alpine glaciers originating in the Delong Mountains scoured the landscape and dammed local drainage, forming the lake basin (Hamilton, 2003a). Subsequent glacier advances in the Noatak Basin were less extensive, including during early Wisconsinan (Itkillik I) and late Wisconsinan (Itkillik II) advances (Hamilton, 2001), and glaciers did not extend across the lake and adjacent terrain during the LGM. During middle and late Pleistocene glacial periods, alpine glaciers emanating from the Delong Mountains extended into the lowlands and repeatedly dammed Noatak River forming Glacial Lake Noatak (Hamilton, 2001; Hamilton and Van Etten, 1984). While the lake was not covered by Itkillik II age (LGM) lacustrine deposits, the lower Anisak River valley and western Noatak Basin were inundated by Glacial Lake Noatak (Hamilton,

2010). During the LGM, alpine glacial erosion resulted in outwash deposition and extensive floodplain aggradation in the Noatak Basin (Hamilton, 2001).

The regional climate in Noatak Basin is characterized by long cold winters and short cool summers. Bieniek et al. (2012) place the upper Noatak Basin within the North Slope climate division, a region defined by arid conditions (maximum precipitation of < 5 cm in the wettest summer month) with seasonal average temperatures ranging from below -25° C in winter to above 10°C in summer. Instrumental weather records from the Noatak Basin are relatively short and discontinuous. Climate normals for stations across northern Alaska (Kotzebue, Bettles, and Barrow) during the period 1981-2010 indicate the majority of annual precipitation occurs during summer months, with peak values typically occurring in July and August (http://climate.gi.alaska.edu/). Summer precipitation to the interior of Alaska is primarily sourced from the North Pacific Ocean (Mock et al., 1998; Streten, 1974). Climatic conditions in northern Alaska are further influenced by ocean-atmosphere interactions and internal modes of climate variability (El Niño Southern Oscillation, Pacific Decadal Oscillation, and Arctic Oscillation) on seasonal to multi-decadal timescales (Bieniek et al., 2012; Hartman and Wendler, 2005; Papineau, 2001).

3.3 METHODS

3.3.1 Sediment coring

Sediment cores were collected from an inflatable raft from the central deep basin in July, 2010 (Figure 3-1). A surface core (A-10 Drive 1) with an intact sediment-water interface was recovered from 21.5 m water depth using a polycarbonate tube fit with a rubber piston. The upper portion of the surface core was dense and therefore packed with floral foam and capped for transport. Multiple overlapping long cores were recovered from core sites A-10 and C-10 in 21.5 m water using a square rod Livingstone corer. Deeper sediments, characterized by greater density, were recovered by coring within the same borehole using 10 cm diameter PVC as casing. Cased drives were offset by 50 cm between core sites A-10 and C-10 to ensure overlap and complete recovery of the sediment sequence. All long cores were packaged in the field and securely transported to the Department of Geology and Planetary Science at the University of Pittsburgh for processing and analysis.

3.3.2 Lithostratigraphy and geochemistry

Sediment cores were split lengthwise and described; notable sedimentary structures, grain size, and Munsell color were characterized for each core. Cores were subsampled using ridged plastic u-channels (2x2 cm cross-sectional area) to investigate environmental magnetic properties as part of a separate study (Dorfman, 2013). Computed Tomography (CT) scans on the u-channels were obtained at the Institut

national de la recherche scientifique, Centre Eau-Terre-Environnement (INRS-ETE) in Quebec City. Select 1 cm samples spanning the composite depth scale were analyzed via smear-slide mineralogy and described according to the lacustrine sediment classification scheme of Schnurrenberger et al. (2003). A total of 5 samples were analyzed for powder x-ray diffraction (XRD) to further characterize core mineralogy. Power XRD analysis was performed using a using a Philips PW3710 x-ray diffractometer at the University of Pittsburgh, Swanson School of Engineering and X'Pert Graphics and Identify® software was used to identify the major mineral assemblages present. All cores were sampled at 1 cm intervals, and dry bulk density was calculated from dry weights of volumetric samples, and percent organic matter and total carbonate values were measured via loss-on-ignition (LOI) at 550° C for 4 hours and 1000° C for 2 hours, respectively (Heiri et al., 2001). Magnetic susceptibility was measured on all split cores at 2 mm intervals using a Bartington MS2E1 high-resolution surface sensor.

Samples for biogenic silica were measured at 2 to 4 cm intervals over the composite core (n = 256) at the Department of Geology and Planetary Science at the University of Pittsburgh using a wet-chemistry, alkaline extraction adapted from Mortlock and Froelich (1989). Wet samples were freeze-dried, homogenized to a fine powder using a mortar and pestle, and treated with 30% H_2O_2 and 1M HCl to remove organic matter and carbonates. Biogenic silica was extracted with a 5% Na_2CO_3 solution and determined by molybdate blue spectrophotometry at 812 nm using a Thermo Scientific Evolution 60s UV-Visible Spectrophotometer. Replicate measurements of unknown samples (n = 44) and an internal sediment standard from

Laguna de Los Anteojos (Stansell et al., 2010) run during sample analysis produced an average error of < 3.2 %.

Samples for total organic carbon (TOC), total nitrogen (TN), and stable carbon ($\delta^{13}C$) and nitrogen ($\delta^{15}N$) isotopes of organic matter were measured at 2 to 4 cm intervals over the composite core (n = 222) at the Stable Isotope Laboratory at Idaho State University. The elemental mass ratio of TOC to TN (C/N) was calculated to further assess the relative proportion of organic matter from terrestrial (C/N > 20) versus aquatic (C/N < 10) sources (Meyers and Teranes, 2001). Prior to analysis, samples were treated with 1M HCl to ensure removal of carbonate minerals, rinsed to neutral pH with MilliQ water, freeze-dried and homogenized. Measurements were obtained using an Elemental Combustion System 4010 interfaced to a Delta V Advantage mass spectrometer through the ConFlo IV system. $\delta^{13}C$ and $\delta^{15}N$ values are reported as ‰ values relative to the VPDB and N_2 scales, respectively. Replicate measurements of internal standards yielded coefficients of variation of 1.61 % and 1.04 % for TOC and TN, and precision equal to 0.2 ‰ for the stable isotope measurements. Surface water samples from Burial Lake collected in August, 1997 were analyzed for pCO2 concentrations via the headspace equilibration technique (Kling et al., 1991) at the Alaska Stable Isotope Facility, University of Alaska Fairbanks.

The split A-10 and C-10 archive cores were scanned for elemental abundances using the ITRAX XRF core scanner at the Large Lakes Observatory, University of Minnesota Duluth. Continuous measurements were obtained at 0.5 cm intervals with 60 second count times. Values are reported as counts per second. To assess controls on elemental abundances, we analyze trends in the incoherent to coherent scatting ratio

(Inc/Coh) and silicon to titanium (Si/Ti) ratio, two commonly used XRF proxies. The Inc/Coh ratio provides a relative measure of the mean atomic number for elements in a sample and therefore is a useful proxy for total organic matter (Croudace et al., 2006). The Si/Ti ratio is another commonly used proxy to estimate the relative proportion of biogenic silica in lake sediments (Brown et al., 2007) and is based on the premise that titanium is sourced solely from detrital sources, while silicon is derived from both biogenic and detrital sources.

3.3.3 Geochronology

Age control of the recovered material was developed from Accelerator Mass Spectrometry (AMS) radiocarbon analyses of 13 terrestrial macrofossils (Table 3.1). Bulk sediment samples were disaggregated with dilute H_2O_2 (7 %), wet-sieved with a 63 μm sieve, and terrestrial macrofossils were identified and picked under a stereographic microscope for AMS radiocarbon measurement. Samples were pre-treated using standard acid-base-acid wash techniques (Abbott and Stafford, 1996) at the University of Pittsburgh and were combusted to CO_2 gas, converted to filamentous graphite, pressed in Aluminum targets, and measured at the W.M. Keck Carbon Cycle AMS Laboratory, University of California, Irvine. Radiocarbon ages were calibrated using CALIB 6.0 and the INTCAL09 calibration curve (Reimer et al., 2009). An age-depth model was created using point to point, linear interpolation with the classical age modeling (CLAM) code for the statistical software R (Blaauw, 2010). The CLAM analysis performed 1,000 age model iterations based on repeated sampling of the calibrated age distributions for each radiocarbon sample to estimate the ‘best fit’ or

weighted mean age for each depth. Given the paucity of materials for radiocarbon dating between 219 cm to 553 cm in the A-10/C-10 composite core sequence (Table 3.1), the linear age uncertainties from the CLAM analysis are inadequate. To further account for chronological uncertainty, we apply a Monte Carlo-based approach that perturbs the interpolated age-depth model 10,000 times following a random draw from a normal distribution between the 2σ calibrated ^{14}C ages (Marcott et al., 2013). The uncertainty between the age control points is modeled as a random walk, after Huybers and Wunsch (2004), with chronological uncertainty assumed to be auto-correlated through time and modeled as a first order autoregressive (AR1) process.

Table 3.1. Burial Lake AMS radiocarbon dates with calibrated 2 sigma error ranges. Samples highlighted with an asterisk (*) are omitted from the age model with explanations in the text.

Sample ID (UCIAMS #)	Core-Drive	Drive Depth (cm)	Total Depth (cm)	Material	^{14}C Age (^{14}C yr)	Error (yr)	Calib 6.0 (yr BP)	Age
89197	A-10 D1	45.0	45.0	plant material	2,535	30	2,493 – 2,745	
109361	A-10 D1	66.5	66.5	wood	3,635	25	3,872 – 4,074	
116878	A-10 D1	87.5	87.5	plant material	4,910	90	5,470 – 5,896	
89198	A-10 D1	111.0	111.0	plant material	6,345	25	7,174 – 7,410	
109362	A-10 D1	141.5	141.5	wood	8,850	110	9,564 – 10,205	
89199	A-10 D2	84.0	166.0	plant material	9,760	40	11,134 – 11,244	
89200	A-10 D3	54.0	173.5	seed	10,085	45	11,398 – 11,959	
89122	C-10 D3	45.0	219.0	wood	13,670	30	16,657 – 16,978	
* 109363	A-10 D5	35.5	359.5	plant material	14,590	550	16,570 – 18,903	
89201	A-10 D7	29.0	553.0	seed	25,300	510	29,173 – 31,074	
* 89123	C-10 D7	64.0	598.0	plant material	31,290	300	35,085 – 36,475	
89124	C-10 D7	72.0	606.0	wood	31,090	210	35,036 – 36,313	
89121	A-10 D8	35.5	636.5	wood	32,150	240	35,699 – 37,342	

3.4 RESULTS

3.4.1 Composite core

A composite 651 cm depth scale was developed from cores A-10 and C-10. Cores were aligned by matching physical properties data (magnetic susceptibility and Inc/Coh from scanning XRF) and visible stratigraphic markers common to both cores

(Figure 3-2). Core A-10 was selected as the primary core due to its greater length and abundance of proxy data sets including radiocarbon samples. The A-10 core stratigraphic section was constructed based on field measurements and subsequently the C-10 cores were aligned to it. No adjustments to subbottom depths in C-10 sections were required to achieve a satisfactory match. The A-10/C-10 composite depth scale (referred to throughout as "depth") is utilized for the production of geochemical proxy data and the age-depth model, in which sediment samples and radiocarbon-dated materials were derived primarily the A-10 cores and the C-10 cores were sampled to span gaps between core sections.

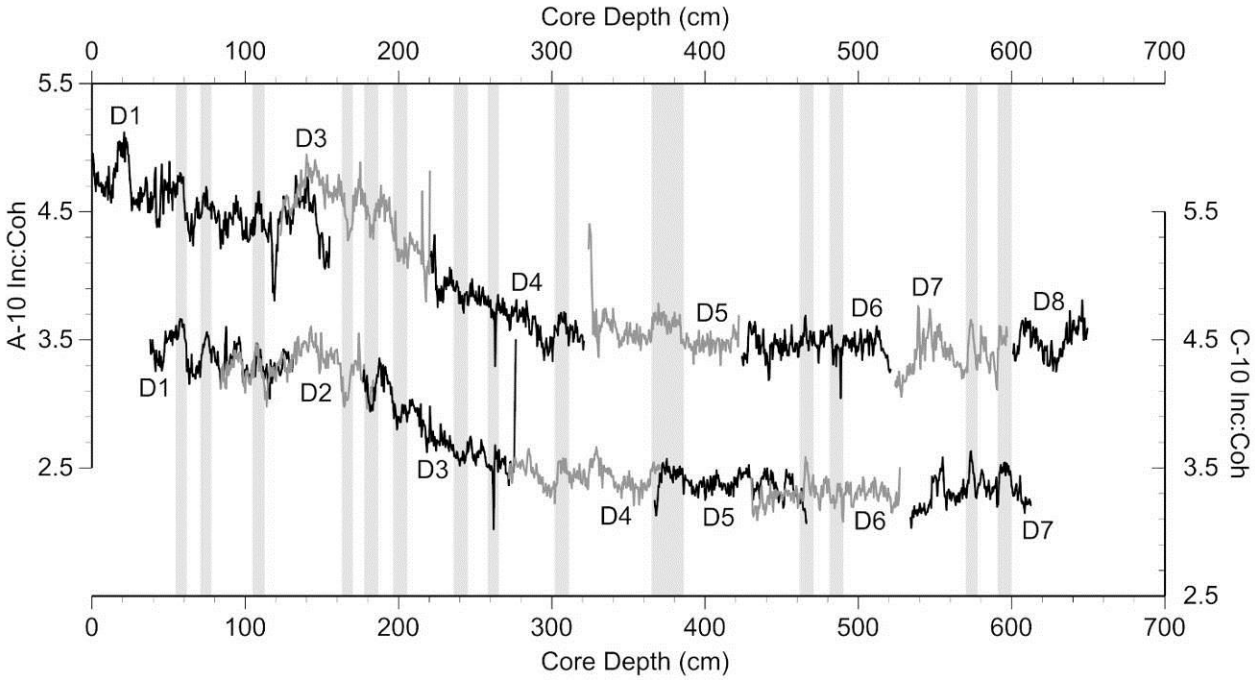

Figure 3-2. Anomaly match between Burial Lake core A-10 and C-10 incoherent/coherent scattering ratio (Inc/Coh) plotted by drive used to develop the composite core depth scale. Grey bars highlight features common to both sets of cores.

3.4.2 Geochronology

The A-10/C-10 composite core age model, maximum variance between age control points, and linear sedimentation rates (cm/ka yr) are presented in Figure 3-3. Two samples (UCIAMS # 109363 and # 89123) were excluded prior to generating the age-depth model. The first sample (UCIAMS # 109363) at 359.5 cm appears anomalously young compared with adjacent ages and, notably, had an extremely small CO_2 yield (0.017 mg C equivalent) prior to graphitization which approaches the threshold limit for AMS radiocarbon analysis. We suggest this sample was contaminated by modern carbon during the combustion and graphitization process given its extremely small mass (Oswald et al., 2005; Santos et al., 2010). In addition, inclusion of this date would require an abrupt increase in sedimentation rate that is not supported by any lithologic evidence or radiocarbon constraints. The second sample (UCIAMS # 89123) at 598 cm displays a modest age reversal with the adjacent sample (#89124) at 606 cm depth. The calibrated age distributions for both samples overlap and therefore we exclude the sample at 598 cm based on its lower carbon yield and slightly larger age uncertainty.

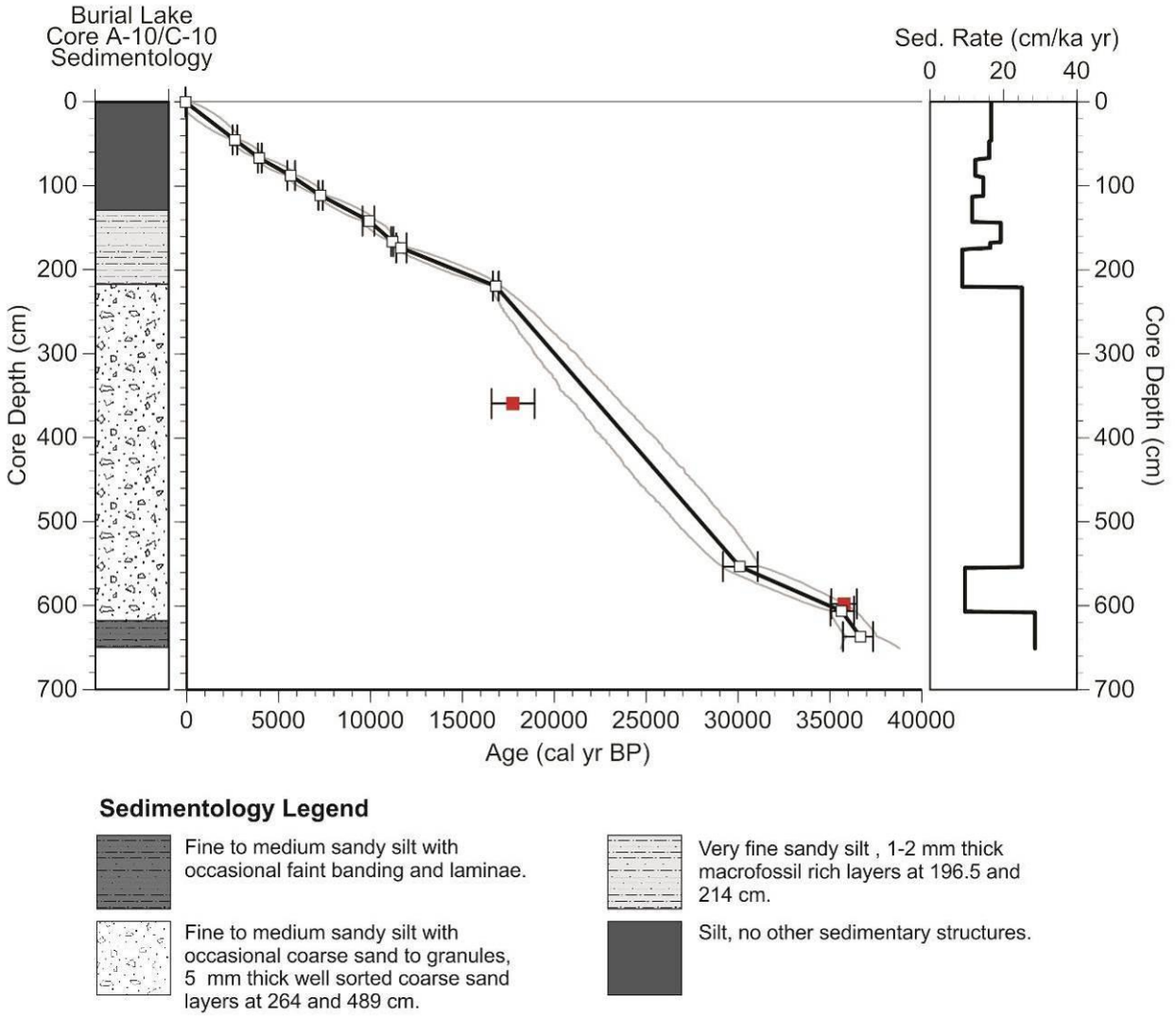

Figure 3-3. Burial Lake A-10/C-10 composite core stratigraphic column showing sedimentology and the age-depth model developed from radiocarbon dates (open squares). Samples designated with a red square are rejected from the age model. Sedimentation rates are presented in cm/ka yr.

3.4.3 Lithostratigraphy

Our paleoenvironmental interpretation of the Burial Lake sediments is based on lithologic subunits based upon core descriptions (Figure 3-3) and sediment physical and geochemical data (Figure 3-4; Figure 3-5; Table 3.2). Variations in organic matter (wt

%), biogenic silica (wt %), magnetic susceptibility, and the availability of terrestrial macrofossils for radiocarbon analysis allow identification of 4 lithologic subunits. Comparison of C/N ratios with organic matter $\delta^{13}C$ (Figure 3-6) and organic matter $\delta^{13}C$ against $\delta^{15}N$ (Figure 3-6) indicates changes in the source (terrestrial versus aquatic) and isotopic composition of organic matter that is consistent with the identified subunits. Lithologic subunits broadly correspond to changes in sediment accumulation rates (Figure 3-3), determined by calculating the time difference between contiguous 1 cm intervals across the composite A-10/C-10 core sequence. The down-core physical and geochemical data are presented versus age in Figure 3-7 and Figure 3-8, which allows us to place our paleo-environmental results in the context of time. Subunit 1 and 2 sediments, extending from the core bottom (651 cm) to 217 cm and spanning the mid-Wisconsinan interstadial through the LGM, are characterized by low in-lake productivity, a higher proportion of mineral sediments, and relatively few organic macrofossils for radiocarbon dating (Figure 3-7; Figure 3-8). In contrast, subunit 3 and 4 sediments extending from 217 cm to the core top and spanning the Lateglacial period through the Holocene, are characterized by higher and fluctuating in-lake productivity, a lower proportion of mineral sediments, and abundant macrofossils (Figure 3-7; Figure 3-8).

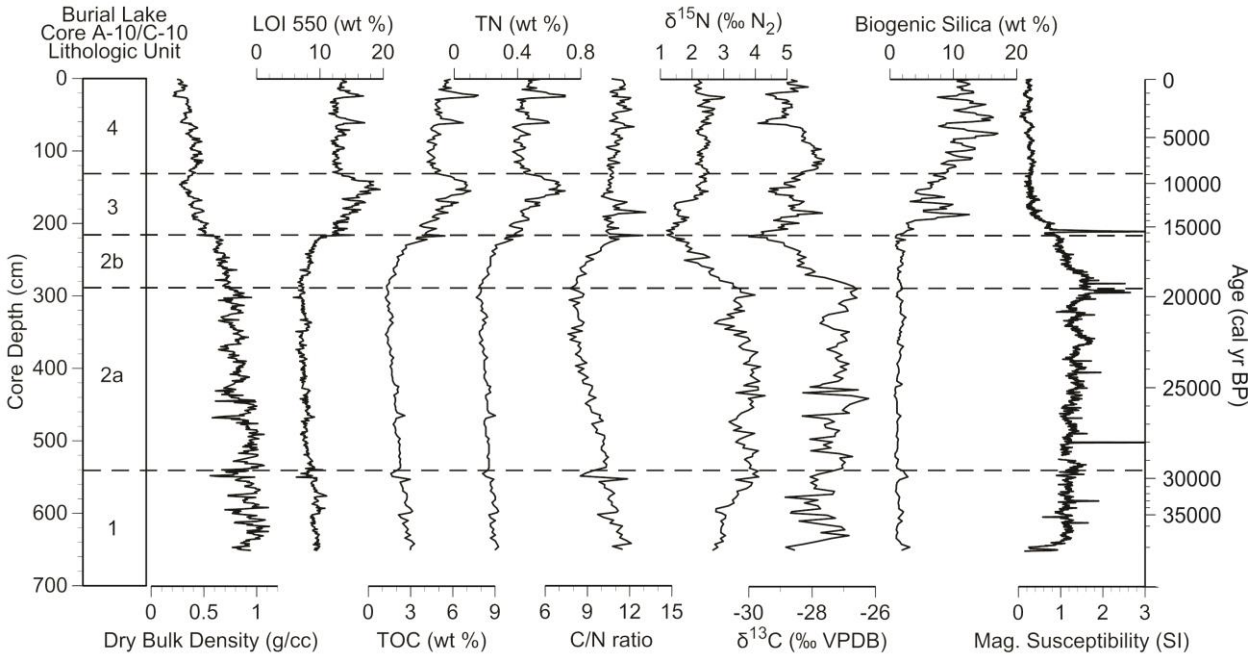

Figure 3-4. Burial Lake A-10/C-10 composite core physical and organic proxy data plotted against depth (cm) and age (cal yr BP).

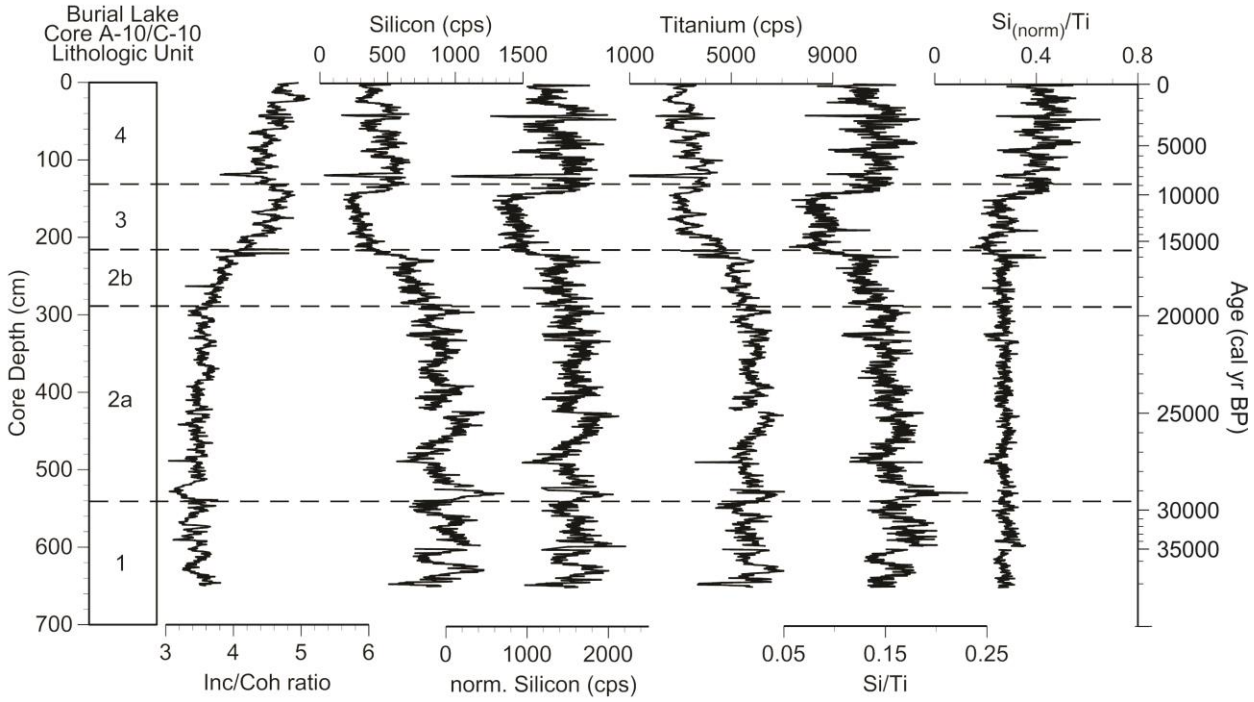

Figure 3-5. Burial Lake A-10/C-10 composite core elemental abundances from scanning XRF analysis plotted against depth (cm) and age (cal yr BP).

Table 3.2. Burial Lake core A-10/C-10 lithologic subunits including depth (cm) intervals and age (cal yr BP) ranges. Mean values for the physical, geochemical, and elemental proxy data are reported for each respective lithologic subunit.

Lithologic Subunit	Core depth cm	Age range cal yr BP	Dry BD g/cc	LOI 550 wt %	LOI 1000 wt %	Bio Si wt %	TOC wt %	TN wt %	C/N ratio
4	0 - 129	8,800 - 2010 AD	0.36	13.1	0	11.6	5.05	0.45	11.1
3	129 - 217	16,500 - 8,800	0.41	15.0	0	5.8	5.43	0.50	10.8
2b	217 - 289	19,600 - 16,500	0.68	7.6	0	1.6	2.29	0.24	9.3
2a	289 - 540	29,600 - 19,600	0.84	7.6	0	1.5	1.80	0.20	9.1
1	540 - 651	37,200 - 29,600	0.91	9.2	0	1.5	2.60	0.24	10.7

Lithologic Subunit	Core depth cm	Age range cal yr BP	$\delta^{15}N$ ‰ N_2	$\delta^{13}C$ ‰ VPDB	Mag. Susc. 10^{-5} SI	Titanium cps	Inc/Coh	$Si_{(norm)}/Ti$
4	0 - 129	8,800 - 2010 AD	2.37	-28.5	0.5	3300	4.5	0.42
3	129 - 217	16,500 - 8,800	1.84	-28.8	0.5	3500	4.5	0.28
2b	217 - 289	19,600 - 16,500	2.35	-28.2	1.2	5200	3.8	0.28
2a	289 - 540	29,600 - 19,600	3.66	-27.2	1.3	5800	3.5	0.28
1	540 - 651	37,200 - 29,600	3.22	-27.8	1.1	5700	3.5	0.28

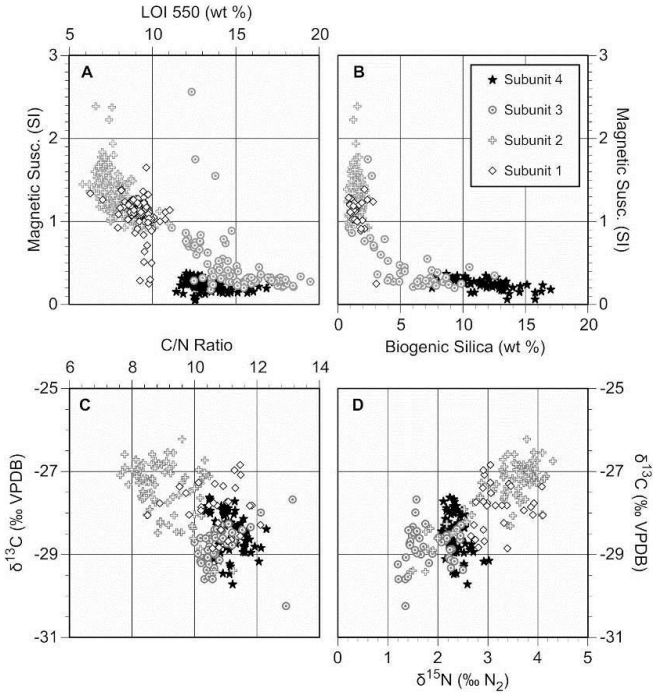

Figure 3-6. Scatterplots of Burial Lake A-10/C-10 composite core proxy data by lithologic subunit showing distinct clustering.

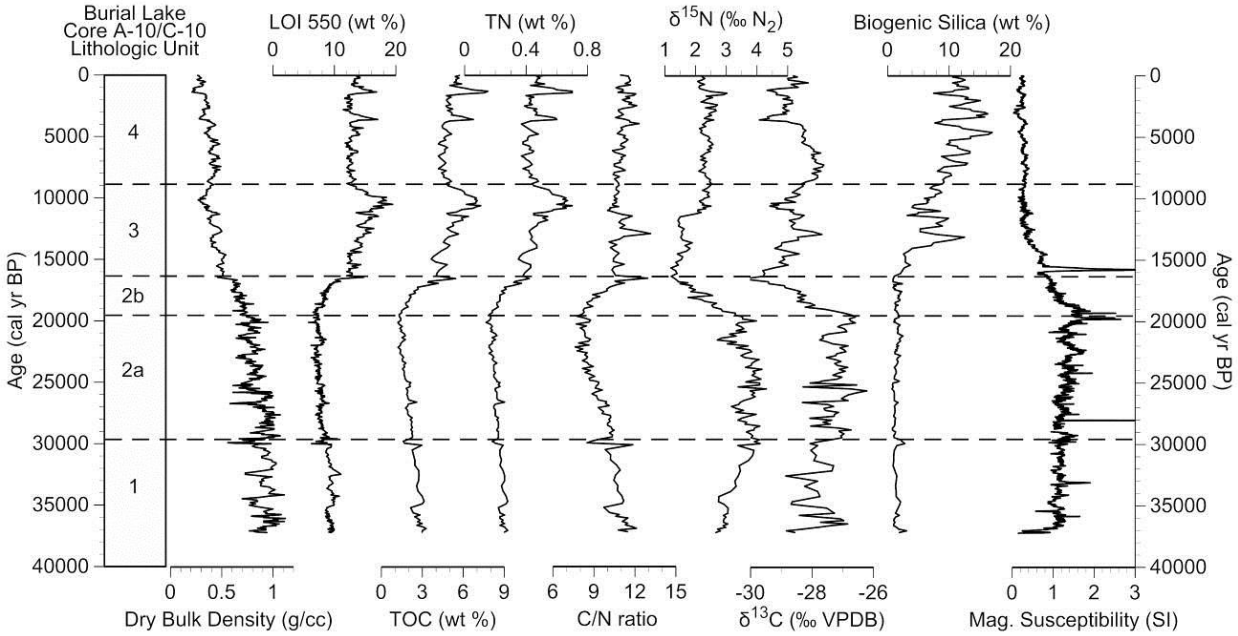

Figure 3-7. Burial Lake A-10/C-10 composite core physical and organic proxy data plotted against age (cal yr BP).

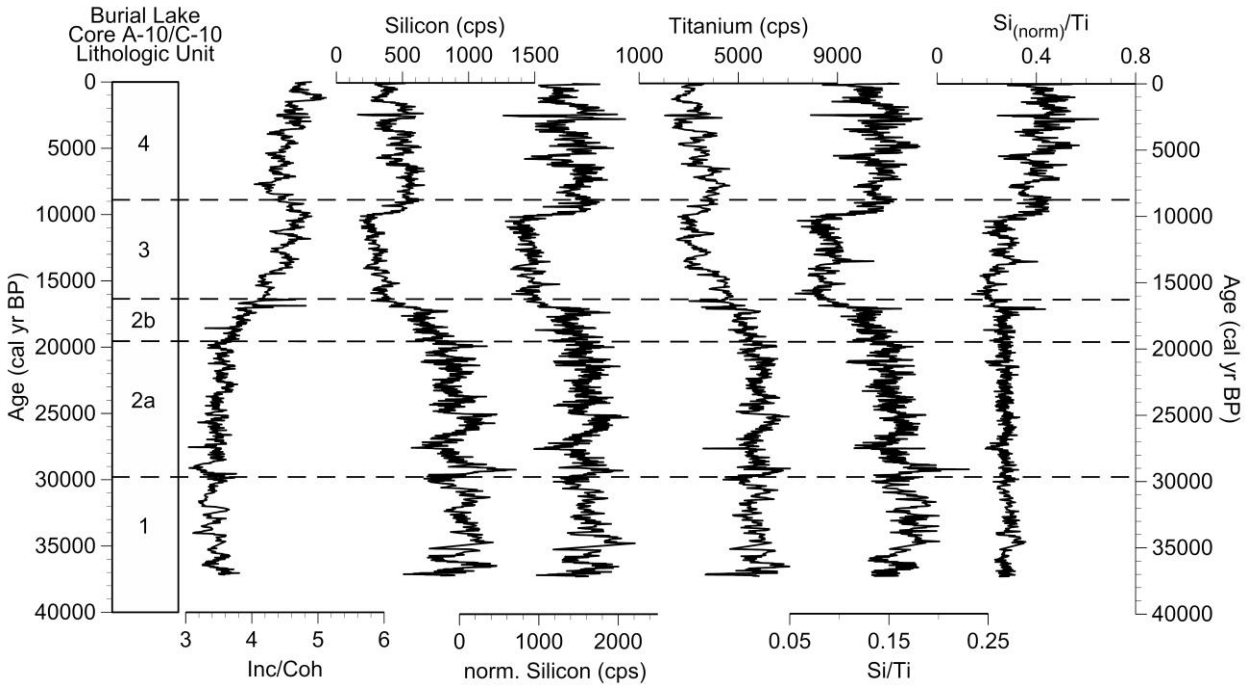

Figure 3-8. Burial Lake A-10/C-10 composite core elemental abundances from scanning XRF analysis plotted against age (cal yr BP).

3.4.4 Scanning XRF Analysis

Comparison of organic matter content determined from LOI 550 (wt %) against the Inc/Coh ratio reveal a significant positive correlation (Figure 3-9; $r^2 = 0.77$, $p < 0.01$). Further, total organic carbon (wt %) is significantly correlated with the Inc/Coh ratio (Figure 3-9; $r^2 = 0.85$, $p < 0.01$). As a result, we use the Inc/Coh ratio as a high resolution (0.5 cm spacing) proxy for the relative proportion of organic matter in Burial Lake sediments.

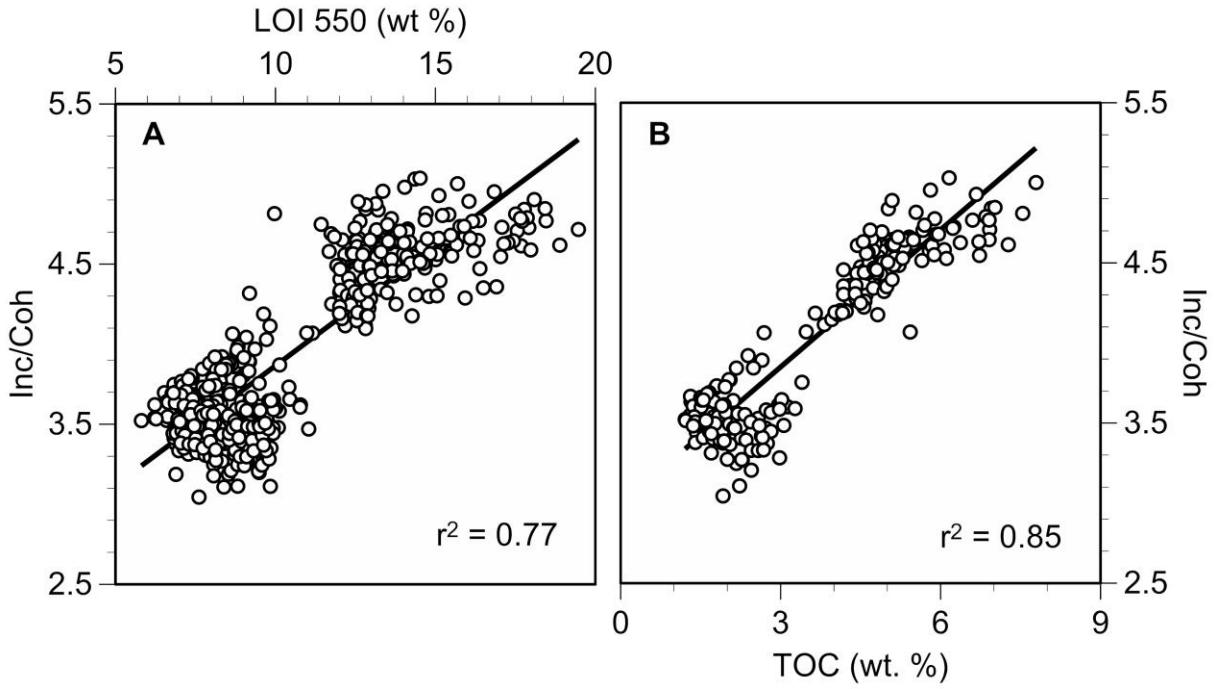

Figure 3-9. Correlation of incoherent to coherent (Inc/Coh) scattering ratio from scanning XRF analysis against A) organic matter (wt. %) and B) total organic carbon (wt %).

Scatterplots of silicon and titanium (Figure 3-10) reveal distinct clustering and separate populations of data. We suspect the large difference in organic matter content between subunit 1 and 2 sediments with low values and subunit 3 and 4 sediments with higher and fluctuating values influenced the XRF counts through matrix effects (Löwemark et al., 2011). To account for the substantial difference in organic matter content, matrix-corrected silicon counts ($Silicon_{(norm)}$) were calculated by normalizing raw silicon counts with the Inc/Coh ratio using an empirically determined formula (Melles et al., 2012):

$$\text{Silicon}_{(\text{norm})} = \frac{Silicon\ (raw)}{3.2994 * e^{-0.505 * Inc/Coh}}$$

Equation 3.1. Empirically determined equation to calculate a matrix-corrected Silicon count with X-Ray Fluorescence derived elemental data (Melles et al., 2012).

Comparison of $Silicon_{(norm)}$ and titanium data (Figure 3-10) indicate clustering between glacial (subunit 1 and 2) sediments while interglacial (subunit 3 and 4) sediments plot in distinct and separate space, indicating changing sources of silicon and titanium over time. For example, $Silicon_{(norm)}$ and titanium from glacial age sediments (37,200 – 16,500 cal yr BP) are well-correlated ($r^2 = 0.52$, $p < 0.01$), suggesting both metals originate from a common detrital source. In contrast, $Silicon_{(norm)}$ and titanium from late-glacial and Holocene sediments (16,500 cal yr BP to 2010 AD) are poorly correlated ($r^2 = 0.11$, $p < 0.01$) and indicate both detrital and biogenic contributions of silicon. Correlation analysis between $Si_{(norm)}$/Ti data against measured biogenic silica values (Figure 3-9) again show distinct clustering and two distinct statistical populations. The correlation between subunit 1 and 2 sediments, characterized by low and stable biogenic silica concentrations, is very poor (Figure 3-9; $r^2 = 0.01$, $p < 0.22$). In comparison, the correlation between subunit 3 and 4 sediments, characterized by rising and fluctuating biogenic silica concentrations, show a strong positive relationship (Figure 3-10; $r^2 = 0.71$, $p < 0.01$) and demonstrate that $Si_{(norm)}$/Ti values track changes in the relative proportion of biogenic silica over the last 16,500 years.

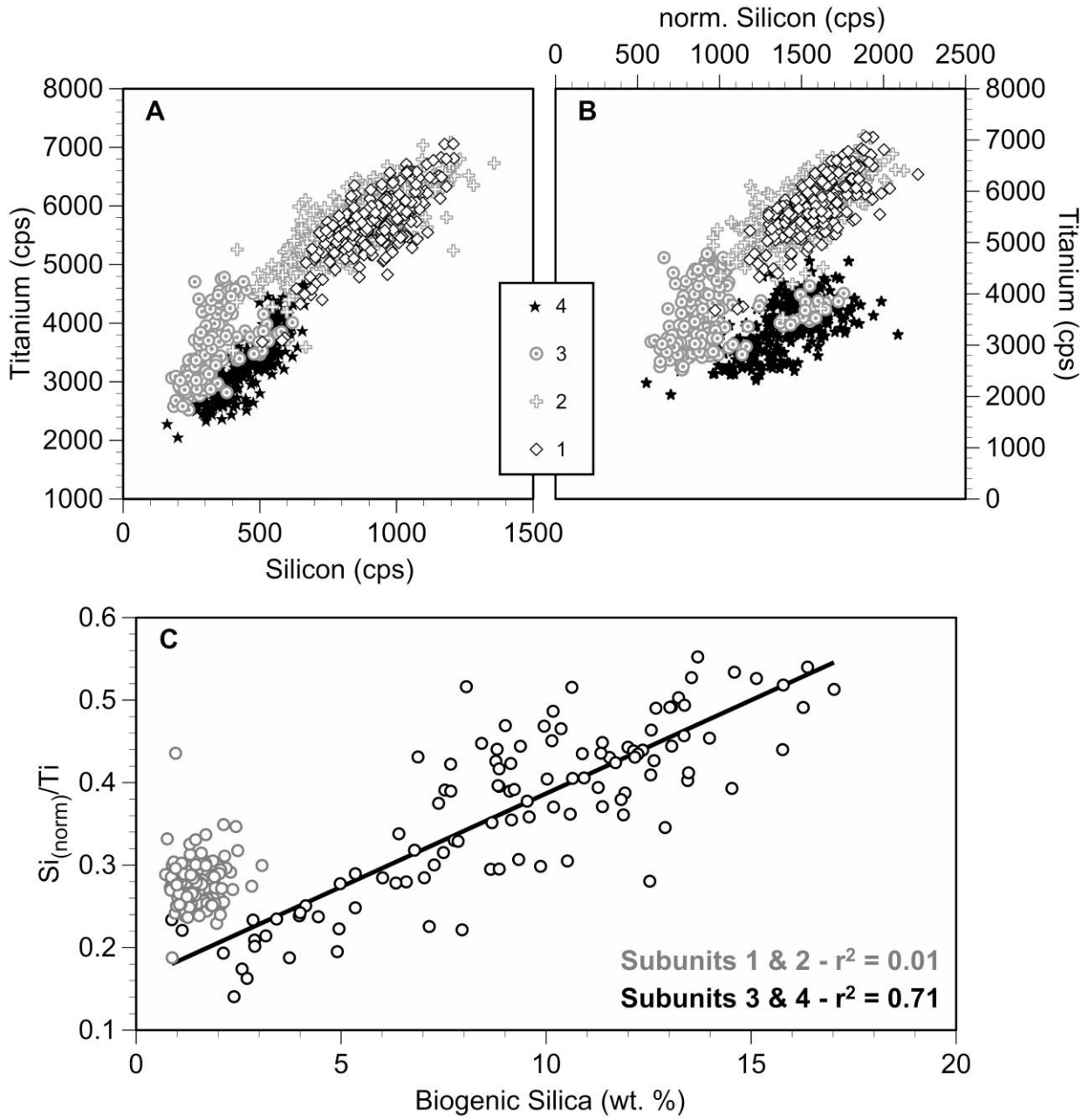

Figure 3-10. Scatterplots of scanning XRF data by lithologic subunit, including A) silicon (cps) against titanium (cps) and B) silicon normalized to Inc/Coh ratio (Melles et al., 2012) against Titanium (cps). C) Correlation between $Si_{(norm)}/Ti$ against biogenic silica (wt. %) for lithologic subunits 1 and 2 (r^2 = 0.01) and lithologic subunits 3 and 4 (r^2 = 0.71).

3.4.5 Lithologic Subunit Descriptions

Subunit 1 extends upward from the base of the composite core (651 cm) to 540 cm and spans the interval ~37,200 to ~29,600 cal yr BP. The basal sediments from 651 to 618 cm consist of dark yellow brown (10YR 4/2) to grayish brown (5YR 3/2), fine to medium sandy argillaceous silt with occasional banding and faint laminae (Figure 3-3). The upper portion from 618 to 540 cm consist of dark yellow brown (10YR 4/2) to grayish brown (5YR 3/2), fine to medium sandy argillaceous silt and a minor proportion of coarse sand and granules, with occasional banding and faint laminae (Figure 3-3). The banding and faint laminae throughout subunit 1 presumably represent small variations in sediment organic matter content or subtle grain size variations. Powder XRD analysis of a sample at 613-614 cm indicate quartz is the dominant mineral phase present (Figure 3-11). Smear-slide analysis of several samples shows very few diatom frustules and a large proportion of silicate mineral matter. Subunit 1 sediments are characterized by relatively high and variable dry bulk density, magnetic susceptibility, and titanium values (Figure 3-4; Figure 3-5; Table 3.2). Biogenic silica is low and stable, and indicates minimal aquatic productivity. Organic matter and Inc/Coh are low with little variability, and gradually decrease up-section towards the subunit 2 boundary. Organic matter $\delta^{13}C$ values are moderate to high and exhibit considerable variability, while organic matter $\delta^{15}N$ values gradually increase through subunit 1 (Figure 3-4). C/N ratios are relatively low during this interval and gradually decrease up-section towards the Zone 2 boundary (Figure 3-4).

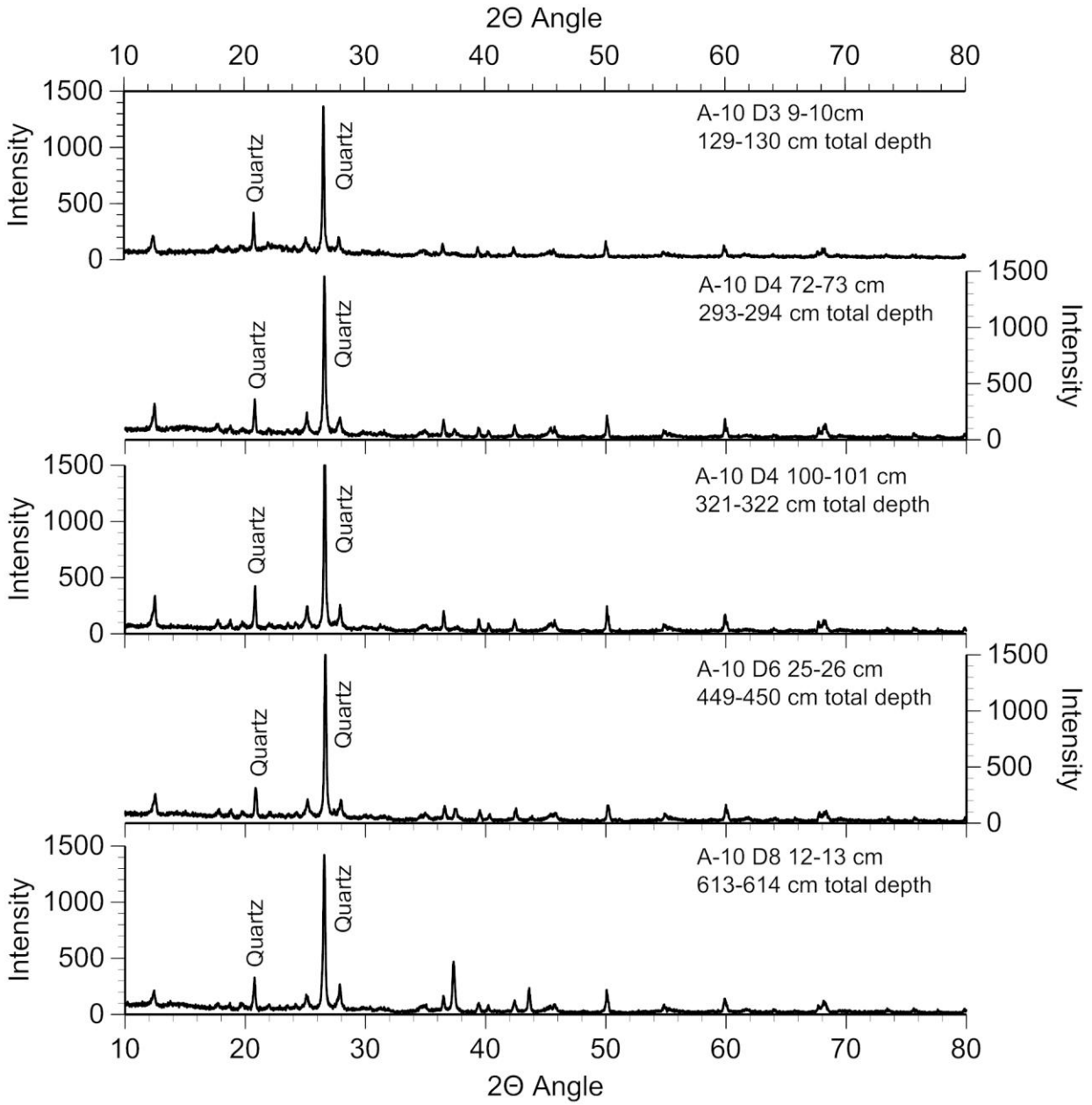

Figure 3-11. Powder x-ray diffraction (XRD) spectra for select samples from the Burial Lake composite core.

Subunit 2 extends from 540 cm to 217 cm and spans the period ~29,600 to ~16,500 cal yr BP. The contact with subunit 1 sediments is gradual and sediments primarily consist of dark yellow brown (10YR 4/2) to grayish brown (5YR 3/2), fine to

medium sandy argillaceous silt and a minor proportion of coarse sand and granules (Figure 3-3). Powder XRD analysis of samples at 449-450 cm, 321-32 cm, and 293-294 cm depth indicate quartz is the dominant mineral phase present (Figure 3-11). Smear-slide analysis of select samples from subunit 2 shows few diatom frustules and a large proportion of silicate mineral matter. Distinct layers of fine sand to granules are present from 489 - 489.5 cm and 264 – 264.5 cm. The layers compositionally represent a mix of lithologies, including mafic to felsic crystalline rocks, gray sandstone particles, and quartz grains that are sub-angular to sub-rounded in shape. The contact between the underlying and overlying finer sediments is horizontal and sharp. Although direct age control in subunit 2 is lacking and is based on interpolation, sedimentation rates are apparently the highest (at ~25 cm/ka yr). Terrestrial macrofossils > 63 μm are virtually absent in subunit 2 sediments, besides a small amount of grass isolated from sediment at 359-360 cm (UCIAMS # 109363). Subunit 2 is divided further into subunit 2a (540 to 289 cm) and subunit 2b (289 to 217 cm) based on subtle variability in the organic and inorganic geochemical proxies, many of which show a change in trend at the 2a/2b boundary.

Subunit 2a extends from 540 cm to 289 cm and spans the period ~29,600 to ~19,600 cal yr BP. The sediments are characterized by high, variable, and gradually declining dry bulk density and the highest magnetic susceptibility and titanium values for the entire record (Figure 3-4; Figure 3-5; Table 3.2). Biogenic silica values are uniformly low, stable, and similar to subunit 1 values. Organic matter is the lowest over the entire record and gradually decreases up-section in subunit 2a and attains the lowest values between 374 and 300 cm (Figure 3-4). Inc/Coh values are low, stable,

and similar to subunit 1 values. Organic matter $\delta^{13}C$ and $\delta^{15}N$ values are the highest (most positive) throughout the entire record and display considerable variability throughout subunit 2a (Figure 3-4). C/N ratios gradually decrease from the base of subunit 2a up-section and attain the lowest values over the entire record toward the subunit 2b boundary (Figure 3-4).

Subunit 2b extends from 289 cm to 217 cm and spans the period 19,600 to 16,500 cal yr BP. The subunit 2b transition is marked by declining dry bulk density, magnetic susceptibility, and titanium values that continue towards the subunit 3 boundary (Figure 3-4; Figure 3-5; Table 3.2). Biogenic silica values are low, stable, and similar to subunit 2a values (Figure 3-4). Organic matter, Inc/Coh, and C/N ratios gradually increase from their minimum values at the base of subunit 2b toward the subunit 3 boundary (Figure 3-4; Figure 3-5;). In addition, organic matter $\delta^{13}C$ and $\delta^{15}N$ gradually decrease from maximum values at the base of subunit 2b and attain their lowest (negative) values at the subunit 3 boundary (Figure 3-4).

Subunit 3 extends from 217 cm to 129 cm and spans the period ~16,500 to ~8,800 cal yr BP. The contact with subunit 2b sediments is rather abrupt (in comparison to the subunit 1 and 2 transition) and sediments consist of homogenous dark yellow brown (10YR 4/2) to pale yellowish brown (10YR 6/2), very fine argillaceous sandy silt (Figure 3-3). Powder XRD analysis of a sample at 129-130 cm indicates quartz is the dominant mineral phase present (Figure 3-11). Organic macrofossil rich, 1-2 mm thick layers are present at 196.5 to 214 cm, respectively. Smear-slide analysis of select samples from subunit 3 shows a substantial increase in the proportion of diatom frustules with no evidence of dissolution and abundant silicate mineral matter.

The subunit 3 transition is characterized by declining and lower dry bulk density, titanium, magnetic susceptibility (Figure 3-4; Figure 3-5; Table 3.2), and a lower but variable sedimentation rate (9 to 19 cm/ka yr), in comparison with the previous (subunit 2) interval. An abrupt spike in magnetic susceptibility occurs at ~ 210 cm (Figure 3-4) and represents a brief return to higher values. Biogenic silica values increase up-section from the base of subunit 3, subsequently peak at 12.5 % at 186 cm, and fluctuate and gradually decrease up-section toward the subunit 4 transition (Figure 3-4). $Si_{(norm)}/Ti$ values track the general trends in biogenic silica through subunit 3 (Figure 3-5). Organic matter and Inc/Coh values increase up-section from the base of subunit 3 and peak at the highest values over the entire record between 153 and 141 cm (10,500 to 9,900 cal yr BP). Organic matter $\delta^{13}C$ values are isotopically lighter on average compared with subunit 1 and 2 sediments, and fluctuate substantially throughout subunit 3 (Figure 3-4; Table 3.2). Similarly, organic matter $\delta^{15}N$ values are lower but generally more stable compared with the previous lithologic zones. C/N ratios are on average the highest throughout subunit 3 (Figure 3-4), and the record is punctuated by several abrupt increases. A greater abundance of terrestrial macrofossils for radiocarbon dating is evident in subunit 3 and sedimentations rates are relatively low and stable (13 cm/ka yr average).

Subunit 4 extends from 129 cm to the core top and spans the period 8,800 cal yr BP to 2010 AD. The contact with subunit 3 is gradual and sediments consist of homogenous grayish brown (5YR 3/2) to dusky brown (5YR 2/2), argillaceous silt sediment with no obvious sedimentary structures (Figure 3-3). Smear-slide analysis of select samples from subunit 4 shows a general abundance and diversity of diatom

frustules, no obvious evidence of dissolution, and substantial variability in diatom proportion over intervals of 5 to 10 cm. Further, smear-slides shows an abundance of silicate mineral matter. Subunit 4 sediments are characterized by low dry bulk density, titanium, and magnetic susceptibility values (Figure 3-4; Figure 3-5; Table 3.2). Organic matter values are generally stable and intermediate, compared to higher values in subunit 3 and lower values in subunits 1 and 2. In contrast, Inc/Coh values gradually increase throughout subunit 4 and attain the highest values over the entire record over the upper 15 cm. Organic matter $\delta^{13}C$ values are quite variable and similar in magnitude while $\delta^{15}N$ values are generally stable and more positive compared to subunit 3 sediments. C/N ratios are stable and on average higher than any time previously. Biogenic silica and $Si_{(norm)}/Ti$ values are higher than any time during the entire record and display substantial variability over 5 to 10 cm intervals (Figure 3-4; Figure 3-5; Table 3.2). Terrestrial macrofossils are present throughout subunit 4 sediments and sedimentation rates are low (15 cm/ka yr average) and generally stable.

3.5 DISCUSSION

The Burial Lake sediment record shows no evidence of major unconformities (e.g. mud cracks, erosional surfaces, etc.) found in intermediate water depth cores (Abbott et al., 2010) that would indicate discontinuous sedimentation in the lake depocenter. However, the distinct 5 mm thick sand and granule layers at 264 cm and 489 cm provide sedimentological evidence for a high energy transport process at the lake depocenter. Given the lack of a surficial input, we hypothesize the sediments are

reworked from the shoreline during a period of lower lake levels (Abbott et al., 2010), when the lake surface area was much smaller and the distance from shoreline to depocenter was substantially reduced. Alternatively, the coarse sediment layers could represent turbidity flows and re-working of shelf sediments. However, this explanation is inconsistent with physical sedimentology that shows sharp underlying and above contacts and a lack of textural grading. Further, the coarse layers could represent sub-aerially exposed shoreline sediments or a lag from winnowing of fine sediments in a very shallow lake from wave-base erosion, both of which might result in disconformities. Unfortunately, radiocarbon constraints throughout lithologic subunit 2 are lacking to directly assess the possibility of these layers representing disconformities. We suggest the nature of the coarse sediment layer contacts (i.e. horizontal and sharp) and minimal thickness (only 5 mm) indicate the features do not represent discontinuous sedimentation. In contrast, the major unconformity present in the intermediate water depth cores from Burial Lake is characterized by a clear erosional and irregular contact (Abbott et al., 2010). The underlying ~ 30 cm of sediment consists of sand and gravel, interpreted to reflect a lag-deposit formed via deflation and winnowing of fine sediments (Abbott et al., 2010), which is sedimentologically distinct compared with the coarse layers in the depocenter cores. We therefore suggest the Burial Lake sediment record is continuous and spans the last 37,200 cal yr BP. However, we acknowledge that age control between 219 cm and 553 cm spanning the period ~ 16,800 to ~ 30,100 cal yr BP (median ages) is based on a linear interpolation (Figure 3-3), and therefore the timing of paleoenvironmental transitions during this time are limited.

To our knowledge, the Burial Lake record provides the oldest continuous lacustrine record to date from northwest Alaska and therefore provides a unique archive to explore environmental changes in Arctic Alaska from the Mid-Wisconsinan interstadial (Marine Isotope Stage 3; MIS3) to the present. We integrate our results with a complimentary environmental magnetic investigation from Burial Lake (Dorfman, 2013) and focus our comparison on S-ratios (Figure 3-12), a sensitive indicator of dust input to the lake. Higher S-ratios are interpreted to reflect periods of increased dust accumulation while lower values indicate periods of diminished flux (Dorfman, 2013). We also interpret the results from our sediment record in light of the gradual changes in in eustatic sea level (Figure 3-12) (Clark et al., 2009 and references therein) and July insolation at 65° North (Figure 3-12) (Berger and Loutre, 1991). Further, we compare our paleoenvironmental interpretations with several regional lacustrine records, the extent of Brooks Range alpine glaciers (Figure 3-12) (Briner and Kaufman, 2008), and several marine sediment records from the Bering and Chukchi seas (Caissie et al., 2010; Keigwin et al., 2006; Max et al., 2012).

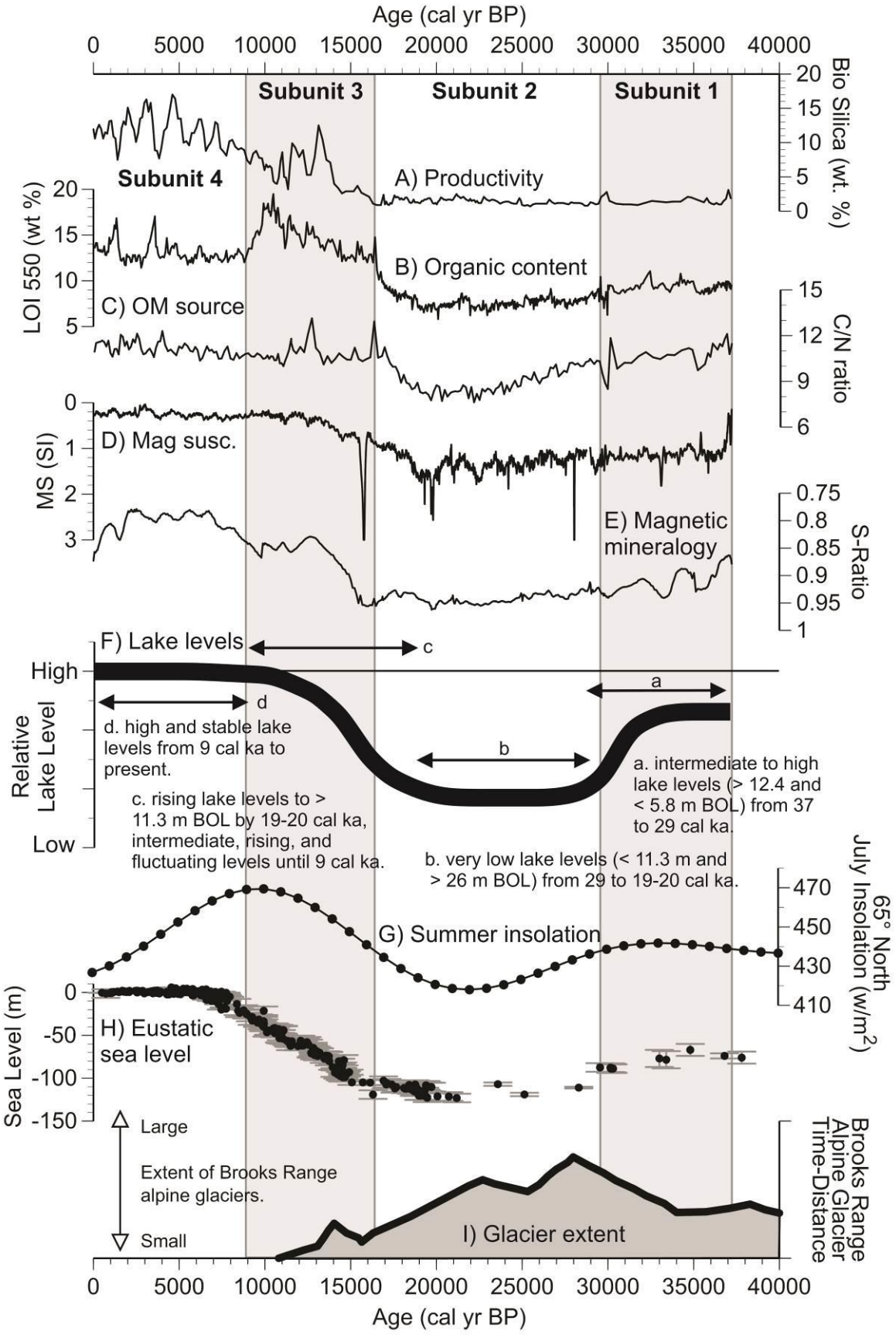
Age (cal yr BP)
0
5000
10000
15000
20000
25000
30000
35000
40000
Subunit 3
Subunit 2
Subunit 1
Subunit 4
Bio Silica (wt. %)
20
15
10
5
0
A) Productivity
LOI 550 (wt %)
B) Organic content
C) OM source
C/N ratio
MS (SI)
D) Mag susc.
E) Magnetic mineralogy
S-Ratio
F) Lake levels
High
Low
Relative Lake Level
d
c
a
b
d. high and stable lake levels from 9 cal ka to present.
c. rising lake levels to > 11.3 m BOL by 19-20 cal ka, intermediate, rising, and fluctuating levels until 9 cal ka.
a. intermediate to high lake levels (> 12.4 and < 5.8 m BOL) from 37 to 29 cal ka.
b. very low lake levels (< 11.3 m and > 26 m BOL) from 29 to 19-20 cal ka.
G) Summer insolation
65° North July Insolation (w/m2)
H) Eustatic sea level
Sea Level (m)
Large
Extent of Brooks Range alpine glaciers.
Small
I) Glacier extent
Brooks Range Alpine Glacier Time-Distance

Figure 3-12. Burial Lake A-10/C-10 composite core proxy data including A) biogenic silica, B) LOI 550, C) C/N ratio, D) magnetic susceptibility (SI), E) s-ratio that describes the relative proportion of low coercivity to high coercivity magnetic material, which is interpreted to reflect the regional input of dust into to Burial Lake (Dorfman, 2013), and F) Burial Lake estimated lake level (m) curve (Abbott et al., 2010). The data is also compared to G) 65° North July insolation (Berger and Loutre, 1991), H) relative eustatic sea level (Clark et al., 2009), and I) time-distance diagram of Brooks Range, Alaska alpine glacier extent (Briner and Kaufman, 2008).

In addition, we present a relative lake-level curve (Figure 3-12) based on previous work of Burial Lake sediments (Abbott et al., 2010) and integrate the results from a chironomid-inferred temperature reconstruction (Kurek et al., 2009). The lake-level curve, based on core-transects and the conceptual model relating fine-grained organic sediments with deeper water and coarse-grained minerogenic sediments with shallower water, presents the major multi-millennial to orbital trends (Figure 3-12). To ensure consistency, the radiocarbon and age model data are updated using the IntCAL09 calibration curve (Reimer et al., 2009). We make two additional changes to the age to depth model presented in Abbott et al. (2010), resulting from re-interpretations based on proxy evidence from the A-10/C-10 composite cores. First, for core C-98 Abbott et al. (2010) extrapolated linearly from a radiocarbon date at 289 cm depth (19,880 cal yr BP) to the unconformity at 340 cm to estimate the upper age of the LGM lake level low stand. Although our age control for the A-10/C-10 core is limited through the LGM (Figure 3-3), proxy evidence shows that very low organic matter and high magnetic susceptibility values persist through subunit 2 (Figure 3-4) until 19,800 cal yr BP. Accordingly, we assert the radiocarbon date at 289 cm in core C-98 (Table 3.3) best constrains the resumption of lake sedimentation at this intermediate water

depth core site, and therefore do not extrapolate ages from this interval down to the unconformity. Second, the basal age from core A-98 at 92 cm (20,060 cal yr BP) consisted of matted grass situated atop coarse gravel sediments (Abbott et al., 2010). The transition to fine-grained lake sediments occurs above the basal gravel in core A-98. The reported basal age from core A-98 therefore only provides a maximum limiting age for the major lake level transgression that inundated this shallow water core site. Accordingly, we utilize the updated calibration data (Table 3.3) and modified C-98 age model (Figure 3-13) to generate an estimated lake-level curve (Figure 3-12) and to integrate the results from previous investigations of Burial Lake sediments with the results of this study.

Table 3.3. AMS radiocarbon dates for Burial Lake core C-98 and A-98 with calibrated 2s error ranges using the IntCAL09 calibration curve. Samples highlighted with an asterisk (*) were omitted from the age to depth model.

Sample ID	Core-Drive	Total Depth (cm)	Material	^{14}C Age (^{14}C yr)	Error (yr)	Calib. Age IntCAL09 (yr BP)
OS-18365	GL-1 D1	20.0	Macrofossil	1,850	110	1,625-1,921
AA-35197	C-98 D2	128.5	Macrofossil	8,390	280	9,011-9,606
CAMS-73172	C-98 D3	216.0	Macrofossil	12,020	380	13,397-14,803
* AA-35195	C-98 D3	220.0	Macrofossil	640	170	516-724
OS-17700	C-98 D3	236.0	Wood	13,150	130	15,269-16,536
OS-18367	C-98 D3	272.5	Wood	15,300	360	18,028-18,848
CAMS-73173	C-98 D3	289.0	Macrofossil	16,740	520	19,404-20,477
* AA-35198	C-98 D4	306.5	Macrofossil	14,660	500	17,193-18,521
* AA-35199	C-98 D4	357.5	Macrofossil	20,330	560	23,585-24,982
OS-18368	C-98 D4	375.5	Wood	30,300	600	34,472-36,160
CAMS-73174	C-98 D5	407.5	Macrofossil	31,680	720	35,161-36,771
CAMS-73175	C-98 D5	407.5	Wood	32,770	940	36,526-38,629
OS-27279	C-98 D5	440.0	Macrofossil	32,780	560	36,669-38,427
* OS-18369	C-98 D5	447.5	Humic extract	42,600	5,600	42,500-50,000
AA-35196	A-98 D1	92.0	Macrofossil	16,900	270	19,438-20,959

1

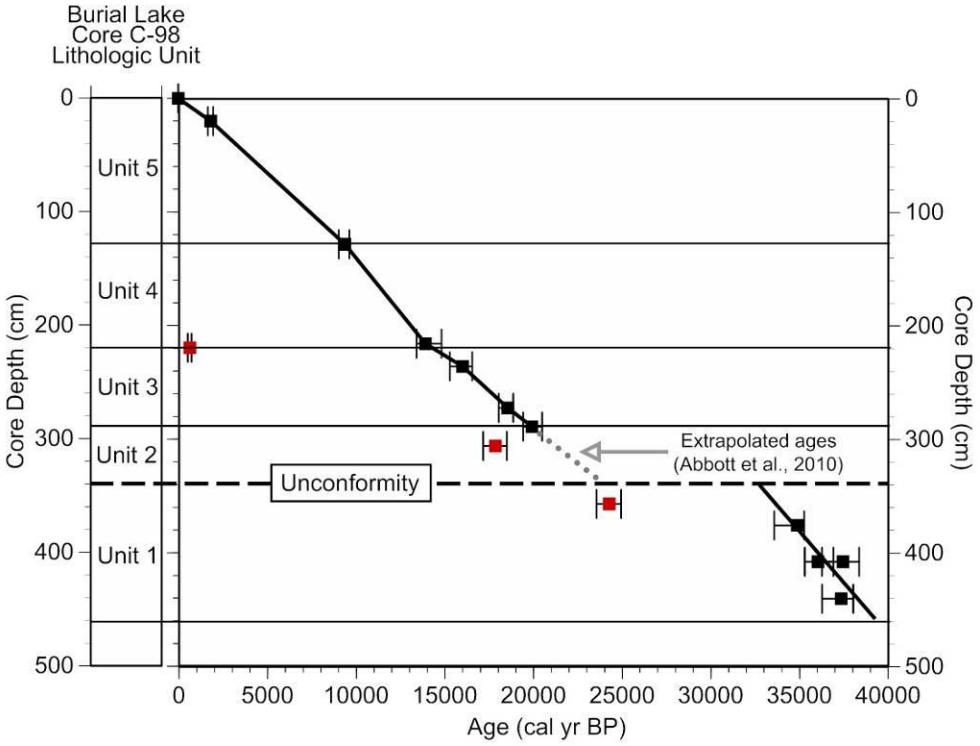

Figure 3-13. Burial Lake C-98 core revised age-depth model. Samples designated with a red square were rejected from the age model.

3.5.1 Interpretation of the carbon and nitrogen isotopic composition of organic matter

The carbon stable isotopic composition ($\delta^{13}C$) of organic matter in lake sediments is controlled by several factors including the contribution of various sources (algal, terrestrial) and changes in the respective photosynthetic pathways, changes in aquatic productivity, and the $\delta^{13}C$ of dissolved inorganic carbon (DIC) inputs to a lake (Finney et al., 2012; Meyers and Ishiwatari, 1993; Meyers and Teranes, 2001). Variations in Burial Lake C/N ratios, which assess the relative proportion of terrestrial (C/N > 20) versus aquatic (C/N < 10) source inputs (Meyers and Teranes, 2001),

indicate a mixed algal-terrestrial and at times primarily algal source of organic matter over the last 37,000 years (Figure 3-7). Pollen analysis of Burial Lake sediments also document changing vegetation patterns and a shift from herb tundra conditions, during the late mid-Wisconsinan interstadial and LGM, to shrub tundra during the Lateglacial and Holocene periods (Abbott et al., 2010). In addition to organic matter source changes, we hypothesize that variations in $\delta^{13}C$ are controlled by changes in aquatic productivity and the $\delta^{13}C$ of CO_2 supplied to Burial Lake for algal utilization. Increasing algal productivity levels correspond with higher $\delta^{13}C$ values, and vice versa for decreasing productivity (Meyers and Teranes, 2001). Variable concentrations of sedimentary biogenic silica attest to changing levels of algal productivity over the last 37,000 years. Further, changes in the $\delta^{13}C$ of dissolved CO_2 supplied to Alaskan lakes has been shown to influence the $\delta^{13}C$ of sedimentary organic matter (Finney et al., 2012). Several Alaskan lakes have surface water pCO_2 concentrations above atmospheric levels, due to inputs of watershed-respired CO_2 from permafrost or organic rich soils (Kling et al., 1991). In such lacustrine systems, increased inputs of watershed-respired CO_2 with relatively low $\delta^{13}C$ values typical of C3 plants (~ -27 ‰) results in relatively low $\delta^{13}C$ organic matter content (Finney et al., 2012). Two surface water samples from Burial Lake were pCO_2 supersaturated (481 ppm, 509 ppm), providing evidence that inputs of watershed respiration products affect the $\delta^{13}C$ of dissolved inorganic carbon inputs to the lake for phytoplankton utilization. Therefore, we interpret organic matter $\delta^{13}C$ trends in light of source changes, but also due to changes in productivity and from variable inputs of landscape derived and respired organic matter.

The interpretation of the nitrogen stable isotopic composition ($\delta^{15}N$) of organic matter in lake sediments is difficult because biogeochemical cycling of nitrogen is more complex than carbon. The lack of modern physical and chemical limnological data further limit our understanding of nitrogen cycling at Burial Lake. Variations in the $\delta^{15}N$ of organic matter might reflect changing productivity and the relative sources and isotopic composition of nitrogen supplied to lakes (Hu et al., 2001; Meyers and Teranes, 2001). In addition, the $\delta^{15}N$ of sedimentary organic matter might be controlled by variations in the availability of reactive nitrogen (relative supply versus demand) inputs arising from hydroclimate variability. Global-scale studies have found that soil and plant $\delta^{15}N$ values increase with decreasing precipitation and increasing N availability (Amundson et al., 2003; Craine et al., 2009), indicating that climate plays a significant role in N cycling. Further, the isotopic composition of atmospheric NOx (Hastings et al., 2005) has changed dramatically over the last 37,000 years, with relatively higher values during MIS3 (and the LGM) compared to the Holocene. Thus, we interpret organic matter $\delta^{15}N$ trends in the Burial Lake sediment record to reflect a combination of changes in productivity, the availability of reactive nitrogen driven by hydroclimate, and from changes in the isotopic composition of atmospheric nitrogen inputs over time.

3.5.2 The Mid-Wisconsinan Interstadial (37,200 to 29,600 cal yr BP)

The presence of fine-grained lacustrine sediment (fine to medium sandy silt) with relatively intermediate organic content at the base of lithologic subunit 1 (Figure 3-3), combined with core-transect data (Abbott et al., 2010), suggest lake levels remained at intermediate to high levels from 37,200 to 36,100 cal yr BP. Specifically, core-transect

data indicate lake levels were > 12.4 m below overflow level (BOL) from 37,200 to 33,000 cal yr BP (Abbott et al., 2010) (Figure 3-12). An erosional unconformity in intermediate water depth core C-98 from Burial Lake indicates a drop in lake level below 11.3 M water depth occurred sometime after 33,000 cal yr BP (Abbott et al., 2010). The transition to coarser sediments (fine to medium sandy argillaceous silt with coarse sand and granules) at 36,100 cal yr BP that persists until 16,500 cal yr BP indicates a change in paleoenvironmental conditions relative to the preceding period at Burial Lake. The lithology during this period is consistent with the process of ice-rafting over the lake (Smith, 2000). Alternatively, the granules could originate from aeolian transport and deposition on the frozen lake surface, with subsequent melting resulting in drop stone deposition (Lewis et al., 2002). Lake ice covers the modern system for 9 months a year, yet coarse sediments (coarse sand to granules) are absent for the last 16,500 cal yr BP. Accordingly, we favor an increase in aeolian activity to explain the coarser sediments. This assertion is supported by relatively high magnetic susceptibility and titanium concentrations over subunit 1, and the distinct magnetic signature originating from wind-blown (aeolian) sources (Dorfman, 2013). Potential local sources of aeolian input to the lake at this time include alluvial sediments along aggrading rivers and sub-aerially exposed glaciolacustrine sediments (Hamilton, 2001), while a far afield source could originate from the exposed Chukchi continental shelf (Dorfman, 2013). Low and gradually declining C/N ratios and relatively heavy (positive) organic matter $\delta^{13}C$ values indicate organic matter originated primarily from aquatic (in-lake) sources (Finney et al., 2012; Meyers and Ishiwatari, 1993), though the low organic matter and biogenic silica values attest to low levels of aquatic productivity (Figure 3-12). The gradual increase in

$\delta^{15}N$ values through the mid-Wisconsinan interstadial (Figure 3-7) corresponds with increasing aridity and lower lake-levels (Abbott et al., 2010), suggesting that changes in $\delta^{15}N$ reflect changing hydroclimate conditions and relatively high N availability (compared with demand) (Amundson et al., 2003; Craine et al., 2009). In addition, increasing and relatively high $\delta^{15}N$ values at Burial Lake could in part reflect relatively high atmospheric NO_x levels during MIS3 (Hastings et al., 2005). Palynological evidence from the C-98 core indicate a tundra landscape with cool and dry conditions compared with the present (Abbott et al., 2010). Overall, proxy evidence from this study and core-transect data demonstrate relatively high lake levels and an interstadial climate with slightly drier and windy conditions compared to the present.

Evidence from Burial Lake provides additional support for interstadial climate conditions > 30,000 cal yr BP in eastern Beringia with warmer and slightly wetter conditions compared with the LGM (Anderson and Lozhkin, 2001 and references therein). In the Noatak Basin, interstadial conditions are reported between 36 to 30 ka ^{14}C years from organic floodplain deposits and palaeosols along Noatak River (Hamilton, 2001). Additional lake records have since been reported from Zagoskin Lake and Arolik Lake in western Alaska, respectively that show slightly more mesic conditions than the following full glacial interval (Ager, 2003; Kaufman et al., 2003). Interstadial conditions occur during a time of relatively high Northern Hemisphere summer insolation (Figure 3-12), reduced alpine glacier extent (Figure 3-12), and when eustatic sea levels were -80 to -60 m lower than modern conditions (Figure 3-12). These intermediate sea levels would have produced a Bering Land Bridge of reduced size compared with the LGM lowstand. As a result, the transport distance of moisture-laden

air masses from the North Pacific Ocean travelling towards Alaska would have been similar to that during the Lateglacial transition (14,000 to 16,000 cal yr BP) where notable increases in effective moisture and higher lake-levels are reported across interior and northern Alaska (Abbott et al., 2000; Finkenbinder et al., 2014; Gaglioti et al., 2014; Mann et al., 2002).

3.5.3 The Last Glacial Maximum (29,600 to 19,600 cal yr BP)

Burial Lake sediments and proxy data across lithologic subunit 2 indicate a two-phase structure that corresponds to the LGM (29,600 – 19,600 cal yr BP) and the last deglaciation (19,600 – 16,500 cal yr BP). The highest magnetic susceptibility values and relatively high titanium concentrations between 29,600 – 19,600 cal yr BP suggests a substantial flux of mineral sediments, which likely originated from wind-blown sources (Dorfman, 2013). The lowest C/N ratios indicate organic matter was primarily sourced from aquatic (in-lake) sources (Meyers and Ishiwatari, 1993) during the LGM. The relatively high $\delta^{13}C$ values coincide with the period of lowest lake-levels and the deposition of coarse-grained mineragenic sediments. We interpret organic matter $\delta^{13}C$ trends to reflect changes driven by decreased productivity and possibly decreased inputs of landscape derived and respired organic matter during this period of dry (Abbott et al., 2010) and cold (Kurek et al., 2009) conditions. Further, $\delta^{15}N$ values are the highest at any time during the record and coincide with the period of low lake levels, again suggesting that aridity controls $\delta^{15}N$ through the LGM. Sustained low levels of organic matter and biogenic silica during the LGM indicate aquatic productivity was minimal likely due to cold conditions and a short ice free, growing season.

The Burial Lake proxy data support existing evidence for extremely arid and windy conditions during the LGM in Arctic Alaska. Evidence for low lake levels and arid conditions at Burial Lake are supported internally by the presence of an erosional unconformity in the C-98 core (Abbott et al., 2010) with a gap in sedimentation between ~33,000 to 24,300 cal yr BP. Abbott et al. (2010) suggest that sedimentation resumed at the C-98 core site by 24,300 cal yr BP, and therefore interpret the early LGM to be the driest period over the entire record. However, this age assignment is extrapolated from a radiocarbon date of 19,880 cal yr BP that is 51 cm above an erosional unconformity. Alternatively, the transition to higher lake-levels is constrained directly to before 19,880 cal yr BP. Our continuous proxy data showing coarse sediments (Figure 3-3) and relatively low organic content (Figure 3-12) are consistent with persistently dry conditions throughout the LGM. Several other lake sediment records from northwest Alaska show evidence for lower lake levels during the LGM (Anderson, 1988; Mann et al., 2002; Oswald et al., 1999) when most small, shallow lakes in the interior of Alaska were dry (Abbott et al., 2000). Thus, evidence from Burial Lake provides additional support for the west-east moisture gradient in Alaska during the LGM, which has been attributed to proximity to marine moisture sources (Guthrie, 2001). The period of low lake levels and minimal aquatic productivity corresponds to the time when most ice sheets attained their maximum late-Wisconsinan extent (Clark et al., 2009) and the LGM sea level lowstand (Figure 3-12). As a result, the Bering Land Bridge attained its greatest extent as lower sea levels exposed the shallow Bering and Chukchi continental shelves (Hopkins, 1982), thereby enhancing the continentality of interior regions in Alaska.

Alpine glaciers in the central Brooks Range attained their maximum extent during the early LGM between 27,000 to 25,500 cal yr BP and experienced a later retreat and re-advance to near the LGM maxima position after 23,000 cal yr BP (Figure 3-12) (Briner and Kaufman, 2008; Hamilton, 1982). The relatively early LGM maximum extent of alpine glaciers in the Brooks Range, compared with elsewhere in Alaska (Briner and Kaufman, 2008), suggests a complex pattern in glacier mass balance. Our re-interpretation of lake-levels at Burial Lake across the LGM (Figure 3-12) and proxy data from this study indicates sustained low lake levels and very low effective moisture levels between 29,600 to ~20,000 cal yr BP. Although our age control is limited, we suggest the relatively early LGM alpine glacial maxima in the central Brooks Range could have occurred during a time of slightly higher effective moisture levels. Therefore, we hypothesize that subsequent more extensive advances were possibly precluded by greater aridity as the Bering Land Bridge increased in size and the distance from marine moisture sources increased.

3.5.4 The Last Deglaciation (19,600 to 16,500 cal yr BP)

Numerous proxies in the Burial Lake record gradually change in trend around ~19,600 cal yr BP at the subunit 2b transition (Figure 3-7; Figure 3-8) consistent with considerable environmental change initiating at this time. Specifically, organic matter concentrations and C/N ratios gradually increase up-section while magnetic susceptibility, titanium, and organic matter $\delta^{13}C$ and $\delta^{15}N$ values gradually decrease up-section towards the subunit 3 boundary (Figure 3-7; Figure 3-8). We interpret these changes to reflect a progressive increase in terrestrial organic matter flux and a

corresponding decrease in clastic sediment delivery to the lake. The decrease in organic matter $\delta^{15}N$ values implies an increase in terrestrial organic matter because the N source of land plants is atmospheric N_2 (expected value of 0 ‰) (Meyers and Teranes, 2001). Decreasing $\delta^{15}N$ values corresponds with rising and higher lake levels at Burial Lake, consistent with increasing supply of reactive N (compared with demand) and the aforementioned relationship between $\delta^{15}N$ and hydroclimate (Amundson et al., 2003). The trend to decreasing organic matter $\delta^{13}C$ values, coincident with increasing C/N values, likely reflects increased inputs of watershed-respired CO_2 from the catchment (Finney et al., 2012).

We acknowledge the lack of direct age control at this time limits a precise age determination for this transition (Figure 3-3). Assuming a constant sediment accumulation rate at Burial Lake through LGM, the estimated uncertainty in the timing of this transition is between 18,600 to 20,700 cal yr BP. However, given the considerable climatic change that transpired in the Alaskan Arctic through the LGM (Abbott et al., 2010; Hamilton, 2001; Kurek et al., 2009), it is very likely that sedimentation rates at Burial Lake were variable and the error estimates associated with this transition could be even greater. Nonetheless, support for major environmental change occurring around this time is provided by the C-98 core, which shows rising and higher lake levels by 19,880 cal yr BP (Figure 3-12). Increasingly mesic conditions beginning at 19,800 cal yr BP inferred from palynological data (Abbott et al., 2010) also coincide with the last deglaciation sediment transition.

The last deglaciation transition is broadly synchronous with gradually rising high-latitude Northern Hemisphere summer insolation (Berger and Loutre, 1991) and retreat

of alpine glaciers in the Central Brooks Range between 22,000 and 18,500 cal yr BP (Hamilton, 1982) (Figure 3-12). Further evidence for climatic change at this time is provided by a chironomid-inferred July temperature reconstruction from Burial Lake, which shows sustained cold temperatures through the LGM until ~ 17,400 cal yr BP (Kurek et al., 2009). Reconstructed July temperatures gradually increase after ~ 17,400 cal yr BP and reflect increasingly warmer and longer summers. Increasing temperatures are broadly synchronous with rising global atmospheric CO_2 levels beginning around ~ 17,000 cal yr BP (Monnin et al., 2001). We therefore suggest the changing trend in sediment properties at ~ 19,600 cal yr BP along with corresponding increases in *Cyperaceae* and *Salix* (Abbott et al., 2010) are driven by increasing effective moisture levels coincident with rising and higher lake-levels (Figure 3-12). Increasing effective moisture levels at this time are possibly related to initial retreat of the Laurentide Ice Sheet at ~ 19,000 cal yr BP (Dyke, 2004) and a re-organization in atmospheric circulation across eastern Beringia. Interestingly, a chironomid-inferred July temperature reconstruction from Zagoskin Lake in western Alaska shows progressive warming of ~3° C during the LGM to last deglaciation from 25,000 to 17,000 cal yr BP (Kurek et al., 2009), possibly reflecting spatial variations in climatic conditions in western Alaska at this time.

3.5.5 The Lateglacial and early Holocene Thermal Maximum (16,500 to 8,800 cal yr BP)

The Lateglacial transition at Burial Lake beginning at ~ 16,500 cal yr BP is marked by an abrupt change in sedimentology, with decreasing grain size (very fine

sandy silt) and absence of coarse sediments (sand or granules) that characterized mid-Wisconsinan interstadial, LGM, and the last deglaciation age sediments. Terrestrial macrofossil abundance increases, suggesting more established vegetation in the surrounding catchment, and sedimentation rates are slower (9 to 19 cm/ka yr). Magnetic susceptibility and titanium values continue to gradually decrease through the Lateglacial, which we interpret a result of decreased windiness, stabilization of watershed soils, and from rising and higher lake-levels (Figure 3-12). Rising and variable biogenic silica and $Si_{(norm)}$/Ti (Figure 3-7; Figure 3-8), and a corresponding increase in the presence and diversity in diatom frustules, indicates increased in-lake (aquatic) productivity likely due to a longer ice-free growing season and increasing nutrients from autochthonous organic matter flux to the lake. Relatively high and variable C/N ratios indicate a higher proportion of organic matter from terrestrial sources during this time. Organic matter $\delta^{15}N$ values attain their most negative values between 16,500 to 11,350 cal yr BP at the same time both terrestrial and aquatic productivity levels are increasing or higher than any previous time. Therefore, we interpret $\delta^{15}N$ dynamics to changes in both decreased relative nitrogen availability relative to demand and increasing input of terrestrial organic matter to the sediment, both of which tend to decrease organic $\delta^{15}N$ (Craine et al., 2009; Meyers and Teranes, 2001). Overall, proxy evidence indicates the Lateglacial and Early Holocene between 16,500 to 8,800 cal yr BP was a time of considerable climatic change with increasing and higher levels of terrestrial and aquatic productivity, decreased windiness and landscape stabilization, and continued rising lake-levels (Figure 3-12) and increasing effective moisture.

The Lateglacial transition at Burial Lake beginning at 16,500 cal yr BP coincides with a decrease in dust accumulation inferred from decreasing and lower s-ratios (Figure 3-12) (Dorfman, 2013). Changing oceanographic conditions in the Bering Sea also indicate broadly synchronous ocean-land responses to warmer climate conditions around this time. For example, Caissie et al. (2010) report a transition from thick perennial pack ice to extensive sea ice with short periods of open water at Umnak Plateaus in the southern Bering Sea beginning at 16,900 cal yr BP. The deglacial transition at 16,500 cal yr BP coincides with evidence of alpine glacier retreat from the range front in the central Brooks Range before ~ 16,000 to 15,000 cal yr BP, and further retreat into cirques by ~ 14,000 cal yr BP (Badding et al., 2013). However, (Hamilton, 2003b) reports evidence of a minor re-advance of alpine glaciers in the central Brooks Range between 15,100 to 13,000 cal yr BP, possibly related to increased effective moisture levels, although geomorphic evidence (moraines) for this advance are lacking. Further, rising eustatic sea levels (Figure 3-12) gradually flooded the Bering Land Bridge and reduced the transport distance of air masses to the Alaskan interior, effectively reducing the continentality of the Alaskan interior over time. Complete submergence of the Bering Land Bridge occurred between 12,000 to 11,000 cal yr BP (Elias et al., 1996; Keigwin et al., 2006), establishing the approximately modern continental configuration of Alaska.

The proxy evidence from Burial Lake is also consistent with other lacustrine records from Alaska that shows considerable and rapid environmental change initiated during the Lateglacial period. For example, Mann et al. (2002) report evidence of higher and fluctuating lake-levels, compared with the preceding glacial period, from Lake of the

Pleistocene (Nikivlik Lake) (Figure 3-1). Relatively high lake-levels and increased effective moisture levels occur between 12,500 – 11,000 ^{14}C yr BP and after 10,000 ^{14}C yr BP, while falling and lower lake-levels with decreased effective moisture occur between 11,000 – 10,000 ^{14}C yr BP (Mann et al., 2002). In addition, core-transect based lake-level reconstructions from Birch Lake (Abbott et al., 2000) and Harding Lake (Finkenbinder et al., 2014) in the interior of Alaska (Figure 3-1) show relatively higher but variable lake-levels with increased effective moisture between ~15,000 to ~9,000 cal yr BP, compared with LGM conditions. Pollen evidence from Burial Lake show a trend to more mesic conditions between 19,800 to 13,900 cal yr BP. Further, an abrupt rise in *Betula* pollen at Burial Lake at 13,900 cal yr BP (Abbott et al., 2010), combined with regional evidence for increasing shrub abundance during the Lateglacial (Anderson and Brubaker, 1994; Higuera et al., 2009; Oswald et al., 1999), provide additional evidence for warmer and wetter conditions at this time. The July temperature reconstruction from Burial Lake shows gradually rising temperatures beginning at ~17,000 cal yr BP that continued to rise to the highest levels over the entire record at 12,300 cal yr BP (Kurek et al., 2009).

Relatively low biogenic silica content and reduced aquatic productivity at Burial Lake between 13,000 to 12,400 cal yr BP possibly provides additional evidence for climatic deterioration during the early Younger Dryas (YD) in Alaska. However, reduced productivity contrasts with the midge-inferred increase and peak summer temperatures at Burial Lake through the early YD (Kurek et al., 2009). This discrepancy is difficult to explain given that both proxies are sensitive to growing season climatic conditions. Further, the apparent lack of a clear YD signal in other physical, geochemical, or

elemental proxies (Figure 3-7; Figure 3-8) suggests the absence of a climatic reversal at this time. This conclusion is consistent with the lack of evidence for YD alpine glacier advances in the central Brooks Range (Badding et al., 2013; Hamilton, 1982) and a review of paleoecological data showing similar to modern temperatures in northern Alaska (Kokorowski et al., 2008). However, this contrasts with regional evidence for the YD in northern Alaska that include low lake-levels and decreased effective moisture at Lake of the Pleistocene (Gaglioti et al., 2014; Mann et al., 2002) and floodplain incision on the Alaskan north slope (Mann et al., 2010) from cooler and potentially drier conditions. Further, evidence for colder temperatures is inferred from fossil beetle assemblages along Noatak River (Elias, 2000) and from a negative $\delta^{18}O$ excursion from the Barrow ice wedge system (Meyer et al., 2010). The apparently discordant evidence for the YD in northern Alaska could reflect seasonal differences in the sensitivity of proxies to environmental or climatic changes used in this study.

The peak in organic matter and highest levels over the entire record along with relatively high C/N ratios at Burial Lake occurs between 10,500 to 9,900 cal yr BP. We interpret this to reflect relatively high terrestrial productivity, which coincides with the latter part of the HTM in Alaska (Kaufman et al., 2004) and with the peak in sea surface temperatures in the northwest Pacific Ocean and Bering Sea (Max et al., 2012) over the last 15,000 years. Regionally, high productivity also coincides with the peak in thermokarst lake development across the circum Arctic (Walter et al., 2007) and peatland initiation across Alaska (Jones and Yu, 2010). Holocene to late Pleistocene age solifluction deposits mapped immediately north of Burial Lake (Hamilton, 2010) represent a local source of autochthonous organic matter delivered to the lake from

permafrost degradation at this time. Additional evidence for regional summertime warming and increased effective moisture from 11,500 to 9,500 cal yr BP is evinced from a period of floodplain aggradation and expansion of Populus balsamifera trees in the Arctic foothills (Mann et al., 2010). These coincident land-ocean environmental changes apparently reflect broadly synchronous responses to the summer insolation maxima (Berger and Loutre, 1991) and enhanced methane emissions from thermokarst lakes (Walter et al., 2007) during the early Holocene in the western Arctic.

3.5.6 The early Holocene to the present (2010 AD)

Burial Lake sediments spanning the early Holocene (8,800 cal yr BP) to the present (2010 AD) consist of fine (silt) sediment and combined with core-transect data (Abbott et al., 2010), indicate high and generally stable lake-levels (Figure 3-12). Low and relatively stable magnetic susceptibility and titanium content are consistent with a low clastic sediments flux, with minimal aeolian sedimentation (Dorfman, 2013). Generally stable organic matter content and low C/N ratios indicate that organic matter primarily originated from a mixed aquatic-terrestrial source through this interval. Organic matter $\delta^{15}N$ values are generally stable and display only minor variability throughout the middle to late Holocene, suggesting that organic N-cycling and the source of reactive N for aquatic productivity remained relatively constant. Excursions to relatively negative $\delta^{13}C$ values also occur at 3,580 and 1,170 cal yr BP and likely reflect a variable flux of terrestrial organic matter delivered to the lake from the catchment. Pollen evidence from Burial Lake shows the *Alnus crispa* expansion occurred at 9,000

cal yr BP and the vegetational mosaic thereafter is moist shrub tundra (Abbott et al., 2010).

The proxy data from Burial Lake spanning the early to late Holocene are consistent with regional-wide evidence for high and generally stable lake levels (Abbott et al., 2000; Finkenbinder et al., 2014), soil development and stabilization (Hu et al., 2001), and increasing and higher levels of aquatic and terrestrial productivity (Finkenbinder et al., 2014; Finney et al., 2012; Hu et al., 2001; Hu et al., 2003; Kaufman et al., 2012). For instance, biogenic silica displays large fluctuations and varies from ~ 6 to ~ 18 (wt. %) at multi-century to millennial time scales over the last 8,800 cal yr BP (Figure 3-12). We interpret changes in biogenic silica to reflect changes in aquatic productivity, given the generally linear sediment accumulation rate over the Holocene (Figure 3-3), no evidence for diatom dissolution, and minimal variability in LOI 550 and TOC (Figure 3-4). Unfortunately, the existing age model and temporal resolution of our biogenic silica record (average 140 yr/sample) do not allow us to address if these changes are related to Holocene millennial variability observed in other paleo records (Bond et al., 2001; Darby et al., 2012; Hu et al., 2003) or to assess the precise mechanism that drives aquatic productivity at Burial Lake. Relatively low S-ratios indicate diminished dust accumulation at Burial Lake compared with the preceding early Holocene and Lateglacial (Figure 3-12). However, increasing S-ratios after ~ 2,000 cal yr BP possibly reflect increasing dust accumulation at Burial Lake (Figure 3-12), which Dorfman (2013) suggest could result from late Holocene alpine glacier advances in the Brooks Range.

3.6 CONCLUSIONS

A detailed investigation of a 6.51 m composite core from the central depocenter of Burial Lake in Arctic Alaska reveals a continuous record of sedimentation that spans the last ~37,000 cal yr BP. The application of AMS radiocarbon dates on terrestrial macrofossils provide a chronological framework to assess changing paleoenvironmental conditions over the late-Quaternary. We identify four distinct lithologic subunits based on an analysis of physical sedimentology and multiple physical and geochemical proxies analyzed at multi-decadal to centennial timescales. Relatively high lake-levels and gradually decreasing in-lake and terrestrial productivity occur during the mid-Wisconsinan interstadial between 37,200 to ~ 29,600 cal yr BP. The subsequent period is defined by falling and lower lake-levels with decreasing effective-moisture, windier conditions, and sustained and low levels of aquatic productivity throughout the LGM between ~ 29,600 to ~19,600 cal yr BP. Although our age control is limited through the LGM, we suggest the relatively early LGM alpine glacial maximum extent in the central Brooks Range could have occurred during a time of slightly higher effective moisture levels. Therefore, we hypothesize that subsequent more extensive advances were possibly precluded by greater aridity as the Bering Land Bridge increased in size and the distance from marine moisture sources increased.

The last deglaciation that commenced by ~19,600 cal yr BP is characterized by gradual changes in several sediment physical and geochemical proxies, including increasing C/N ratios and terrestrial productivity, decreasing magnetic susceptibility and clastic sediment flux, along with rising and relatively higher lake-levels. The lack of direct age control in the Burial Lake record constraining the last deglaciation limits a

precise age determination for this transition. However, support for environmental change occurring at this time is provided by core-transects that show rising and higher lake levels along with palynological data that show increasingly mesic conditions by ~ 19,800 cal yr BP (Abbott et al., 2010). We suggest this transition is related to initial retreat of the Laurentide Ice Sheet at ~ 19,000 cal yr BP and a re-organization in atmospheric circulation across eastern Beringia, resulting in increasing effective moisture levels and terrestrial productivity at Burial Lake. A decrease in aeolian activity after 16,500 cal yr BP is inferred from the appearance of fine (very fine sandy silt) sediment, compared to coarse sediments through the LGM and last deglaciation. The highest levels of terrestrial productivity along with increasing and variable aquatic productivity occurs during the Lateglacial to early Holocene interval between 16,500 to 8,800 cal yr BP. The absence of multi-proxy evidence for a climatic reversal during the Younger Dryas from Burial Lake sediments contrasts with other paleorecords showing cooler temperatures and/or dry conditions in northern Alaska at this time. Peak levels of sediment organic content and terrestrial productivity at Burial Lake between ~ 10,500 to 9,900 cal yr BP coincide with the early Holocene summer insolation maxima and Holocene Thermal Maximum in the western Arctic, which likely represents summertime warming and an enhanced flux of watershed derived organic matter from permafrost degradation. The remainder of the Holocene (since 8,800 cal yr BP) at Burial Lake is characterized by relatively high and stable lake levels, landscape stabilization, and relatively high and variable levels of aquatic productivity.

The Burial Lake record provides one of the oldest lacustrine records from the North American Arctic to continuously span the period prior to the last glacial period

through to the present. High-resolution proxy analysis at multi-decadal to centennial time scales provides new insights into the sensitivity of Arctic ecosystems to climatic, environmental, and landscape changes across glacial to interglacial timescales. Unfortunately, the absence of terrestrial macrofossils for radiocarbon dating across the LGM and last deglaciation, during the period of cold, extremely arid, and windy conditions, limits our ability to assess the precise timing of environmental changes at key times. Further, the lack of evidence for dramatic environmental changes throughout the LGM and across the Younger Dryas, suggests the physical and geochemical proxies used in this study were possibly less sensitive to climatic changes at these times. Alternately, the absence of evidence for environmental changes could reflect seasonal differences in the sensitivity of productivity proxies (organic content, biogenic silica) used in this study, which primarily respond to summer growing season conditions. These apparent discrepancies highlight the need to carefully interpret proxy indicators to infer environmental changes, which by their nature respond to myriad environmental factors and often towards seasonal climate conditions.

4.0 MILLENNIAL-SCALE VARIABILITY IN HOLOCENE CLIMATE FROM BURIAL LAKE, ARCTIC ALASKA

Millennial-scale fluctuations in Holocene climate conditions have been observed in a variety of paleoclimate archives, however relatively few observations exist from continental sites in high-latitude regions. Further, the underlying mechanism that drives these variations, including whether they might arise from internal and intrinsic variations within the climate system compared with an external forcing mechanism, are still actively debated. Here we present the first evidence for cyclical millennial-scale fluctuations in Holocene climate conditions in Arctic Alaska using sedimentological and geochemical analyses from Burial Lake in the western Brooks Range. We interpret changes in sedimentary biogenic silica (BSi) to result from variability in aquatic productivity, which is indirectly mediated by climate through changes in the duration of the ice-free growing season and the availability of limiting nutrients at this oligotrophic, tundra lake. Large BSi fluctuations and related proxies at millennial timescales in Burial Lake occur over the last 10,000 years. Time series analysis of the BSi record indicates a significant ~1,500-yr periodicity emerges by ~6,000 cal yr BP that disappears after ~3,000 cal yr BP. Comparison of aquatic productivity against a sea-ice inferred reconstruction of the Arctic Oscillation (AO) (Darby et al., 2012) shows that periods of reduced productivity at Burial Lake coincide with positive phases of the AO.

Specifically, reconstructed AO+ conditions that correspond with lower summer temperatures and a shortened ice free season result in a decreased flux of limiting nutrients from permafrost degradation and lower levels of aquatic productivity at Burial Lake. Further, the reconstructed aquatic productivity and the AO display similar millennial scale periodicities with ~1,500-yr variability during the middle Holocene that transitions to ~1,000-yr variability during the late Holocene. We propose that aquatic productivity at Burial Lake is related to state changes in the AO and that millennial variability that the record exhibits is related to internal oscillations within the climate system. These results shed light on the sensitivity of aquatic ecosystems in northern Alaska to changes in growing season temperature and Arctic Ocean sea ice extent over the Holocene.

4.1 INTRODUCTION

Millennial-scale fluctuations in Holocene climate conditions have been observed in a variety of paleoclimate archives (Bond et al., 2001), however the meaning of these variations including whether they might arise from internal or external forcing are still actively debated. The 1,500-yr cycle in Holocene climate records has been attributed to external solar forcing (Bond et al., 2001; Hu et al., 2003), geomagnetic field intensity variations (St-Onge et al., 2003), internally driven changes in the strength of Atlantic Meridional Overturning Circulation (AMOC) and variations in the formation of North Atlantic Deep Water (NADW) (Bianchi and McCave, 1999; Debret et al., 2007), and to internal modes of climate variability (Darby et al., 2012; Sorrel et al., 2012). Proxy

evidence for millennial scale variability is most clearly present in the North Atlantic region, but it remains unclear whether the lack of evidence from many other regions is the result of limited observations or an absence of expression. Evidence for a 1,500-yr cycle in Holocene climate from Alaska and the North Pacific is relatively scarce with a few notable exceptions. For example, Wiles et al. (2008) use glacial-geologic studies in Alaska that reveal multi-century to millennial-scale fluctuations in the advance and retreat of alpine glaciers over the late Holocene linked to solar variability. Hu et al. (2003) report evidence of a prominent 950-yr cycle, and a weaker 1,500-yr cycle, in aquatic productivity from Arolik Lake in southwest Alaska over the Holocene, and suggested a direct solar irradiance control. More recently, Darby et al. (2012) report evidence for a 1500-yr cycle in Arctic sea-ice drift and attribute these variations to changes in the mean-state of the Arctic Oscillation.

Paleoclimate records that display millennial-scale variations are often analyzed for frequency patterns using classical spectral analysis, which seeks to detect significant periodicities within a signal. Debret et al. (2007) demonstrated the limitations of conventional spectral analysis methods to detect periodic signals that evolve through time from reanalysis of a North Atlantic ice-rafted debris stack Bond et al. (1997). Wavelet analysis is an additional time series analysis technique used to explore the evolution of frequency patterns in climate records, which permits visualization of the changing statistical properties in stochastic processes with time (Torrence and Compo, 1998). For example, wavelet analysis of North Atlantic climate proxies and cosmogenic radionuclides (^{14}C production rate, ^{10}Be) showed that Holocene millennial variability consists of 1000 and 2500-yr periodicities linked to solar forcing. In addition, the

analysis revealed a 1500-yr periodicity and linked these variations to internal oceanic or ocean-atmosphere forcings (Debret et al., 2007). Further, wavelet analysis revealed the 1500-yr periodicity found in global paleoclimate records was not continuous through the Holocene and appears by the middle to late Holocene (4,000 to 6,000 calendar years before present; cal yr BP) (Debret et al., 2009). However, these wavelet analysis studies did not include proxy records from the North Pacific and Arctic regions, and further emphasized marine records with limited analysis of terrestrial climate records. As a result, the existence and temporal evolution of millennial-scale climate variability in Arctic Alaska is still uncertain. Additional paleoclimate records from northern Alaska will help further understand the potential forcings and spatial patterns of millennial-scale climate fluctuations in the Arctic during the Holocene.

Here we present new evidence for millennial-scale climate variations in Arctic Alaska from sedimentological and geochemical analyses of Burial Lake in the western Brooks Range. A multiproxy approach is used to reconstruct paleoenvironmental changes over the last 10,000 years, which is used to hypothesize and test that algal productivity is sensitive to climatic conditions on millennial to orbital timescales. We utilize a combination of time series methods to detect and investigate the temporal evolution of frequency patterns in aquatic productivity. Last, We compare the Burial Lake biogenic silica (BSi) record to paleoclimate records from the North Atlantic (Bianchi and McCave, 1999; Hoogakker et al., 2011; Thornalley et al., 2009) and Alaskan region that include; a midge-inferred temperature reconstruction (Clegg et al., 2011), sea-ice records from the Bering and Chukchi Seas (de Vernal et al., 2005; Katsuki et al., 2009), and a recently developed sea-ice inferred record of the Arctic

Oscillation (Darby et al., 2012) to investigate potential mechanisms that drive this variability in the Alaskan Arctic.

4.2 SITE DESCRIPTION

Burial Lake (68.43°N, 159.17°W; 460 m above sea level, asl) is a small (0.8 km^2), hydrologically open, oligotrophic lake located in the Noatak River basin in northwest Alaska (Figure 4-1). The surrounding catchment is small (3.3 km^2) with steep (3-5 m high) slopes along most of the lake's shoreline that transition to a low-relief plateau (Figure 4-2). The lake receives inflow from several ephemeral gullies along the northern shoreline and contains a small outlet stream at the southwest shoreline. The catchment and surrounding region is underlain by continuous permafrost at depths below 200 to 300 m (Jorgenson et al., 2008). Vegetation surrounding the lake is characterized as low-arctic tundra, consisting of sedges, Salix, shrub-Betula, and Alnus with occasional stands of Populus balsamifera in river valleys (Abbott et al., 2010). Physical observations and a review of monthly Landsat satellite imagery (http://landsatlook.usgs.gov/) indicate that ice covers the lake for approximately 9 months a year, resulting in a short, 3 month long ice-free growing season.

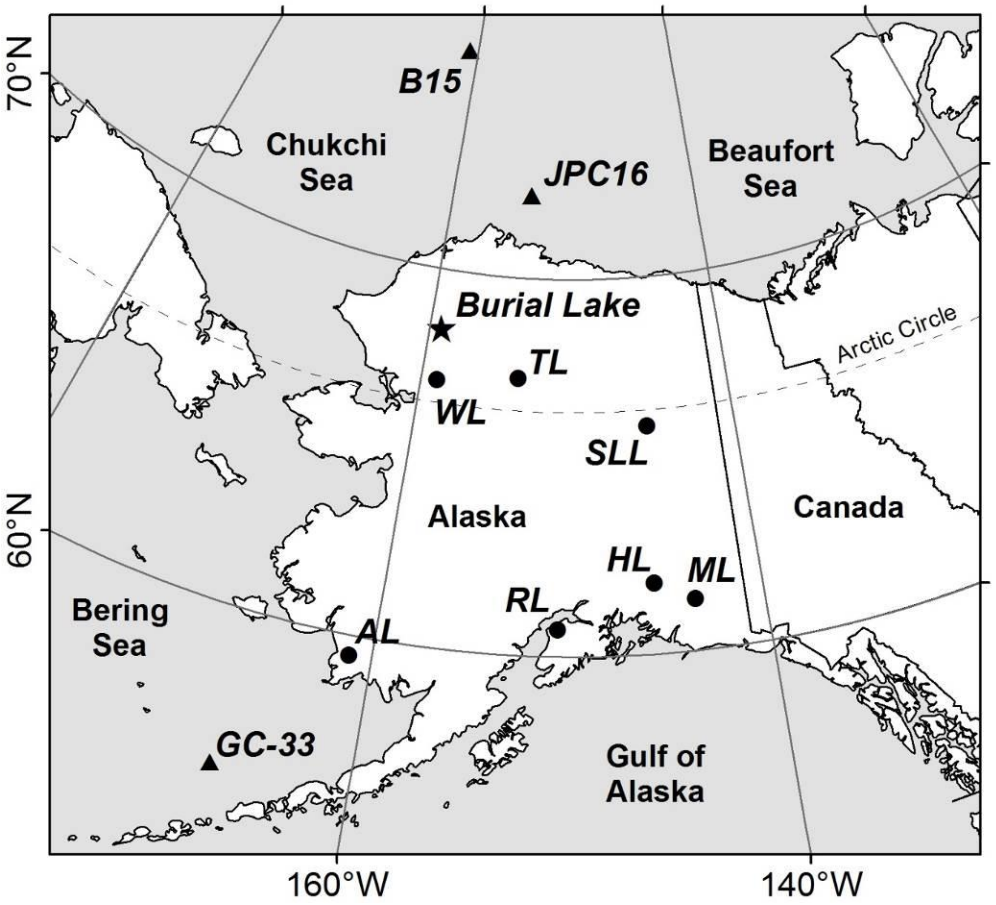

Figure 4-1. Map of Map of Alaska showing Burial Lake and other sites mentioned in the text. Other sites include Arolik Lake (AL), Rainbow Lake (RL), Hudson Lake (HL), Moose Lake (ML), Screaming Lynx Lake (SL), Wolverine Lake (WL), and Takahula Lake (TL). Marine records include core JPC16 in the Beaufort Sea, core GC-33 in the Bering Sea, and core B15 in the Chukchi Sea.

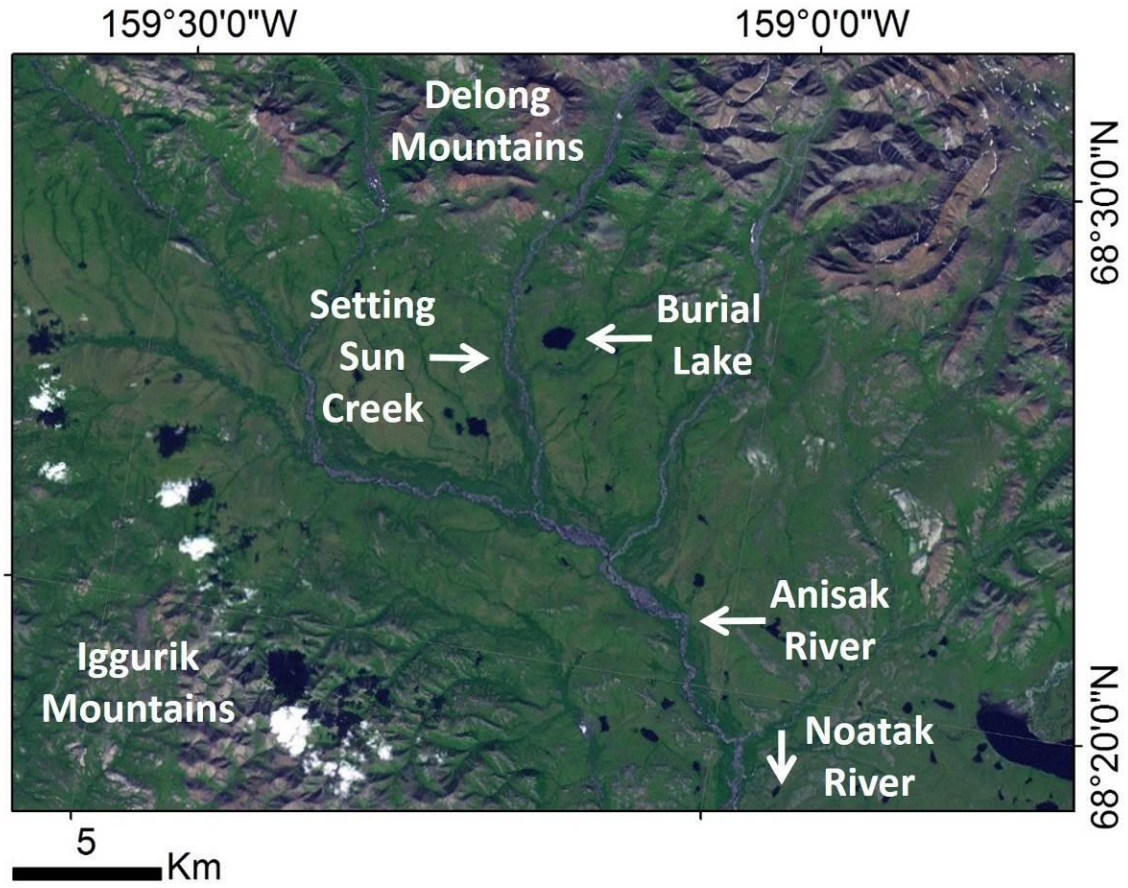

Figure 4-2. Satellite photo showing the location of Burial Lake with respect to local streams in the upper Anisak River drainage basin.

The regional climate around Burial Lake is characterized by long cold winters and short cool summers. Bieniek et al. (2012) place the upper Noatak Basin within the North Slope climate division, a region defined by arid conditions (maximum precipitation of < 5 cm in the wettest summer month) with seasonal average temperatures ranging from below -25° C in winter to above 10°C in summer. Climatic conditions in Alaska are further influenced by ocean-atmosphere interactions and internal modes of climate variability on seasonal to multi-decadal timescales. For example, variations in the El Niño Southern Oscillation (ENSO) correlate with cold season conditions in Alaska, with

the negative phase of ENSO (La Niña) associated with lower than average winter temperature (Bieniek et al., 2012; Papineau, 2001). Similarly, the Pacific Decadal Oscillation (PDO), or dominant mode of Pacific Ocean sea surface temperatures northward of 20° N latitude, also influences Alaskan climates whereby colder winters typically occur with the cool phase of the PDO (Bieniek et al., 2012; Hartman and Wendler, 2005; Papineau, 2001). The Arctic Oscillation (AO), or a leading mode of Northern Hemisphere sea level pressure variability that effects hemisphere-wide atmospheric circulation (Thompson and Wallace, 1998) impacts Alaskan weather with positive phase AO conditions associated with colder wintertime conditions (Bieniek et al., 2012). The influence of ENSO and PDO variations on summer temperatures in Alaska is comparatively weak (Hartman and Wendler, 2005; Papineau, 2001), while the influence of the wintertime AO on temperatures persists through most of the following year through interannual effects with Arctic sea ice (Rigor et al., 2002). The summer climate of interior and northern Alaska is primarily affected by mid-tropospheric variations of ridges and troughs (Edwards et al., 2001).

4.3 MATERIALS AND METHODS

4.3.1 Lithostratigraphy and geochemistry

Sediment cores were collected from the deepest part of the central basin at Burial Lake in July, 2010. A surface core (A-10 Drive 1) with intact sediment-water interface was recovered in 21.5 m water using a polycarbonate tube fit with a rubber

piston. The upper portion of the surface core was packed with floral foam and capped for transport. Overlapping cores were recovered from the same location in 21.5 m water using a modified square rod Livingstone corer (Wright et al., 1984). Sediment cores were split lengthwise and described at the Department of Geology and Planetary Science at the University of Pittsburgh. Notable sedimentary structures, grain-size, and Munsell color were characterized for each core. Samples for dry bulk density were measured at continuous 1 cm intervals using a 1 cm^3 piston sampler, subsequently dried for 48 hours in a 60° C oven, and weighed thereafter. Magnetic susceptibility was measured at 2 mm intervals on the split-core surface using a Bartington MS2 Magnetic Susceptibility Meter.

Sedimentary organic matter proxies are often used to evaluate changes in the source and production of vegetation growing in and around lacustrine systems (Meyers and Teranes, 2001). Samples for total organic carbon (TOC) and total nitrogen (TN) were measured at 2 cm intervals using an Elemental Combustion System 4010 interfaced to a Delta V Advantage mass spectrometer through the ConFlo IV system. The elemental mass ratio of TOC to TN (C/N) was calculated to further assess the relative proportion of organic matter from terrestrial (C/N > 20) versus aquatic (C/N < 10) sources (Meyers and Teranes, 2001). Prior to analysis, samples were treated with 1M HCl to ensure removal of carbonate minerals, rinsed to neutral pH with MilliQ water, freeze-dried and homogenized.

Biogenic silica (BSi) is a measure of the amorphous component of silica (SiO_2) in sediments that has been shown to be a reliable proxy for the abundance of diatoms, or single celled algae that produce a siliceous frustule (Conley and Schelske, 2001). In

the Arctic, diatoms are typically the most prevalent algae in lakes and sedimentary BSi is often used as an index of primary productivity (Douglas and Smol, 1999). BSi content was measured at 1 cm intervals using a wet-chemistry, alkaline extraction adapted from Mortlock and Froelich (1989). Briefly, homogenized sediment samples were treated with 30% H_2O_2 and 1M HCl to oxidize organic matter and carbonates prior to analysis. BSi was extracted with a 5% Na_2CO_3 solution and determined by molybdate blue spectrophotometry at 812 nm using a Thermo Scientific Evolution 60s UV-Visible Spectrophotometer.

4.3.2 Composite core and geochronology

A composite sediment record was developed using overlapping core segments based on matching magnetic susceptibility and visible stratigraphic markers. Age control is based on 11 accelerator mass spectrometry ^{14}C dates on terrestrial macrofossils (Table 4.1) plus a core top age assignment of 2010 AD. Radiocarbon samples were pre-treated using standard acid-base-acid wash techniques (Abbott and Stafford, 1996) at the University of Pittsburgh and were combusted, converted to filamentous graphite, and measured at the W.M. Keck Carbon Cycle AMS Laboratory, University of California, Irvine. Radiocarbon ages were calibrated to calendar years BP (1950 A.D.) using Calib 7.0 and the IntCAL13 calibration curve (Reimer et al., 2013). An age-depth model was created using point to point, linear interpolation with the classical age modeling (CLAM) code v2.2 for the statistical software R (Blaauw, 2010). To further account for chronological uncertainty, I apply a Monte Carlo-based approach

that perturbs the interpolated age-depth model 10,000 times following a random draw from a normal distribution between the 2σ calibrated ^{14}C ages (Marcott et al., 2013). The uncertainty between the age control points is modeled as a random walk, after Huybers and Wunsch (2004), with chronological uncertainty assumed to be auto-correlated through time and modeled as a first order autoregressive (AR1) process.

Table 4.1. Burial Lake AMS radiocarbon dates from core A-10.

Sample ID (UCIAMS #)	Depth (cm)	Material	^{14}C Age (yr BP)	± (yr)	Calib 7.0 Age (cal yr BP)
152065	16.5	twig	950	180	562 - 1,261
89197	45.0	plant material	2,535	30	2,493 - 2,745
152066	53.5	bryophyte	3,030	60	3,042 - 3,378
109361	66.5	wood	3,635	25	3,872 - 4,074
152067	74.5	plant material	4,055	25	4,437 - 4,783
116878	87.5	plant material	4,910	90	5,470 - 5,896
152068	99.5	twig	5,765	30	6,491 - 6,651
89198	111.0	plant material	6,345	25	7,174 - 7,410
109362	141.5	wood	8,850	110	9,564 - 10,205
89199	166.0	plant material	9,760	40	11,134 - 11,244
89200	173.5	seed	10,085	45	11,398 - 11,959

4.4 RESULTS

4.4.1 Geochronology

Radiocarbon measurements (Table 4.1) indicate the Burial Lake core continuously spans the latest Pleistocene and Holocene epochs, although this investigation focuses on the upper 143 cm of the sediment sequence that spans the last 10,000 years. The age model indicates sedimentation rates are nearly constant, ranging from 0.12 to 0.19 mm/yr (Figure 4-3). A detailed analysis of core sedimentology show they consist of homogenous grayish brown (5YR 3/2) to dusky brown (5YR 2/2), homogeneous silt with no obvious sedimentary structures. Smear-slide analyses indicate a large proportion of silicate mineral matter, a general abundance and high diversity of diatom frustules, no obvious evidence of dissolution, and substantial variability in diatom proportion over intervals of 5-10 cm.

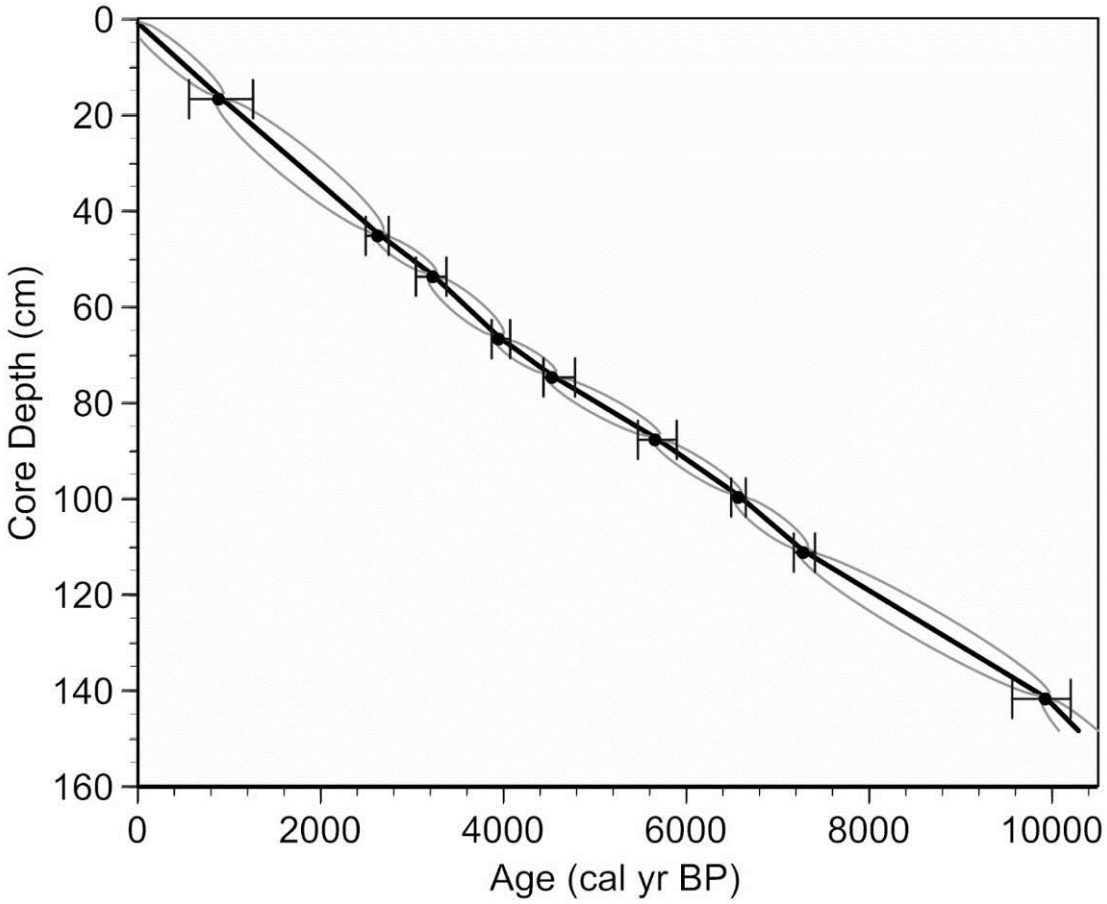

Figure 4-3. Burial Lake core A-10 age model developed using point to point, linear interpolation with the classical age modeling code.

4.4.2 Lithostratigraphy and geochemistry

Geochemical proxies from the Burial Lake sediment record exhibit large fluctuations over the last 10,000 cal yr BP (Figure 4-4). BSi varies between 6 % to 17 % and displays multi-century to millennial fluctuations superimposed on a long-term orbital trend. Values are relatively low during the early (10,000 to ~ 6,000 cal yr BP) and late (~ 2,000 to 0 cal yr BP) Holocene, while higher values occur between ~ 6,000 to ~ 2,000 cal yr BP. BSi and BSi flux, calculated by normalizing weight percent values with

sediment dry bulk density (g/cm^3) and sedimentation rates (cm/yr), display a similar trend (Figure 4-4) and are highly correlated (r^2 = 0.71; Figure 4-5). In combination with a generally constant sediment accumulation rate (Figure 4-3) and no evidence for diatom frustule dissolution, we interpret variations in BSi to reflect relative changes in aquatic productivity.

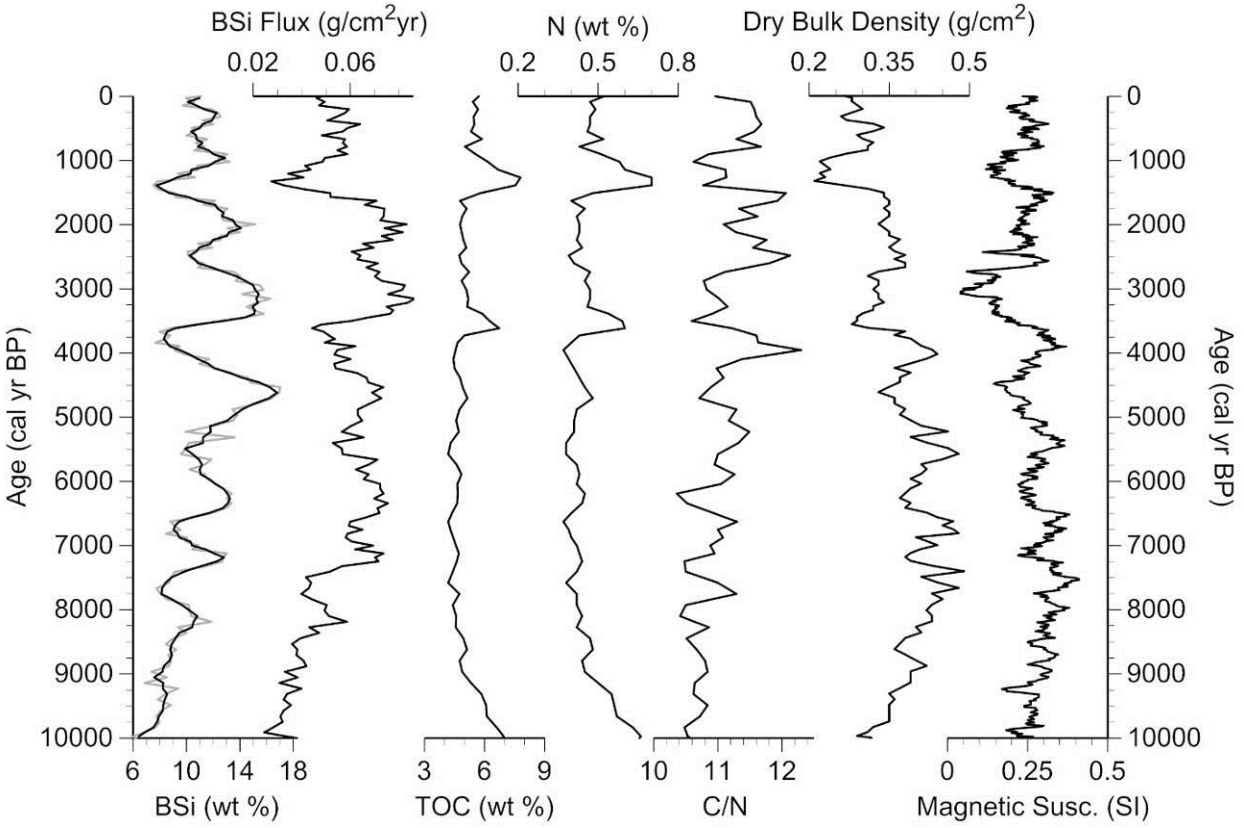

Figure 4-4. Proxy data from the Burial Lake core sequence for the last 10,000 cal yr BP. The biogenic silica record is plotted in its entirety (grey line) and with a 3-point moving average (black line).

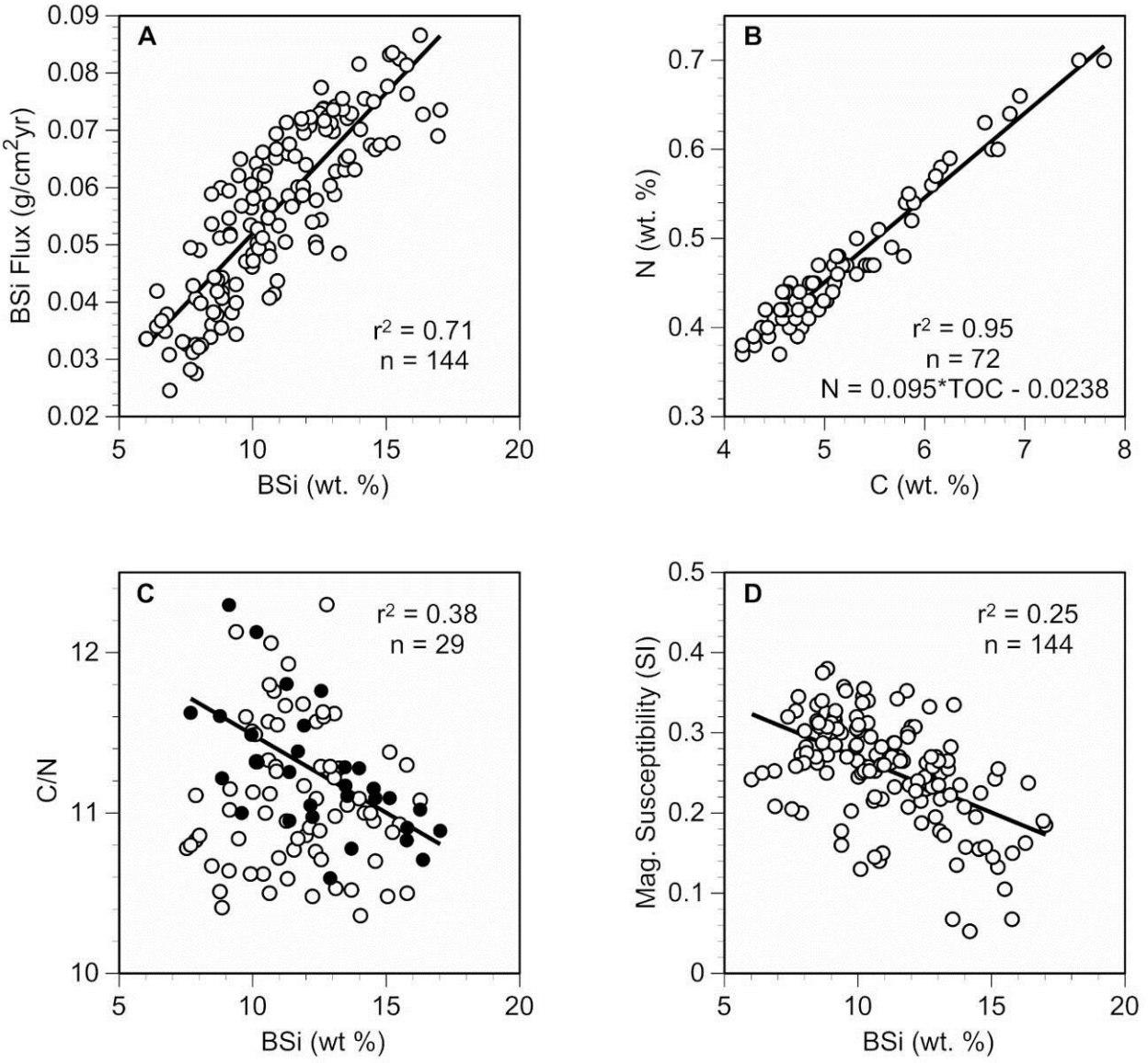

Figure 4-5. Scatter plots of Burial Lake proxy data including A) biogenic silica (wt. %) against biogenic silica flux (g/cm2yr), B) total organic carbon (wt. %) against nitrogen (wt. %), C) biogenic silica (wt. %) against C/N ratio and D) biogenic silica (wt. %) against magnetic susceptibility (SI).

Sedimentary TOC and N display similar variability (Figure 4-4) and range from 4.2 % to 7.8 % and 0.37 % to 0.7 %, respectively. TOC and N are significantly correlated (r^2 = 0.95; Figure 4-5) and the y-intercept from a linear regression between TOC and N is negative, suggesting N is derived from organic matter (Hu et al., 2001).

Values are relatively high at ~ 10,000 cal yr BP and decrease thereafter to lower values by ~ 8,000 cal yr BP. Both TOC and N values are relatively low and stable for the remainder of the record (Figure 4-4), with the exception of two distinct peaks to higher values that are centered on 3,600 and 1,400 cal yr BP. The mass ratio of TOC to N (C/N) ranges from 10.3 to 12.3 and also exhibits multi-century to millennial scale fluctuations (Figure 4-4). The relatively low C/N ratios (< 12.3) support our inference that organic matter is primarily sourced from algal (in-lake) sources and to a lesser extent from terrestrial sources (Meyers and Terranes, 2001). C/N ratios and BSi are negatively correlated between 6,000 to 2,000 cal yr BP (r^2 = 0.38; Figure 4-5), suggesting that variations in the relative source of sedimentary TOC is related to variations in BSi.

Magnetic susceptibility ranges from 0.04 to 0.41 x 10^{-5} SI and also displays multi-century to millennial scale variations (Figure 4-4). The variability in magnetic susceptibility is negatively correlated with BSi (r^2 = 0.25; Figure 4-5). This inverse relationship is likely reflecting the dilution of the clastic content of sediments by increasing BSi content. Dry bulk density ranges from 0.21 to 0.49 g/cm^3 over the study interval (Figure 4-4). The correlation between dry bulk density and BSi over the last 10,000 cal yr BP is very low (r^2 = 0.04; not shown), providing additional support that variations in BSi reflect aquatic productivity and not dilution/concentration from the flux of clastic sediments.

4.4.3 Time series analysis

Time-series analyses were performed on the de-trended and normalized (mean removed) BSi record to detect if any significant periodicities occur within the data. Spectral analysis of the BSi record using the Lomb-Scargle periodogram with the REDFIT code (Schulz and Mudelsee, 2002) shows a broad peak in spectral power between 1300-yr to 1620-yr that is significant above the 95% confidence level (Figure 4-6). The mean value of the spectral peak is centered at 1500-yr. No other significant periodicities on millennial time scales were detected in this analysis, although a less prominent peak at 1000-yr is identified above red-noise but with low (<80%) significance (Figure 4-6). To investigate the temporal evolution of millennial variability at Burial Lake, I performed wavelet analysis on the evenly interpolated, de-trended and normalized BSi record (70 yr) using the Morlet function (Torrence and Compo, 1998). Wavelet analysis shows the 1500-yr cycle in BSi gradually appears during the middle Holocene by ~ 6,000 cal yr BP and later disappears by ~ 3,000 cal yr BP. Further, the analysis reveals a less significant 1000-yr cycle between ~ 8,000 to ~ 6,000 cal yr BP and ~3,000 to ~1000 cal yr BP, consistent with the findings of spectral analysis.

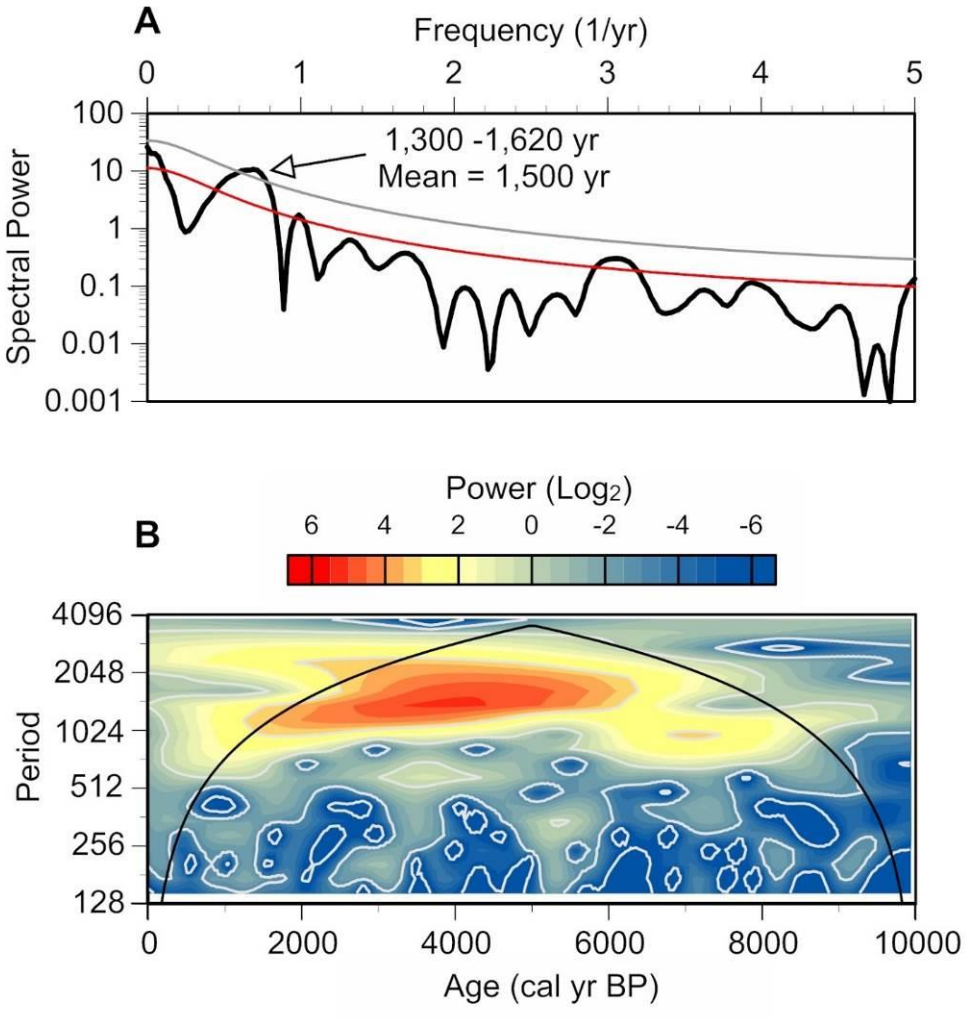

Figure 4-6. Spectral analysis of the Burial Lake biogenic silica record for the last 10,000 cal yr BP. A) Power spectrum of biogenic silica (black curve), theoretical red noise spectrum (red curve), and false alarm level for 95% significance (grey curve). B) Wavelet analysis of biogenic silica showing the power of cycles. The triangular region denoted by the solid black line is the cone of influence and signals above this area may be distorted.

4.5 DISCUSSION

4.5.1 Interpretation of Biogenic Silica Record

The variability in BSi indicates that cyclical changes in aquatic (diatom) productivity have occurred over millennial time scales during the Holocene (Figure 4-4). Changes in diatom productivity in lakes is controlled by light for photosynthesis, lake-water pH, the availability of limiting nutrients (Si, N, and P), and growing season water temperatures (Anderson, 2000; Wetzel, 2001). However, in High Arctic Lakes, where nutrients are often limited, the extent and duration of ice and snow cover is considered the overriding control on diatom productivity (Douglas and Smol, 1999). Warmer summer temperatures result in a longer ice-free growing season, which consequently allows for algal production to be higher. Warmer spring temperatures could cause greater nutrient delivery to Arctic lakes from accelerated snowmelt, permafrost degradation and active-layer thaw, and greater surface runoff from the catchment (Douglas and Smol, 1999). In addition, changes in water balance (precipitation – evaporation) and vegetation patterns can also influence aquatic productivity in Alaskan lakes (Hu et al., 2001; Hu et al., 2003). For example, the presence of the shrub Alnus has been linked with higher levels of aquatic productivity at Grandfather Lake in southwest Alaska (Hu et al., 2001), because it can fix atmospheric N_2 and increase reactive N inputs to lakes. Higher temperatures and increased effective moisture at Arolik Lake in southwest Alaska coincided with an increase in the abundance of Betula shrubs, a lengthened ice-free growing season, higher nutrient inputs, and increased aquatic productivity on centennial to millennial timescales (Hu et al., 2003). Several

other studies across Alaska have demonstrated a relationship between climate and aquatic productivity inferred from sedimentary biogenic silica in lakes (Finney et al., 2012; Kaufman et al., 2012; McKay et al., 2008).

We hypothesize that changes in the duration of the ice-free growing season and nutrient inputs, which are ultimately mediated by climate, controls algal productivity and the overall concentration of sedimentary BSi at Burial Lake. However, the specific mechanism(s) that controls the extent of ice-free conditions and nutrient inputs to Burial Lake over the Holocene are unclear. Core-transect and palynological evidence from Burial Lake indicate stable and overflowing lake-levels are established by ~9,400 cal yr BP, coincident with the appearance of Alnus shrubs in the region (Abbott et al., 2010). Unfortunately, the temporal resolution of pollen analysis from Burial Lake is too coarse to assess the relationship between terrestrial and aquatic ecosystem variability and core-transect data are insensitive to further low magnitude changes in effective moisture. However, proxy evidence from Wolverine Lake (Figure 4-1) in the Kobuk Valley and at Takahula Lake (Figure 4-1) in the central Brooks Range indicate multi-century to millennial variability in effective moisture over the last 8,000 years. It is therefore reasonable that similar patterns in effective moisture affected Burial Lake over this time. Today the majority of annual precipitation at Burial Lake and across the interior of Alaska is received during the summer (June through September) months (Bieniek et al., 2012). Increased summer precipitation would likely result in higher nutrient inputs to Burial Lake through runoff and erosion of permafrost and soils in the surrounding watershed, leading to higher levels of aquatic productivity. Therefore, we

suspect that variations in aquatic productivity are also controlled in part by changes in effective moisture.

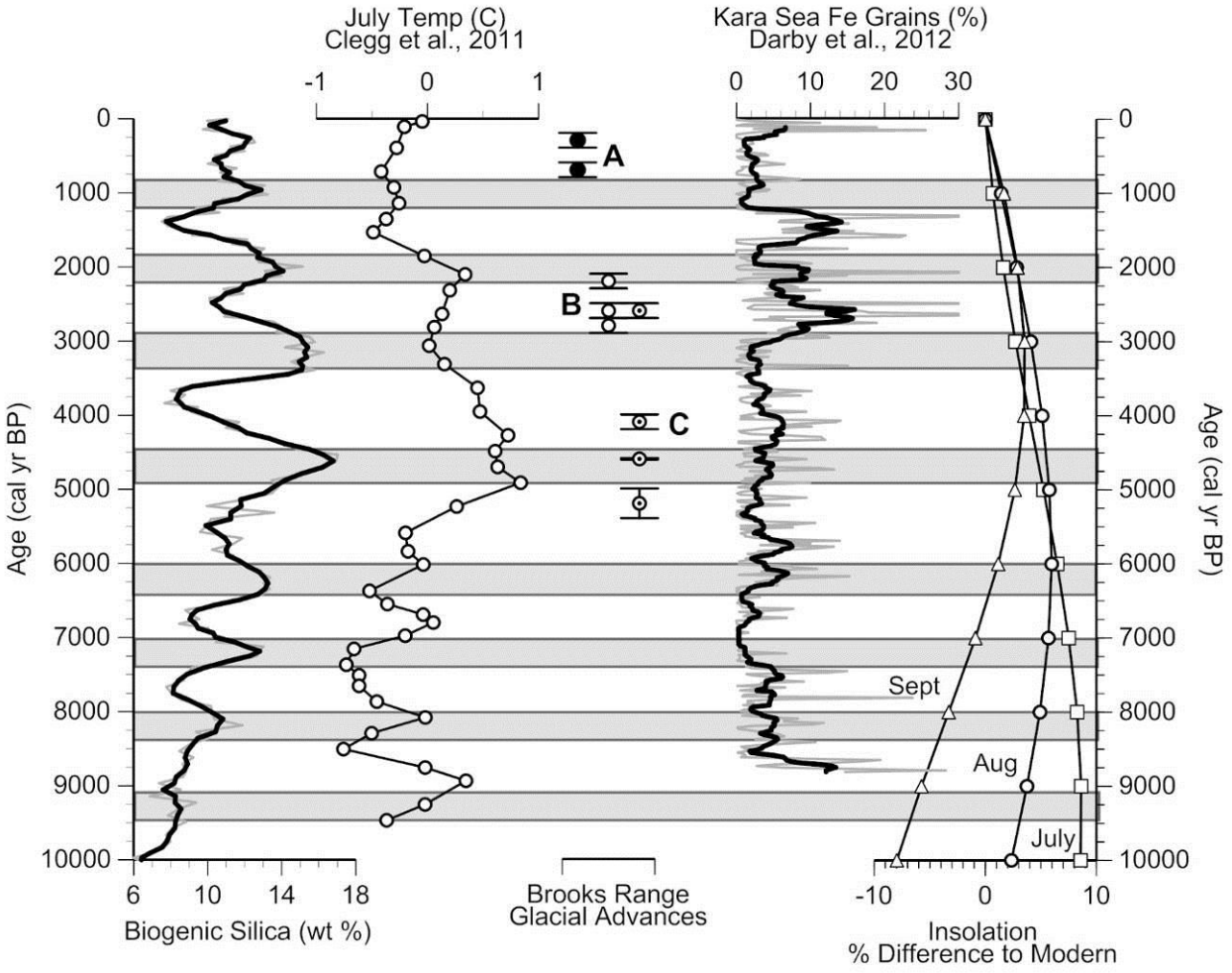

Figure 4-7. Comparison of the Burial Lake biogenic silica record against paleo records from the Alaskan region. July temperature is a composite midge-inferred record (Clegg et al., 2011). Brooks Range alpine glacier moraine ages include A) lichenometry based moraine ages from Sagavinerktok River valley and Oolah Valley (Sikorski et al., 2009), B) ^{10}Be ages on moraines from Kurupa River valley (Badding et al., 2013), and C) ^{10}Be ages on moraines from Atigun River valley (Badding et al., 2013). Core JPC16 Fe grain (%) interpreted as a proxy for the Arctic Oscillation (Darby et al., 2012). Insolation at 65° North latitude for July, August, and September (Laskar et al., 2004).

On orbital timescales, changes in high latitude (65° N) summer insolation should provide a first-order control on the duration of the summer growing season. July insolation levels were 8 % greater than modern between 11,000 to 9,000 cal yr BP (Figure 4-7) during the Holocene thermal maximum in the western Arctic, when proxy evidence suggests warmer than present conditions across Alaska (Kaufman et al., 2004; Kurek et al., 2009). The gradual decline in July insolation levels through the Holocene (Figure 4-7) resulted in alpine glacier advances during the Neoglacial and Little Ice Age in Arctic Alaska (Figure 4-7) (Badding et al., 2013; Ellis and Calkin, 1984; Sikorski et al., 2009), suggesting a nearly linear response to insolation forcing. However, a midge-inferred July temperature reconstruction from central and southern Alaska reveals a more complicated pattern in temperature variability (Figure 4-7) (Clegg et al., 2011). Summer temperatures were lower than modern prior to ~ 5,500 cal yr BP (Figure 4-7), discordant with high levels in July insolation during the early Holocene, but consistent with a reduced summer growing season and low levels of aquatic productivity at Burial Lake. The orbital trend in August and September insolation (Figure 4-7) better matches the long-term trend in BSi, suggesting a potential connection with changes in late summer insolation. Clegg et al. (2011) suggested that summer temperatures responded non-linearly to (summer) insolation forcing resulting from ocean-atmosphere interactions and their interplay with Arctic sea ice. For instance, dinoflagellate analysis from marine core B15 in the western Chukchi Sea (Figure 4-1) indicates extensive summer sea ice and relatively cool sea surface temperatures (SST) between ~12,000 to ~6,000 cal yr BP (de Vernal et al., 2005). Further, diatom analysis from marine core GC-33 in the Southern Bering (Sea) Continental Shelf (Figure 4-1) indicate extensive

sea-ice during the early Holocene before ~7,000 cal yr BP probably because of a weakened and split Aleutian Low pressure system over the western Bering Sea and Gulf of Alaska (Katsuki et al., 2009). ENSO influences the Aleutian Low on interannual time scales, with La Nina-like conditions resulting in a weakened and more westerly Aleutian Low (Niebauer et al., 1999). Evidence from Mt. Logan (Canada) and Laguna Palcacocha (Ecuador) provides support for this interpretation with weakened ENSO or La-Niña like conditions during the early Holocene (Fisher et al., 2008; Rodbell et al., 1999). Today La Niña conditions result in colder winter temperatures across Alaska (Bieniek et al., 2012). Thus, low aquatic productivity at Burial Lake until ~5,500 cal yr BP likely resulted from cooler summer temperatures in Alaska (Clegg et al., 2011) and persistent La Niña-like conditions that produced extensive sea ice and relatively cool SST's in the Bering Sea.

Increasing aquatic productivity at Burial Lake coincides with a shift to higher than modern summer temperatures across Alaska at ~ 5,500 cal yr BP (Figure 4-7). Higher temperatures likely resulted in a lengthened ice-free growing season, an increase in permafrost degradation and flux of limiting nutrients to the lake, and an increase in aquatic productivity. The interval of greatest aquatic productivity between ~5,000 to ~ 2,000 cal yr BP occurs as July insolation continues to decrease from peak values during the early Holocene, again highlighting a divergent response to insolation forcing. However, increasing and peak late summer insolation (August to September) at this time (Figure 4-7) could have lengthened the ice-free season and increased productivity at Burial Lake. Specifically, August insolation levels peaked and were 6% higher than modern during the middle Holocene between ~6,000 to ~5,000 cal yr BP (Figure 4-7),

which had a substantial influence on the late summer surface energy budget and likely extended the ice-free season in Arctic Alaska. Changing oceanographic conditions in the Chukchi Sea provides support for ameliorating paleoenvironmental conditions at this time with a decrease in summer sea ice extent and warmer SST's after ~ 6,000 cal yr BP (de Vernal et al., 2005). Decreasing sea ice extent between ~7,000 to ~3,000 cal yr BP in the Southern Bering Sea from a weakened Aleutian Low (Katsuki et al., 2009) likely contributed to warmer conditions in the Alaskan interior. Increasing aquatic productivity at Burial Lake also broadly coincides with establishment of El Niño-like conditions by ~5,000 cal yr BP in the tropical Pacific Ocean (Rodbell et al., 1999). El Niño and neutral ENSO conditions result in warm temperature anomalies in interior Alaska during the winter months (Papineau, 2001) and the interaction with sea ice accumulation in the Bering Sea likely influenced summer climatic conditions after ~ 5,000 cal yr BP.

The onset of Neoglaciation during the middle to late Holocene resulted in several alpine glacial advances and periods of moraine construction in the Brooks Range (Badding et al., 2013; Ellis and Calkin, 1984; Hamilton, 1994; Sikorski et al., 2009). The age of moraines in the central Brooks Range broadly corresponds with periods of reduced aquatic productivity at Burial Lake (Figure 4-7) during the Little Ice Age (Sikorski et al., 2009) and around ~2,500 (^{10}Be) cal yr BP (Badding et al., 2013). If this observation is valid, it provides additional support for the hypothesis that cool summers and a shorter ice-free season result in lower algal productivity at Burial Lake. However, the correlation between productivity and the timing of moraine stabilization is not perfect. A peak in aquatic productivity at ~4,700 cal yr BP appears synchronous with a

glacial advance centered at ~4,600 ± 500 (^{10}Be) cal yr BP at the Atigun River Valley in the north central Brooks Range (Badding et al., 2013). The large uncertainty in the age of this advance overlaps with preceding and subsequent periods of reduced productivity at Burial Lake, suggesting the possibility that mean ^{10}Be ages on moraines with a limited number of samples (n=4) do not adequately capture the time of this glacial advance. Other climatic factors (e.g. increased winter precipitation) may have contributed to glacial advance at this time, however evidence from Takahula Lake in the south-central Brooks Range indicates low effective moisture at this time (Clegg and Hu, 2010). Alternatively, it is likely the substantial distance between Burial Lake and the Atigun River Valley resulted in spatially heterogeneous climate conditions at this time.

4.5.2 Evaluation of Millennial Variability

The millennial variability in aquatic productivity at Burial Lake implicates a forcing mechanism that has operated on these time scales over the Holocene. Previous work in Alaska suggested that changes in solar variability underlie multi-century to millennial variability in Holocene climate conditions (Hu et al., 2003; Wiles et al., 2008). Comparison of the Burial Lake BSi record against a 9,300-yr reconstruction of total solar irradiance (TSI) (Steinhilber et al., 2009) shows that BSi displays an independent temporal history and different millennial periodicities with respect to TSI (Figure 4-8). Further, the correlation between BSi (interpolated to 70-yr time steps) and TSI is very low (r^2 = 0.003; not shown). Wavelet analysis of the TSI reconstruction (Darby et al., 2012; Khider et al., 2014) has shown significant spectral power around ~1000 and 2500-yr periodicities, while the 1500-yr periodicity present in the BSi record (Figure 4-7)

is noticeably absent. Therefore I conclude there is no direct solar forcing of the 1500-yr cycle in BSi at Burial Lake over the Holocene. The appearance of the statistically significant 1500-yr cycle at Burial Lake by ~ 6,000 cal yr BP is consistent with the hypothesis of Debret et al. (2009) showing a strong middle Holocene transition in millennial variability, that is reportedly linked to internal variability within the climate system.

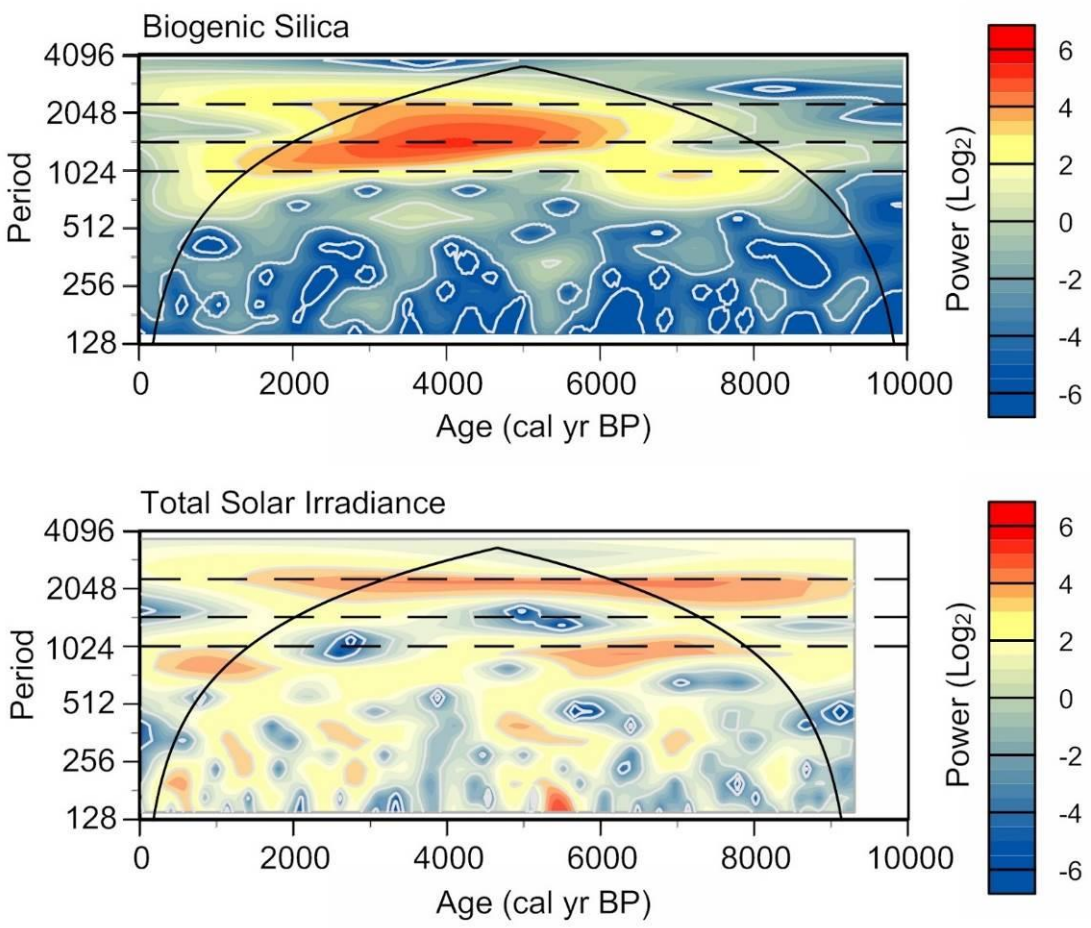

Figure 4-8. Comparison of spectral properties using wavelet analysis between the Burial Lake biogenic silica record (top) against a reconstruction of total solar irradiance (bottom) spanning the last 9,300 cal yr BP (Steinhilber et al., 2009).

Oceanographic records from the North Atlantic region sensitive to AMOC variations and NADW formation changes display prominent millennial scale variations and a 1500-year periodicity during the Holocene (Bianchi and McCave, 1999; Hoogakker et al., 2011; Thornalley et al., 2009). Further, wavelet analysis of these records shows the 1500-year periodicity emerges by the middle Holocene (Debret et al., 2007; Hoogakker et al., 2011), consistent with the findings from the Burial Lake biogenic silica record. To facilitate comparison of millennial variations in climate between the records, I bandpass filtered the Burial Lake biogenic silica and North Atlantic records at 1250-1750 years (Figure 4-9) based on the signal processing routine employed by Khider et al. (2014). Because the 1500-yr cycle at Burial Lake only exists between ~ 6,000 to 3,000 cal yr BP, I limit discussion to this time period. Notably, peaks in aquatic productivity at Burial Lake correspond with a strengthened AMOC, high flow speeds in NADW, and a weak sub-polar gyre circulation which contributes freshwater to the Atlantic inflow. This comparison suggests the millennial variations in biogenic silica at Burial Lake could be related to changes in North Atlantic Ocean circulation, via a common forcing or through an ocean-atmosphere interaction that transmits this signal to Arctic Alaska.

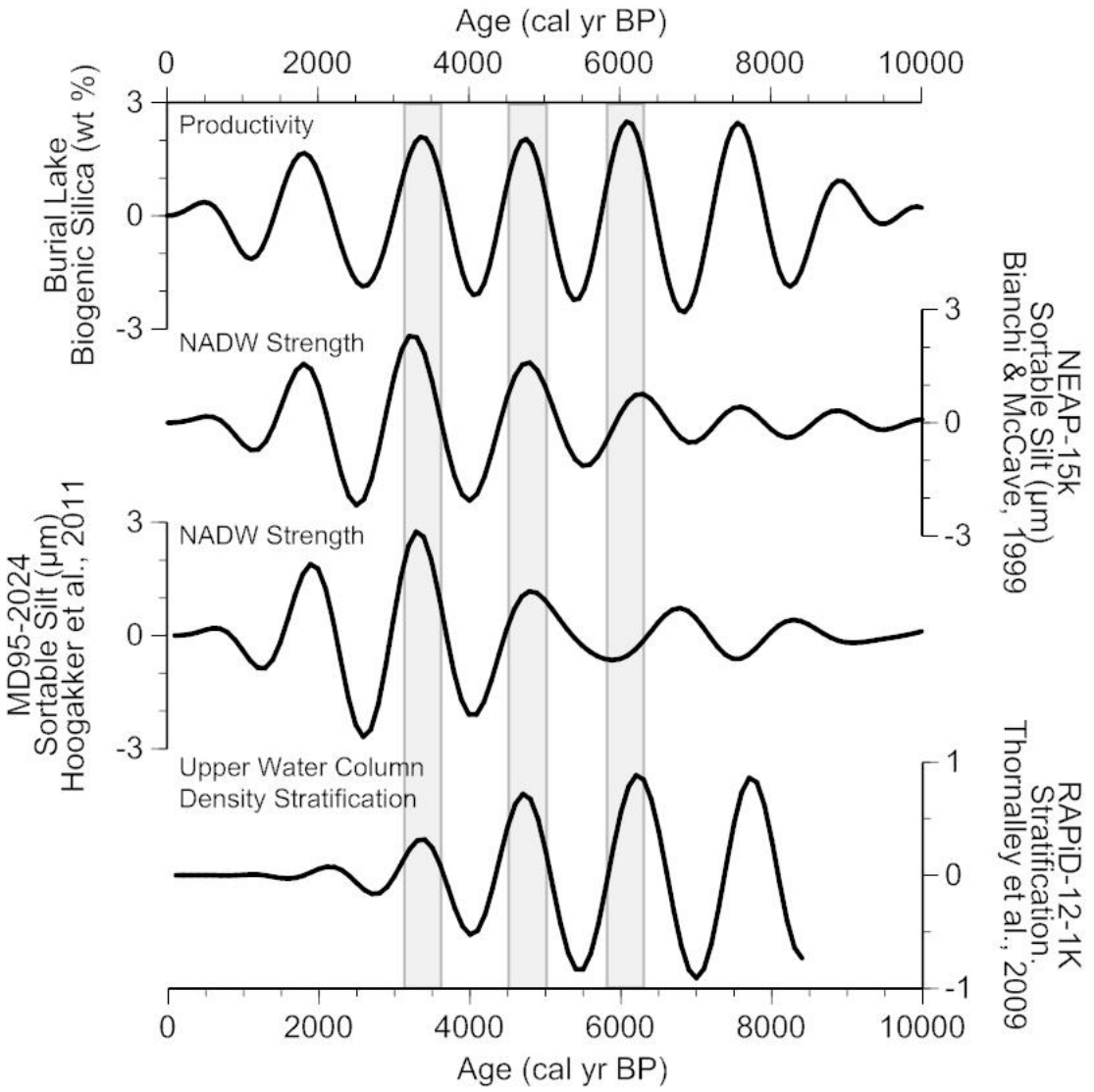

Figure 4-9. Comparison of the Burial Lake productivity record against North Atlantic variability over the Holocene. All records were bandpass filtered at 1250–1750 years to highlight variability on this timescale.

Sedimentological evidence from the western Arctic Ocean reveals a similar pattern of Holocene millennial climate variations, potentially providing a link between the North Atlantic and Arctic regions. For instance, ice-rafted debris analysis from marine core JPC16 in the Beaufort Sea (Figure 4-1) displays millennial variability in Arctic sea

ice drift, interpreted to reflect variations in the mean state of the Arctic Oscillation (AO) over the last 8,800 cal yr BP (Figure 4-7) (Darby et al., 2012). Time series analysis of the AO proxy indicates a significant 1,500-yr periodicity in sea ice drift that is distinct from changes in TSI (Darby et al., 2012). Today the AO provides an important control on the winter climate of Alaska, with AO+ conditions associated with cold temperature anomalies (Bieniek et al., 2012). The effect of the wintertime AO persists through most of the subsequent year through the influence on the thickness of wintertime sea ice and its control on heat transfer between the Arctic Ocean and overlying atmosphere in summer and fall (Rigor et al., 2002). Comparison of aquatic productivity at Burial Lake with the AO proxy (Figure 4-7) indicate that troughs in BSi coincide with AO+ conditions and colder temperatures over the last ~3,000 cal yr BP. For example, strong AO+ conditions correspond with distinct minima in aquatic productivity at ~2,500 and ~1,400 cal yr BP (Figure 4-7).

This observation suggests a physical link exists between the mean state of the AO and aquatic productivity at Burial Lake on millennial time scales. AO+ conditions likely result in lower (colder) summer temperatures in northern Alaska and a short ice-free growing season, a thinner active layer in permafrost during the summer and a decreased flux of limiting nutrients to the lake, and reduced aquatic productivity at Burial Lake. Relatively high aquatic productivity over the last ~1,000 cal yr BP coincides with AO- conditions, which results warmer winters in Alaska today (Bieniek et al., 2012). The interpretation linking the Arctic Oscillation and sea ice dynamics in the Beaufort Sea to climatic conditions in northern Alaska is supported by a recent analysis of satellite derived sea ice and weather data for the period 1979-2012. During this time, a

strong decrease in sea ice concentration in the Beaufort and Chukchi Sea's coincides with a mean annual temperature increase of 2.7° C in northern Alaska (Wendler et al., 2014). The net radiation budget at Barrow in northern Alaska is primarily controlled by the regional surface albedo (Wendler and Eaton, 1990). Specifically, increased sea ice concentration in the Beaufort and Chukchi Sea's results in a reduced radiation receipt and colder temperatures at Barrow. In addition, the decrease of sea ice and warmer atmosphere resulted in a 42% increase in annual precipitation and an increase in brush taxa (willow and dwarf birch) in northern Alaska over the 34 year period. Comparison of sea ice concentration in the Beaufort Sea with the AO index during this time shows a high and significant correlation (r^2 = 0.49) (Wendler et al., 2014). Therefore, it is apparent that sea ice dynamics directly influence temperature and precipitation conditions in northern Alaska and we hypothesize this physical link acted in a similar way over the last 10,000 years.

Wavelet cross coherence analysis between the Burial Lake BSi record and the AO proxy permits analysis of the evolution of millennial variability over time (Grinsted et al., 2004). The squared wavelet coherence between productivity and the AO highlights periodicities common to both time series in red (Figure 4-10). Both records display strong ~1,500-yr variability during the middle Holocene between ~6,000 to ~3,000 cal yr BP and a transition to ~1,000-yr variability over the last ~3,000 cal yr BP. The similarity in millennial periodic variability between productivity and the AO does not explicitly indicate a direct cause and effect relationship. However, the area of significant common power and phase arrows over the last ~3,000 cal yr BP indicate an anti-phase relationship between the AO and productivity (Figure 4-10), consistent with the

aforementioned observation that AO+ conditions coincide with reduced productivity at Burial Lake. We therefore suggest that variations in the mean state of the AO are partly responsible for millennial variability in aquatic productivity at Burial Lake at least over the late Holocene. The anti-phase relationship between the AO and productivity is not consistent through time, however. Between ~6,000 to ~3,000 cal yr BP, the phase arrows indicate the AO leads productivity by roughly half the millennial periodicity (1500-yr) during this time. This discrepancy could result from age-model inconsistencies between the two independently, radiocarbon dated proxy records. Further, the application of a constant marine reservoir correction (ΔR = 506 yr) to correct the radiocarbon dated JPC16 core sequence could lead to inconsistencies between the records (Darby et al., 2012). Alternatively, the apparent offset might suggest a different climate forcing that operates on millennial time scales that affects both the AO and aquatic productivity at Burial Lake. Regardless, the similarity in the evolution of millennial variability between the records implicates a physical connection has existed between ecosystem variability in northern Alaska and ocean-atmosphere interactions in the western Arctic Ocean region over the Holocene.

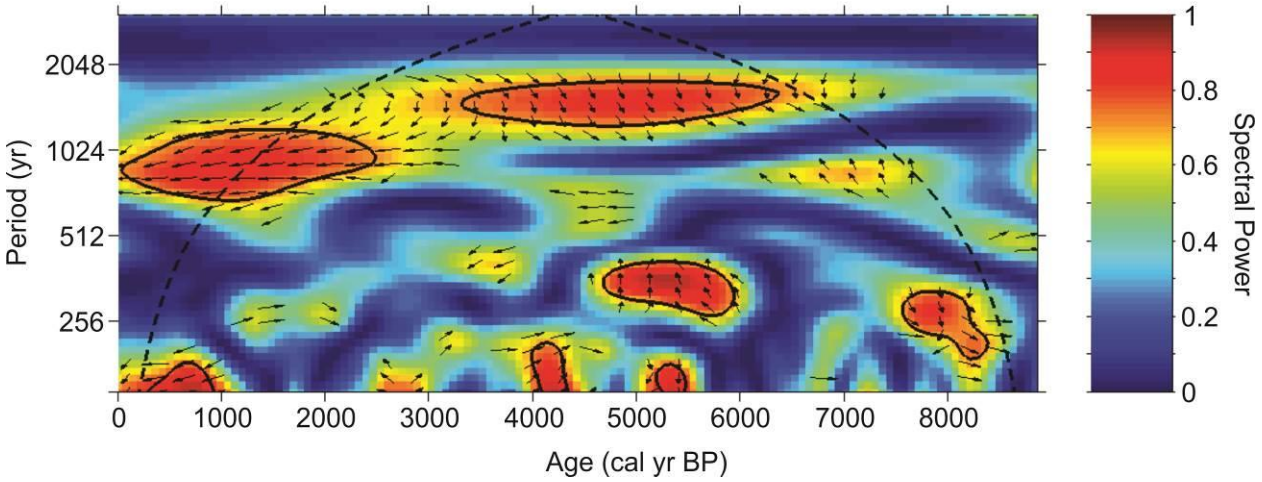

Figure 4-10. Wavelet cross coherence of the Burial Lake biogenic silica record against Fe grain (%) from core JPC16 from the Beaufort Sea interpreted as a proxy for the Arctic Oscillation.

4.6 CONCLUSIONS

The Burial Lake aquatic productivity record highlights the sensitivity of aquatic ecosystems in northern Alaska to changes in growing season temperature and western Ocean-atmosphere interactions. Spectral analysis results are consistent with the notion that the 1500-yr signal observed in Holocene paleoclimate records emerges during the middle Holocene around ~6,000 cal yr BP (Debret et al., 2007; Debret et al., 2009). Further, comparison of the aquatic productivity record against a reconstruction of total solar irradiance indicates there is no direct solar forcing of millennial climate variations at Burial Lake. This result lends additional support for the hypothesis that the 1500-yr cycle in Holocene climate records is not a result of external forcing. Reduced aquatic productivity at Burial Lake coincides with positive phases of the Arctic Oscillation, which result in colder summers, a shortened ice-free (summer) growing season, and a

reduced flux of nutrients to the lake. We therefore propose that aquatic productivity variations are related to state changes in the AO and that millennial variability that the record exhibits is related to internal oscillations within the climate system. This observation has important implications for aquatic ecosystem variability in the Alaskan Arctic, in light of the observed decrease in the extent and volume of Arctic sea ice (Stroeve et al., 2007) over the late 20th century from increasing greenhouse gas emissions and climate change. Sea ice model projections from the Intergovernmental Panel on Climate Change 4th Assessment Report indicate a seasonally ice free Arctic Ocean by the mid-21st century under the business as usual emissions scenario (Zhang and Walsh, 2006). The transition to a new mean state in Arctic sea ice will undoubtedly effect the surface energy budget and future patterns of aquatic ecosystem variability in Arctic Alaska.

5.0 HOLOCENE CLIMATE FROM NEWFOUNDLAND SENSITIVE TO NORTH ATLANTIC OCEAN-ATMOSPHERE INTERACTIONS ON MILLENNIAL TO ORBITAL TIME SCALES

Open-basin lakes that precipitate carbonate minerals have the potential to provide excellent archives to reconstruct past variations in the oxygen isotopic composition of precipitation ($\delta^{18}O_{ppt}$). Existing $\delta^{18}O_{ppt}$ records from the circum North Atlantic region spanning the Holocene show dramatic fluctuations with rapid ice sheet deglaciation, followed by more stable conditions as interglacial boundary conditions were achieved. However, relatively few quantitative hydroclimate records exist from the eastern Canadian Maritime Provinces, and therefore questions remain regarding the magnitude of century to millennial-scale $\delta^{18}O_{ppt}$ variations in precipitation over the Holocene. Here we present a lacustrine oxygen isotope ($\delta^{18}O$) record spanning the period 10,200 to 1,200 calendar years before present (cal yr BP) from Cheeseman Lake, a small, alkaline, hydrologically open lake located in west-central Newfoundland, Canada. Water stable isotope data from regional lakes, rivers, and monthly precipitation indicate the surface waters at Cheeseman Lake plot along the local meteoric water line and that the $\delta^{18}O$ of lake water reflects the annual moisture surplus (precipitation - evaporation) weighted $\delta^{18}O_{ppt}$. Climate sensitivity simulations conducted with a lake hydrologic and isotope mass balance model further indicate that Cheeseman

Lake is sensitive to cold-season (October-March) temperature changes, and to a much lesser extent the seasonality of precipitation. To infer past changes in the $\delta^{18}O_{ppt}$, we measured the stable isotopic composition of fine-grained (< 63 μm) authigenic calcite ($\delta^{18}O_{cal}$) sampled continuously at an average temporal resolution of ~ 48 years. A general trend of increasing and more positive $\delta^{18}O_{cal}$ values between ~ 10,200 to ~ 7,950 cal yr BP is interpreted to reflect warming temperatures. This period coincides with melting of the Laurentide Ice Sheet, changing surface ocean $\delta^{18}O$ from enhanced meltwater delivery, and rising eustatic sea levels. The increasing trend is interrupted by abrupt $\delta^{18}O_{ca}$ anomalies to more negative values at ~ 9,700 and ~ 8,500 cal yr BP, that coincide with cooling events in the adjacent Labrador Sea and circum North Atlantic region. After ~ 7,950 cal yr BP, $\delta^{18}O_{cal}$ values decrease to gradually more negative values until ~ 4,300 cal yr BP, which we interpret as a cooling trend related to declining Boreal summer insolation and cooling sea surface temperatures in the western North Atlantic Ocean. $\delta^{18}O_{cal}$ values return to slightly more positive values after ~ 4,300 cal yr BP and thereafter remain relatively stable until ~ 1,200 cal yr BP. The transition at ~4,300 cal yr BP corresponds with a shift to wetter conditions in Newfoundland evinced from other paleo-proxy records. The discordance between Cheeseman Lake $\delta^{18}O_{cal}$ values and declining insolation could in part reflect warmer temperatures and/or changes in the seasonality of precipitation resulting from an abrupt and mean-state shift in atmospheric circulation.

5.1 INTRODUCTION

The oxygen isotopic composition of precipitation ($\delta^{18}O_{ppt}$) is an effective tracer of the global hydrologic cycle (Araguás-Araguás et al., 2000; Gat, 1995). $\delta^{18}O_{ppt}$ is controlled by the initial $\delta^{18}O_{ppt}$ at the moisture source and isotopic fractionation processes that occur during the movement of water molecules through the hydrological cycle (Bowen and Wilkinson, 2002; Dansgaard, 1964; Rozanski et al., 1992). As a result, reconstructions of paleo $\delta^{18}O_{ppt}$ from ice cores (Grootes and Stuiver, 1997; NGRIP, 2004), speleothems (Ersek et al., 2012), tree rings (Bale et al., 2010; Brienen et al., 2012), and lake sediments (Anderson et al., 2005; Daley et al., 2009; Edwards et al., 1996; Steinman et al., 2014; Steinman et al., 2012) have provided invaluable information concerning paleohydrological and paleoclimatic conditions over the Holocene. For instance, high-resolution $\delta^{18}O_{ppt}$ records from Greenland ice cores reveal substantial changes in atmospheric temperature and snowfall accumulation over the current interglacial (Grootes and Stuiver, 1997). Greenland ice core records also show the presence of early Holocene abrupt climate events at 9,300 and 8,200 cal yr BP that have been linked to catastrophic drainage of proglacial lakes (Barber et al., 1999; Clarke et al., 2004), routing of meltwater and freshening of the North Atlantic Ocean (Licciardi et al., 1999), a reduction or partial shut-down of North Atlantic Deep Water (NADW) formation (Clark et al., 2001), and abrupt but short-lived cooling events (Alley et al., 1997; Yu et al., 2010). After the 8,200 cal yr BP event, Greenland ice core records display generally more stable and gradually decreasing $\delta^{18}O_{ppt}$ values towards the present (Grootes and Stuiver, 1997) consistent with cooling (Vinther et al., 2009) and the monotonic decline in 65° N summer insolation (Laskar et al., 2004). While very

informative, $\delta^{18}O_{ppt}$ records from Greenland ice cores are restricted geographically and therefore much less is known concerning spatial variability in paleo- $\delta^{18}O_{ppt}$ over the Holocene. Although the terrestrial climate signature of early Holocene abrupt climate events is well-expressed in the North Atlantic region (Daley et al., 2011; Marshall et al., 2007; von Grafenstein et al., 1999), relatively few $\delta^{18}O_{ppt}$ records exist from the western North Atlantic region in eastern Canada (Daley et al., 2009).

To date, the only reported $\delta^{18}O_{ppt}$ reconstruction from the island of Newfoundland is a bog sphagnum cellulose $\delta^{18}O$ record from Nordan's Pond Bog (Daley et al., 2009). The large range (-9.67 to -4.12 ‰) in reconstructed $\delta^{18}O_{ppt}$ values and the isotopic composition of water samples suggest the possibility that evaporative modification of bog waters exerts a dominant influence on the reported cellulose $\delta^{18}O$ values, yielding a record of moisture balance (precipitation – evaporation) rather than meteoric precipitation. Given these uncertainties, additional $\delta^{18}O_{ppt}$ records from the Maritime Provinces of eastern Canada are necessary to confirm the patterns identified by Daley et al. (2009) and to disentangle the relationship between atmospheric temperature and potential circulation variations over the Holocene.

Here we present a lacustrine oxygen isotope ($\delta^{18}O$) record from a small, alkaline lake (Cheeseman Lake) located in west-central Newfoundland, Canada spanning the period 10,200 to 1,200 calendar years before present (cal yr BP). To investigate hydroclimate variability and North Atlantic Ocean-land interactions over the Holocene in Newfoundland, we analyzed the stable isotopic composition of authigenic calcite ($\delta^{13}C$ and $\delta^{18}O$) from the Cheeseman Lake sedimentary record at continuous 1 cm intervals (n = 189). We further analyzed surface water samples for stable isotopes (δD and

$\delta^{18}O$), instrumental climate data from a proximal weather station, and monthly precipitation δD and $\delta^{18}O$ data from a Canadian Network of Isotopes in Precipitation (CNIP) station to investigate modern lake-catchment hydrologic and water isotope relationships. To provide a framework for interpreting the Cheeseman Lake $\delta^{18}O$ record, we utilized a coupled lake hydrologic and water isotope mass balance model (Steinman et al., 2010a; Steinman et al., 2010b) to assess the sensitivity of the lake to hydroclimate forcing (Stansell et al., 2013; Steinman and Abbott, 2013). Specifically, we performed a series of climate sensitivity tests to determine the response of lake water $\delta^{18}O$ and calcite $\delta^{18}O$ to changes in mean annual temperature (± 2° C) and the seasonality of precipitation (± 20% winter). We interpret the Cheeseman Lake $\delta^{18}O$ record with respect to changes in Laurentide Ice Sheet extent (Dyke and Prest, 1987), eustatic sea level (Clark et al., 2009), and 50° N insolation (Laskar et al., 2004). Further, we compare our paleoenvironmental interpretations to ice core $\delta^{18}O$ from southern (Dye-3) (Daansgaard et al., 1985) and central Greenland (North Greenland Ice Core Project, NGRIP) (NGRIP, 2004), sea surface temperature and foraminiferal $\delta^{18}O$ records from the Labrador Sea (Andrews et al., 1999; Hoffman et al., 2012) and western North Atlantic Ocean (Keigwin et al., 2005; Sachs, 2007), and terrestrial hydroclimate records from Newfoundland (Amesbury et al., 2013; Daley et al., 2009; Daley et al., 2011) to evaluate the underlying causes of orbital to centennial scale climate variability during the Holocene.

5.2 SITE LOCATION AND REGIONAL SETTING

Cheeseman Lake (informal name; 49.351° N, 57.603° W, 180 m asl) is a small (0.2 km^2), alkaline, open-basin lake located near the coast of west-central Newfoundland (Figure 5-1; Figure 5-2). The lake is elliptical in shape and the surrounding watershed is small (1.9 km^2), characterized by moderately steep slopes along much of the lakes shoreline. The lake receives inflow from a small stream on the southwest shoreline and drains to Lomond River through a small outlet stream on the northeast shoreline. The lake had a maximum water depth of 4.1 m near the geometric center of the basin in August, 2012. The catchment contains second-growth forests that are characterized by a Dryopteris-Hylocomium-Balsam Fir forest type (South, 1983). Balsam Fir (Abies balsamea) is the dominant forest cover, however Yellow Birch (Betula alleghaniensis) and Red Maple (Acer rubrum) are also common and robust in the Western Newfoundland ecoregion (Newfoundland, 2007). The isotopic composition of lake surface waters collected in August, 2012 had $\delta^{18}O$ and δD values of -9.02 and -65.05 ‰ VSMOW, respectively.

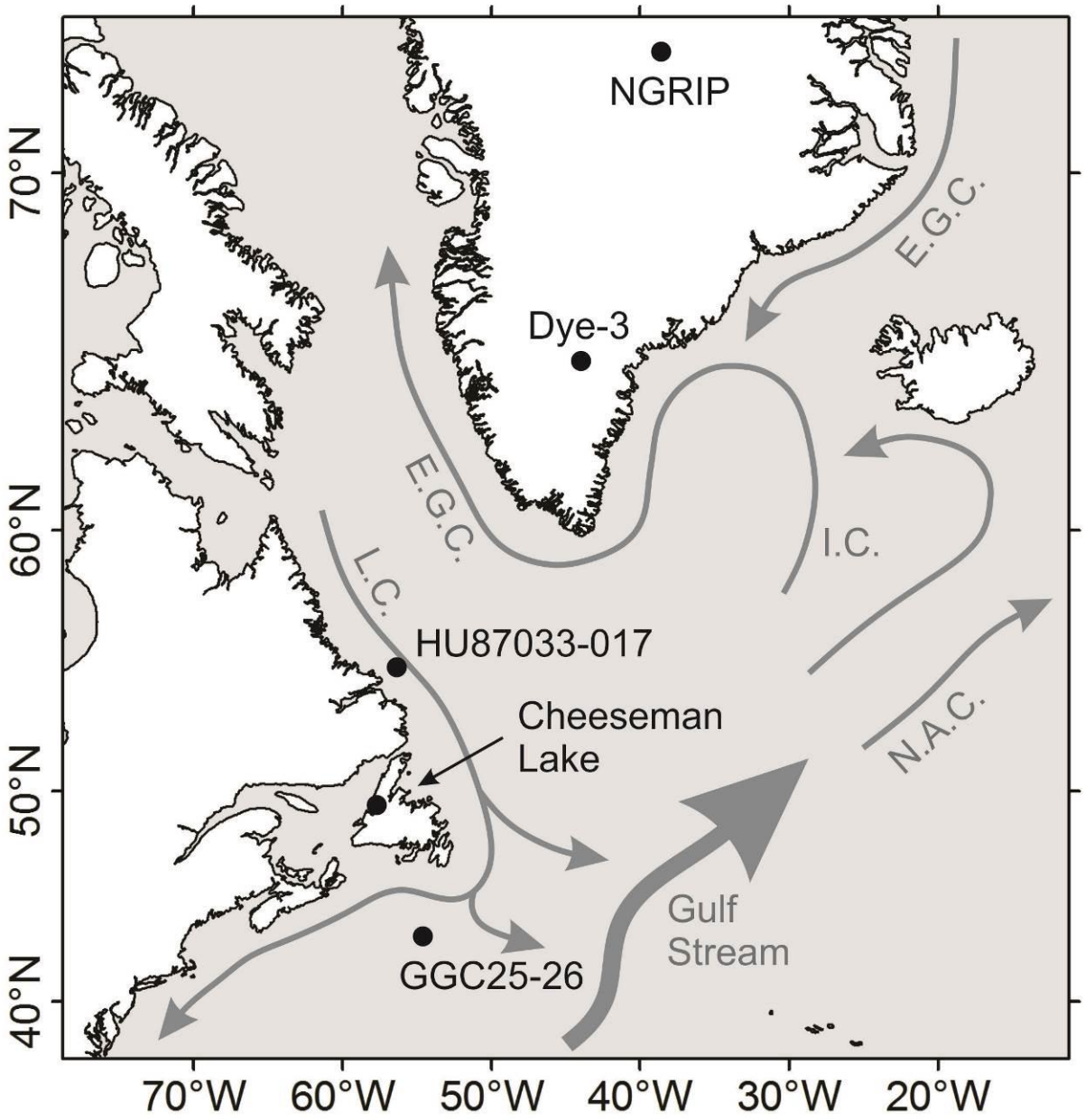

Figure 5-1. Map of the western North Atlantic region showing modern surface ocean currents and sites mentioned in the text. Ocean currents include, N.A.C. – North Atlantic Current, E.G.C. – East Greenland Current, I.C. – Irminger Current, and L.C. – Labrador Current.

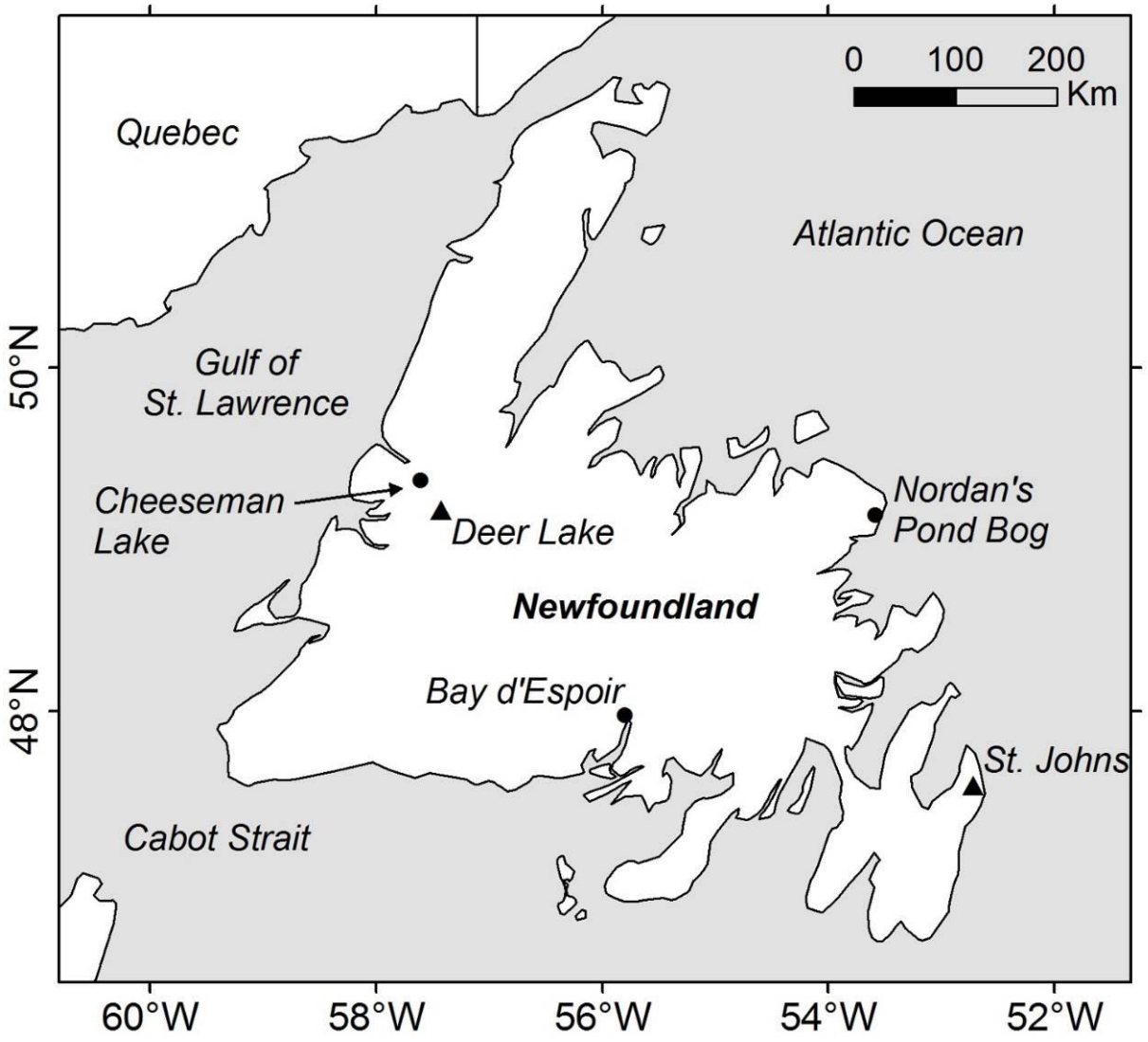

Figure 5-2. Map of Newfoundland with Cheeseman Lake (informal name) and other sites mentioned in the text.

The lake and surrounding area is located in the West Coast Calcareous Uplands physiographic province, characterized by hilly terrain and irregular topography (South, 1983). Marl ponds that precipitate carbonate minerals, similar to Cheeseman Lake, are a common feature of the province (South, 1983). Bedrock geology in the catchment consists of Cambrian to Ordovician age limestone, dolostone, and shale (Colman-Sadd

et al., 2000). Surficial geology in the immediate area is mapped as till veneer, which is composed of a thin (< 1.5 m) discontinuous sheet of lodgment till (Liverman and Taylor, 1990). The Island of Newfoundland was covered by the Laurentide Ice Sheet during the last glacial period (Dyke and Prest, 1987; Shaw et al., 2006). Retreat of the Laurentide Ice Sheet by 13,000 ^{14}C yr BP (~ 15,200 cal yr BP) formed an isolated Newfoundland Ice Cap, which thereafter was increasingly topographically controlled as the ice retreated inland (Batterson and Catto, 2001). The Deer Lake valley, located ~ 20 km southwest of Cheeseman Lake, was deglaciated by 12,000 ^{14}C yr BP (~ 13,800 cal yr BP) (Batterson and Catto, 2001). Post-glacial isostatic depression resulted in higher relative sea level compared with the present and presumably an unstable land surface. A relative sea level curve for the Bay of Islands, based on radiocarbon dates on marine micro-fauna, indicates levels at ~ 30 m asl at 12,000 ^{14}C yr BP (~ 13,800 cal yr BP) that approach modern levels by 10,000 ^{14}C yr BP (~ 11,500 cal yr BP) (Batterson and Catto, 2001). Cheeseman Lake was not inundated by higher relative sea levels during deglaciation (Batterson and Catto, 2001), however the lake and catchment were presumably influenced by general landscape instability as isostatic adjustment was achieved.

The climate of Newfoundland is principally controlled by the marine influence of the Gulf of St. Lawrence and Atlantic Ocean along with hemispheric-wide atmospheric circulation patterns (Ullah, 1992). The island climate is influenced by the Labrador Current that transports cold, ex-Arctic waters along the eastern continental margin and the warm, northeastward flowing North Atlantic Current (Figure 5-1). The resultant climate of Newfoundland is characterized by generally mild winters and cool summers

(Ullah, 1992). Climate data from Deer Lake (Figure 5-3) record average winter (January-February-March) and summer (June-July-August) temperatures of -6.8° C and 15.0 ° C (Figure 5-3), respectively (Canada, 2010). Modern climate data indicate that precipitation is generally distributed equally over the year, with slightly lower amounts during the late winter/early spring but otherwise no distinct wet season (Figure 5-3). Climatic conditions in Newfoundland are further influenced by internal modes of climate variability on seasonal to multi-decadal timescales. The North Atlantic Oscillation (NAO) provides an important control on the cold-season climate of the North Atlantic region (Hurrell, 1995) and Newfoundland specifically. The NAO, generally defined by the pressure difference between the Azores high and the Icelandic low, influences the hemisphere-wide circulation and exerts a dominant influence on wintertime temperatures across the Northern Hemisphere (Hurrell and Deser, 2010). For example, the positive phase of the NAO index is associated with below average (colder) winter temperatures across Newfoundland (Figure 5-4) (Banfield and Jacobs, 1998). Cold-season precipitation and the NAO index across Newfoundland display no significant correlation (Figure 5-4) (Banfield and Jacobs, 1998). The influence of the NAO on the climate of Newfoundland is restricted to the winter months, with no significant relationship between the summer-time NAO index and temperature or precipitation (Banfield and Jacobs, 1998).

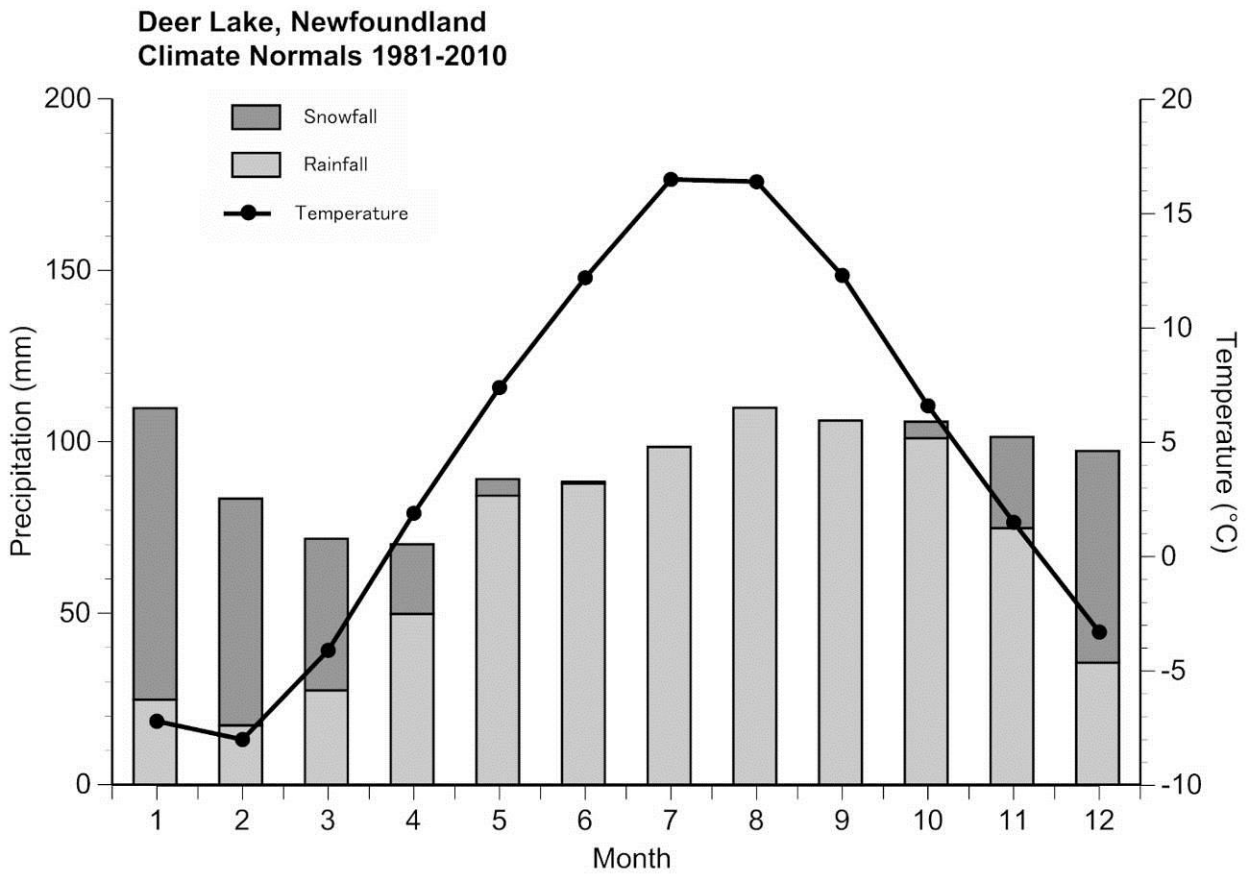

Figure 5-3. Climate normals for the period 1981 to 2010 for Deer Lake, Newfoundland. Data source is from Environment Canada.

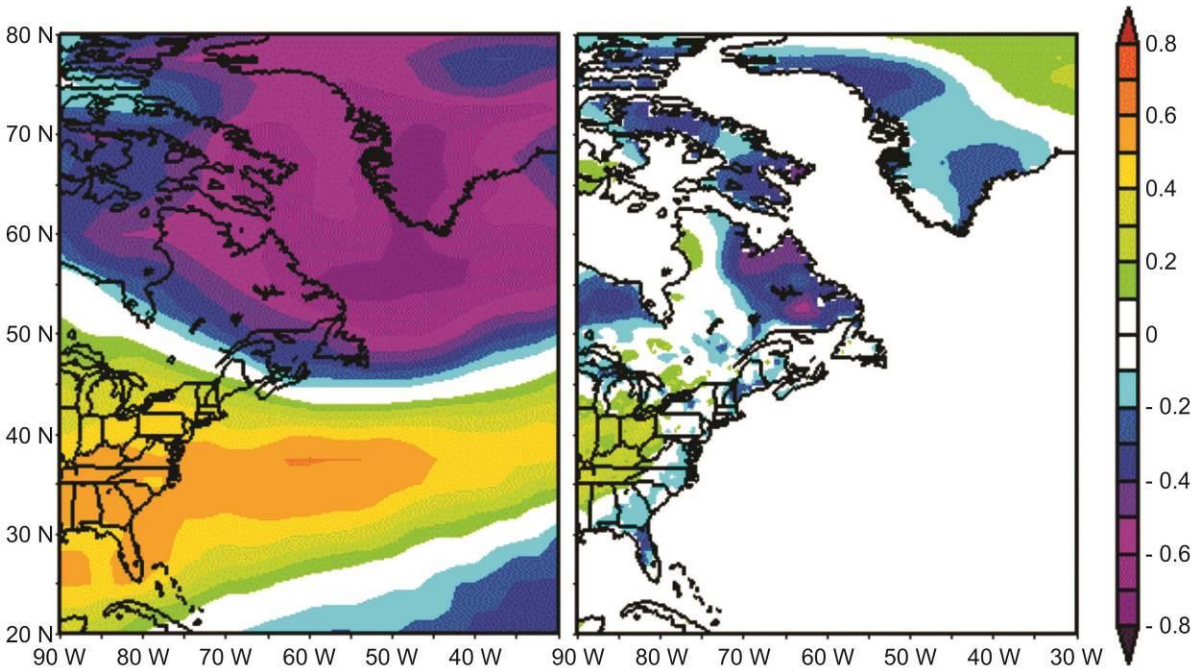

Figure 5-4. NCEP/NCAR reanalysis showing the correlation between surface air temperature (left) and University of Delaware v3.0 reanalysis precipitation (right) with the NAO index during the winter season (December-January-February) for the period 1949-2010.

5.3 METHODS

5.3.1 Sediment coring and sample collection

Sediment cores were collected from the center of the lake in August, 2012. A surface core (A-12 Drive 1) with an intact sediment-water interface was recovered from 3.5 m water depth using a polycarbonate tube fit attached to a rod-driven piston corer. The flocculate upper 32 cm of the surface core was extruded in the field at 1 cm intervals into sterilized whirl-pak® bags. Multiple overlapping long cores were

recovered from an adjacent core site (B-12) in 4.1 m water depth using a square rod Livingstone corer. All long cores were packaged in the field and securely transported to the Department of Geology and Planetary Science at the University of Pittsburgh for processing and analysis.

Water samples for oxygen ($\delta^{18}O$) and hydrogen isotope (δD) analyses were collected from the surface water of regional lakes and streams in August, 2012. Samples were collected in 30 mL polyethylene bottles after rinsing three times with sample water and then capping the bottle underwater. Water samples were measured for stable isotopes at the University of Arizona Environmental Isotope Laboratory on a gas-source isotope ratio mass spectrometer (Finnigan Delta S). For hydrogen, samples were reacted at 750°C with Cr metal using a Finnigan H/Device coupled to the mass spectrometer. For oxygen, samples were equilibrated with CO_2 gas at approximately 15°C in an automated equilibration device coupled to the mass spectrometer. Standardization is based on the international reference materials Vienna Standard Mean Ocean Water (VSMOW) and Standard Light Antarctic Precipitation (SLAP). Precision is 0.9 per mil (‰) or better for δD and 0.08 ‰ or better for $\delta^{18}O$ on the basis of repeated internal standard measurement. The isotopic composition of modern precipitation was also used to investigate modern lake-catchment hydrologic and water isotope relationships. Monthly precipitation $\delta^{18}O$ and δD data from a Canadian Network for Isotopes in Precipitation (CNIP) station at Bay d'Espoir, Newfoundland (Figure 5-2) for the period 1997 to 2010 were analyzed to estimate the sensitivity of Cheeseman Lake water isotopes to hydroclimate forcing. Surface water samples from regional lakes and

rivers were also collected to determine total carbonate (alkalinity) concentrations via H_2SO_4 acid titration using a Hach® Digital Titrator.

5.3.2 Lithostratigraphy

Sediment cores were split lengthwise and described at the Department of Geology and Planetary Science at the University of Pittsburgh. Notable sedimentary structures, grain size, and Munsell color were characterized for each core. All cores were sampled at 1 cm intervals and dry bulk density was calculated from dry weights of volumetric samples. Loss-on-ignition (LOI) analysis was conducted at 550° C for 4 hours and 1000° C for 2 hours to estimate the weight percent organic matter and total carbonate (Heiri et al., 2001). A composite sediment core sequence was developed by matching visible stratigraphic markers between the A-12 surface core and B-12 Livingstone cores.

5.3.3 Geochronology

Age control of the recovered material was developed from ^{210}Pb dating of surface sediments and Accelerator Mass Spectrometry (AMS) radiocarbon analyses of 10 terrestrial macrofossils (Table 5.1). Freeze dried and homogenized aliquots of the top 32 cm of surface core A-12 were analyzed for radioisotope (^{210}Pb, ^{214}Pb, ^{137}Cs and ^{226}Ra) activities by direct gamma counting using a high purity germanium detector (Canberra model BE-3825) with a closed-end coaxial well located in the Department of Geology and Planetary Science at the University of Pittsburgh. Detector efficiency was

determined by counting a Canberra MGS-1 standard for which peak efficiencies have been established using a National Institute of Standards traceable standard. Excess ^{210}Pb activities were calculated by subtracting the background ^{214}Pb activity, sourced from in-situ decay of ^{226}Ra within the sediment matrix, from the ^{210}Pb activity sourced from direct atmospheric deposition. Sediment ages were calculated using the Constant Rate of Supply (CRS) method, which accounts for variability in both the sedimentation rate and dry bulk density, according to the methodology of Binford (1990). Bulk sediment samples were disaggregated with dilute (7 %) H_2O_2, wet-sieved with a 150 μm sieve, and terrestrial macrofossils were identified and picked under a stereographic microscope for AMS radiocarbon measurement. Samples were pre-treated using standard acid-base-acid wash techniques (Abbott and Stafford, 1996) at the University of Pittsburgh and were combusted to CO_2 gas, converted to filamentous graphite, pressed in Aluminum targets, and measured at the W.M. Keck Carbon Cycle AMS Laboratory, University of California, Irvine. Radiocarbon ages were calibrated using CALIB 7.0 and the IntCAL13 calibration curve (Reimer et al., 2013). An age-depth model was created using a cubic spline interpolator with the classical age modeling (CLAM) code v2.2 for the statistical software R (Blaauw, 2010). The CLAM analysis performed 1,000 age model iterations based on repeated sampling of the calibrated age distributions for each radiocarbon sample to estimate the ‘best fit’ or weighted mean age for each depth.

Table 5.1. Cheeseman Lake AMS radiocarbon dates with calibrated 2s error ranges. The sample highlighted with an asterisk was rejected from the age model.

UCIAMS #	Core	Total Depth (cm)	Material	^{14}C age yr BP	± yr	Calib 2σ yr BP
* 131491	A-12 66-67cm	66.5	plant material	1,650	70	1,389-1,711
131491	A-12 75-76cm	75.5	plant material	1,485	40	1,301-1,518
116881	B-12 D1 15cm	102	plant material	2,250	20	2,159-2,339
131492	B-12 D1 35-36cm	122.5	plant material	3,520	35	3,698-3,887
122242	B-12 D1 80-81cm	167.5	plant material	5,010	45	5,651-5,895
122243	B-12 D2 22-23cm	191.5	plant material	5,980	70	6,660-6,993
141393	B-12 D2 43cm	212	plant material	7,040	35	7,795-7,947
116882	B12 D2 62-63cm	231.5	plant material	7,955	30	8,649-8,985
141394	B-12 D2 76cm	244.5	plant material	8,680	35	9,544-9,727
131493	B12 D2 90cm	259	plant material	8,980	150	9,614-10,491

5.3.4 Geochemistry

A total of 5 samples from the composite were analyzed for x-ray diffraction (XRD) and scanning electron microscopy (SEM) to characterize the carbonate mineralogy. For XRD analysis, 2 cm thick samples were treated with dilute (7 %) H_2O_2 for 8 hours to disaggregate the sediment and to oxidize organic matter. Samples were subsequently rinsed with Milli-Q™ water, frozen, lyophilized, and homogenized with an agate mortar and pestle. Power XRD analysis was performed using a using a Philips PW3710 X'Pert® x-ray diffractometer in the Materials Micro-Characterization Laboratory at the University of Pittsburgh, Swanson School of Engineering. X'Pert Graphics and

Identify® software was used to identify the major mineral assemblages present. For SEM analysis, sediment samples were smeared on a glass slide, dried in a 60° C low-temperature Precision® oven, and coated with Palladium prior to analysis. The samples were imaged using a JEOL 6610V variable pressure SEM system in the Materials Micro-Characterization Laboratory at the University of Pittsburgh, Swanson School of Engineering.

The composite core sequence was sampled at continuous 1 cm intervals for carbonate stable isotope analysis of oxygen ($\delta^{18}O$) and carbon ($\delta^{13}C$). Sediment samples were disaggregated for approximately 24 h in dilute (7 %) H_2O_2 solution and sieved at 63 μm to isolate fine-grained authigenic carbonate material and to minimize contamination from shell material. The <63 μm fraction of the sediment was settled from rinse water and then centrifuged, and the remaining liquid was decanted. The resulting fine-grained carbonate sediment was treated with a dilute (3 %) NaClO solution, rinsed three times with Milli-Q™ water, frozen, lyophilized, and homogenized using an agate mortar and pestle. Isotope ratios were measured at the Regional Stable Isotope Laboratory for Earth and Environmental Science at the University of Pittsburgh using a dual-inlet GV Instruments, Ltd. (now Isoprime, Ltd) IsoPrime™ stable isotope ratio mass spectrometer and MultiPrep™ inlet module. Powdered carbonate samples were reacted with dehydrated phosphoric acid under vacuum at 90 °C. Measurements were calibrated to the NBS-18 and NBS-19 calcite standards and values are reported in standard delta (δ) notation as the per mil (‰) deviation from Vienna Pee Dee Belemnite (VPDB). Precision is ± 0.09 for $\delta^{18}O$ and ± 0.03 for $\delta^{13}C$ (1σ) based on replicate measurements of NBS-18 and NBS-19 standards.

5.4 LAKE HYDROLOGY AND ISOTOPE MODELLING

5.4.1 Lake modelling

To investigate the sensitivity of Cheeseman Lake $\delta^{18}O_{lw}$ to specific climate variables and to develop a quantitative basis for the interpretation of sediment $\delta^{18}O_{cal}$ values, we conducted simulations using a coupled lake hydrologic and isotope mass balance model. Similar models have been used previously to provide a quantitative basis for the interpretation of lacustrine $\delta^{18}O$ records (Jones et al., 2007; Steinman and Abbott, 2013; Steinman et al., 2013). In this study, we utilize the model to characterize the $\delta^{18}O$ values of lake water and sediment calcite from changes in atmospheric temperature and the seasonality of precipitation. Given the relatively short water residence time in the lake and the negligible influence of evaporation, these climatic variables should primarily control lake geochemical responses to climate forcing. The results of these sensitivity tests provide support for the interpretation of Cheeseman Lake sediment $\delta^{18}O_{cal}$ values.

5.4.2 Model structure

The hydrologic and isotope mass balance model applied in this study is based on the lake-catchment model developed by (Steinman et al., 2010a; Steinman et al., 2010b) and subsequently modified by Steinman et al. (2013), Steinman and Abbott (2013) and Stansell et al. (2013). For the purpose of this study, the catchment component of the model was replaced with a lake water input algorithm that simulates

catchment derived surface and groundwater inflows. Additional model adjustments include the application of 1) a simplified lake hypsography algorithm that assumes a conic lake shape and requires maximum lake depth and surface area as inputs, 2) a lake overflow sub-model based on maximum basin volume defined by the lake hypsography algorithm, and 3) an outseepage sub-model wherein lake bed outseepage varies exponentially as a function of offshore distance (with values decreasing toward the lake center). These adjustments were necessary given the paucity of data concerning Cheeseman Lake catchment hydrologic characteristics. As a result, the model presented in this study is meant for simulating the general isotope dynamics of a shallow, perennially overflowing, hydrologically open lake with a relatively short water-residence time and located in a mid-latitude temperate climate with a more or less even monthly distribution of precipitation. The model inputs are therefore meant to reflect a lake similar but not necessarily identical to Cheeseman Lake.

5.4.3 Model inputs

Model simulations utilized monthly weather data derived from weather station and satellite measurements, observational data, and climate model reanalysis experiments (Table 5.2). Mean monthly precipitation $\delta^{18}O$ and δD values were calculated from the Bay d'Espoir, Newfoundland Canadian Network of Isotopes in Precipitation (CNIP) station for the period AD 1997-2010. Mean monthly temperature (°C) and precipitation (mm) were derived from the Deer Lake, Newfoundland 1981-2010 Climate Normals (Canada, 2010). Average lake water temperature is estimated to be +2.5 °C relative to air temperature. Mean monthly incoming solar insolation (MJ m^{-2} d^{-}

^{1}), relative humidity (%) and wind speed (m/s) were determined using data from the NOAA 20th Century Reanalysis Project version 2 using the 1981-2010 AD data (Compo et al., 2011). The maximum lake depth (m) was determined in August, 2012 from field measurements when Cheeseman Lake was overflowing. The lake surface area was calculated using high-resolution aerial imagery in ArcMAP software.

5.4.4 Model calibration

The lake water input algorithm defines the flux of surficial and groundwater inflows into the lake and therefore determines the water residence time and sensitivity to evaporative modification (water loss via fractionating and non-fractionating pathways). Steady state simulations were conducted whereby the water input flux was increased from a value of 1,000 to 30,000, at which point modeled lake depth and $\delta^{18}O_{lw}$ values were similar to observations. This model configuration produced realistic seasonal lake water $\delta^{18}O$ changes, given the monthly variations in precipitation $\delta^{18}O$ values over the course of a year, with the most negative $\delta^{18}O_{lw}$ values occurring in May (-10.83 ‰ VSMOW) and most positive occurring in September (-9.85 ‰ VSMOW). Theoretical $\delta^{18}O_{cal}$ values were estimated using the $\delta^{18}O_{lw}$ values and water temperature values for late summer (July and August) using the following equation for equilibrium precipitation of calcite (Kim and Oneil, 1997):

$$1000 \ln \alpha (\text{Calcite-}H_2O) = 18.03(10^3 T^{-1}) - 32.42$$

Equation 5.1. Equation for equilibrium precipitation of calcite based on a defined temperature (Kim and Oneil, 1997).

5.4.5 Model sensitivity tests to climate variables

The objective of the model simulations was to assess the sensitivity of Cheeseman Lake $\delta^{18}O_{lw}$ and $\delta^{18}O_{cal}$ to changes in atmospheric temperature and the seasonality of precipitation. Changes in temperature modify $\delta^{18}O_{ppt}$ through the temperature-dependent transformation of water vapor to precipitation (+0.6 ‰/1° C) (Rozanski et al., 1992) and via the temperature-dependent fractionation of the water to calcite (-0.24 ‰/1° C) (Craig, 1965). Likewise, cold-season $\delta^{18}O_{ppt}$ is isotopically more negative (lighter) compared with more positive (heavier) values for the warm-season (Table 5.2). Model Simulations were conducted on a monthly time-step over 1000 model months (83 years). In the 501st month, the tested climate variable was either increased or decreased by a constant amount and maintained until the end of the test.

5.5 RESULTS

5.5.1 Composite core and physical sedimentology

A composite 300 cm core sequence was developed from surface core A-12 and long cores B-12 Drive 1, B-12 Drive 2, and B-12 Drive 3 by matching visible stratigraphic markers (Figure 5-5). The basal sediments from 300 to 271 cm consist of moderate brown (5 YR 4/4) to pale reddish brown (10 R 5/4) clay and silty clay minerogenic sediment with occasional fine sand laminae. The unit is primarily homogenous with occasional faint bands. The contact at 271 cm with the overlying

sediments is abrupt and irregular, suggestive of an unconformable (erosion) surface or a disconformable hiatus. The sediments from 271 to 263 cm consist of dusky brown (5 YR 2/2) silt, organic and minerogenic sediment with occasional coarser clasts (sand, granules, and pebbles) in a matrix. Above 263 cm, there is an abrupt transition to grayish orange (10 YR 7/4) to pale yellowish brown (10 YR 6/2), banded to laminated calcareous sediment with gastropod and bivalve shells that persists to 125 cm. The sediments from 125 to 119 cm consist of dusky brown (5 YR 2/2) to grayish brown (5 YR 3/2) homogenous organic silt with rare gastropod and bivalve shells. The overlying sediments from 119 to 70 cm consist of grayish orange (10 YR 7/4) to pale yellowish brown (10 YR 6/2) banded to laminated calcareous sediment with gastropod and bivalve shells with generally increasing organic content up-section. Above 70 cm, there is an abrupt transition to dusky brown (5 YR 2/2) to grayish brown (5 YR 3/2) homogenous organic silt with aquatic vegetation remains along with gastropod and bivalve shells that decrease towards the core top.

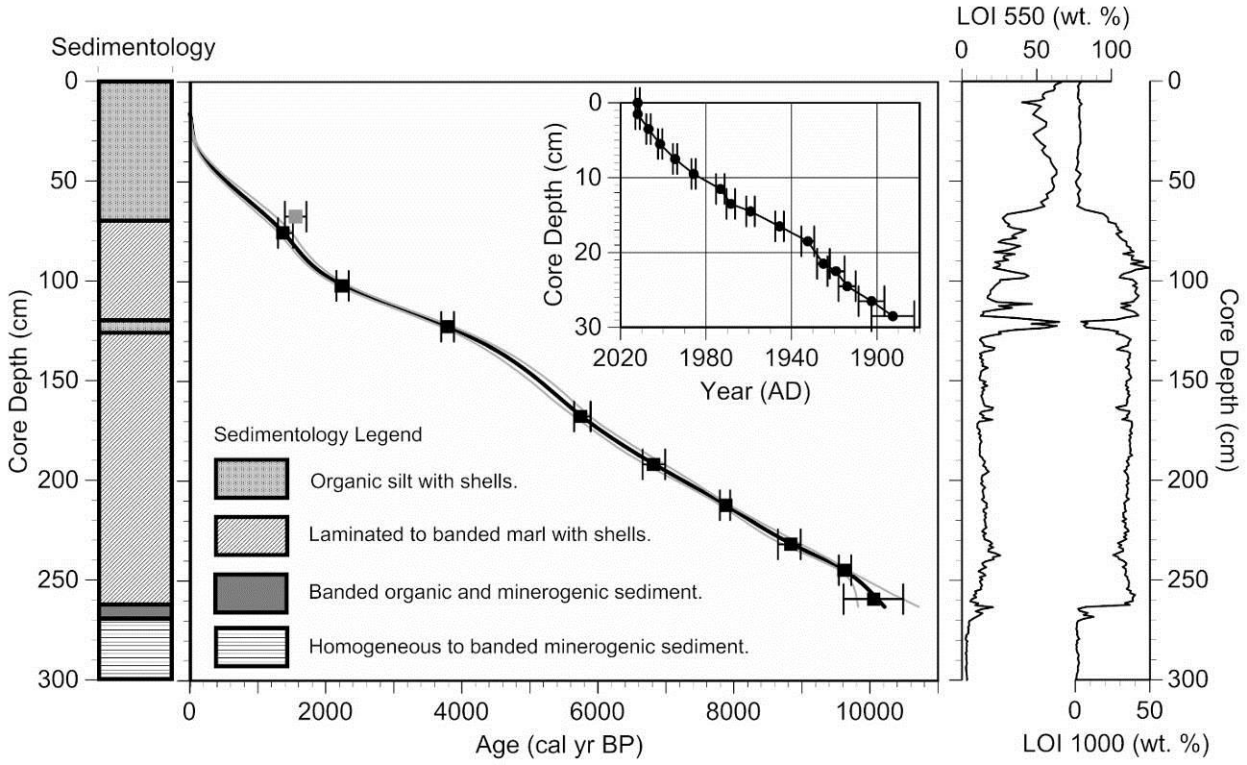

Figure 5-5. Stratigraphic column and age model for the Cheeseman Lake core sequence developed from radiocarbon and ^{210}Pb dates. The sample at 67.5 cm depth highlighted with a gray square is rejected from the age model. Weight percent organic matter and total carbonate from LOI 550 (wt. %) and LOI 1000 (wt. %) analysis.

5.5.2 Chronology

The ^{210}Pb inferred CRS age model for the surface sediments indicates the upper 28 cm of the core dates to ~ 1890 AD (Figure 5-5). The 1963 AD maximum concentration of ^{137}Cs from above-ground thermonuclear weapons testing occurs from 11.5 to 14.5 cm depth, broadly consistent with the CRS inferred age of this interval between 1959 to 1973 AD. The uppermost radiocarbon sample (UCIAMS # 116880) at 66-67 cm depth was excluded prior to generating the age model, based on a slight age

reversal between the oldest reliable ^{210}Pb date and adjacent radiocarbon sample (UCIAMS # 131490). The rejected sample appears anomalously old for its stratigraphic position and has a slightly larger analytical uncertainty compared to the adjacent date. This sample was likely an aquatic or submerged macrophyte that incorporated ^{14}C depleted dissolved inorganic carbon, resulting in a dead carbon contribution and too old age. This hypothesis is consistent with core sedimentology that shows the presence of aquatic vegetation in the upper 70 cm of the composite core (Figure 5-5). The resulting age model indicates generally low and variable sedimentation rates between ~ 0.01 to ~ 0.04 cm/yr from 28 to 259 cm depth (Figure 5-5). Sedimentation rates increase from ~ 0.04 cm/yr at 28 cm to ~ 0.5 cm/yr towards the core top (Figure 5-5).

5.5.3 Modern water isotopes

The global meteoric water line (GMWL) (Rozanski et al., 1992) and local meteoric water line (LMWL), developed with monthly average precipitation δD and δ^{18}O data from the Bay d'Espoir CNIP station (Table 5.2) (Figure 5-6), along with regional lake and river water samples are presented in Figure 5-6. Cheeseman Lake surface waters (δ^{18}O = -9.02 ‰, δD = -65.05 ‰ [VSMOW]) plot along the LMWL (Figure 5-6), suggesting that lake waters reflect the isotopic composition of precipitation.

Table 5.2. Model input and meteorological station data. [A] Deer Lake, Newfoundland Climate Normals 1981-2010 (Canada, 2010), [B] NOAA 20th Century Gridded Re-analysis Project data (Compo et al., 2011), [C] Bay d'Espoir Precipitation Isotope data (http://www.science.uwaterloo.ca/~twdedwar/cnip/)

Month	Precipitation[a] (mm)	Temperature[a] (°C)	Relative Humidity (%)[b]	Wind Speed (m/s)[b]	Incoming Solar rad. (MJ m^{-2} d^{-1})[b]	$\delta^{18}O$ (‰)[c]	δD (‰)[c]
Jan	109.8	-7.2	94.4	6.3	4.7	-12.5	-89.5
Feb	83.5	-8.0	95.4	5.8	7.8	-11.6	-80.3
Mar	71.7	-4.1	95.0	5.8	11.9	-11.5	-81.5
Apr	70.1	1.9	93.0	5.3	15.6	-9.3	-64.0
May	89.2	7.4	84.7	4.7	19.3	-8.1	-57.9
Jun	88.3	12.2	80.0	4.6	21.1	-7.7	-52.2
Jul	98.5	16.5	80.1	4.7	21.0	-6.7	-46.4
Aug	109.9	16.4	78.6	4.7	18.4	-6.3	-39.9
Sep	106.2	12.3	80.0	5.0	13.2	-8.0	-53.0
Oct	105.7	6.6	85.7	5.5	7.8	-8.2	-54.5
Nov	101.3	1.5	89.4	5.9	4.6	-8.5	-55.2
Dec	97.3	-3.3	93.1	6.2	3.6	-11.7	-79.3

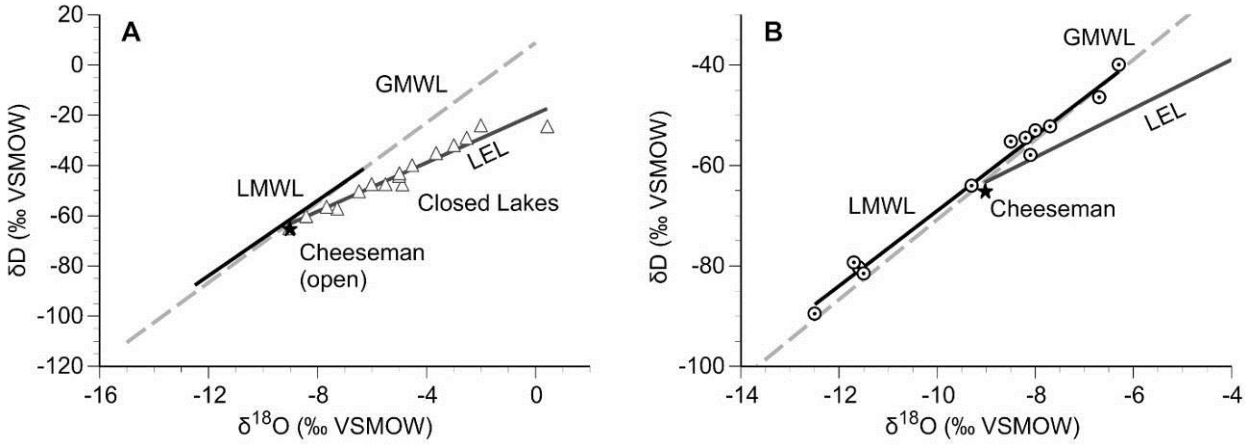

Figure 5-6. (a) Surface water sample from Cheeseman Lake (black star) and surface water samples from regional lakes (open triangles) collected in July, 2012 in $\delta^{18}O$-δD (VSMOW) space. The Cheeseman Lake surface water sample plots along the Local Meteoric Water Line (LMWL, black line) that parallels the Global Meteoric Water Line (GMWL, dashed gray line). Regional lakes with closed-basin conditions

sensitive to evaporation plot along a Local Evaporation Line (LEL, solid gray line) that is oblique to the LMWL and GMWL. (b) Same as in (a) but focused on the LMWL developed with a linear, best-fit line from monthly average precipitation δ18O and δD from the Bay d'Espoir Canadian Network of Isotopes in Precipitation (CNIP) station.

The average weighted $\delta^{18}O$ of precipitation, calculated by normalizing monthly average precipitation $\delta^{18}O$ from the Bay d'Espoir CNIP station with the monthly proportion of annual precipitation from Deer Lake (Figure 5-3), is -9.10 ‰ VSMOW (Henderson and Shuman, 2009). However, we hypothesize that the $\delta^{18}O$ of lake water should reflect the annual moisture surplus, given precipitation losses in the summer months from plant interception and catchment scale evapotranspiration. We therefore calculate the annual moisture surplus $\delta^{18}O$ of precipitation using a coupled lake hydrologic and isotope mass balance model (see Lake Modeling section), which estimates precipitation losses via catchment potential evapotranspiration and lake surface evaporation (Valiantzas, 2006), using the Bay d'Espoir CNIP precipitation $\delta^{18}O$ data and mean monthly meteorological data (Table 5.2) (Canada, 2010; Compo et al., 2011). Using this approach the annual moisture surplus $\delta^{18}O$ of precipitation is -10.35 ‰ VSMOW, which is more negative than the observed $\delta^{18}O$ of lake water. Several regional lakes have isotope values that plot down and to the right of the LMWL on the local evaporation line (LEL) (Figure 5-6), indicating these closed-basin lacustrine systems are influenced by evaporative modification.

5.5.4 Geochemistry

The results of XRD analysis for select samples from the composite core sequence are presented in Figure 5-7. The primary carbonate mineral present in the cores is identified as calcite. No other calcite polymorphs (i.e. aragonite, veterite) were present in the measured samples, suggesting that carbonate minerals in the core sequence are single phase and consist of calcite. SEM analysis further shows the presence of near perfect, rhombic (euhedral) calcite crystal form (Figure 5-8) in the sediment samples. Collectively, these results indicate that carbonate minerals within the sediment core consist of in-lake (authigenic) precipitated calcite. Physical observations of Cheeseman Lake in August, 2012 showed a lack of littoral marl around the lake shoreline, suggesting that either carbonate precipitation and/or a lack of preservation preclude calcareous sedimentation over the upper 70 cm of the core sequence (Figure 5-5). However, a review of monthly Landsat satellite imagery (http://landsatlook.usgs.gov/) appear to show 'whiting' events of carbonate precipitation during the summer months. Accordingly, we hypothesize that modern calcareous sedimentation (over the upper 70 cm) is limited by calcite preservation at the A-12 and B-12 core sites. Regardless of the precise mechanism, the lack of carbonate sediments at the core top limit stable isotope analysis to 262 to 70 cm from the composite core sequence (Figure 5-5) that spans the interval ~ 10,200 to ~ 1,200 cal yr BP.

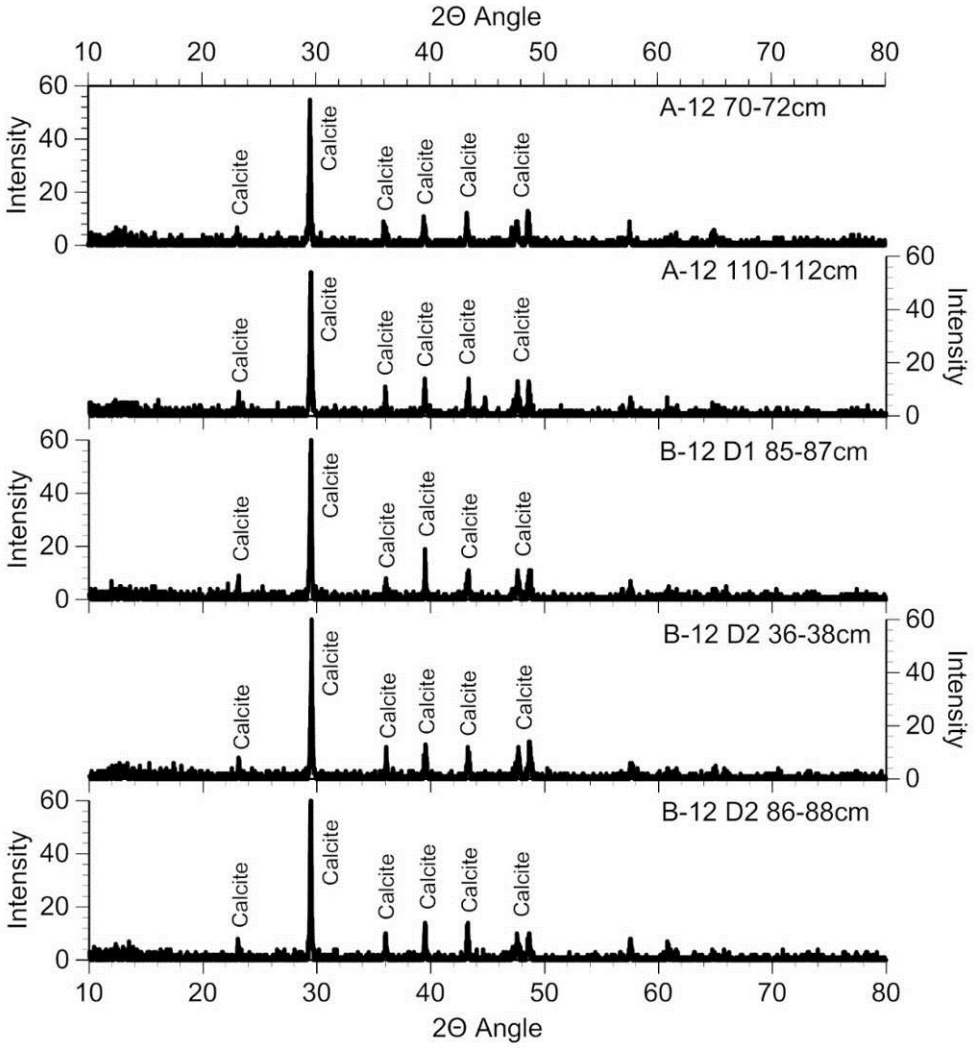

Figure 5-7. X-ray Diffraction spectra for select sediment samples from the Cheeseman Lake core sequence. Major peaks are identified as the mineral calcite.

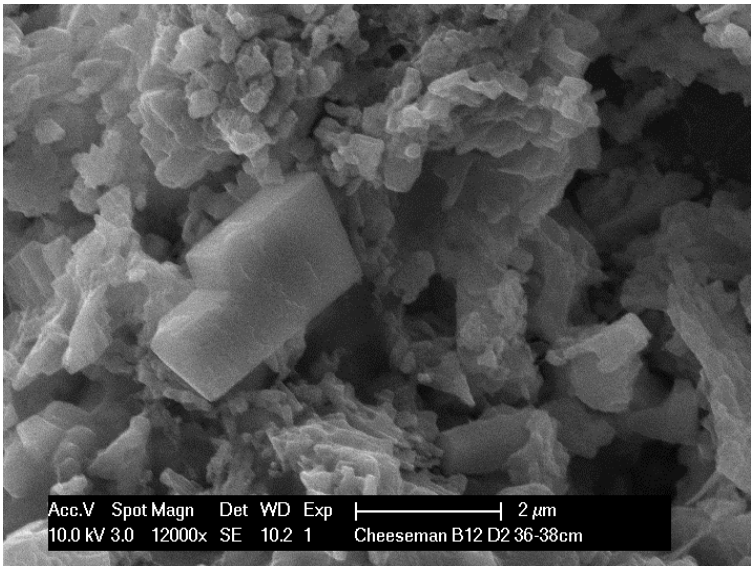

Figure 5-8. Scanning electron microscope image of euhedral calcite crystal from core B-12 D2 36-38 cm.

5.5.5 Carbonate stable isotopes

Our paleoenvironmental interpretation of the Cheeseman Lake sedimentary record is based on calcite oxygen stable isotope data (Figure 5-9). Variations in calcite $\delta^{18}O$ ($\delta^{18}O_{cal}$) allow identification of 2 isotope zones. Zone 1 begins at the transition of minerogenic to carbonate sediments at 262 cm and extends to 213 cm and spans the interval ~ 10,200 to ~ 7,950 cal yr BP. Cheeseman $\delta^{18}O_{cal}$ decreased abruptly between ~ 10,200 to ~ 10,100 cal yr BP from -10.95 ‰ to -11.54 ‰ (Figure 5-9). After ~ 10,100 cal yr BP, $\delta^{18}O_{cal}$ values increased from -11.54 ‰ with century-scale variability and reached the most positive $\delta^{18}O_{cal}$ values of -9.98 ‰ at the Zone 2 boundary (~ 7,950 cal yr BP). Increasing $\delta^{18}O_{cal}$ values are abbreviated by rapid excursions to more negative $\delta^{18}O_{cal}$ values beginning at ~ 9,700 and ~ 8,500 cal yr BP that persist for ~ 200 years (Figure 5-9). $\delta^{18}O_{cal}$ values increased rapidly after ~ 8,300 cal yr BP from -10.95 ‰ to -9.98 ‰ by ~ 7,950 cal yr BP. Zone 2 extends from 213 cm to 70 cm and spans the

interval ~ 7,950 to ~ 1,200 cal yr BP. Cheeseman $\delta^{18}O_{cal}$ values gradually decreased from ~ 7,950 to ~ 4,300 cal yr BP from -9.98 ‰ to -11.11 ‰ with distinct centennial scale variability (Figure 5-9). Between ~ 4,300 to ~ 2,500 cal yr BP slightly more positive $\delta^{18}O_{cal}$ values (-10.6 ‰) are apparent with increased variability. $\delta^{18}O_{cal}$ values generally decreased after ~ 2,500 cal yr BP and remained relatively negative (-11.0 ‰) with minimal variability until ~ 1,200 cal yr BP.

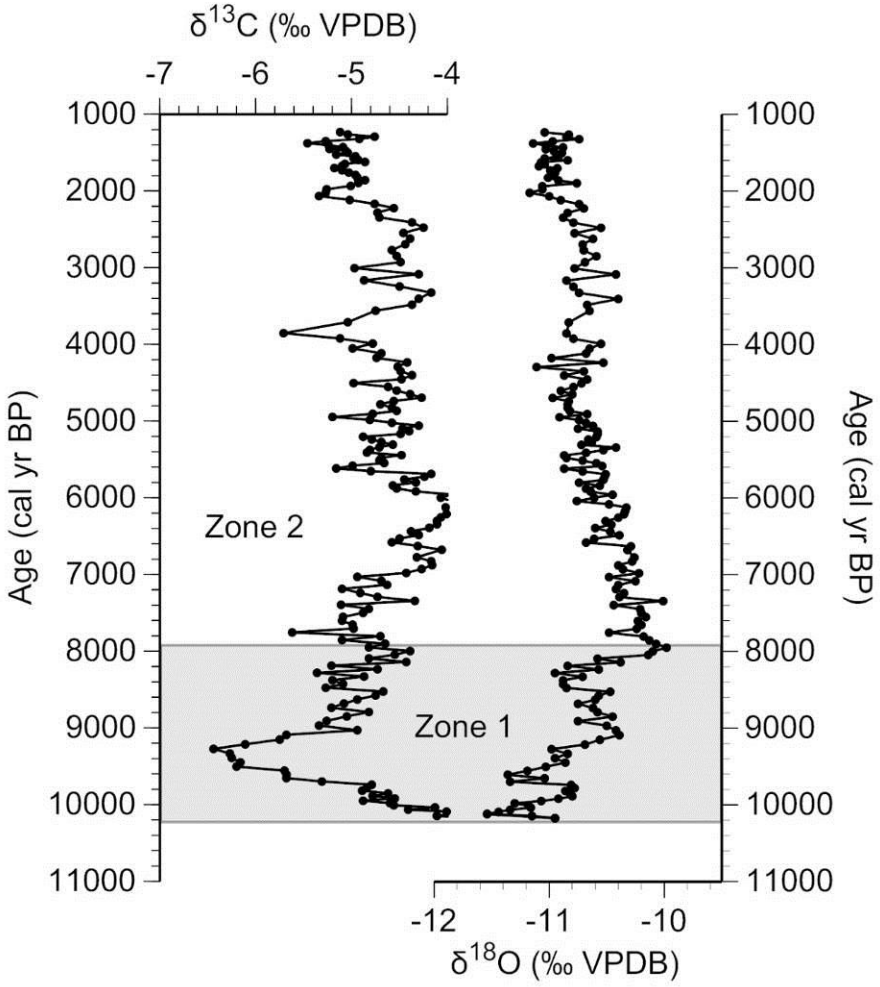

Figure 5-9. Cheeseman Lake carbonate stable isotope data of $\delta^{13}C$ (‰ VPDB) and $\delta^{18}O$ (‰ VPDB).

5.5.6 Model calibration and sensitivity test results

The steady-state model simulation produced a theoretical $\delta^{18}O_{cal}$ value of -10.71 ‰ (VPDB), which is similar to the measured $\delta^{18}O_{cal}$ value of -11.04 ‰ (VPDB) at ~ 1,200 cal yr BP. Atmospheric temperature changes of ± 2 ° C resulted in $\delta^{18}O_{lw}$ anomalies of +1.21 ‰ and -1.26 ‰ (VSMOW) (Figure 5-10). The same test produced theoretical equilibrium summer $\delta^{18}O_{cal}$ anomalies of +0.78 ‰ and -0.68 ‰ VPDB (Figure 5-10). Notably, the amplitude of simulated summer $\delta^{18}O_{cal}$ anomalies agrees with the range in measured Cheeseman Lake $\delta^{18}O_{cal}$ values. Precipitation seasonality tests focus on changes in winter variability (herein defined as the period between October to March). We emphasize precipitation seasonality changes in the cold-season, because the annual moisture surplus weighted $\delta^{18}O_{ppt}$ reflects losses of summer precipitation due to evapotranspiration from the catchment and lake surface, and is therefore weighted towards cold-season values. Winter season precipitation seasonality changes of ± 20% resulted in $\delta^{18}O_{lw}$ anomalies of -0.12 ‰ and +0.17 ‰ (VSMOW) (Figure 5-11). The same test produced theoretical equilibrium summer $\delta^{18}O_{cal}$ anomalies of -0.11 ‰ and +0.17 ‰ VPDB (Figure 5-11).

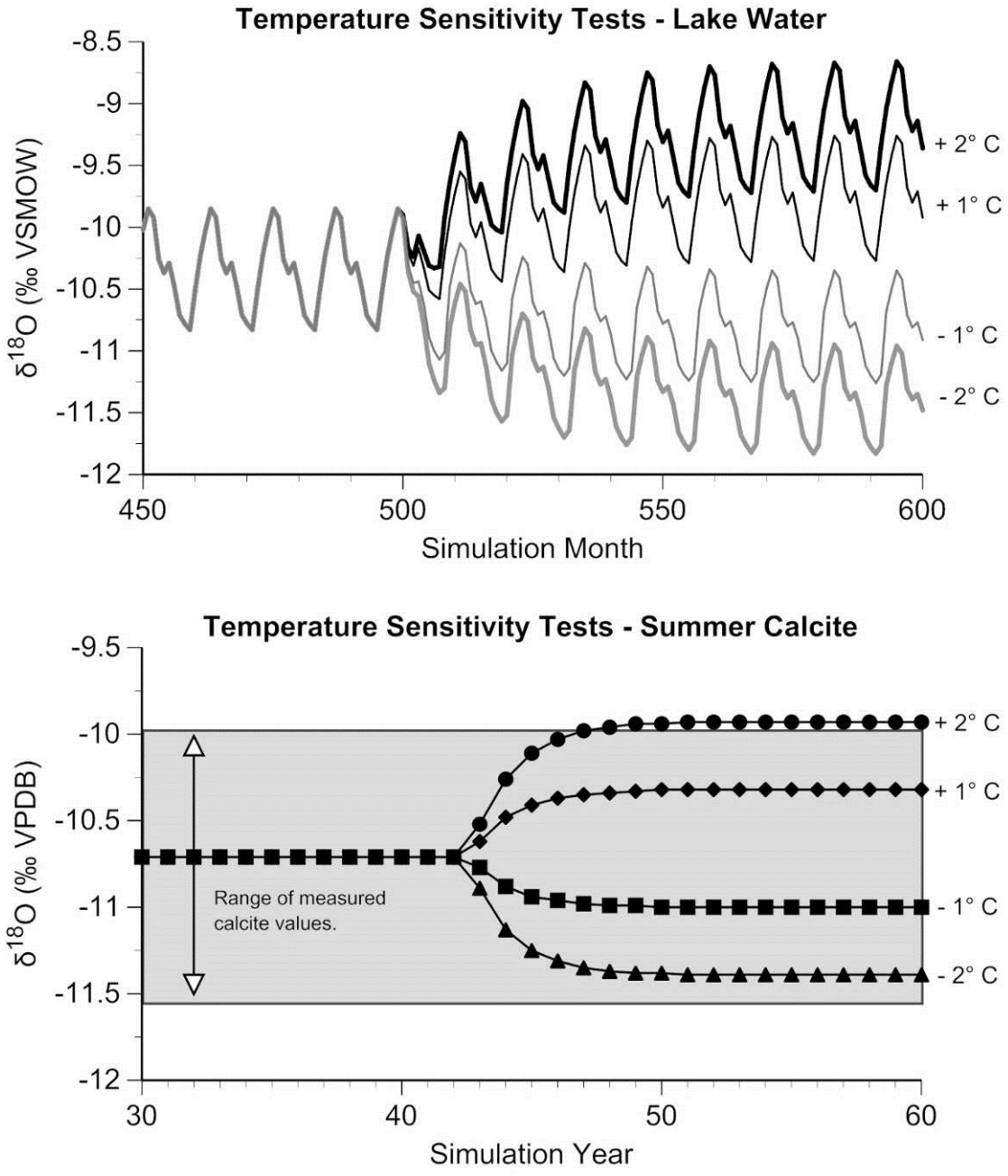

Figure 5-10. Simulated lake water $\delta^{18}O$ (‰ VSMOW) and summer calcite $\delta^{18}O$ (‰ VPDB) values from sensitivity tests for ± 1° C and ± 2° C annual temperature changes.

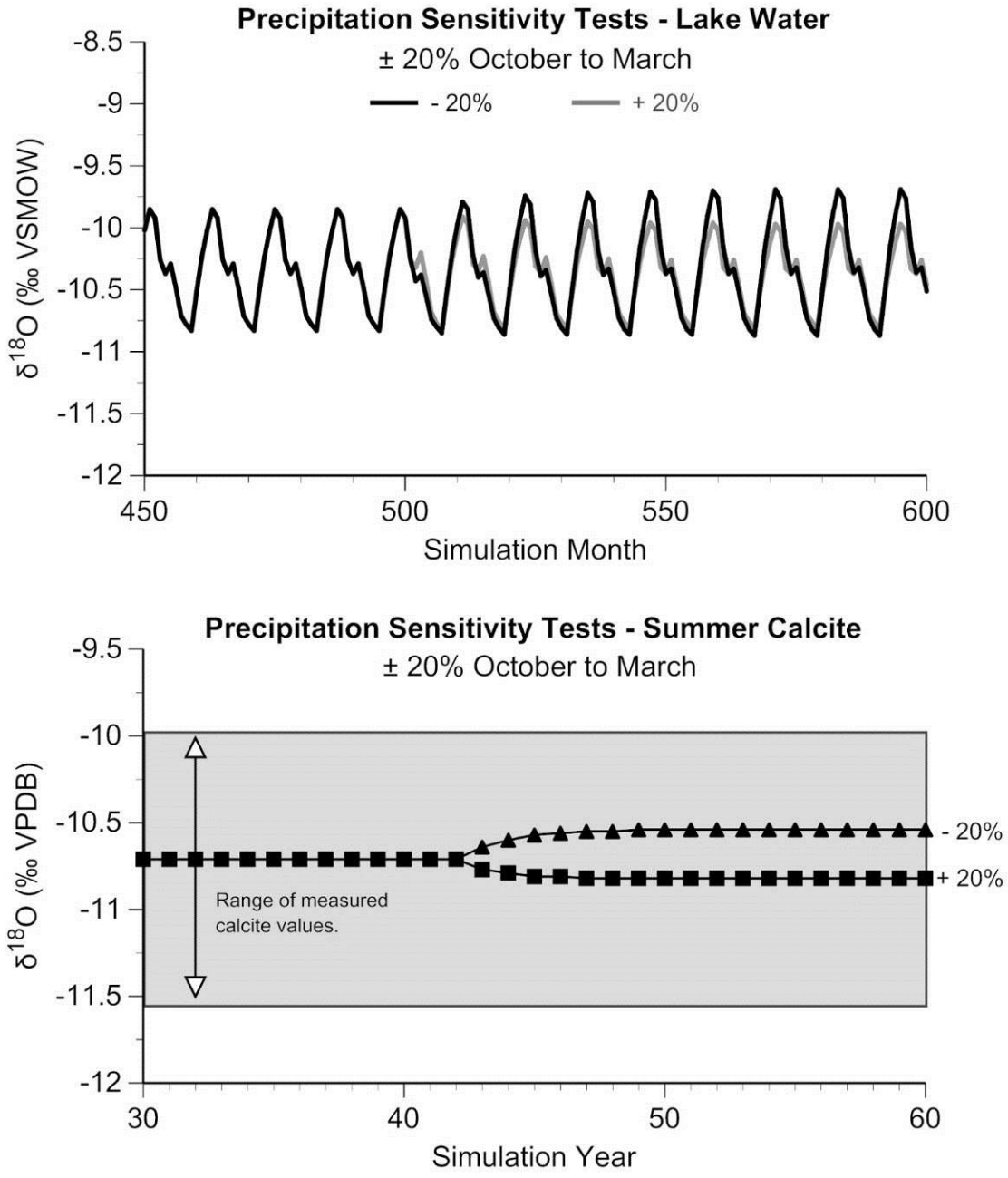

Figure 5-11. Simulated lake water $\delta^{18}O$ (‰ VSMOW) and summer calcite $\delta^{18}O$ (‰ VPDB) values from sensitivity tests for changes in the seasonality of cold-season (± 20% October to March) precipitation.

5.6 DISCUSSION

5.6.1 Interpretation of calcite oxygen isotopes

The oxygen isotope composition of lacustrine authigenic calcite ($\delta^{18}O_{cal}$) is a function of the isotopic composition of lake water ($\delta^{18}O_{lw}$) and the temperature of calcite precipitation (Gat, 1995; Kim and Oneil, 1997). In open-basin lakes with short water residence times, like that of Cheeseman Lake, the $\delta^{18}O_{lw}$ is principally controlled by the oxygen isotopic composition of meteoric precipitation ($\delta^{18}O_{ppt}$) (Gat, 1995; Leng and Marshall, 2004). At mid to high-latitude sites, the $\delta^{18}O_{ppt}$ is systematically related to atmospheric temperature (Dansgaard, 1964), with the global relationship showing ~ 0.6 ‰ increase in $\delta^{18}O_{ppt}$ per 1° C (Rozanski et al., 1992). Seasonal variations in temperature coincide with concomitant changes in $\delta^{18}O_{ppt}$ for Newfoundland (Table 5.2), whereby cold-season $\delta^{18}O_{ppt}$ values are more negative compared with more positive values during the warm-season (Clark and Fritz, 1997; Rozanski et al., 1992). The $\delta^{18}O_{ppt}$ is also controlled by the rain-out history of an air mass, through the latitude, altitude, and continental effects that results in a progressive depletion of $\delta^{18}O_{ppt}$ through a Rayleigh-type distillation process (Dansgaard, 1964), and changes in the isotopic composition of and/or the oceanic moisture source (Araguás-Araguás et al., 2000).

Cheeseman Lake surface waters plot on the LMWL (Figure 5-6), suggesting that evaporative modification of lake waters are negligible and that water loss is primarily through non-fractionating pathways (surficial outflow and groundwater outseepage). When combined with physical observations showing a distinct open-basin hydrology and $\delta^{18}O_{lw}$ data suggesting a short-water residence time, we interpret changes in

Cheeseman Lake $\delta^{18}O_{cal}$ to reflect changes in the oxygen isotope composition of precipitation ($\delta^{18}O_{ppt}$) and atmospheric temperature. Unfortunately, the lack of authigenic calcite in lake surface sediments make the comparison of $\delta^{18}O_{lw}$ against $\delta^{18}O_{cal}$ difficult, which is necessary to demonstrate the precipitation of calcite in isotopic equilibrium with lake water. In the past, authigenic calcite precipitation at Cheeseman Lake likely occurred during the summer months from photosynthetically mediated increases in pH resulting from algal utilization of dissolved CO_2, leading to saturation of HCO_3- and carbonate precipitation (Kelts and Hsu, 1978). This interpretation is supported by satellite imagery that show 'whiting' events of carbonate precipitation in the summer months from regional marl lakes. Accordingly, Cheeseman Lake $\delta^{18}O_{cal}$ should reflect the $\delta^{18}O_{lw}$ and the summer lake water temperature at the time of calcification.

Model sensitivity test results provide support for the interpretation that $\delta^{18}O_{lw}$ and theoretical equilibrium Cheeseman Lake $\delta^{18}O_{cal}$ are most sensitive to changes in atmospheric temperature. Temperature changes of ± 2 ° C produce theoretical $\delta^{18}O_{cal}$ values within the range of measured down-core $\delta^{18}O_{cal}$ values (Figure 5-10), suggesting that temperature forced changes in $\delta^{18}O_{ppt}$ are the primary control on in $\delta^{18}O_{lw}$. Conversely, cold-season precipitation seasonality changes of ± 20% yield theoretical $\delta^{18}O_{cal}$ anomalies that are too low to explain the range of measured $\delta^{18}O_{cal}$ values (Figure 5-11). Accordingly, changes in the seasonality of precipitation must be considered a less important control affecting $\delta^{18}O_{ppt}$ and the resultant $\delta^{18}O_{cal}$ over time.

In addition, other factors affecting the $\delta^{18}O_{ppt}$ must be considered, including changes in the moisture source and temporal variability in the isotopic composition of

ocean source water over the Holocene. The modern source of precipitation for Newfoundland is dominantly from the western Atlantic Ocean south of the island that originates via cyclonic or frontal activity (Milrad et al., 2010). The influence of Arctic or Pacific Ocean derived-moisture to Newfoundland is presumably negligible, at least on centennial to millennial time scales, given the small range in Cheeseman Lake $\delta^{18}O_{cal}$ values (~ 1.5 ‰) over the Holocene. However, the surface ocean $\delta^{18}O$ composition varied substantially during the early Holocene as a result of Laurentide Ice Sheet deglaciation and meltwater flux to the Labrador Sea and western Atlantic Ocean (Andrews et al., 1999; Hoffman et al., 2012; Keigwin et al., 2005).

Holocene paleoclimate conditions in eastern North America were influenced by changes in Earth's orbital parameters (Laskar et al., 2004) and surface boundary conditions (COHMAP, 1988; Dyke and Prest, 1987). Northern hemisphere high-latitude (50° N) summer (July) insolation was 8% greater than modern at 10,000 cal yr BP (Laskar et al., 2004). Summer insolation levels gradually decreased towards the present while winter (January) insolation increased, leading to decreasing Northern Hemisphere seasonality from the early to late Holocene. The early Holocene climate was influenced by relatively lower but rapidly rising sea levels (Clarke et al., 2004) resulting from deglaciation (Dyke and Prest, 1987), which produced enhanced freshwater flux to the North Atlantic Ocean (Licciardi et al., 1999). Isostatic depression of the land surface and a large meltwater flux resulted in formation of large proglacial lakes at the southern edge of the Laurentide Ice Sheet during deglaciation (Teller and Leverington, 2004; Teller et al., 2002). Lake Agassiz was the largest proglacial lake in the North American interior during the last deglaciation, which formed by 11,700 ^{14}C yr

BP (~ 13,500 cal yr BP) and drained completely by about 7,700 ^{14}C yr BP (~ 8,450 cal yr BP) (Clarke et al., 2004). Substantial changes in the extent and depth (lake-level) of Lake Agassiz resulted from the interaction between changes in the ice-margin position, isostatic rebound, and shifting outlets (Teller and Leverington, 2004) that lead to episodic release of large volumes of freshwater to the oceans. Catastrophic drainage of Lake Agassiz and related proglacial lakes (i.e. Ojibway, Minong) from ice-dam failure or outlet erosion at 9,300 cal yr BP (Yu et al., 2010) and 8,450 cal yr BP (Barber et al., 1999) lead to enhanced freshwater flux to the North Atlantic Ocean and abrupt but short-lived cooling events (Alley et al., 1997). Abrupt climate change at these times is linked to a reduction in North Atlantic Deep Water (NADW) formation and a weakening or partial shut-down of the Atlantic Meridional Overturning Circulation (AMOC) (Clark et al., 2001). The final drainage of Lake Agassiz, rapid disintegration of the Laurentide Ice Sheet after ~ 8,000 cal yr BP (Dyke, 2004), and transition from glacial to interglacial boundary conditions resulted in relative climate stability for the remainder of the Holocene (Grootes and Stuiver, 1997). In addition, eustatic sea levels approached near modern levels shortly after ~ 8,000 cal yr BP (Clark et al., 2009).

Changes in Earth's boundary conditions before and after ~ 8,000 cal yr BP produced variations in Newfoundland precipitation regimes, which are recorded by $\delta^{18}O$ values in Cheeseman Lake sediment. For example, a gradually increasing trend in $\delta^{18}O_{cal}$ from 10,200 to 7,950 cal yr BP (Figure 5-9) occurs along with ice sheet retreat and rising eustatic sea levels. Generally decreasing $\delta^{18}O_{cal}$ from 7,950 cal yr BP towards the middle to late Holocene (Figure 5-9) occurs as interglacial boundary conditions are achieved defined by relative Laurentide Ice Sheet extent (Dyke and

Prest, 1987), eustatic sea level stabilization (Clark et al., 2009), and 50° N insolation (Laskar et al., 2004). Further, we compare our paleoenvironmental interpretations to ice core $\delta^{18}O$ from southern (Dye-3) (Dansgaard et al., 1985) and central Greenland (NGRIP) (NGRIP, 2004), sea surface temperature and foraminiferal $\delta^{18}O$ records from the Labrador Sea (Andrews et al., 1999; Hoffman et al., 2012) and western North Atlantic Ocean (Keigwin et al., 2005; Sachs, 2007), and terrestrial hydroclimate records from Newfoundland (Amesbury et al., 2013; Daley et al., 2009).

5.6.2 Newfoundland regional comparison

The Nordan's Pond Bog $\delta^{18}O_{ppt}$ reconstruction (Figure 5-12) provides the only other quantitative precipitation isotope record for direct comparison with the Cheeseman Lake record. The major difference between the records is the much larger range in $\delta^{18}O$ values present in the reconstruction from Nordan's Pond Bog, which varies between -9.67 to -4.12 ‰ (VSMOW), a total range of 5.55 ‰. In contrast, the range in Cheeseman Lake $\delta^{18}O_{cal}$ values that vary between -11.54 to -9.98 ‰ (VPDB), is much smaller. While there is certainly spatial variability in $\delta^{18}O_{ppt}$ across eastern North America during the Holocene (Edwards et al., 1996; Hardt et al., 2010; Kirby et al., 2002; Yu et al., 2010; Zhao et al., 2010), the distance between Cheeseman Lake and Nordan's Pond Bog is only ~ 300 km. We therefore assert that spatial variations in $\delta^{18}O_{ppt}$ across such a short distance cannot explain the apparent discordance between the records. Alternatively, we suggest that differences in the seasonality of Cheeseman Lake calcite precipitation and Nordan's Pond Bog cellulose synthesis could explain the large differences in reconstructed $\delta^{18}O_{ppt}$. Further, evaporative modification of bog

waters could in part explain the rather large variations in $\delta^{18}O_{ppt}$ at Nordan's Pond Bog. This idea is supported by the isotopic composition of bog waters (n=8) collected in July of 2004, which Daley et al. (2009) state "are within the scatter of regional precipitation values." However, the bog water samples plot along a local evaporation line in VSMOW space (Daley et al., 2009), demonstrating that evaporation is a significant flux in the bog hydrologic system. This apparent discrepancy suggests that the Nordan's Pond Bog $\delta^{18}O_{ppt}$ reflects the precipitation – evaporation (P-E) or moisture balance. Relatively positive $\delta^{18}O_{ppt}$ values are interpreted to reflect some combination of warmer temperatures, greater warm-season precipitation, or enhanced evaporation and relatively dry conditions. Conversely, relatively negative $\delta^{18}O_{ppt}$ values reflect the opposite – namely colder temperatures, greater cold-season precipitation, and relatively wet conditions. The interpretation that the Nordan's Pond Bog $\delta^{18}O_{ppt}$ record reflects the P-E balance is supported by a testate-amoeba based water-table depth reconstruction (Figure 5-12) (Amesbury et al., 2013), which shows substantial shifts in moisture balance coincident with $\delta^{18}O_{ppt}$ variations.

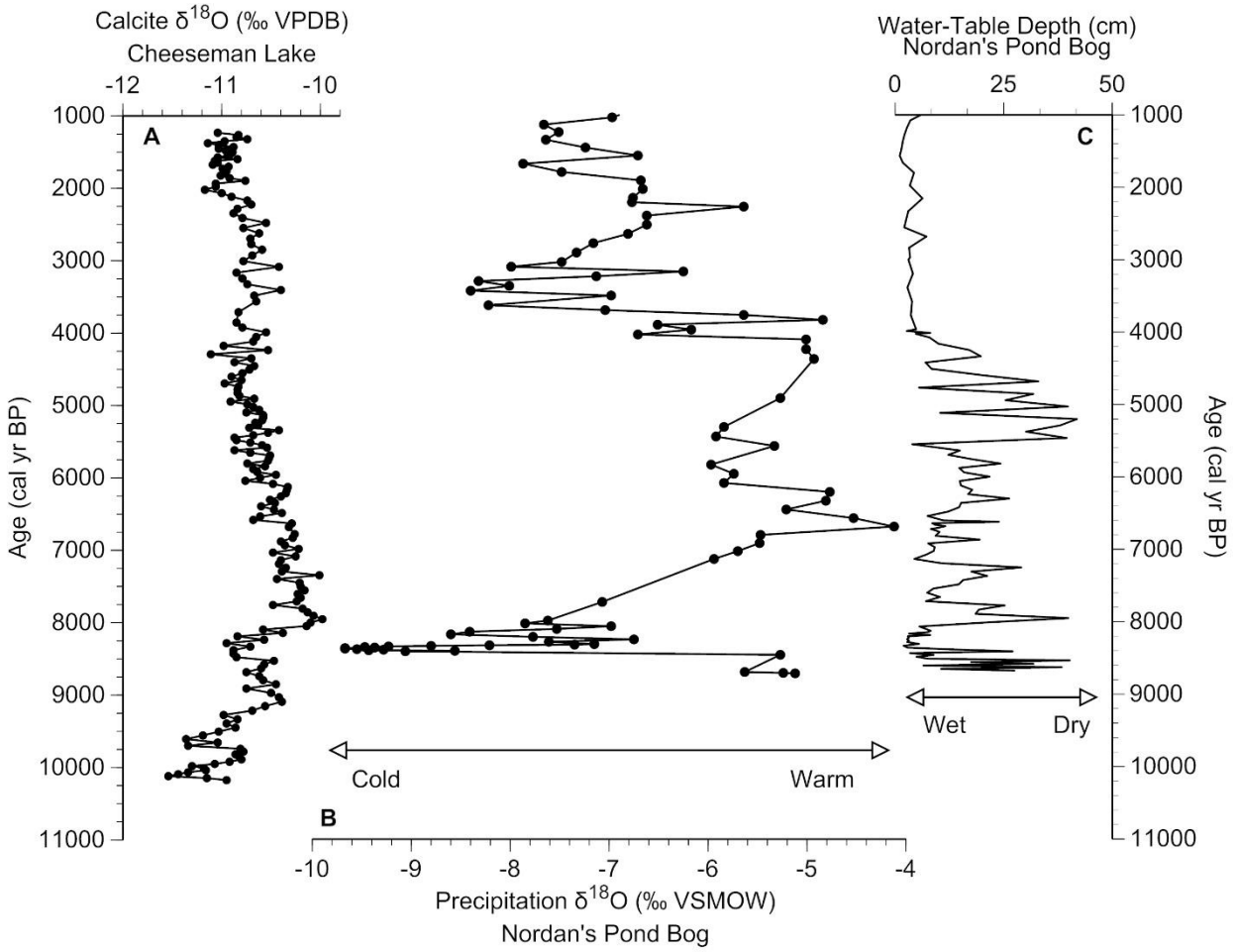

Figure 5-12. Regional comparison of quantitative hydroclimate reconstructions from Newfoundland including (a) Cheeseman Lake carbonate $\delta^{18}O$ (‰ VPDB), (b) Nordan's Pond Bog $\delta^{18}O$ (‰ VSMOW) (Daley et al., 2009), and (c) Nordan's Pond Bog testate-amoeba based water-table depth reconstruction (Amesbury et al., 2013).

The Cheeseman Lake $\delta^{18}O_{cal}$ record and Nordan's Pond Bog $\delta^{18}O_{ppt}$ reconstruction are strikingly different, yet there are a few similarities (Figure 5-12). For instance, both records show anomalies to more negative $\delta^{18}O$ values during the early Holocene associated with the 8,200 cal yr BP abrupt climate change event (Alley et al., 1997; Barber et al., 1999). The transition to more negative values at Cheeseman Lake occurs at ~ 8,500 cal yr BP and is characterized by a -0.38 ‰ (VPDB) excursion. At

Nordan's Pond Bog, the transition begins at ~ 8,400 cal yr BP and is characterized by an initial -3.79 ‰ (VSMOW) excursion. We can convert these $\delta^{18}O$ anomalies to changes in temperature, assuming that temperature is the only forcing that controls these variations. We use the long-term average temperature-$\delta^{18}O_{ppt}$ relationship (Dansgaard, 1964) that accounts for interannual and longer term variations by removing the seasonal component (Rozanski et al., 1992), which is more relevant as it concerns isotope-based paleo reconstructions. In contrast, the seasonal relationship defined by directly comparing monthly average $\delta^{18}O_{ppt}$ and temperature time-series yield temperature-$\delta^{18}O_{ppt}$ coefficients that are substantially smaller (Daley et al., 2009), resulting in a much greater temperature sensitivity.

Using the globally defined temperature-$\delta^{18}O_{ppt}$ relationship of 0.6 ‰/°C and accounting for the temperature dependence of the water-calcite transformation (Craig, 1965), these changes correspond with a 1°C cooling at Cheeseman Lake and a 6.3°C cooling at Nordan's Pond Bog. The apparent discordance in the magnitude of $\delta^{18}O$ anomalies and associated shifts in temperature between these records highlights differences inherent to each of the reconstructions. For instance, the Cheeseman Lake proxy resolution across the 8,200 cal yr BP event is ~ 50 years/sample. Therefore, each $\delta^{18}O_{cal}$ value integrates at least ~ 50 years or more than likely an even greater time period, given mixing at the sediment-water interface. The Cheeseman Lake $\delta^{18}O_{cal}$ record therefore reflects multi-decadal to sub-century scale variations in $\delta^{18}O_{ppt}$ and atmospheric temperature. The Nordan's Pond Bog $\delta^{18}O_{ppt}$ reconstruction has a similar proxy resolution during this time of ~ 40 years/sample, which should yield a similar anomaly. As a result, we interpret the large differences observed between the records

across the 8,200 cal yr BP event (Figure 5-12) to reflect seasonal differences in the formation of the proxies and/or evaporative modification at Nordan's Pond Bog. For instance, the Nordan's Pond Bog water-table depth reconstruction shows a transition from relatively dry to wet conditions at ~ 8,400 cal yr BP (Figure 5-12), synchronous with the negative shift in $\delta^{18}O_{ppt}$. Accordingly, we argue the rather large $\delta^{18}O_{ppt}$ excursion at Nordan's Pond Bog is confounded in variations in the P-E balance and not solely changes in $\delta^{18}O_{ppt}$. This result has implications for climate model simulations (Daley et al., 2011; Tindall and Valdes, 2011) and isotope anomalies associated with the 8,200 cal yr BP abrupt climate event, which posits that greater $\delta^{18}O$ excursions are experienced proximal to the Labrador Sea.

After the 8,200 cal yr BP event, Cheeseman Lake $\delta^{18}O_{cal}$ values increase and attain the most positive values (-9.98 ‰ VPDB) during the entire record at ~ 7,950 cal yr BP (Figure 5-12). Thereafter, Cheeseman Lake $\delta^{18}O_{cal}$ values decrease and eventually attain minimum values (-11.11 ‰ VPDB) around ~ 4,300 cal yr BP. We interpret these variations to represent the warmest conditions and/or enhanced warm-season precipitation at ~ 7,900 cal yr BP and gradual cooling thereafter. In contrast, Nordan's Pond Bog $\delta^{18}O_{ppt}$ values increase after 8,200 cal yr BP and are relatively high (~ -4 to -6 ‰) between 6,800 to 3,900 cal yr BP (Figure 5-12). We interpret this discrepancy to show increased evaporation at Nordan's Pond Bog, resulting in more positive $\delta^{18}O_{ppt}$ values, consistent with drier conditions during this time (Amesbury et al., 2013). After 3,900 cal yr BP, $\delta^{18}O_{ppt}$ values at Nordan's Pond Bog decrease abruptly by ~ 4 ‰ and remain relatively low (between ~ -6 to -8 ‰) for the remainder of the Holocene (Figure 5-12). This transition likely reflects the onset of wetter conditions and reduced

evaporation of bog waters. This interpretation is consistent with a transition to a higher and stable water-table depth at Nordan's Pond Bog after ~ 4,000 cal yr BP (Figure 5-12) (Amesbury et al., 2013), reflecting wetter conditions. Meanwhile, Cheeseman Lake $\delta^{18}O_{cal}$ briefly returns to relatively higher values of -10.4 ‰ (VPDB) between ~ 3,400 to ~ 3,000 cal yr BP and a slight trend towards more negative and generally stable values thereafter.

5.6.3 North Atlantic comparison: 10,200 to 7,950 cal yr BP

The Cheeseman Lake $\delta^{18}O_{cal}$ record shows an overall trend to more positive values from 10,200 to 7,950 cal yr BP during the early Holocene (Figure 5-13). The range in $\delta^{18}O_{cal}$ values over this time is from -11.54 ‰ VPDB (at 11,100 cal yr BP) to -9.98 ‰ VPDB (at 7,950 cal yr BP). If the 1.56 ‰ increase in $\delta^{18}O_{cal}$ values was entirely a result of changes in atmospheric temperature, this would imply a 4.0° C increase. Notably, a similar trend is found in the Dye-3 and NGRIP Greenland ice core $\delta^{18}O$ records at this time (Figure 5-13), which has been interpreted to reflect rising temperatures during the final stages of deglaciation (Vinther et al., 2009). Further, the early Holocene increase in Cheeseman Lake $\delta^{18}O_{cal}$ coincides with Laurentide Ice Sheet retreat (Dyke, 2004), increasing eustatic sea levels (Clark et al., 2009), and changing oceanographic conditions in the Labrador Sea and western Atlantic Ocean. For example, gradually decreasing planktonic foraminiferal (N. pachyderma sinistral) $\delta^{18}O$ values recorded south of Newfoundland at the Laurentian Fan (Figure 5-13) reflect changes in the $\delta^{18}O$ of the surface ocean from ice sheet retreat (Keigwin et al., 2005). Changing surface ocean $\delta^{18}O$ values south of Newfoundland likely influenced $\delta^{18}O_{ppt}$ at

Cheeseman Lake, given this area represents the source of atmospheric moisture. Increasing Cheeseman Lake $\delta^{18}O_{cal}$ is interrupted by abrupt negative excursions at ~ 9,700 cal yr BP and ~8,500 cal yr BP. The ~ 9,700 cal yr BP feature occurs too early to be linked with the ~ 9,300 cal yr BP abrupt climate change event (Yu et al., 2010), suggesting that our $\delta^{18}O_{cal}$ record is too coarsely resolved in time to detect this rather short-lived event. However, the ~ 9,700 cal yr BP anomaly at Cheeseman Lake coincides with a shift toward colder sea surface temperatures (SSTs) and decreasing surface ocean $\delta^{18}O$ ($\delta^{18}O_{sw}$) from Cartwright Saddle in the western Labrador Sea (Figure 5-13). Hoffman et al. (2012) interpret this shift after 9,700 cal yr BP to reflect enhanced meltwater flux and renewed Laurentide Ice Sheet retreat.

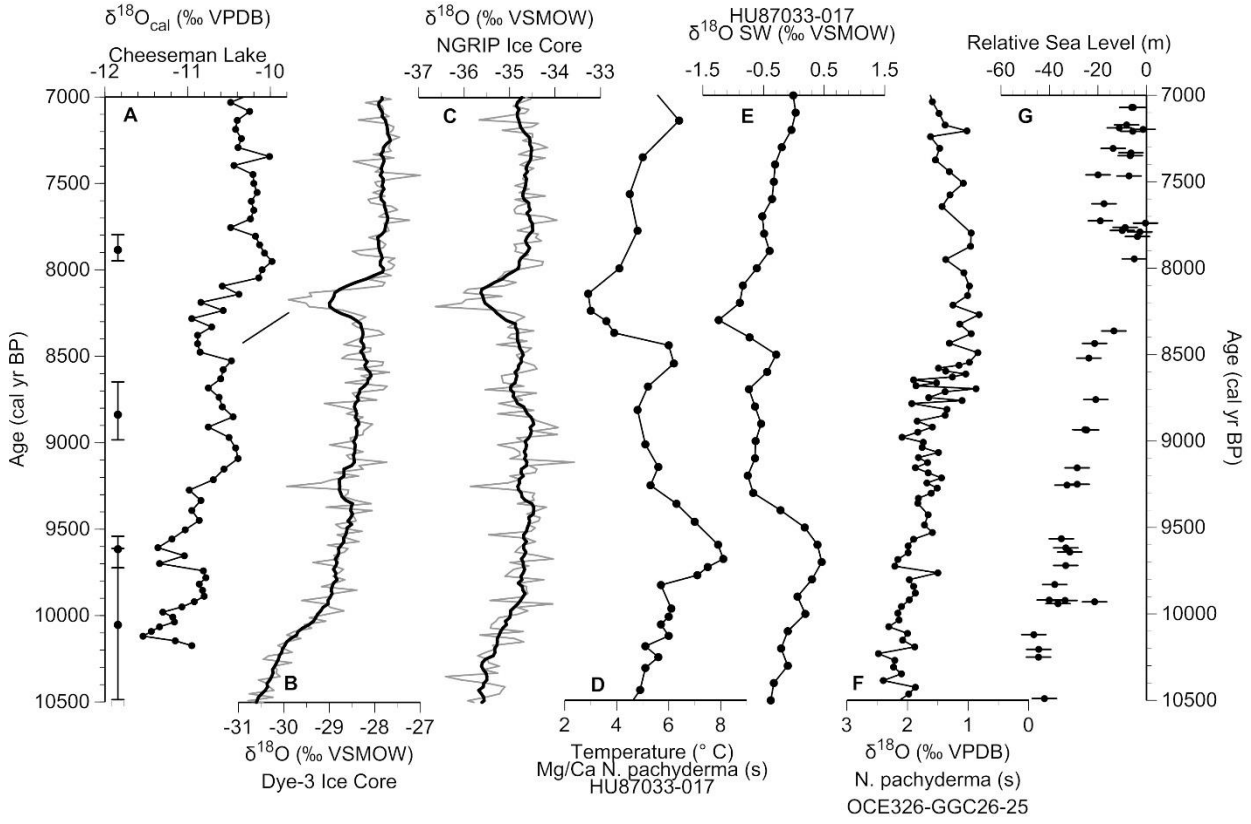

Figure 5-13. Comparison of early Holocene climate records from the North Atlantic region, including (a) Cheeseman Lake carbonate $\delta^{18}O$ (‰ VPDB) with calibrated radiocarbon ages and the 95% error bounds

on the left. (b) Dye-3 $\delta^{18}O$ (grey line) and 200-yr moving average (black line) (‰ VSMOW) (Dansgaard et al., 1985). (c) NGRIP $\delta^{18}O$ (grey line) and 200-yr moving average (black line) (‰ VSMOW) (NGRIP, 2004). (d) Mg/Ca inferred calcification temperature of the planktonic foraminifer N. pachyderma sinistral from marine core HU87033-017 from the Cartwright Saddle in the Labrador Sea (Hoffman et al., 2012). (e) $\delta^{18}O$ (‰ VSMOW) of sea water from marine core HU87033-017 (Hoffman et al., 2012). (f) N. pachyderma sinistral $\delta^{18}O$ (‰ VPDB) from marine core OCE326-GGC26-25 from the Laurentian Fan south of Newfoundland (Keigwin et al., 2005). (g) Relative eustatic sea level (Clark et al., 2009).

The 8,200 cal yr BP event (Alley et al., 1997) represents the last major abrupt climate change event experienced during the last glacial to interglacial transition. The Cheeseman Lake $\delta^{18}O_{cal}$ excursion at ~ 8,500 cal yr BP again coincides with a shift to colder SSTs at Cartwright Saddle (Hoffman et al., 2012) associated with the final drainage of Glacial Lake Agassiz (Barber et al., 1999), indicating a synchronous response between the ocean-atmosphere system at this time. A similar phasing is found in the Nordan's Pond Bog $\delta^{18}O_{ppt}$, wherein the primary anomaly begins at ~ 8,400 cal yr BP (Daley et al., 2009; Daley et al., 2011). However, the $\delta^{18}O_{cal}$ excursion begins almost ~ 300 years earlier than the observed $\delta^{18}O$ anomaly found in Greenland ice cores (Figure 5-13). Daley et al. (2011) discuss the phasing and implications of this age off-set in their review of stable isotope records from the circum North Atlantic region spanning the 8,200 cal yr BP event. Specifically, they consider the apparent age off-set to result from 1) age model errors and inconsistencies between the proxies that confounds identification of the event as 'synchronous' across the Atlantic and 2) a delayed transmission of the event because of interactions in the ocean-atmosphere system (Daley et al., 2011). The authors reject the second option, because a time-transgressive response to the underlying forcing mechanism should result in a spatial

pattern showing a delayed response with increasing distance from the Labrador Sea. As a result, Daley et al. (2011) consider the $\delta^{18}O$ anomalies among paleoclimate records in the North Atlantic region to be broadly synchronous, with the age discrepancies linked with local climatic responses. After ~ 8,280 cal yr BP and the primary negative isotope anomaly, Cheeseman Lake $\delta^{18}O_{cal}$ values increase from -10.95 ‰ (VPDB) to maximum values of -9.98 ‰ (VPDB) by ~ 7,950 cal yr BP (Figure 5-13). Converting this 1.07 ‰ increase in $\delta^{18}O_{cal}$ values yields a temperature increase of 2.8° C spanning the ~ 350 year period. However, $\delta^{18}O_{ppt}$ across Newfoundland at this time must be controlled by various factors, including changes in moisture balance (Amesbury et al., 2013), the seasonality of precipitation (Denton et al., 2005; Prasad et al., 2009; Rohling and Palike, 2005), the surface ocean $\delta^{18}O$ (Hoffman et al., 2012; Keigwin et al., 2005), atmospheric circulation (Kirby et al., 2002), and temperature (Vinther et al., 2009), among others. Thus, we conclude the post 8,200 cal yr BP event transition to the most positive $\delta^{18}O_{cal}$ values reflects some combination of warmer temperatures, a shift back to greater warm-season precipitation, and potentially wetter conditions.

5.6.4 North Atlantic comparison: 7,950 to 1,200 cal yr BP

Evidence from the Cheeseman Lake $\delta^{18}O_{cal}$ record suggests the period immediately after ~ 7,950 cal yr BP represents the warmest conditions spanning the entire record (Figure 5-14). This result is consistent with a synthesis of temperature reconstructions from the North Atlantic region, which shows the warmest temperatures in eastern Canada between 8,000 to 6,000 cal yr BP (Kaplan and Wolfe, 2006).

Additional evidence for relatively warm conditions at this time comes from Greenland ice core $\delta^{18}O$ records (Figure 5-14), which show the warmest temperatures of the entire Holocene at ~ 7,900 cal yr BP (Vinther et al., 2009). This period of time, known as the Holocene Thermal Maximum (HTM), lags the early Holocene 50° N summer insolation maxima by 1,000 to 3,000 years in the western Atlantic Ocean sector. The delay in peak temperatures with respect to insolation forcing is attributed to the close proximity of the residual Laurentide Ice Sheet (Kaufman et al., 2004), which still dominated atmospheric circulation and exerted a 'chilling effect' on Newfoundland, prior to ice sheet disintegration before the 8,200 cal yr BP event.

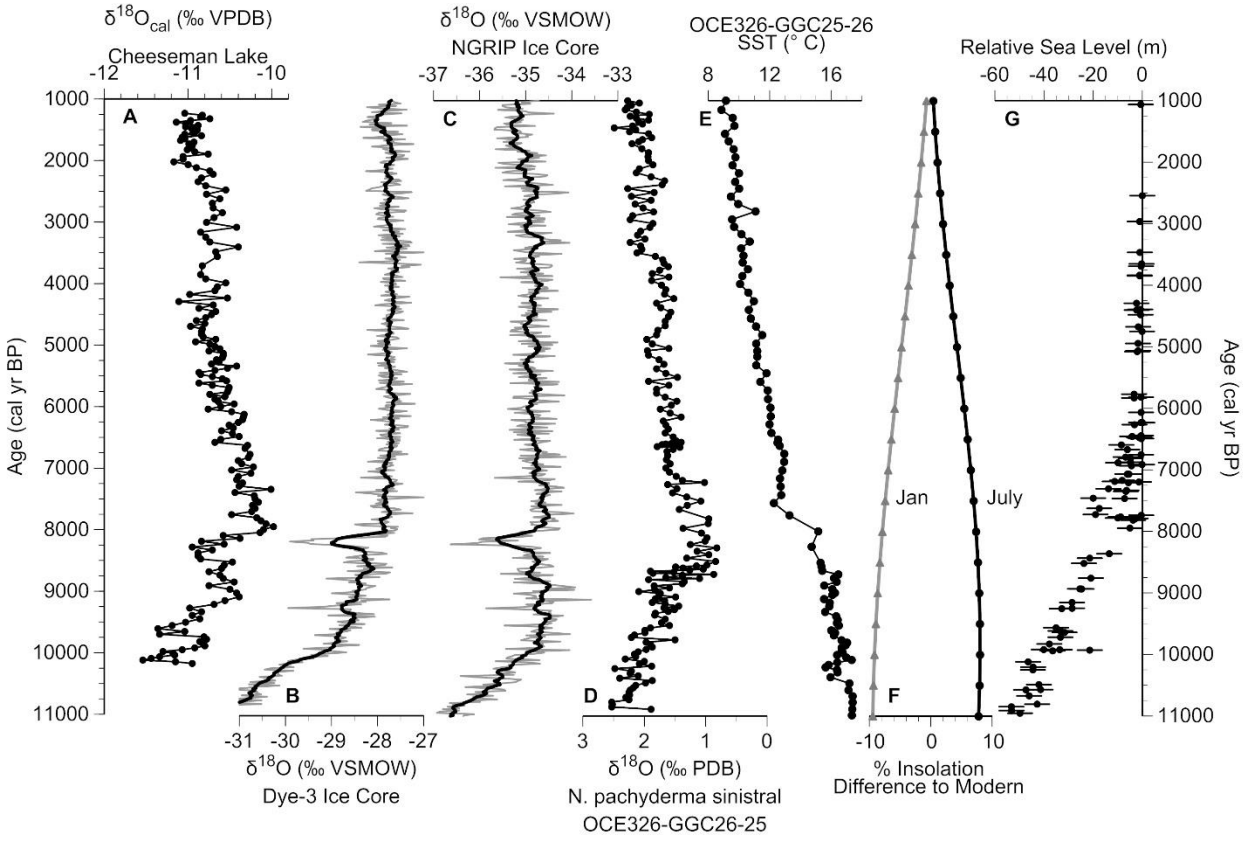

Figure 5-14. (a) Cheeseman Lake carbonate $\delta^{18}O$ (‰ VPDB). (b) Dye-3 $\delta^{18}O$ (grey line) and 200-yr moving average (black line) (‰ VSMOW) (Dansgaard et al., 1985). (c) NGRIP $\delta^{18}O$ (grey line) and 200-yr moving average (black line) (‰ VSMOW) (NGRIP, 2004). (d) N. pachyderma sinistral $\delta^{18}O$ (‰ VPDB)

from marine core OCE326-GGC26-25 (Keigwin et al., 2005). (e) Alkenone derived sea surface temperatures (SST) also from marine core OCE326-GGC26-25 (Keigwin et al., 2005; Sachs, 2007). (f) Percent insolation difference to modern for 50° North (Laskar et al., 2004). (g) Relative eustatic sea level (Clark et al., 2009).

Cheeseman Lake $\delta^{18}O_{cal}$ gradually decreases between ~ 7,950 to ~ 4,300 cal yr BP (Figure 5-14) consistent with the monotonic decline in high-latitude northern hemisphere summer insolation (Laskar et al., 2004). The 1.13 ‰ decrease in $\delta^{18}O_{cal}$ values over this time period represents a 3.3° C cooling, assuming temperature is the only factor influencing $\delta^{18}O_{ppt}$ at Cheeseman Lake. At the same time, a similar response is observed in the Greenland ice core $\delta^{18}O$ records (Figure 5-14) and ice-core inferred temperatures (Vinther et al., 2009). For example, a 2.74° C cooling is found between ~ 7,950 to ~ 4,300 cal yr BP based on temperature change in Greenland derived from the Agassiz and Renland ice core $\delta^{18}O$ records (Vinther et al., 2009). Evidence for cooling at this time is also found in proximal oceanographic records south of Newfoundland at the Laurentian Fan, where planktonic foraminiferal (N. pachyderma sinistral) $\delta^{18}O$ values gradually increase and alkenone-derived SSTs decrease from ~ 8,000 cal yr BP to the resent (Keigwin et al., 2005; Sachs, 2007). Keigwin et al. (2005) suggest the long term decrease in foraminiferal $\delta^{18}O$ values and SSTs is probably driven by decreasing seasonality of Northern Hemisphere insolation, forced by gradually decreasing summer and increasing winter insolation through the Holocene (Figure 5-14) (Laskar et al., 2004). More specifically, Sachs (2007) attributes cooling of continental slope waters at the Laurentian Fan and along the eastern seaboard of North America to result from declining insolation, increasing convection in the Labrador Sea, and

equatorward shifting of the Gulf Stream path. Thus, the concurrent shifts in Cheeseman Lake $\delta^{18}O_{cal}$ and inferred cooling support the notion of a coupled ocean-atmosphere response to insolation forcing at centennial time scales, at least between ~ 7,950 to ~ 4,300 cal yr BP.

The spatial pattern in reconstructed SSTs from the Laurentian Fan and across the Atlantic Ocean during the Holocene implicate a possible role of the North Atlantic Oscillation (NAO) driving the decline in temperatures. The NAO, defined by the cold-season pressure difference between the Azores High and Iceland Low, causes colder conditions in Newfoundland during the NAO+ phase (Hurrell and Deser, 2010), and vice versa during the NAO- phase. Accordingly, NAO+ conditions and cooler winter conditions in Newfoundland should result in more negative $\delta^{18}O_{ppt}$ and $\delta^{18}O_{cal}$ at Cheeseman Lake. Based on the pattern of Atlantic wide SSTs over the Holocene, Sachs (2007) suggest a transition from NAO- conditions in the early Holocene gave way to NAO+ conditions by the late Holocene. This interpretation is supported by excursions in the Transpolar Drift Stream evinced from driftwood in the Canadian Arctic Archipelago, driven by high-latitude atmospheric circulation patterns, which shows early Holocene NAO- or NAO neutral conditions and NAO+ conditions during the late Holocene (Tremblay et al., 1997). If we assume the spatial pattern of NAO-type conditions observed during the 20th century (Figure 5-4) persisted throughout the Holocene, such a pattern identified by Sachs (2007) would produce gradually colder conditions in Newfoundland through the Holocene. The decline in Cheeseman Lake $\delta^{18}O_{cal}$ and inferred temperatures between ~7,950 to ~ 4,300 cal yr BP provides evidence to support the hypothesis set forth by Sachs (2007). However, other

paleoclimate synthesis studies show the opposite, that the early Holocene was typified by NAO+ conditions that transitioned to NAO- conditions during the later Holocene (Rimbu et al., 2004). This discrepancy highlights the need for additional paleo records sensitive to NAO-like variability, to refine our understanding of natural variations and mean-state shifts in hemisphere wide circulation patterns.

After ~ 4,300 cal yr BP, the pattern of decreasing Cheeseman Lake $\delta^{18}O_{cal}$ is interrupted (Figure 5-14), discordant with the continual decline in high-latitude northern hemisphere summer insolation (Laskar et al., 2004). A return to slightly more positive and relatively stable $\delta^{18}O_{cal}$ values could in part reflect slightly warmer temperatures and/or a decrease in cold-season or increase in warm-season precipitation (Figure 5-10; Figure 5-11). Alternatively, the $\delta^{18}O_{cal}$ trend could be in part controlled by increased evaporative modification, leading to preferential loss of $H_2{}^{16}O$ via evaporation. However, this transition coincides with a shift to wet conditions between ~ 4,500 to ~ 4,000 cal yr BP evinced from the water-table depth reconstruction at Nordan's Pond Bog in eastern Newfoundland (Figure 5-12) (Amesbury et al., 2013). Additional support for major environmental change at this time is seen in the $\delta^{18}O_{ppt}$ reconstruction from Nordan's Pond Bog, which shows a ~ 4 ‰ negative shift at 3,900 cal yr BP (Figure 5-12) (Daley et al., 2009). Collectively, the regional proxy evidence suggests a major reorganization of atmospheric circulation occurred at this time across Newfoundland.

Notably, the inflection point in Cheeseman Lake $\delta^{18}O_{cal}$ and proxy evidence from Nordan's Pond Bog coincides with widespread regional and global evidence for abrupt climate change initiating at this time (Booth et al., 2005; Liu et al., 2014). For instance, Booth et al. (2005) synthesize mid-continent North American hydroclimate records and

report evidence for a severe drought between 4,300 to 4,100 cal yr BP. Interestingly, low to middle latitude sites in North America experienced severely dry conditions at the same time many higher latitude sites experienced a shift to wetter conditions (Booth et al., 2005). Evidence for changes in climate teleconnections and internal modes of variability from proxy records are reported across North America around this time. For instance, variations in the Mt. Logan ice core $\delta^{18}O$ record are interpreted to reflect enhanced meridional atmospheric circulation and an increase in the positive phase of the El Niño Southern Oscillation at 4,200 cal yr BP (Fisher et al., 2008). In addition, evidence for a mean-state shift in the Pacific-North American (PNA) pattern is found in paleoclimate records around 4,000 cal yr BP (Liu et al., 2014). The PNA influences North American weather patterns through its attendant effect on the strength and location of the East Asian jet stream, which determines the mode of atmospheric circulation (zonal vs. meridional flow) traversing the continent, primarily during the winter months. Variations in the PNA are driven by internal atmospheric variability and external forcing. In a synthesis of several $\delta^{18}O$ records from across North America, Liu et al. (2014) report evidence for PNA negative conditions during the middle Holocene and a shift to PNA positive conditions after 4,000 cal yr BP. This shift would correspond with a transition from zonal to greater meridional atmospheric circulation through the middle to late Holocene, which in turn influences the position of the winter time polar front, atmospheric temperature, and the $\delta^{18}O_{ppt}$ across North America. Additional proxy evidence showing a shift in atmospheric circulation during the middle Holocene between ~ 5,000 to ~ 4,000 cal yr BP are reported from New York State (Kirby et al., 2002) and southern Ontario (Edwards et al., 1996; Yu et al., 1997). While it is uncertain what if

any connection exists between these large scale climate teleconnections and the Cheeseman Lake $\delta^{18}O_{cal}$ record, existing proxy evidence from Newfoundland (Amesbury et al., 2013; Daley et al., 2009) provides support for major climatic change at this time in eastern North America.

5.7 CONCLUSIONS

The Cheeseman Lake $\delta^{18}O_{cal}$ record provides insights into the Holocene evolution of $\delta^{18}O_{ppt}$ in eastern North America. Lake hydrology and isotope mass balance model simulations support the interpretation that $\delta^{18}O_{cal}$ records variations in the annual moisture surplus weighted $\delta^{18}O_{ppt}$. Lake model simulations further indicate that Cheeseman Lake is sensitive to cold-season (October-March) temperature changes, and to a much lesser extent the seasonality of precipitation. Variations in Cheeseman Lake $\delta^{18}O_{cal}$ permit identification of two distinct isotopic zones, based on overall differences in the trend of $\delta^{18}O_{cal}$ over time, which are broadly consistent with the disparity in Earth's boundary conditions before and after ~ 8,000 cal yr BP. A general trend of increasing and more positive $\delta^{18}O_{cal}$ values between ~ 10,200 to ~ 7,950 cal yr BP is interpreted to reflect warming temperatures, coinciding with Laurentide Ice Sheet deglaciation, changing surface ocean $\delta^{18}O$ from enhanced meltwater, rising eustatic sea levels, and warming temperatures inferred from Greenland ice cores. The increasing trend is interrupted by abrupt $\delta^{18}O_{cal}$ anomalies to more negative values at ~ 9,700 and ~ 8,500 cal yr BP, that coincide with cooling events in the adjacent Labrador Sea and circum North Atlantic region. After ~ 7,950 cal

yr BP, $\delta^{18}O_{cal}$ values decrease to gradually more negative values until ~ 4,300 cal yr BP, which we interpret as a cooling trend, consistent with declining Boreal summer insolation and cooling sea surface temperatures in the western North Atlantic Ocean. $\delta^{18}O_{cal}$ values return to slightly more positive values after ~ 4,300 cal yr BP and thereafter remain relatively stable until ~ 1,200 cal yr BP. The transition at ~4,300 cal yr BP corresponds with a shift to wetter conditions in Newfoundland evinced from other paleo-proxy records. The discordance between Cheeseman Lake $\delta^{18}O_{cal}$ values and declining insolation could in part reflect warmer temperatures and/or changes in the seasonality of precipitation resulting from an abrupt and mean-state shift in atmospheric circulation. For instance, a transition to the positive phase of the El Niño Southern Oscillation, the positive phase of the Pacific-North American pattern, and regional to global evidence for climate change occur around ~ 4,200 cal yr BP. Accordingly, proxy evidence from Cheeseman Lake and other paleo records from Newfoundland provide additional support for climatic change at this time from eastern North America.

6.0 SUMMARY AND CONCLUSIONS

This dissertation uses the sedimentary record from lakes combined with detailed analysis of physical sedimentology, geochemical proxies, and radiometric dating to reconstruct lake-levels, hydroclimate conditions, and paleoenvironmental changes in Alaska and Newfoundland spanning the late-Quaternary. The geographic focus is on high-latitude regions in North America, which are climatically sensitive regions due to ice-albedo processes and associated positive feedbacks (ACIA, 2005). Arctic regions have experienced accelerated warming over the late 20th century (Miller et al., 2010), resulting in adverse impacts including the drying up and disappearance of lakes from increased evaporation and permafrost degradation. Lake sediment reconstructions provide a long-term geological perspective of past changes in hydroclimate and environmental conditions that allow direct comparison with the instrumental record to assess the natural range of climatic conditions spanning the late-Quaternary. Further, paleo observations provide important constraints to validate and test the performance of climate model simulations that quantitatively investigate paleoclimate conditions (Bartlein et al., 2011), which ultimately helps to better predict the range of future climate scenarios.

In the interior of Alaska, a 31,000 year record of lake-level and paleoenvironmental change from Harding Lake shows very low lake-levels along with

extremely arid and windy conditions during the global LGM until 15,700 cal yr BP. The Lateglacial to early Holocene period between 15,700 to 9,400 cal yr BP is marked by higher and fluctuating lake-levels, a decrease in windiness, and increases in terrestrial and aquatic productivity. The expansion of *Betula* forest at ~ 14,600 cal yr BP provides additional support for wetter and warmer conditions compared with the preceding glacial period. A rapid increase in sedimentation rate, terrestrial and aquatic productivity, and rising lake lake-levels to near the overflow indicates considerable environmental change between 9,400 to 8,700 cal yr BP. Generally high and stable lake-levels persist after 8,700 cal yr BP to the present with conditions similar to the modern lake. Increases in *Alnus* by 7,000 cal yr BP and *Picea* by 5,600 cal yr BP, combined with continued predominance of *Betula* through the Holocene, indicate substantial expansion of boreal forest during the middle Holocene at Harding Lake.

In northwest Arctic Alaska, a 37,000 year record of paleoenvironmental change from Burial Lake provides the oldest continuous lacustrine record from eastern Beringia to date. Relatively high lake-levels and gradually decreasing in-lake and terrestrial productivity occur during the mid-Wisconsinan interstadial between 37,200 to ~ 29,600 cal yr BP. The subsequent period is defined by falling and lower lake-levels with decreasing effective-moisture, windier conditions, and sustained and low levels of aquatic productivity throughout the LGM between ~ 29,600 to ~19,600 cal yr BP. Although our age control is limited through the LGM, we suggest the relatively early LGM alpine glacial maximum extent in the central Brooks Range could have occurred during a time of slightly higher effective moisture levels. Therefore, we hypothesize that subsequent more extensive advances were possibly precluded by greater aridity as the

Bering Land Bridge increased in size and the distance from marine moisture sources increased. The last deglaciation that commenced by ~19,600 cal yr BP is characterized by gradual changes in several sediment physical and geochemical proxies, including increasing C/N ratios and terrestrial productivity, decreasing magnetic susceptibility and clastic sediment flux, along with rising and relatively higher lake-levels. We suggest this transition is related to initial retreat of the Laurentide Ice Sheet at ~ 19,000 cal yr BP and a re-organization in atmospheric circulation across eastern Beringia, resulting in increasing effective moisture levels and terrestrial productivity at Burial Lake. A decrease in aeolian activity after 16,500 cal yr BP is inferred from the appearance of fine (very fine sandy silt) sediment, compared to coarse sediments through the LGM and last deglaciation. The highest levels of terrestrial productivity along with increasing and variable aquatic productivity occurs during the Lateglacial to early Holocene interval between 16,500 to 8,800 cal yr BP. The absence of multi-proxy evidence for a climatic reversal during the Younger Dryas from Burial Lake sediments contrasts with other paleorecords showing cooler temperatures and/or dry conditions in northern Alaska at this time. Peak levels of sediment organic content and terrestrial productivity at Burial Lake between ~ 10,500 to 9,900 cal yr BP coincide with the early Holocene summer insolation maxima. The remainder of the Holocene (since 8,800 cal yr BP) at Burial Lake is characterized by relatively high and stable lake levels, landscape stabilization, and relatively high and variable levels of aquatic productivity.

At Burial Lake, a multiproxy approach is used to investigate the evolution of Holocene climate at multi-decadal to sub-century scale resolution. In this chapter, we report the first evidence for cyclical and millennial scale fluctuations in climate from

Arctic Alaska. Large fluctuations in biogenic silica and related proxies at millennial timescales in Burial Lake occur over the last 10,000 years. We interpret changes in biogenic silica (BSi) to result from variability in aquatic productivity, which is indirectly mediated by climate through changes in the duration of the ice-free growing season and the availability of limiting nutrients at this oligotrophic, tundra lake. Time series analysis of the BSi record indicates a significant ~1,500-yr periodicity emerges by ~6,000 cal yr BP that disappears after ~3,000 cal yr BP. Comparison of aquatic productivity against a sea-ice inferred reconstruction of the Arctic Oscillation (AO) shows that periods of reduced productivity at Burial Lake coincide with positive phases of the AO. Reconstructed AO+ conditions that correspond with lower summer temperatures and a shortened ice free season result in a decreased flux of limiting nutrients from permafrost degradation and lower levels of aquatic productivity at Burial Lake. Further, the reconstructed aquatic productivity and the AO display similar millennial scale periodicities with ~1,500-yr variability during the middle Holocene that transitions to ~1,000-yr variability during the late Holocene. We propose that aquatic productivity at Burial Lake is related to state changes in the AO and that millennial variability that the record exhibits is related to internal oscillations within the climate system.

In west-central Newfoundland, a record of the oxygen isotopic composition of lacustrine carbonate minerals ($\delta^{18}O_{cal}$) from Cheeseman Lake provides insights into the Holocene evolution in $\delta^{18}O_{ppt}$ from eastern North America. A general trend of increasing and more positive $\delta^{18}O_{cal}$ values between ~ 10,200 to ~ 7,950 cal yr BP is interpreted to reflect warming temperatures, coincides with Laurentide Ice Sheet deglaciation, changing surface ocean $\delta^{18}O$ from enhanced meltwater, rising eustatic sea

levels, and warming temperatures inferred from Greenland ice cores. The increasing trend is interrupted by abrupt $\delta^{18}O_{cal}$ anomalies to more negative values at ~ 9,700 and ~ 8,500 cal yr BP, that coincide with cooling events in the adjacent Labrador Sea and circum North Atlantic region. After ~ 7,950 cal yr BP, $\delta^{18}O_{cal}$ values decrease to gradually more negative values until ~ 4,300 cal yr BP, which we interpret as a cooling trend, consistent with declining Boreal summer insolation and cooling sea surface temperatures in the western North Atlantic Ocean. $\delta^{18}O_{cal}$ values return to slightly more positive values after ~ 4,300 cal yr BP and thereafter remain relatively stable until ~ 1,200 cal yr BP, possibly reflecting warmer temperatures and/or changes in the seasonality of precipitation resulting from an abrupt and mean-state shift in atmospheric circulation.

BIBLIOGRAPHY

Abbott, M.B., Edwards, M.E., Finney, B.P., 2010. A 40,000-yr record of environmental change from Burial Lake in Northwest Alaska. Quaternary Research 74, 156-165.

Abbott, M.B., Finney, B.P., Edwards, M.E., Kelts, K.E., 2000. Lake-level reconstructions and paleohydrology of Birch Lake, central Alaska, based on seismic reflection profiles and core transects. Quaternary Research 53, 154-166.

Abbott, M.B., Stafford, T.W., 1996. Radiocarbon geochemistry of modern and ancient Arctic lake systems, Baffin Island, Canada. Quaternary Research 45, 300-311.

ACIA, A.C.I.A., 2005. Arctic Climate: Past and Present. Cambridge University Press, New York.

Adrian, R., O'Reilly, C.M., Zagarese, H., Baines, S.B., Hessen, D.O., Keller, W., Livingstone, D.M., Sommaruga, R., Straile, D., Van Donk, E., Weyhenmeyer, G.A., Winderl, M., 2009. Lakes as sentinels of climate change. Limnology and Oceanography 54, 2283–2297.

Ager, T.A., 1975. Late Quaternary environmental history of the Tanana Valley, Alaska, Institute of Polar Studies, Report No. 54. Ohio State University, Columbus, p. 117.

Ager, T.A., 1983. Holocene vegetational history of Alaska, In: Wright Jr., H. (Ed.), Late Quaternary Environments of the United States, The Holocene. University of Minnesota Press, Minneapolis, pp. 128-141.

Ager, T.A., 2003. Late Quaternary vegetation and climate history of the central Bering land bridge from St. Michael Island, western Alaska. Quaternary Research 60, 19-32.

Alley, R.B., Mayewski, P.A., Sowers, T., Stuiver, M., Taylor, K.C., Clark, P.U., 1997. Holocene climatic instability: a prominent, widespread event 8200 years ago. Geology 25, 483-486.

Amesbury, M.J., Mallon, G., Charman, D.J., Hughes, P.D.M., Booth, R.K., Daley, T.J., Garneau, M., 2013. Statistical testing of a new testate amoeba-based transfer function for water-table depth reconstruction on ombrotrophic peatlands in north-eastern Canada and Maine, United States. Journal of Quaternary Science 28, 27-39.

Amundson, R., Austin, A.T., Schuur, E.A.G., Yoo, K., Matzek, V., Kendall, C., Uebersax, A., Brenner, D., Baisden, W.T., 2003. Global patters of the isotopic composition of soil and plant nitrogen. Global Biogeochemical Cycles 17, 1031.

Anderson, L., Abbott, M.B., Finney, B.P., Burns, S.J., 2005. Regional atmospheric circulation change in the North Pacific during the Holocene inferred from

lacustrine carbonate oxygen isotopes, Yukon Territory, Canada. Quaternary Research 64, 21-35.
Anderson, N.J., 2000. Diatoms, temperature and climatic change. European Journal of Phycology 35, 307-314.
Anderson, P.M., 1985. Late Quaternary vegetational change in the Kotzebue Sound area, northwestern Alaska. Quaternary Research 24, 307-321.
Anderson, P.M., 1988. Late Quaternary pollen records from the Kobuk and Noatak River drainages, northwestern Quaternary Research 29, 263-276.
Anderson, P.M., Brubaker, L.B., 1994. Vegetation history of northcentral Alaska: a mapped summary of late-Quaternary pollen data. Quaternary Science Reviews 41, 306-315.
Anderson, P.M., Lozhkin, A.V., 2001. The Stage 3 interstadial complex (Karginskii/middle Wisconsinan interval) of Beringia: variations in paleoenvironments and implications for paleoclimatic interpretations. Quaternary Science Reviews 20, 93-125.
Andresen, C.G., Lougheed, V.L., 2015. Disappearing Arctic tundra ponds: Fine-scale analysis of surface hydrology in drained thaw lake basins over a 65year period (1948-2013). Journal of Geophysical Research-Biogeosciences 120, 466-479.
Andrews, J.T., Keigwin, L., Hall, F., Jennings, A.E., 1999. Abrupt deglaciation events and holocene palaeoceanography from high-resolution cores, Cartwright Saddle, Labrador Shelf, Canada. Journal of Quaternary Science 14, 383-397.
Araguás-Araguás, L., Froehlich, K., Rozanski, K., 2000. Deuterium and oxygen-18 isotope composition of precipitation and atmospheric moisture. Hydrological Processes 14, 1341-1355.
Badding, M.E., Briner, J.P., Kaufman, D.S., 2013. 10Be ages of late Pleistocene deglaciation and Neoglaciation in the north-central Brooks Range, Arctic Alaska. Journal of Quaternary Science 28, 95-102.
Balascio, N.L., Bradley, R.S., 2012. Evaluating Holocene climate change in northern Norway using sediment records from two contrasting lake systems. Journal of Paleolimnology 48, 259-273.
Bale, R.J., Robertson, I., Leavitt, S.W., Loader, N.J., Harlan, T.P., Gagen, M., Young, G.H.F., Csank, A.Z., Froyd, C.A., McCarroll, D., 2010. Temporal stability in bristlecone pine tree-ring stable oxygen isotope chronologies over the last two centuries. Holocene 20, 3-6.
Balser, A.W., Jones, J.B., Gens, R., 2014. Timing of retrogressive thaw slump initiation in the Noatak Basin, northwest Alaska, USA. Journal of Geophysical Research-Earth Surface 119, 1106-1120.
Banfield, C.E., Jacobs, J.D., 1998. Regional patterns of temperature and precipitation for Newfoundland and Labrador during the past century. The Canadian Geographer 42, 354-364.
Barber, D.C., Dyke, A., Hillaire-Marcel, C., Jennings, A.E., Andrews, J.T., Kerwin, M.W., Bilodeau, G., McNeely, R., Southon, J., Morehead, M.D., Gagnon, J.M., 1999. Forcing of the cold event of 8,200 years ago by catastrophic drainage of Laurentide lakes. Nature 400, 344-348.

Barber, V.A., Finney, B.P., 2000. Late Quaternary paleoclimatic reconstructions for interior Alaska based on paleolake-level data and hydrologic models. Journal of Paleolimnology 24, 29-41.
Bartlein, J.P., Anderson, P.M., Edwards, M.E., McDowell, P.F., 1991. A framework for interpreting paleoclimatic variations in eastern Beringia. Quaternary International 10, 73-83.
Bartlein, P.J., Harrison, S.P., Brewer, S., Connor, S., Davis, B.A.S., Gajewski, K., Guiot, J., Harrison-Prentice, T.I., Henderson, A., Peyron, O., Prentice, I.C., Scholze, M., Seppa, H., Shuman, B., Sugita, S., Thompson, R.S., Viau, A.E., Williams, J., Wu, H., 2011. Pollen-based continental climate reconstructions at 6 and 21 ka: a global synthesis. Climate Dynamics 37, 775-802.
Batterson, M.J., Catto, N.R., 2001. Topographically-controlled deglacial history of the Humber River Basin, western Newfoundland. Geographie Physique Et Quaternaire 55, 213-228.
Berger, A., Loutre, M.F., 1991. Insolation values for the climate of the last 10 million years. Quaternary Sciences Review 10, 297-317.
Bianchi, G.G., McCave, I.N., 1999. Holocene periodicity in North Atlantic climate and deep-ocean flow south of Iceland. Nature 397, 515-517.
Bieniek, P.A., Bhatt, U.S., Thoman, R.L., Angeloff, H., Partain, J., Papineau, J., Fritsch, F., Holloway, E., Walsh, J.E., Daly, C., Shulski, M., Hufford, G., Hill, D.F., Calos, S., Gens, R., 2012. Climate Divisions for Alaska Based on Objective Methods. Journal of Applied Meteorology and Climatology 51, 1276-1289.
Bigelow, N.H., 1997. Late-Quaternary climate and vegetation in interior Alaska. University of Alaska, Fairbanks.
Bigelow, N.H., Edwards, M.E., 2001. A 14,000 yr paleoenvironmental record from Windmill Lake, Central Alaska: evidence for high-frequency climatic and vegetation fluctuations. Quaternary Science Reviews 20, 203-215.
Binford, M.W., 1990. Calculation and uncertainty analysis of 210Pb dates for PIRLA project sediment cores. Journal of Paleolimnology 3, 253-267.
Blaauw, M., 2010. Methods and code for 'classical' age-modelling of radiocarbon sequences. Quaternary Geochronology 5, 512-518.
Blackwell, J., 1965. Surficial geology and geomorphology of the Harding Lake area, Big Delta Quadrangle, Alaska. University of Alaska, Fairbanks, Fairbanks.
Bond, G., Kromer, B., Beer, J., Muscheler, R., Evans, M.N., Showers, W., Hoffmann, S., Lotti-Bond, R., Hajdas, I., Bonani, G., 2001. Persistent solar influence on north Atlantic climate during the Holocene. Science 294, 2130-2136.
Bond, G., Showers, W., Cheseby, M., Lotti, R., Almasi, P., deMenocal, P., Priore, P., Cullen, H., Hajdas, I., Bonani, G., 1997. A pervasive millennial-scale cycle in North Atlantic Holocene and glacial climates. Science 278, 1257-1266.
Booth, R.K., Jackson, S.T., Forman, S.L., Kutzbach, J.E., Bettis, E.A., Kreig, J., Wright, D.K., 2005. A severe centennial-scale drought in mid-continental North America 4200 years ago and apparent global linkages. The Holocene 15, 321-328.
Bowen, G.J., Wilkinson, B., 2002. Spatial distribution of delta O-18 in meteoric precipitation. Geology 30, 315-318.
Brienen, R.J.W., Helle, G., Pons, T.L., Guyot, J.-L., Gloor, M., 2012. Oxygen isotopes in tree rings are a good proxy for Amazon precipitation and El Nino-Southern

Oscillation variability. Proceedings of the National Academy of Sciences of the United States of America 109, 16957-16962.
Briner, J.P., Kaufman, D.S., 2008. Late Pleistocene mountain glaciation in Alaska: key chronologies. Journal of Quaternary Science 23, 659-670.
Briner, J.P., Kaufman, D.S., Manley, W.E., Finkel, R.C., Caffee, M.W., 2005. Cosmogenic exposure dating of late Pleistocene moraine stabilization in Alaska. Geological Society of America Bulletin 117, 1108-1120.
Brown, E.T., Johnson, T.C., Scholz, C.A., Cohen, A.S., King, J.W., 2007. Abrupt change in tropical African climate linked to the bipolar seesaw over the past 55,000 years. Geophysical Research Letters 34.
Caissie, B.E., Brigham-Grette, J., Lawrence, K.T., Herbert, T.D., Cook, M.S., 2010. Last Glacial Maximum to Holocene sea surface conditions at Umnak Plateau, Bering Sea, as inferred from diatom, alkenone, and stable isotope records. Paleoceanography 25.
Canada, E., 2010. Canadian Monthly Climate Data and 1981-2010 Normals: Deer Lake, Newfoundland, In: Canada, E. (Ed.).
Carlson, L.J., Finney, B.P., 2004. A 13,000-year history of vegetation and environmental change at Jan Lake, east-central Alaska. The Holocene 14, 818–827.
Carpenter, S.R., Benson, B.J., Biggs, R., Chipman, J.W., Foley, J.A., Golding, S.A., Hammer, R.B., Hanson, P.C., Johnson, P.T.J., Kamarainen, A.M., Kratz, T.K., Lathrop, R.C., McMahon, K.D., Provencher, B., Rusak, J.A., Solomon, C.T., Stanley, E.H., Turner, M.G., Vander Zanden, M.J., Wu, C.-H., Yuan, H., 2007. Understanding regional change: A comparison of two lake districts. Bioscience 57, 323-335.
Cassano, E.N., Cassano, J.J., Nolan, M., 2011. Synoptic weather pattern controls on temperature in Alaska. Journal of Geophysical Research-Atmospheres 116.
Clark, I., Fritz, I., 1997. Environmental Isotopes in Hydrogeology. Lewis Publishers, Boca Raton, Florida.
Clark, P.U., Dyke, A.S., Shakun, J.D., Carlson, A.E., Clark, J., Wohlfarth, B., Mitrovica, J.X., Hostetler, S.W., McCabe, A.M., 2009. The Last Glacial Maximum. Science 325, 710-714.
Clark, P.U., Marshall, S.J., Clarke, G.K.C., Hostetler, S.W., Licciardi, J.M., Teller, J.T., 2001. Freshwater forcing of abrupt climate change during the last glaciation. Science 293, 283-287.
Clarke, G.K.C., Leverington, D.W., Teller, J.T., Dyke, A.S., 2004. Paleohydraulics of the last outburst flood from glacial Lake Agassiz and the 8200 BP cold event. Quaternary Science Reviews 23, 389-407.
Clegg, B.F., Hu, F.S., 2010. An oxygen-isotope record of Holocene climate change in the south-central Brooks Range, Alaska. Quaternary Science Reviews 29, 928-939.
Clegg, B.F., Kelly, R., Clarke, G.H., Walker, I.R., Hu, F.S., 2011. Nonlinear response of summer temperature to Holocene insolation forcing in Alaska. Proceedings of the National Academy of Sciences of the United States of America 108, 19299-19304.
COHMAP, M., 1988. Climatic changes of the last 18,000 years: observations and model simulations. Science 241, 1043-1052.

Colman-Sadd, S.P., Hayes, J.P., Knight, I., 2000. Geology of the Island of Newfoundland (digital version of Map 90-01 with minor revisions) Newfoundland Department of Mines and Energy, Geological Survey.

Compo, G.P., Whitaker, J.S., Sardeshmukh, P.D., Matsui, N., Allan, R.J., Yin, X., Gleason, B.E., Jr., Vose, R.S., Rutledge, G., Bessemoulin, P., Broennimann, S., Brunet, M., Crouthamel, R.I., Grant, A.N., Groisman, P.Y., Jones, P.D., Kruk, M.C., Kruger, A.C., Marshall, G.J., Maugeri, M., Mok, H.Y., Nordli, O., Ross, T.F., Trigo, R.M., Wang, X.L., Woodruff, S.D., Worley, S.J., 2011. The Twentieth Century Reanalysis Project. Quarterly Journal of the Royal Meteorological Society 137, 1-28.

Conley, D.L., Schelske, C.L., 2001. Biogenic silica, In: Last, W.M., Smol, J.P. (Eds.), Tracking Environmental Changes Using Lake Sediments - Volume II: Physical and Chemical Techniques. Kluwer, Dordecht, pp. 281-293.

Coulter, H.W., Hopkins, D.M., Karlstrom, T.N.V., Péwé, T.L., Wahrhaftig, C., Williams, J.R., 1965. Map showing extent of glaciations in Alaska. U.S. Geological Survey Map, I-415.

Craig, H., 1965. The measurement of oxygen isotope palaeotemperatures, In: Tongiorgi, E. (Ed.), Stable Isotopes in Oceanographic Studies and Palaeotemperatures. Consiglio Nazionale delle Ricerche Laboratorio di Geologia Nucleare, Pisa, pp. 161-182.

Craine, J.M., Elmore, A.J., Aidar, M.P.M., Bustamante, M., Dawson, T.E., Hobbie, E.A., Kahmen, A., Mack, M.C., McLauchlan, K.K., Michelsen, A., Nardoto, G.B., Pardo, L.H., Penuelas, J., Reich, P.B., Schuur, E.A.G., Stock, W.D., Templer, P.H., Virginia, R.A., Welker, J.M., Wright, I.J., 2009. Global patterns of foliar nitrogen isotopes and their relationships with climate, mycorrhizal fungi, foliar nutrient concentrations, and nitrogen availability. New Phytologist 183, 980-992.

Croudace, I.W., Rindby, A., Rothwell, R.G., 2006. ITRAX: description and evaluation of a new multi-function X-ray core scanner. New Techniques in Sediment Core Analysis. Geological Society, London Special Publications 267, 51-63.

Daansgaard, W., Clausen, H.B., Gundestrup, N., Johnsen, S.J., Rygner, C., 1985. Dating and climatic interpretation of two deep Greenland ice cores. Geophysical Monograph 33, 71-76.

Daley, T.J., Street-Perrott, F.A., Loader, N.J., Barber, K.E., Hughes, P.D.M., Fisher, E.H., Marshall, J.D., 2009. Terrestrial climate signal of the "8200 yr BP cold event" in the Labrador Sea region. Geology 37, 831-834.

Daley, T.J., Thomas, E.R., Holmes, J.A., Street-Perrott, F.A., Chapman, M.R., Tindall, J.C., Valdes, P.J., Loader, N.J., Marshall, J.D., Wolff, E.W., Hopley, P.J., Atkinson, T., Barber, K.E., Fisher, E.H., Robertson, I., Hughes, P.D.M., Roberts, C.N., 2011. The 8200 yr BP cold event in stable isotope records from the North Atlantic region. Global and Planetary Change 79, 288-302.

Dansgaard, W., 1964. Stable isotopes in precipitation. Tellus 16, 436-468.

Dansgaard, W., Clausen, H.B., Gundestrup, N., Johnsen, S.J., Rygner, C., 1985. Dating and climatic interpretation of two deep Greenland ice cores. Geophysical Monograph 33, 71-76.

Dansgaard, W., Johnsen, S.J., Clausen, H.B., Dahljensen, D., Gundestrup, N.S., Hammer, C.U., Hvidberg, C.S., Steffensen, J.P., Sveinbjornsdottir, A.E., Jouzel,

J., Bond, G., 1993. Evidence for general instability of past climate from a 250-kyr ice-core record. Nature 364, 218-220.
Darby, D.A., Ortiz, J.D., Grosch, C.E., Lund, S.P., 2012. 1,500-year cycle in the Arctic Oscillation identified in Holocene Arctic sea-ice drift. Nature Geoscience 5, 897-900.
Davies, M.H., Mix, A.C., Stoner, J.S., Addison, J.A., Jaeger, J., Finney, B., Wiest, J., 2011. The deglacial transition on the southeastern Alaska Margin: Meltwater input, sea level rise, marine productivity, and sedimentary anoxia. Paleoceanography 26.
de Vernal, A., Hillaire-Marcel, C., Darby, D.A., 2005. Variability of sea ice cover in the Chukchi Sea (western Arctic Ocean) during the Holocene. Paleoceanography 20.
Debret, M., Bout-Roumazeilles, V., Grousset, F., Desmet, M., McManus, J.F., Massei, N., Sebag, D., Petit, J.R., Copard, Y., Trentesaux, A., 2007. The origin of the 1500-year climate cycles in Holocene North-Atlantic records. Climate of the Past 3, 569-575.
Debret, M., Sebag, D., Crosta, X., Massei, N., Petit, J.R., Chapron, E., Bout-Roumazeilles, V., 2009. Evidence from wavelet analysis for a mid-Holocene transition in global climate forcing. Quaternary Science Reviews 28, 2675-2688.
Denton, G.H., Alley, R.B., Comer, G.C., Broecker, W.S., 2005. The role of seasonality in abrupt climate change. Quaternary Science Reviews 24, 1159-1182.
Dorfman, J.M., 2013. A 37,000-year Record of Paleomagnetic and Environmental Magnetic Variability from Burial Lake, Arctic Alaska, College of Earth, Ocean, and Atmospheric Science. Oregon State University, p. 126.
Douglas, M.S.V., Smol, J.P., 1999. Freshwater diatoms as indicators of environmental change in the High Arctic, In: Stoermer, E., Smol, J.P. (Eds.), The Diatoms: Applications for the Environment and Earth Sciences. Cambridge University Press, Cambridge, pp. 227-244.
Dyke, A., 2004. An outline of the deglaciation of North America with emphasis on central and northern Canada, In: Ehlers, J., Gibbard, P.L. (Eds.), Quaternary Glaciations, Extent and Chronology. Part II. North America. Elsevier, Amsterdam.
Dyke, A., Prest, V.K., 1987. Late Wisconsinan and Holocene history of the Laurentide Ice Sheet. Geographie Physique et Quaternaire 41, 237-263.
Edwards, M.E., Bigelow, N.H., Finney, B.P., Eisner, W.R., 2000. Records of aquatic pollen and sediment properties as indicators of late-Quaternary Alaskan lake levels. Journal of Paleolimnology 24, 55-68.
Edwards, M.E., Mock, C.J., Finney, B.P., Barber, V.A., Bartlein, P.J., 2001. Potential analogues for paleoclimatic variations in eastern interior Alaska during the past 14,000 yr: atmospheric-circulation controls of regional temperature and moisture responses. Quaternary Science Reviews 20, 189-202.
Edwards, T.W.D., Wolfe, B.B., MacDonald, G.M., 1996. Influence of changing atmospheric circulation on precipitation delta O-18-temperature relations in Canada during the Holocene. Quaternary Research 46, 211-218.
Eisner, W.R., Colinvaux, P.A., 1992. Late Quaternary Pollen Records from Oil Lake and Feniak Lake, Alaska, U.S.A. Arctic and Alpine Research 24, 56-63.
Elias, S.A., 2000. Late Pleistocene climates of Beringia, based on analysis of fossil beetles. Quaternary Research 53, 229-235.

Elias, S.A., Hamilton, T.D., Edwards, M.E., Beget, J.E., Krumhardt, A.P., Lavoie, C., 1999. Late Pleistocene environments of the western Noatak basin, northwestern Alaska. Geological Society of America Bulletin 111, 769-789.

Elias, S.A., Short, S.K., Nelson, C.H., Birks, H.H., 1996. Life and times of the Bering land bridge. Nature 382, 60-63.

Ellis, J.M., Calkin, P.E., 1984. Chronology of Holocene glaciation, central Brooks Range, Alaska. Geological Society of America Bulletin 95, 897-912.

Ersek, V., Clark, P.U., Mix, A.C., Cheng, H., Edwards, R.L., 2012. Holocene winter climate variability in mid-latitude western North America. Nature Communications 3, 1-8.

Faegri, K., Kaland, P.E., Krzywinski, K., 1989. Textbook of Pollen Analysis, 4th ed. Wiley, New York.

Finkenbinder, M.S., Abbott, M.B., Edwards, M.E., Langdon, C.T., Steinman, B.A., Finney, B.P., 2014. A 31,000 year record of paleoenvironmental and lake-level change from Harding Lake, Alaska, USA. Quaternary Science Reviews 87, 98-113.

Finney, B.P., Bigelow, N.H., Barber, V.A., Edwards, M.E., 2012. Holocene climate change and carbon cycling in a groundwater-fed, boreal forest lake: Dune Lake, Alaska. Journal of Paleolimnology 48, 43-54.

Fisher, D., Dyke, A., Dahl-Jensen, D., Demuth, M., Zdanowicz, C., Bourgeois, J., Koerner, R.M., Mayewski, P., Wake, C., Kreutz, K., Steig, E., Zheng, J., Yalcin, K., Goto-Azuma, K., Luckman, B., Rupper, S., 2008. The Mt. Logan Holocene and late Wisconsin isotope record: tropical Pacific-Yukon connections. The Holocene 19, 667-677.

Gaglioti, B.V., Mann, D.H., Jones, B.M., Pohlman, J.W., Kunz, M.L., Wooller, M.J., 2014. Radiocarbon age-offsets in an arctic lake reveal the long-term response of permafrost carbon to climate change. Journal of Geophysical Research-Biogeosciences 119, 1630-1651.

Gat, R.J., 1995. Stable Isotopes of Fresh and Saline Lakes, In: Lerman, A., Imboden, D.M., Gat, J.R. (Eds.), Physics and Chemistry of Lakes. Berlin, Springer Berlin Heidelberg, pp. 139-165.

Grimm, E.C., 1990. TILIA and TILIA GRAPH PC spreadsheet and graphics software for pollen data. INQUA Working Group on Data-Handling Methods Newsletter 4, 5-7.

Grinsted, A., Moore, J.C., Jevrejeva, S., 2004. Application of the cross wavelet transform and wavelet coherence to geophysical time series. Nonlinear Processes in Geophysics 11, 561-566.

Grootes, P.M., Stuiver, M., 1997. Oxygen 18/16 variability in Greenland snow and ice with 10(-3)- to 10(5)-year time resolution. Journal of Geophysical Research-Oceans 102, 26455-26470.

Grybeck, D., Beikman, H.M., Brosge, W.P., Tailleur, I.L., Mull, C.G., 1977. Geologic Map of the Brooks Range, Alaska, U.S. Geological Survey Open File Map OF 77-166B. U.S. Geological Survey.

Guthrie, D.A., 2001. Origin and causes of the mammoth steppe: a story of cloud cover, woolly mammal tooth pits, buckles, and inside-out Beringia. Quaternary Science Reviews 20, 549-574.

Hamilton, T.D., 1982. A late Pleistocene glacial chronology for the southern Brooks Range: Stratigraphic record and regional significance. Geological Society of America Bulletin 93, 700-716.
Hamilton, T.D., 1994. Late Cenozoic glaciation of Alaska, The Geology of North America, pp. 813-844.
Hamilton, T.D., 2001. Quaternary glacial, lacustrine, and fluvial interactions in the western Noatak basin, Northwest Alaska. Quaternary Science Reviews 20, 371-391.
Hamilton, T.D., 2003a. Surficial Geologic Map of parts of the Misheguk Mountain and Baird Mountains Quadrangles, Noatak National Preserve, Alaska, U.S. Geological Survey Open File Report 03-367. U.S. Geological Survey.
Hamilton, T.D., 2003b. Surficial Geology of the Dalton High (Itkillik-Sagavanirktop Rivers) Area, Southern Arctic Foothills, Alaska, Professional Report 121. Alaska Division of Geological and Geophysical Surveys, p. 32.
Hamilton, T.D., 2010. Surficial Geologic Map of the Noatak National Preserve, Alaska, U.S. Geological Survey Scientific Investigations Map 3036. U.S. Geological Survey.
Hamilton, T.D., Craig, J.L., Sellmann, P.V., 1988. The Fox Permafrost Tunnel - A Late Quaternary Geologic Record in Central Alaska. Geological Society of America Bulletin 100, 948-969.
Hamilton, T.D., Lancaster, G.A., Trimble, D.A., 1987. Glacial advance of late Wisconsin (Itkillik II) age in the upper Noatak River valley—A radiocarbon-dated stratigraphic record, In: Survey, U.S.G. (Ed.), Geologic studies in Alaska by the U.S. Geological Survey during 1986, pp. 35-39.
Hamilton, T.D., Van Etten, D.P., 1984. Late Pleistocene glacial dams in the Noatak valley, The United States Geological survey in Alaska -accomplishments during 1981: U.S. Geological Survey Circular 868. U.S. Geological Survey, pp. 21-23.
Hardt, B., Rowe, H.D., Springer, G.S., Cheng, H., Edwards, R.L., 2010. The seasonality of east central North American precipitation based on three coeval Holocene speleothems from southern West Virginia. Earth and Planetary Science Letters 295, 342-348.
Hartman, B., Wendler, G., 2005. The Significance of the 1976 Pacific Climate Shift in the Climatology of Alaska. Journal of Climate 18, 4824-4839.
Hastings, M.G., Sigman, D.M., Steig, E.J., 2005. Glacial/interglacial changes in the isotopes of nitrate from the Greenland Ice Sheet Project 2 (GISP2) ice core. Global Biogeochemical Cycles 19.
Hays, J.D., Imbrie, J., Shackleton, N.J., 1976. Variations in Earth's Orbit - Pacemaker of the Ice Ages. Science 194, 1121-1132.
Heiri, O., Lotter, A.F., Lemcke, G., 2001. Loss on ignition as a method for estimating organic and carbonate content in sediments: reproducibility and comparability of results. Journal of Paleolimnology 25, 101-110.
Henderson, A.K., Shuman, B.N., 2009. Hydrogen and oxygen isotopic compositions of lake water in the western United States. Geological Society of America Bulletin 121, 1179-1189.

Higuera, P.E., Brubaker, L.B., Anderson, P.M., Hu, F.S., Brown, T.A., 2009. Vegetation mediated the impacts of postglacial climate change on fire regimes in the south-central Brooks Range, Alaska. Ecological Monographs 79, 201-219.
Hoffman, J.S., Carlson, A.E., Winsor, K., Klinkhammer, G.P., LeGrande, A.N., Andrews, J.T., Strasser, J.C., 2012. Linking the 8.2 ka event and its freshwater forcing in the Labrador Sea. Geophysical Research Letters 39.
Hoogakker, B.A.A., Chapman, M.R., McCave, I.N., Hillaire-Marcel, C., Ellison, C.R.W., Hall, I.R., Telford, R.J., 2011. Dynamics of North Atlantic Deep Water masses during the Holocene. Paleoceanography 26.
Hopkins, D.M., 1982. Aspects of the paleogeography of Beringia during the Late Pleistocene, In: Hopkins, D.M., Matthews, J.V., Schweger, C.E., Young, S.B. (Eds.), Paleoecology of Beringia. Academic Press, New York, pp. 3-28.
Hu, F.S., Brubaker, L.B., Anderson, P.M., 1993. A 12,000 year record of vegetation change and soil development from Wien Lake, central Alaska. Canadian Journal of Botany 71, 1133-1142.
Hu, F.S., Brubaker, L.B., Anderson, P.M., 1996. Boreal ecosystem development in the northwestern Alaska range since 11,000 yr BP. Quaternary Research 45, 188-201.
Hu, F.S., Finney, B.P., Brubaker, L.B., 2001. Effects of holocene Alnus expansion on aquatic productivity, nitrogen cycling, and soil development in southwestern Alaska. Ecosystems 4, 358-368.
Hu, F.S., Kaufman, D., Yoneji, S., Nelson, D., Shemesh, A., Huang, Y., Tian, J., Bond, G., Clegg, B., Brown, T., 2003. Cyclic variation and solar forcing of Holocene climate in the Alaskan subarctic. Science 301, 1890-1893.
Hurrell, J.W., 1995. Decadal Trends in the North-Atlantic Oscillation - Regional Temperatures and Precipitation. Science 269, 676-679.
Hurrell, J.W., Deser, C., 2010. North Atlantic climate variability: The role of the North Atlantic Oscillation. Journal of Marine Systems 79, 231-244.
Huybers, P., Wunsch, C., 2004. A depth-derived Pleistocene age model: Uncertainty estimates, sedimentation variability, and nonlinear climate change. Paleoceanography 19.
IPCC, I.P.C.C., 2007. Climate Change 2007: The Physical Science Basis. Cambridge University Press, New York.
Jepsen, S.M., Voss, C.I., Walvoord, M.A., Rose, J.R., Minsley, B.J., Smith, B.D., 2013. Sensitivity analysis of lake mass balance in discontinuous permafrost: the example of disappearing Twelvemile Lake, Yukon Flats, Alaska (USA). Hydrogeology Journal 21, 185-200.
Jones, M.C., Yu, Z., 2010. Rapid deglacial and early Holocene expansion of peatlands in Alaska. Proceedings of the National Academy of Sciences of the United States of America 107, 7347-7352.
Jones, M.D., Roberts, C.N., Leng, M.J., 2007. Quantifying climatic change through the last glacial-interglacial transition based on lake isotope palaeohydrology from central Turkey. Quaternary Research 67, 463-473.
Jorgenson, M.T., Yoshikawa, K., Kanveskiy, M., Shur, Y.L., Romanovsky, V., Marchenko, S., Grosse, G., Brown, J., Jones, B., 2008. Permafrost

characteristics of Alaska, Ninth International Conference on Permafrost, Fairbanks, Alaska, pp. 121-122.
Kaplan, M.R., Wolfe, A.P., 2006. Spatial and temporal variability of Holocene temperature in the North Atlantic region. Quaternary Research 65, 223-231.
Katsuki, K., Khim, B.-K., Itaki, T., Harada, N., Sakai, H., Ikeda, T., Takahashi, K., Okazaki, Y., Asahi, H., 2009. Land-sea linkage of Holocene paleoclimate on the Southern Bering Continental Shelf. Holocene 19, 747-756.
Kaufman, D.S., Ager, T.A., Anderson, N.J., Anderson, P.M., Andrews, J.T., Bartlein, P.J., Brubaker, L.B., Coats, L.L., Cwynar, L.C., Duvall, M.L., Dyke, A.S., Edwards, M.E., Eisner, W.R., Gajewski, K., Geirsdottir, A., Hu, F.S., Jennings, A.E., Kaplan, M.R., Kerwin, M.N., Lozhkin, A.V., MacDonald, G.M., Miller, G.H., Mock, C.J., Oswald, W.W., Otto-Bliesner, B.L., Porinchu, D.F., Ruhland, K., Smol, J.P., Steig, E.J., Wolfe, B.B., 2004. Holocene thermal maximum in the western Arctic (0-180 degrees W). Quaternary Science Reviews 23, 529-560.
Kaufman, D.S., Axford, Y., Anderson, R.S., Lamoureux, S.F., Schindler, D.E., Walker, I.R., Werner, A., 2012. A multi-proxy record of the Last Glacial Maximum and last 14,500 years of paleoenvironmental change at Lone Spruce Pond, southwestern Alaska. Journal of Paleolimnology 48, 9-26.
Kaufman, D.S., Hu, F.S., Briner, J.P., Werner, A., Finney, B.P., Gregory-Eaves, I., 2003. A 33,000 year record of environmental change from Arolik Lake, Ahklun Mountains, Alaska, USA. Journal of Paleolimnology 30, 343-362.
Kaufman, D.S., Young, N.E., Briner, J.P., Manley, W.F., 2011. Alaska Paleo Glacier Atlas version 2, Quaternary Glaciations - Extent and Chronology: North America. Developments in Quaternary Sciences pp. 427-445.
Keigwin, L.D., Donnelly, J.P., Cook, M.S., Driscoll, N.W., Brigham-Grette, J., 2006. Rapid sea-level rise and Holocene climate in the Chukchi Sea. Geology 34, 861-864.
Keigwin, L.D., Sachs, J.P., Rosenthal, Y., Boyle, E.A., 2005. The 8200 year BP event in the slope water system, western subpolar North Atlantic. Paleoceanography 20.
Kelts, K., Hsu, K.J., 1978. Freshwater Carbonate Sedimentation, In: Lerman, A. (Ed.), Lakes: Chemistry, Geology, Physics. Berlin, Springer-Verlag Berlin Heidelberg, pp. 295-323.
Khider, D., Jackson, C.S., Stott, L.D., 2014. Assessing millennial-scale variability during the Holocene: A perspective from the western tropical Pacific. Paleoceanography 29, 143-159.
Kim, S.T., Oneil, J.R., 1997. Equilibrium and nonequilibrium oxygen isotope effects in synthetic carbonates. Geochimica Et Cosmochimica Acta 61, 3461-3475.
Kirby, M.E., Mullins, H.T., Patterson, W.P., Burnett, A.W., 2002. Late glacial-Holocene atmospheric circulation and precipitation in the northeast United States inferred from modern calibrated stable oxygen and carbon isotopes. Geological Society of America Bulletin 114, 1326-1340.
Kling, G.W., Kipphut, G.W., Miller, M.C., 1991. Arctic lakes and rivers as gas conduits to the atmosphere: implications for tundra carbon budgets. Science 251, 298–301.
Kokorowski, H.D., Anderson, P.M., Mock, C.J., Lozhkin, A.V., 2008. A re-evaluation and spatial analysis of evidence for a Younger Dryas climatic reversal in Beringia. Quaternary Science Reviews 27, 1710-1722.

Kurek, J., Cwynar, L.C., Ager, T.A., Abbott, M.B., Edwards, M.E., 2009. Late Quaternary Paleoclimate of Western Alaska Inferred from Fossil Chironomids and it Relation to Vegetation Histories. Quaternary Science Reviews 28, 799-811.

LaPerriere, J.D., 2003. Limnology of Harding Lake, Alaska: A deep, subarctic lake. Lake and Reservoir Management 19, 93-107.

Laskar, J., Robutel, P., Joutel, F., Gastineau, M., Correia, A.C.M., Levrard, B., 2004. A long-term numerical solution for the insolation quantities of the Earth. Astronomy & Astrophysics 428, 261-285.

LeGrande, A.N., Schmidt, G.A., 2009. Sources of Holocene variability of oxygen isotopes in paleoclimate archives. Climate of the Past 5, 441-455.

Leng, M.J., Marshall, J.D., 2004. Palaeoclimate interpretation of stable isotope data from lake sediment archives. Quaternary Science Reviews 23, 811-831.

Lewis, T., Gilbert, R., Lamoureux, S.F., 2002. Spatial and temporal changes in sedimentary processes at proglacial Bear Lake, Devon Island, Nunavut, Canada. Arctic Antarctic and Alpine Research 34, 119-129.

Licciardi, J.M., Teller, J.T., Clark, P.U., 1999. Freshwater routing by the Laurentide Ice Sheet during the last deglaciation, In: Clark, P.U., Webb, R.S., Keigwin, L.D. (Eds.), Mechanisms of Global Climate Change at Millennial Time Scales. American Geophysical Union Monograph 112. American Geophysical Union, Washington D.C., pp. 177-201.

Liu, Z., Yoshimura, K., Bowen, G.J., Buenning, N.H., Risi, C., Welker, J.M., Yuan, F., 2014. Paired oxygen isotope records reveal modern North American atmospheric dynamics during the Holocene. Nature Communications 5, 3701.

Liverman, D., Taylor, D., 1990. Surficial geology map of insular Newfoundland, Report 90-1 ed. Newfoundland Department of Mines and Energy, Geological Survey.

Löwemark, L., Chen, H.F., Yang, T.N., Kylander, M., Yu, E.F., Hsu, Y.W., Lee, T.Q., Song, S.R., Jarvis, S., 2011. Normalizing XRF-scanner data: A cautionary note on the interpretation of high-resolution records from organic-rich lakes. Journal of Asian Earth Sciences 40, 1250-1256.

Mann, D.H., Groves, P., Reanier, R.E., Kunz, M.L., 2010. Floodplains, permafrost, cottonwood trees, and peat: What happened the last time climate warmed suddenly in arctic Alaska? Quaternary Science Reviews 29, 3812-3830.

Mann, D.H., Peteet, D.M., Reanier, R.E., Kunz, M.L., 2002. Responses of an arctic landscape to Lateglacial and early Holocene climatic changes: the importance of moisture. Quaternary Science Reviews 21, 997-1021.

Marcott, S.A., Shakun, J.D., Clark, P.U., Mix, A.C., 2013. A Reconstruction of Regional and Global Temperature for the Past 11,300 Years. Science 339, 1198-1201.

Marshall, J.D., Lang, B., Crowley, S.F., Weedon, G.P., van Calsteren, P., Fisher, E.H., Holme, R., Holmes, J.A., Jones, R.T., Bedford, A., Brooks, S.J., Bloemendal, J., Kiriakoulakis, K., Ball, J.D., 2007. Terrestrial impact of abrupt changes in the North Atlantic thermohaline circulation: Early Holocene, UK. Geology 35, 639-642.

Matmon, A., Briner, J.P., Carver, G., Bierman, P., Finkel, R., 2010. Moraine chronosequence of the Donnelly Dome region, Alaska: Implications for the late Pleistocene glacial history of interior Alaska. Quaternary Research 74, 63-72.

Matthews, J.V., 1974. Wisconsin environment of interior Alaska: Pollen and macrofossil analysis of a 27 meter core from the Isabella Basin (Fairbanks, Alaska). Canadian Journal of Earth Science 11, 828-841.

Max, L., Riethdorf, J.-R., Tiedemann, R., Smirnova, M., Lembke-Jene, L., Fahl, K., Nuernberg, D., Matul, A., Mollenhauer, G., 2012. Sea surface temperature variability and sea-ice extent in the subarctic northwest Pacific during the past 15,000 years. Paleoceanography 27.

McKay, N.P., Kaufman, D.S., Michelutti, N., 2008. Biogenic silica concentration as a high-resolution, quantitative temperature proxy at Hallet Lake, south-central Alaska. Geophysical Research Letters 35.

Melles, M., Brigham-Grette, J., Minyuk, P.S., Nowaczyk, N.R., Wennrich, V., DeConto, R.M., Anderson, P.M., Andreev, A.A., Coletti, A., Cook, T.L., Haltia-Hovi, E., Kukkonen, M., Lozhkin, A.V., Rosen, P., Tarasov, P., Vogel, H., Wagner, B., 2012. 2.8 Million Years of Arctic Climate Change from Lake El'gygytgyn, NE Russia. Science 337, 315-320.

Meyer, H., Schirrmeister, L., Yoshikawa, K., Opel, T., Wetterich, S., Hubberten, H.-W., Brown, J., 2010. Permafrost evidence for severe winter cooling during the Younger Dryas in northern Alaska. Geophysical Research Letters 37.

Meyers, P.A., Ishiwatari, R., 1993. Lacustrine organic geochemistry - an overview of indicators of organic matter sources and diagenesis in lake sediments. Organic Geochemistry 20, 867-900.

Meyers, P.A., Teranes, J.L., 2001. Sediment organic matter, In: Last, W.M., Smol, J.P. (Eds.), Tracking Environmental Changes Using Lake Sediments - Volume II: Physical and Chemical Techniques. Kluwer, Dordecht, pp. 239–269.

Miller, G.H., Alley, R.B., Brigham-Grette, J., Fitzpatrick, J.J., Polyak, L., Serreze, M.C., White, J.W.C., 2010. Arctic amplification: can the past constrain the future? Quaternary Science Reviews 29, 1779-1790.

Milrad, S.M., Atallah, E.H., Gyakum, J.R., 2010. Synoptic Typing of Extreme Cool-Season Precipitation Events at St. John's, Newfoundland, 1979-2005. Weather and Forecasting 25, 562-+.

Mock, C.J., Bartlein, P.J., Anderson, P.M., 1998. Atmospheric circulation patterns and spatial climatic variations in Beringia. International Journal of Climatology 18, 1085-1104.

Monnin, E., Indermuhle, A., Dallenbach, A., Fluckiger, J., Stauffer, B., Stocker, T.F., Raynaud, D., Barnola, J.M., 2001. Atmospheric CO2 Concentrations over the Last Glacial Termination. Science 291, 112-114.

Mortlock, R.A., Froelich, P.N., 1989. A simple method for the rapid determination of biogenic opal in pelagic marine sediments. Deep-Sea Research 35, 1415-1426.

Muhs, D.R., Ager, T.A., Bettis, E.A., McGeehin, J., Been, J.M., Beget, J.E., Pavich, M.J., Stafford, T.W., Stevens, D.S.P., 2003. Stratigraphy and palaeoclimatic significance of Late Quaternary loess-palaeosol sequences of the Last Interglacial-Glacial cycle in central Alaska. Quaternary Science Reviews 22, 1947-1986.

Nakao, K., Ager, T.A., 1985. Climatic changes and vegetational history of the interior of Alaska inferred from drilled cores at Harding Lake, In: Nakao, K. (Ed.), Hydrological regime and climatic changes in the Arctic Circle - Report of the

Alaskan Paleohydrology Research Project. Laboratory of Hydrology, Department of Geophysics, Faculty of Science, Hokkaido University, Japan.
Nakao, K., Tanoue, R., Yokoyama, T., 1981. Origin of Harding Lake in interior Alaska. Journal of the Faculty of Science Hokkaido University 7, 1-12.
Newfoundland, G.o.L.a., 2007. Ecoregions of Newfoundland.
NGRIP, M., 2004. High-resolution record of Northern Hemisphere climate extending into the last interglacial period. Nature 431, 147-151.
Niebauer, H.J., Bond, N.A., Yakunin, L.P., Plotnikov, V.V., 1999. An update on the climatology and sea ice of the Bering Sea, In: Loughlin, T.R., Ohtani, K. (Eds.), Dynamics of the Bering Sea. University of Alaska Sea Grant, pp. 22-59.
Oswald, W.W., Anderson, P.M., Brown, T.A., Brubaker, L.B., Hu, F.S., Lozhkin, A.V., Tinner, W., Kaltenrieder, P., 2005. Effects of sample mass and macrofossil type on radiocarbon dating of arctic and boreal lake sediments. Holocene 15, 758-767.
Oswald, W.W., Brubaker, L.B., Anderson, P.M., 1999. Late Quaternary vegetational history of the Howard Pass area, northwestern Alaska. Canadian Journal of Botany 77, 570-581.
Otto-Bliesner, B.L., Brady, E.C., Clauzet, G., Tomas, R., Levis, S., Kothavala, Z., 2006. Last Glacial Maximum and Holocene climate in CCSM3. Journal of Climate 19, 2526–2544.
Papineau, J.M., 2001. Wintertime temperature anomalies in Alaska correlated with ENSO and PDO. International Journal of Climatology 21, 1577-1592.
Peltier, W.R., Fairbanks, R.G., 2006. Global glacial ice volume and Last Glacial Maximum duration from an extended Barbados sea level record. Quaternary Science Reviews 25, 3322-3337.
Péwé, T.L., 1975. The Quaternary Geology of Alaska, USGS Professional Paper 385, p. 145.
Pompeani, D.P., Steinman, B.A., Abbott, M.B., 2012. A Sedimentary and Geochemical Reconstruction of Water Level Changes from Rantin Lake, Yukon Territory, Canada. Journal of Paleolimnology 48, 147-158.
Prasad, S., Witt, A., Kienel, U., Dulski, P., Bauer, E., Yancheva, G., 2009. The 8.2 ka event: Evidence for seasonal differences and the rate of climate change in western Europe. Global and Planetary Change 67, 218-226.
Reimer, P.J., Baillie, M.G.L., Bard, E., Bayliss, A., Beck, J.W., Blackwell, P.G., Ramsey, C.B., Buck, C.E., Burr, G.S., Edwards, R.L., Friedrich, M., Grootes, P.M., Guilderson, T.P., Hajdas, I., Heaton, T.J., Hogg, A.G., Hughen, K.A., Kaiser, K.F., Kromer, B., McCormac, F.G., Manning, S.W., Reimer, R.W., Richards, D.A., Southon, J.R., Talamo, S., Turney, C.S.M., van der Plicht, J., Weyhenmeye, C.E., 2009. IntCAL09 and Marine09 Radiocarbon Age Calibration Curves, 0-50,000 Years CAL BP. Radiocarbon 51, 1111-1150.
Reimer, P.J., Bard, E., Bayliss, A., Beck, J.W., Blackwell, P.G., Ramsey, C.B., Buck, C.E., Cheng, H., Edwards, R.L., Friedrich, M., Grootes, P.M., Guilderson, T.P., Haflidason, H., Hajdas, I., Hatte, C., Heaton, T.J., Hoffmann, D.L., Hogg, A.G., Hughen, K.A., Kaiser, K.F., Kromer, B., Manning, S.W., Niu, M., Reimer, R.W., Richards, D.A., Scott, E.M., Southon, J.R., Staff, R.A., Turney, C.S.M., van der

Plicht, J., 2013. IntCAL13 and Marine13 Radiocarbon Age Calibration Curves 0-50,000 Years Cal BP. Radiocarbon 55, 1869-1887.
Rigor, I.G., Wallace, J.M., Colony, R.J., 2002. Response of the sea ice to the Arctic Oscillation. Journal of Climate 15, 2648-2663.
Rimbu, N., Lohmann, G., Lorenz, S.J., Kim, J.H., Schneider, R.R., 2004. Holocene climate variability as derived from alkenone sea surface temperature and coupled ocean-atmosphere model experiments. Climate Dynamics 23, 215-227.
Rodbell, D.T., Seltzer, G.O., Anderson, D.M., Abbott, M.B., Enfield, D.B., Newman, J.H., 1999. A 15,000-year record of El Nino-driven alluviation in southwestern Ecuador. Science 283, 516-520.
Rohling, E.J., Palike, H., 2005. Centennial-scale climate cooling with a sudden cold event around 8,200 years ago. Nature 434, 975-979.
Rozanski, K., Araguasaraguas, L., Gonfiantini, R., 1992. Relation Between Long-Term Trends of O-18 Isotope Composition of Precipitation and Climate. Science 258, 981-985.
Sachs, J.P., 2007. Cooling of Northwest Atlantic slope waters during the Holocene. Geophysical Research Letters 34.
Santos, G.M., Southon, J.R., Drenzek, N.J., Ziolkowski, L.A., Druffel, E., Xu, X., Zhang, D., Trumbore, S., Eglinton, T.I., Hughen, K.A., 2010. Blank Assessment for Ultra-Small Radiocarbon Samples: Chemical Extraction and Separation Versus AMS. Radiocarbon 52, 1322-1335.
Schnurrenberger, D., Russell, J., Kelts, K., 2003. Classification of lacustrine sediments based on sedimentary components. Journal of Paleolimnology 29, 141-154.
Schulz, M., Mudelsee, M., 2002. REDFIT: estimating red-noise spectra directly from unevenly spaced paleoclimatic time series. Computers & Geosciences 28, 421-426.
Shaw, J., Piper, D.J.W., Fader, G.B.J., King, E.L., Todd, B.J., Bell, T., Batterson, M.J., Liverman, D.G.E., 2006. A conceptual model of the deglaciation of Atlantic Canada. Quaternary Science Reviews 25, 2059-2081.
Sikorski, J.J., Kaufman, D.S., Manley, W.F., Nolan, M., 2009. Glacial-Geologic Evidence for Decreased Precipitation during the Little Ice Age in the Brooks Range, Alaska. Arctic Antarctic and Alpine Research 41, 138-150.
Smith, I.R., 2000. Diamictic sediments within high Arctic lake sediment cores: evidence for lake ice rafting along the lateral glacial margin. Sedimentology 47, 1157-1179.
Sorrel, P., Debret, M., Billeaud, I., Jaccard, S.L., McManus, J.F., Tessier, B., 2012. Persistent non-solar forcing of Holocene storm dynamics in coastal sedimentary archives. Nature Geoscience 5, 892-896.
South, G.R., 1983. Biogeography and Ecology of the Island of Newfoundland. W. Junk Publishers, Boston.
St-Onge, G., Stoner, J.S., Hillaire-Marcel, C., 2003. Holocene paleomagnetic records from the St. Lawrence Estuary, eastern Canada: centennial- to millennial-scale geomagnetic modulation of cosmogenic isotopes. Earth and Planetary Science Letters 209, 113-130.
Stafford, J.M., Wendler, G., Curtis, J., 2000. Temperature and precipitation of Alaska: 50 year trend analysis. Theoretical and Applied Climatology 67, 33-44.

Stansell, N.D., Abbott, M.B., Rull, V., Rodbell, D.T., Bezada, M., Montoya, E., 2010. Abrupt Younger Dryas cooling in the northern tropics recorded in lake sediments from the Venezuelan Andes. Earth and Planetary Science Letters 293, 154-163.

Stansell, N.D., Steinman, B.A., Abbott, M.B., Rubinov, M., Roman-Lacayo, M., 2013. Lacustrine stable isotope record of precipitation changes in Nicaragua during the Little Ice Age and Medieval Climate Anomaly. Geology 41, 151-154.

Steinhilber, F., Beer, J., Fröhlich, C., 2009. Total solar irradiance during the Holocene. Geophysical Research Letters 36, L19704.

Steinman, B.A., Abbott, M.B., 2013. Isotopic and hydrologic responses of small, closed lakes to climate variability: Hydroclimate reconstructions from lake sediment oxygen isotope records and mass balance models. Geochimica Et Cosmochimica Acta 105, 342-359.

Steinman, B.A., Abbott, M.B., Mann, M.E., Ortiz, J.D., Pompeani, D.P., Stansell, N.D., Anderson, L., Finney, B.P., Bird, B.W., 2014. Ocean-atmosphere forcing of centennial hydroclimate variability in the Pacific Northwest. Geophysical Research Letters 41, 2553–2560.

Steinman, B.A., Abbott, M.B., Mann, M.E., Stansell, N.D., Finney, B.P., 2012. 1500-year Quantitative Reconstruction of Precipitation in the Pacific Northwest. Proceedings of the National Academy of Sciences of the United States of America 109, 11619–11623.

Steinman, B.A., Abbott, M.B., Nelson, D.B., Stansell, N.D., Rosenmeier, M.F., 2013. Isotopic and hydrologic responses of small, closed lakes to climate variability: Comparison of measured and modeled lake level and sediment core oxygen isotope records. Geochimica et Cosmochimica Acta 105, 455-471.

Steinman, B.A., Rosenmeier, M.F., Abbott, M.B., 2010a. The isotopic and hydrologic response of small, closed-basin lakes to climate forcing from predictive models: Simulations of stochastic and mean-state precipitation variations. Limnology and Oceanography 55, 2246-2261.

Steinman, B.A., Rosenmeier, M.F., Abbott, M.B., Bain, D.J., 2010b. The isotopic and hydrologic response of small, closed-basin lakes to climate forcing from predictive models: Application to paleoclimate studies in the upper Columbia River basin. Limnology and Oceanography 55, 2231-2245.

Streten, N.A., 1974. Some features of the summer climate of interior Alaska. Arctic 27, 272-286.

Stroeve, J., Holland, M.M., Meier, W., Scambos, T., Serreze, M., 2007. Arctic sea ice decline: Faster than forecast. Geophysical Research Letters 34.

Surdu, C.M., Duguay, C.R., Brown, L.C., Prieto, D.F., 2014. Response of ice cover on shallow lakes of the North Slope of Alaska to contemporary climate conditions (1950-2011): radar remote-sensing and numerical modeling data analysis. Cryosphere 8, 167-180.

Swanson, D.K., 2010. Satellite Greenness Data Summary for the Arctic Inventory and Monitoring Network, 1990-2009, In: Department of the Interior, N.P.S. (Ed.), pp. 1-20.

Teller, J.T., Leverington, D.W., 2004. Glacial Lake Agassiz: A 5000 yr history of change and its relationship to the delta O-18 record of Greenland. Geological Society of America Bulletin 116, 729-742.

Teller, J.T., Leverington, D.W., Mann, J.D., 2002. Freshwater outbursts to the oceans from glacial Lake Agassiz and their role in climate change during the last deglaciation. Quaternary Science Reviews 21, 879-887.
Thompson, D.W.J., Wallace, J.M., 1998. The Arctic Oscillation signature in the wintertime geopotential height and temperature fields. Geophysical Research Letters 25, 1297-1300.
Thornalley, D.J.R., Elderfield, H., McCave, I.N., 2009. Holocene oscillations in temperature and salinity of the surface subpolar North Atlantic. Nature 457, 711-714.
Tindall, J.C., Valdes, P.J., 2011. Modeling the 8.2 ka event using a coupled atmosphere-ocean GCM. Global and Planetary Change 79, 312-321.
Torrence, C., Compo, G.P., 1998. A practical guide to wavelet analysis. American Meteorological Society 79, 61-78.
Tremblay, L.B., Mysak, L.A., Dyke, A.S., 1997. Evidence from driftwood records for century-to-millennial scale variations of the high latitude atmospheric circulation during the Holocene. Geophysical Research Letters 24, 2027-2030.
Ullah, W., 1992. Water resources atlas of Newfoundland. Water Resources Division, Government of Newfoundland and Labrador, St. John, Newfoundland.
Valiantzas, J.D., 2006. Simplified versions for the Penman evaporation equation using routine weather data. Journal of Hydrology 331, 690-702.
Viau, A.E., Gajewski, K., Sawada, M.C., Bunbury, J., 2008. Low- and high-frequency climate variability in eastern Beringia during the past 25 000 years. Canadian Journal of Earth Sciences 45, 1435-1453.
Vinther, B.M., Buchardt, S.L., Clausen, H.B., Dahl-Jensen, D., Johnsen, S.J., Fisher, D.A., Koerner, R.M., Raynaud, D., Lipenkov, V., Andersen, K.K., Blunier, T., Rasmussen, S.O., Steffensen, J.P., Svensson, A.M., 2009. Holocene thinning of the Greenland ice sheet. Nature 461, 385-388.
von Grafenstein, U., Erlenkeuser, H., Brauer, A., Jouzel, J., Johnsen, S.J., 1999. A mid-European decadal isotope-climate record from 15,500 to 5000 years BP. Science 284, 1654-1657.
Waelbroeck, C., Labeyrie, L., Michel, E., Duplessy, J.C., McManus, J.F., Lambeck, K., Balbon, E., Labracherie, M., 2002. Sea-level and deep water temperature changes derived from benthic foraminifera isotopic records. Quaternary Science Reviews 21, 295-305.
Wahrhaftig, C., 1965. Physiographic divisions of Alaska, U.S. Geological Survey Professional Paper 482, p. 52.
Walter, K.M., Edwards, M.E., Grosse, G., Zimov, S.A., Chapin, F.S., III, 2007. Thermokarst lakes as a source of atmospheric CH4 during the last deglaciation. Science 318, 633-636.
Wendler, G., Eaton, F., 1990. Surface Radiation Budget at Barrow, Alaska. Theoretical and Applied Climatology 41, 107-115.
Wendler, G., Moore, B., Galloway, K., 2014. Strong Temperature Increase and Shrinking Sea Ice in Arctic Alaska. The Open Atmospheric Science Journal 8, 7-15.
Wetzel, R.G., 2001. Limnology: Lake and River Ecosystems. Academic Press, San Diego, California.

Wiles, G.C., Barclay, D.J., Calkin, P.E., Lowell, T.V., 2008. Century to millennial-scale temperature variations for the last two thousand years indicated from glacial geologic records of Southern Alaska. Global and Planetary Change 60, 115-125.

Wilson, F.H., Dover, J.H., Bradley, D.C., Weber, F.R., Bundtzen, T.K., Haeussler, P.J., 1998. Geologic Map of Central (Interior) Alaska, U.S. Geological Survey Open-File Report OF 98-133. U.S. Geological Survey.

Wooller, M.J., Kurek, J., Gaglioti, B.V., Cwynar, L.C., Bigelow, N., Reuther, J.D., Gelvin-Reymiller, C., Smol, J.P., 2012. An 11,200 year paleolimnological perspective for emerging archaeological findings at Quartz Lake, Alaska. Journal of Paleolimnology 48, 83-99.

Wright, H.E., Jr., Mann, D.H., Glaser, P.H., 1984. Piston corers for peat and lake sediments. Ecology 65, 657-659.

Young, N.E., Briner, J.P., Kaufman, D.S., 2009. Late Pleistocene and Holocene glaciation of the Fish Lake valley, northeastern Alaska Range, Alaska. Journal of Quaternary Science 24, 677-689.

Yu, S.-Y., Colman, S.M., Lowell, T.V., Milne, G.A., Fisher, T.G., Breckenridge, A., Boyd, M., Teller, J.T., 2010. Freshwater Outburst from Lake Superior as a Trigger for the Cold Event 9300 Years Ago. Science 328, 1262-1266.

Yu, Z.C., McAndrews, J.H., Eicher, U., 1997. Middle Holocene dry climate caused by change in atmospheric circulation patterns: Evidence from lake levels and stable isotopes. Geology 25, 251-254.

Zhang, X., Walsh, J.E., 2006. Toward a seasonally ice-covered Arctic Ocean: Scenarios from the IPCC AR4 model simulations. Journal of Climate 19, 1730-1747.

Zhao, C., Yu, Z., Ito, E., Zhao, Y., 2010. Holocene climate trend, variability, and shift documented by lacustrine stable-isotope record in the northeastern United States. Quaternary Science Reviews 29, 1831-1843.